SCDAP/RELAP5 ANALYSIS SUPPORTING A REVIEW OF ANO2 SG INSPECTION INTERVAL

Task Order 1

for

Technical Assignment Control Number MA7226

under

Technical Support for Risk Informed Activities Licensing Submittals

JCN J2824

August 2000

D. L. Knudson
Idaho National Engineering and Environmental Laboratory
Idaho Falls, Idaho 83415

Prepared for
Office of Nuclear Reactor Regulation
U. S. Nuclear Regulatory Commission
through
U. S. Department of Energy
Under DOE Idaho Operations Office
Contract DE-AC07-99ID13727

CONTENTS

CONTENTS iii
FIGURES iv
TABLES v
1. INTRODUCTION 1
2. SCDAP/RELAP5 MODEL 1
3. SCDAP/RELAP5 CALCULATIONS 7
4. RESULTS 10
4.1. Case 01 13
4.2. Case 02 18
4.3. Case 03 20
4.4. Case 04 23
4.5. Case 05 24
4.6. Case 06 27
4.7. Case 07 29
4.8. Case 08 33
5. CONCLUSIONS 38
6. REFERENCES 40
Appendix A - Selected Results from Case 01 . . . . . A-1
Appendix B - Selected Results from Case 02 . . . . . B-1
Appendix C - Selected Results from Case 03 . . . . . C-1
Appendix D - Selected Results from Case 04 . . . . . D-1
Appendix E - Selected Results from Case 05 . . . . . E-1
Appendix F - Selected Results from Case 06 . . . . . F-1
Appendix G - Selected Results from Case 07 . . . . . G-1
Appendix H - Selected Results from Case 08 . . . . . H-1

FIGURES

1. ANO2 loop nodalization without provisions for hot leg countercurrent natural circulation. 2
2. ANO2 reactor vessel nodalization. 3
3. Natural circulation flow patterns that can develop during severe accidents in PWRs with U-tube SGs. 5
4. ANO2 loop nodalization with provisions for hot leg countercurrent natural circulation. 6
5. Schematic showing the surge line connection to the split hot leg. 7
6. Case 01 RCS pressure. 15
7. Case 01 hydrogen generation (oxidation) rate. 16
8. Non-condensable quality in the top of SGA U-tubes in Case 01. 16
9. Mass flow rates in hot and cold SGA tubes in Case 01. 17
10. Mass flow rates in hot and cold SGB tubes in Case 01. 17
11. Volume-averaged temperatures of hot and cold SGB tubes in Case 01. 18
12. Hot leg B mass flows in Case 02. 19
13. Case 03 RCS pressure. 20
14. SGB tube mass flows in Case 03. 21
15. SGB tube temperatures in Case 03. 22
16. Non-condensable quality in SGA tubes in Cases 03 and 04. 24
17. Total hydrogen generated in Cases 03 and 04. 25
18. Pressurizer SRV liquid fraction in Case 05. 25
19. SGA hot tube temperatures in Cases 04 and 05. 26
20. SGB hot tube temperatures in Cases 04 and 05. 27
21. RCS pressures in Cases 05 and 06. 28
22. SG hot tube temperatures in Case 06. 29
23. RCS pressure in Case 07. 30
24. Core exit temperature in Case 07. 31
25. Core exit temperature near the time of operator action in Case 07. 31
26. SGB tube temperatures in Case 07. 32
27. Core exit temperature in Case 08. 34
28. Core exit temperature near the time of operator action in Case 08. 35
29. Core liquid fractions at the seventh axial level of the center channel in Cases 07 and 08. 36
30. Total hydrogen generation in Cases 07 and 08. 37

TABLES

1. Variations considered in the SCDAP/RELAP5 station blackout calculations. 8
2. SCDAP/RELAP5 steady state results. 9
3. Countercurrent natural circulation parameters and benchmark results. 10
4. Sequence of transient events in the SCDAP/RELAP5 station blackout calculations. 10
5. Summary of SCDAP/RELAP5 predicted creep rupture timing. 14

1. INTRODUCTION

The licensee for the Arkansas Nuclear One Unit Two (ANO2) power reactor has applied to the U. S. Nuclear Regulatory Commission (NRC) for a change in the plant's license related to the management of steam generator (SG) tube degradation. Because the application is risk-informed (in accordance with Regulatory Guide 1.174), it addresses the potential consequences of SG tube degradation in the context of severe accident sequences that are beyond the plant's design basis. The NRC requested technical assistance from the Idaho National Engineering and Environmental Laboratory (INEEL) in evaluating the severe accident portions of the application. Specifically, the NRC requested a SCDAP/RELAP5[1] analysis of ANO2 during station blackout accidents with an emphasis on the effects on SG tube integrity. The analysis was directed toward understanding the effects of primary and secondary systems leakage and the effectiveness of a strategy proposed by the licensee to mitigate any challenge to SG tube integrity.

This report contains documentation the ANO2 SCDAP/RELAP5 analysis as requested by the NRC. Specifically, the SCDAP/RELAP5 model used during the course of this analysis is described in Section 2, all calculations that were completed are defined in terms of assumed boundary and initial conditions in Section 3, calculational results are discussed in Section 4, and conclusions are summarized in Section 5.

2. SCDAP/RELAP5 MODEL

ANO2 is a pressurized water reactor (PWR) with a Combustion Engineering nuclear steam supply system. The plant has a power rating of 2,815 MW_t derived from a core of 177 16x16 assemblies with an active fuel height of approximately 3.81 m. ANO2 has two primary coolant loops where each includes a hot leg, a U-tube SG, two reactor coolant pumps (RCPs), and two cold legs. A single pressurizer is attached to the hot leg piping in one of the two loops. The pressurizer surge line is made of stainless steel, the hot/cold leg piping is made of carbon steel with a stainless steel inner lining, and the SG U-tubes are made of inconel. ANO2 has two safety relief valves (SRVs) with a combined capacity of 99.5 kg/s for release of excess reactor coolant system (RCS) pressure from the top of the pressurizer. One safety injection tank (SIT), with ~44.7 m^3 (~44,200 kg) of borated water at ~322 K, is attached to each cold leg. The SITs, which are initially pressurized to ~4.31 MPa by a nitrogen cover gas, are the only operational part of the emergency core cooling system (ECCS) during the station blackout scenario being considered. A large, dry containment building surrounds the reactor systems.

An existing SCDAP/RELAP5 model, which has been documented elsewhere,[2] was used in this analysis to represent those features of the ANO2 PWR. A SCDAP/RELAP5 nodalization of the model is shown in Figure 1. Corresponding reactor vessel nodalization details are shown in Figure 2. Arrows indicate directions associated with positive flows. Shaded areas represent fuel rods, cross-hatched areas represent all other pipe/vessel structures, and remaining regions represent the hydrodynamic volume within the plant. Nodalizations shown in Figures 1 and 2 were used to establish full power steady state conditions, which provided the necessary initialization for the station blackout scenario.

The specific station blackout scenario considered is initiated by the loss of off site power. On-site alternating current (AC) power is also unavailable because diesel generators fail to start or fail to supply power. Decay heat removal cannot be maintained because there is no power for electrical feedwater pumps and steam driven auxiliary feedwater pumps fail to supply water. As the transient begins, control rod drives lose power, the reactor scrams, and the main feedwater pumps and RCPs begin to coastdown. The flow of

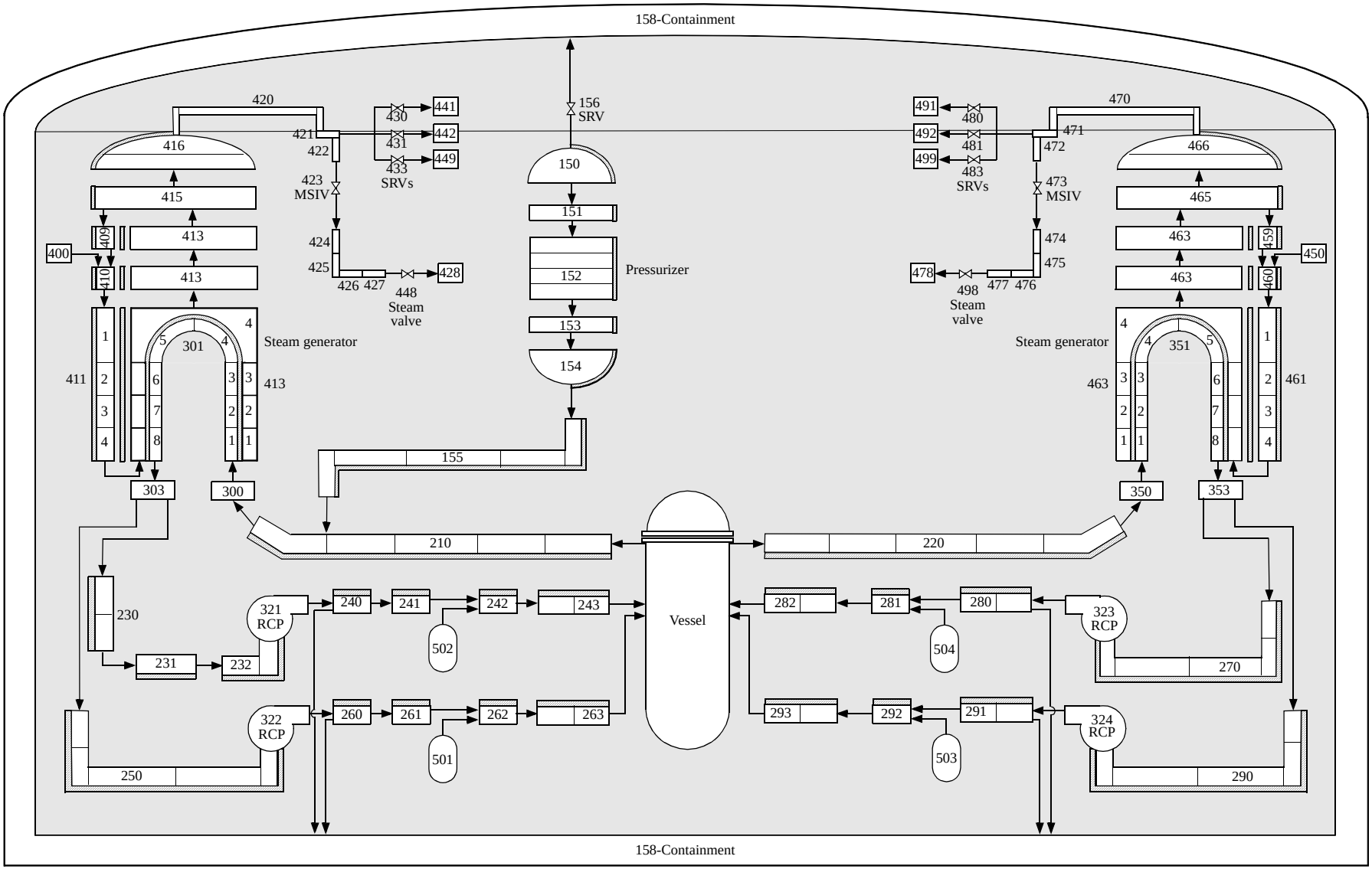

Figure 1. ANO2 loop nodalization without provisions for hot leg countercurrent natural circulation.

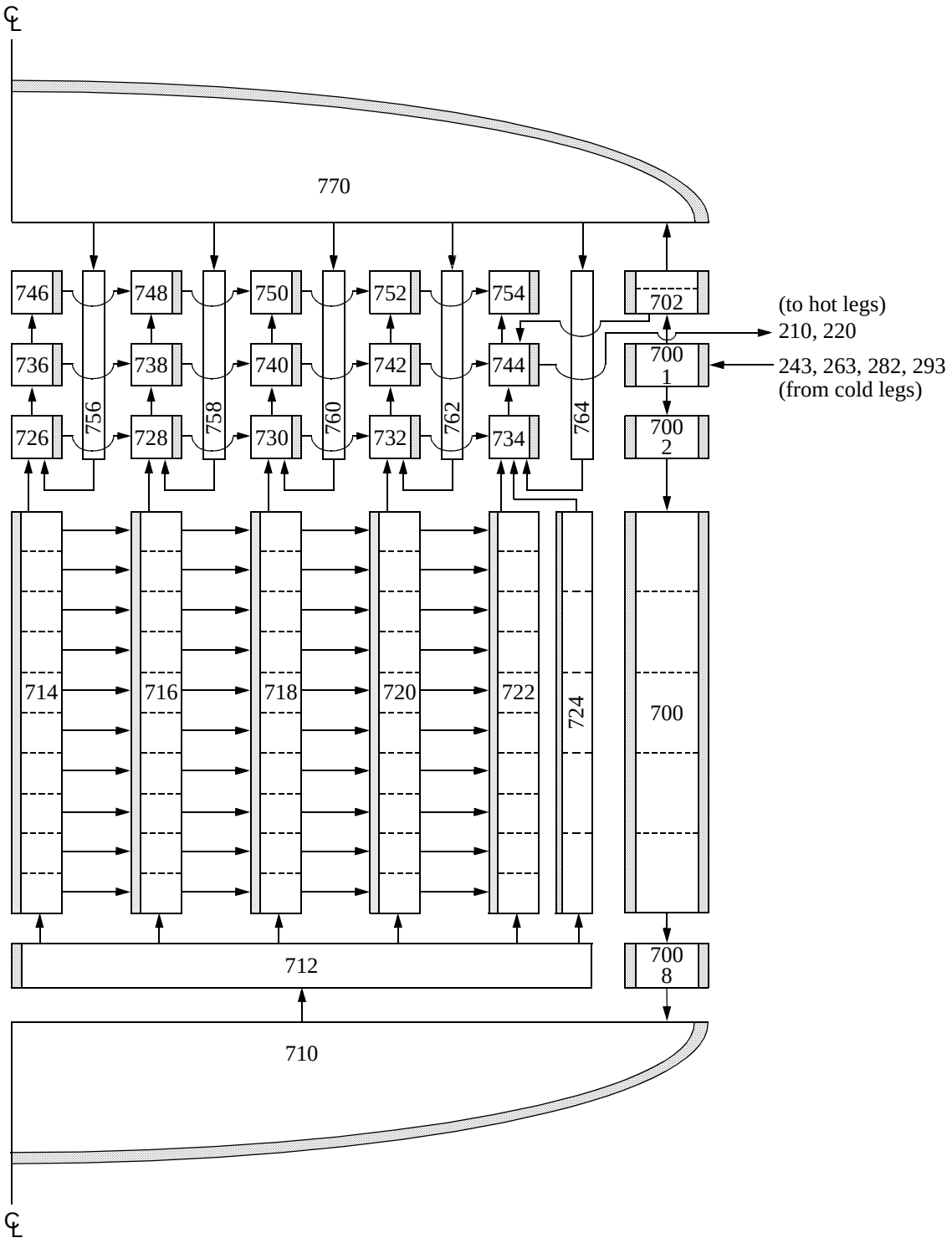

Figure 2. ANO2 reactor vessel nodalization.

feedwater is reduced to zero before pump coastdown is complete because the main feedwater valves close quickly. The turbine stop valves then close, effectively isolating the SG secondaries. After isolation, SG pressures increase as a result of boiling associated with decay heat transfer from the core until relief valves open. SG pressures are normally maintained between the opening and closing pressures of the relief valves thereafter. Water in the SG secondaries is ultimately boiled away as heat is transferred from the RCS. Once water in the secondaries is depleted, the SGs no longer remove significant amounts of heat. Core decay energy then heats the RCS, resulting in system pressurization normally controlled by cycling pressurizer SRVs. The RCS pressure can also be influenced by RCP seal leaks, which could develop following the loss of seal cooling associated with the loss of AC power. After the RCS is heated to saturated conditions, a high pressure boiloff begins, ultimately leading to core uncovery and heatup. Without recovery of power or equipment, the transient proceeds to severe core damage and fuel melting.

Variations of in-vessel and full loop natural circulation flow patterns, as depicted in Figure 3, can develop during the early phases of a station blackout scenario. SCDAP/RELAP5 nodalizations shown in Figures 1 and 2 can accommodate simulation of those flow patterns if/when the appropriate conditions occur. However, a potential for hot leg countercurrent natural circulation (also depicted in Figure 3) exists as the RCS boiloff proceeds and the hot legs are eventually voided. At that point, the nodalization shown in Figure 4 was used in place of the Figure 1 nodalization to provide the additional flow paths needed if/when hot leg countercurrent natural circulation develops. Those flow paths include a split hot leg to carry hot flow away from the reactor vessel and cooler return flow back to the reactor vessel, a split SG inlet plenum to allow simulation of experimentally observed mixing of hot and cold flow streams, and a split SG tube bundle to carry hot flow toward the outlet plenum and cooler return flow back to the inlet plenum. Details associated with the surge line/hot leg connection during countercurrent natural circulation as adopted for use in this analysis are shown in Figure 5.

Simulation of all modes of natural circulation is a vital capability of the SCDAP/RELAP5 model because those flows transfer decay energy from the core to other parts of the RCS. The associated heatup of RCS structures can lead to pressure boundary failures; with notable vulnerabilities in the pressurizer surge line, the hot leg nozzles, and the SG tubes. SCDAP/RELAP5 calculation of in-vessel and full loop natural circulation was based on loss coefficients derived from full power steady state operating data. However, flow areas and loss coefficients for all SG plena connections shown in Figure 4 (from the split hot leg to the split SG inlet plenum, from the split SG inlet plenum to the split SG tube bundle, and from the split SG tube bundle to the SG outlet plenum for a total of 10 connections in each primary coolant loop) were modified for consistency with hot leg countercurrent natural circulation flows observed during Westinghouse 1/7th scale experiments.[3]

Two different approaches were used to model SG plena connections needed for simulation of hot leg countercurrent natural circulation. In the first approach, which was used only for the first two SCDAP/RELAP5 calculations (Cases 01 and 02), flow areas and loss coefficients were simply fixed at values needed for consistency with the Westinghouse experiments. This approach, which was not introduced in the affected calculations until hot leg countercurrent natural circulation was imminent, is acceptable as long as the reactor vessel water level is above the bottom of the downcomer skirt and RCP loop seals remain water filled. If the bottom of the downcomer skirt is uncovered and water in the loop seals happens to clear, countercurrent natural circulation can transition to full loop natural circulation. In such a case, flow areas and loss coefficients fixed for consistency with the Westinghouse experiments may not be appropriate.

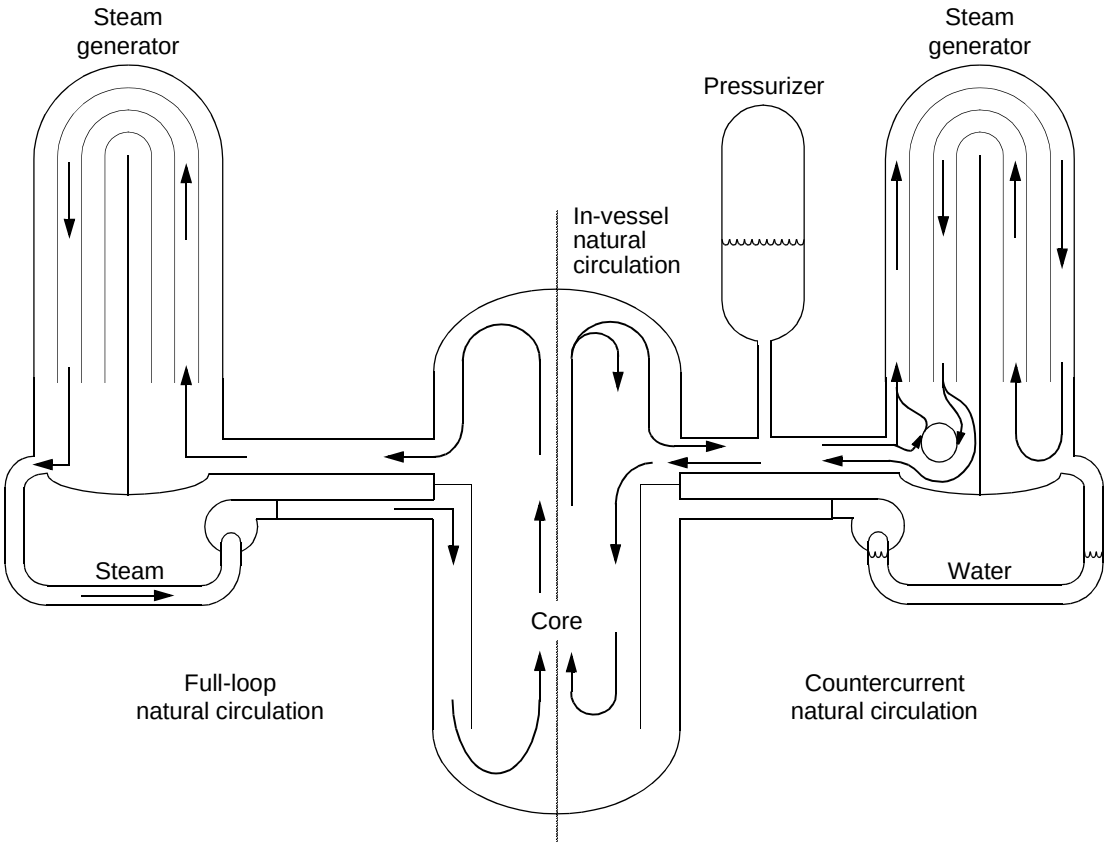

Figure 3. Natural circulation flow patterns that can develop during severe accidents in PWRs with U-tube SGs.

Servo valves were used to model SG plena connections in the second approach, which was adopted for the other SCDAP/RELAP5 calculations (Cases 03 through 08). The valves were configured with two sets of flow areas and loss coefficients; one set appropriate for full loop natural circulation and one set appropriate for hot leg countercurrent natural circulation. If the bottom of the reactor vessel downcomer skirt is covered and the horizontal portion of RCP loop seals in a given loop are full of water, control logic directs the use of countercurrent loss coefficients in all servo valves in that loop. Alternately, if the bottom of the downcomer skirt begins to uncover and voids begin to form in horizontal portions of RCP loop seals, control logic directs a loss coefficient transition to values used for full loop circulation. As a result, this servo valve approach allows simulation of both full-loop and countercurrent natural circulation flows in each loop if/when loop conditions change during accident progression.

Servo valves were also used in all SCDAP/RELAP5 calculations to model surge line to hot leg connections. Those servo valves, numbered 157 and 159 in Figure 5, were needed to accommodate pressurizer draining and the mixing that would be expected when pressurizer SRVs open. Specifically, while the pressurizer drains and SRVs are closed, control logic opens Valve 159 and closes Valve 157. Consequently, all water draining from the pressurizer appropriately flows into the bottom half of the split hot leg. After pressurizer dryout, Valve 157 opens and Valve 159 closes whenever SRVs are closed to appropriately expose

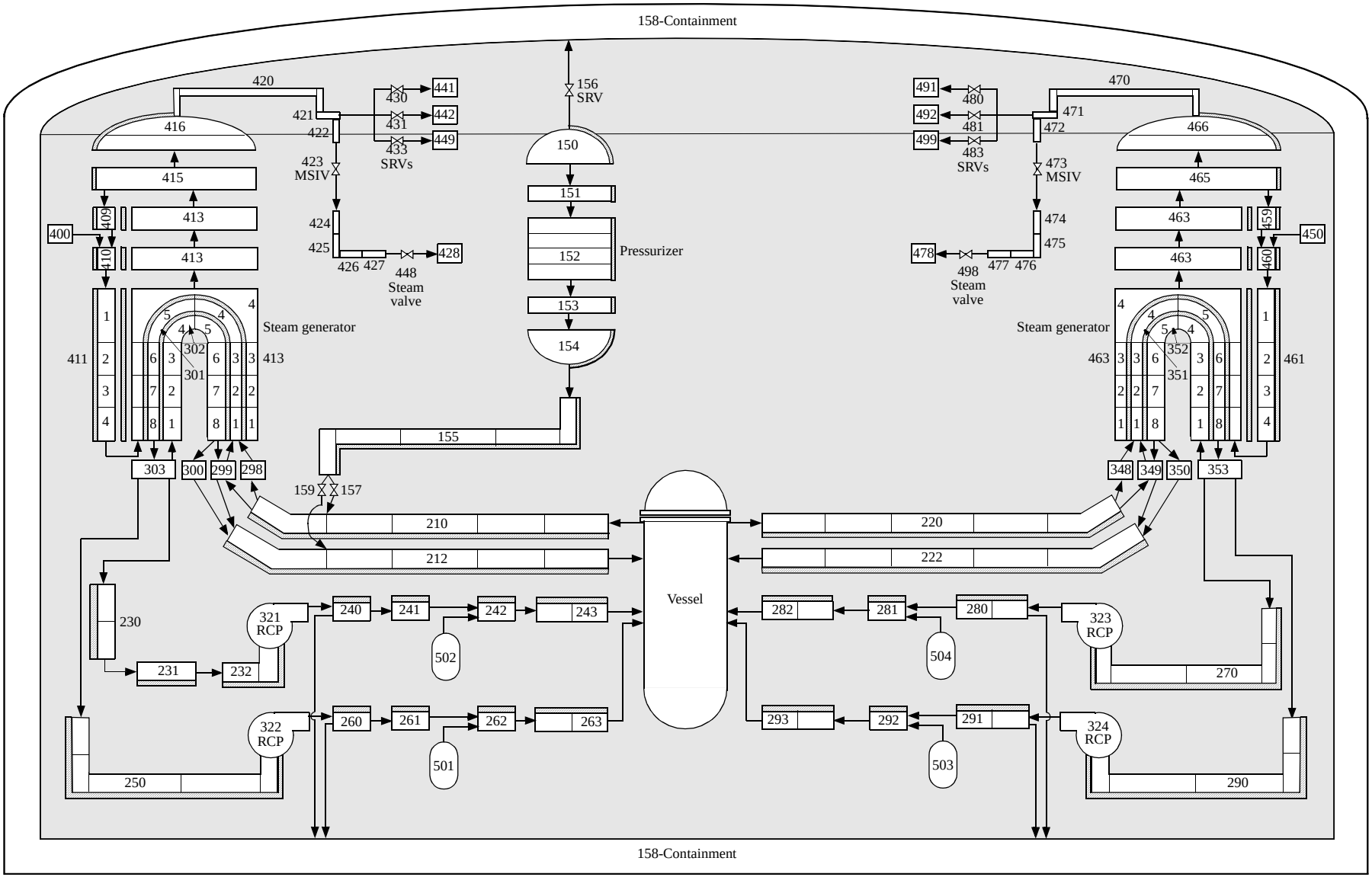

Figure 4. ANO2 loop nodalization with provisions for hot leg countercurrent natural circulation.

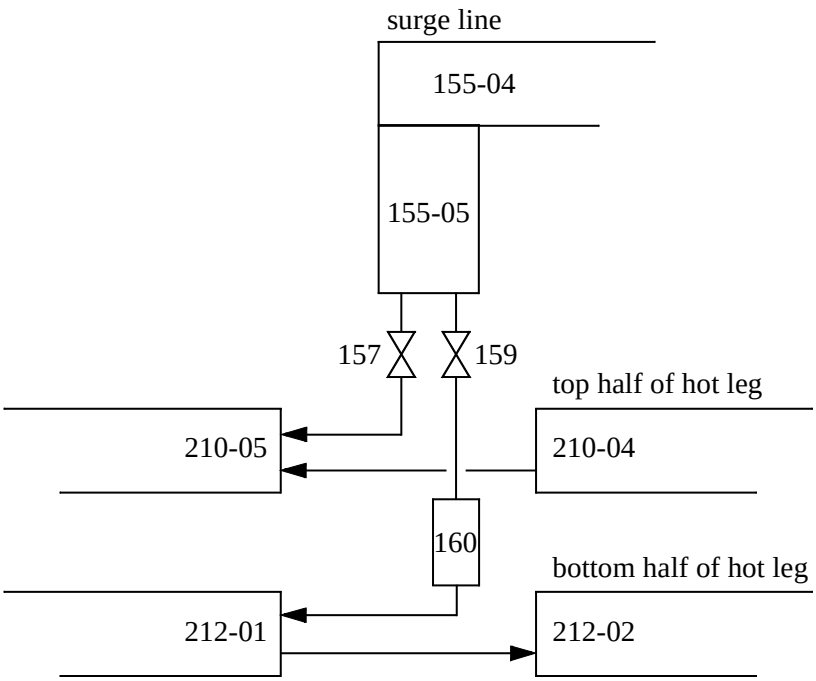

Figure 5. Schematic showing the surge line connection to the split hot leg.

the surge line to the hottest flow stream. And finally, control logic opens both valves (half way) whenever pressurizer SRVs open. Countercurrent natural circulation is interrupted when SRVs open because fluid from the core tends to flow in both halves of the split hot leg toward the surge line. It is reasonable to expect a high degree of mixing as those flow streams reach the entrance to the surge line and respond to the large pressure differential generated by the open SRVs. Valves 157 and 159 were opened (half way) when SRVs opened as a way to approximate conditions that would result from that mixing. Other details associated with (relatively minor) alterations of the existing ANO2 SCDAP/RELAP5 model for use in this analysis are documented elsewhere.[4]

3. SCDAP/RELAP5 CALCULATIONS

A total of eight different SCDAP/RELAP5 calculations, hereafter referred to as Cases 01 through 08, were completed during the course of this analysis. All of the calculations were completed using Version 8ht1 of SCDAP/RELAP5/MOD3.2. Version 8ht1 includes a few minor error corrections (relative to the transmittal version of 8ht) as well as updates to allow user specification of stress multiplication factors in the calculation of creep damage (although that capability was not available at the time Cases 01 and 02 were completed).

All calculations were designed to simulate variations of a station blackout accident. The variations considered are listed in Table 1. Those variations can be grouped into one of three categories including (a) variations in SG secondary pressures as represented by items 1 through 3, (b) variations in RCS pressure as

represented by items 4 through 10, and (c) variations in heat transfer as represented by item 11. (Items 12 and 13 were included in the table for the sake of completeness, although they are more accurately classified as model refinements rather than calculational variables.) Of the listed variations, nine (including items 1 through 8 and item 11) were selected in an attempt to cover those conditions that could reasonably be expected to develop during a station blackout accident and have an impact on SG tube integrity. The remaining variations (items 9 and 10) were considered because ANO2 operators may take such actions to depressurize the RCS in an effort to mitigate accident consequences. (Notation used in the table, and throughout the remainder of this document, includes assignment of the letter 'A' to the RCS loop containing the pressurizer and the letter 'B' to the RCS loop without the pressurizer.)

Table 1. Variations considered in the SCDAP/RELAP5 station blackout calculations.

Item/Description		Case							
		01	02	03	04	05	06	07	08
1	SGA secondary depressurization through SRV that fails open on first challenge	x	x	x	x	x	x	x	x
2	SGB secondary depressurization through SRV that fails open on first challenge						x	x	x
3	SGB secondary depressurization from 0 s through a steam valve leak of 9.3e-5 m^2			x					
4	Pressurizer SRV open/close set points reduced by 6.9 MPa on first challenge		x						
5	One of two pressurizer SRVs fails to fully close (@ 13% of full open area) when surge line creep damage begins to accumulate			x					
6	One of two pressurizer SRVs fail to fully close (@ 13% of full open area) when surge line temperature exceeds the maximum SGA tube temperature during hot leg countercurrent heating				x				
7	One of two pressurizer SRVs fail to fully close (@ 13% of full open area) after water discharge through the valve is complete					x			
8	Both pressurizer SRVs fail to fully close (@ 13% of full open area) after water discharge through the valves is complete						x		
9	Operators open ECCS vent valves 1,380 s after reaching 700 K at the core exit without simulation of the ECCS vent valve tail pipe							x	
10	Operators open ECCS vent valves 1,620 s after reaching 700 K at the core exit with simulation of the ECCS vent valve tail pipe								x
11	SG flow and heat transfer area reductions to approximate 17.7% plugging (or 1,489 of 8,411 SG tubes)							x	x
12	Use of SG plena servo valves[a]			x	x	x	x	x	x
13	Use of stress multipliers for calculating SG tube creep damage[a]			x	x	x	x	x	x

a. Although this is more of a modeling refinement rather than a calculation variable, it is included here for the sake of completeness.

All calculations were completed without credit for predicted failures in the RCS pressure boundary. In other words, all calculations were allowed to progress without depressurization of the RCS associated with any predicted pressure boundary failure. This approach was used as a way to estimate the earliest possible failure time for all vulnerable components by minimizing the time between various failures.

Before any station blackout transients could be completed, steady state calculations and benchmarking of hot leg countercurrent natural circulation were required. Steady state calculations were needed to provide initial conditions for simulating the various station blackout accidents. As indicated in Table 2, two SCDAP/RELAP5 steady state calculations were actually completed because SG tube plugging considered in Cases 07 and 08 affects steady state (as calculated for Cases 01 through 06 without tube plugging). In this analysis, a reduced SG secondary pressure was accepted as indicated in the table to achieve target core and hot leg temperatures in Cases 07 and 08. This approach, which may or may not be consistent with actual practice at ANO2, yields initial core stored energy comparable to all other calculations with only a small disparity (increase) in initial SG secondary heat capacity.

Table 2. SCDAP/RELAP5 steady state results.

Parameter	Target Value[a]	Calculated Result	
		Cases 01 through 06	Cases 07 and 08[b]
Reactor power (MW_t)	2,815	2,815	2,815
Pressurizer pressure (MPa)	15.51	15.51	15.51
SG pressure (MPa)	6.21	6.21	5.93
Pressure drop across the core (kPa)	110	110	110
Total pressure drop across the vessel (kPa)	250	273	273
Pressurizer level (%)	49.2	49.2	49.8
SG narrow range mass (lbm/SG)	130,910	130,910	130,910
Reactor coolant flow (kg/s)	15,170	15,170	15,170
Core flow (kg/s)	14,640	14,620	14,620
Steam flow (kg/s)	815	794	793
Feedwater flow (kg/s)	787	794	793
Nozzle clearance flow (0.4% of reactor flow in kg/s)	60.68	59.91	59.91
Alignment keyway flow (0.4% of reactor flow in kg/s)	60.68	62.88	62.98
Cold leg temperature (K)	562.9	562.8	562.8
Hot leg temperature (K)	595.7	595.5	595.5
Maximum clad surface temperature (K)	620.1	618.5	618.5

a. Based on information taken from the ANO2 Final Safety Analysis Report.
b. Steady state initialization associated with Cases 01 through 06 was not applicable because SG tube plugging was simulated in these cases.

Benchmarking of hot leg countercurrent natural circulation consists of adjusting flow areas and loss coefficients associated with all (ten) SG plena junctions (in each loop) to obtain agreement with Westinghouse experimental data. Results of that effort are provided in Table 3. As indicated, three different benchmark calculations were actually performed. Three benchmarks were required because of differences between the calculations. Specifically, the benchmark completed for Cases 01 and 02 was not applicable to Cases 03 through 06 because fixed SG plena flow areas and loss coefficients used in Cases 01 and 02 were not appropriate for the servo valves used in Cases 03 through 06. In addition, servo valve flow areas and loss coefficients determined for Cases 03 through 06 were not appropriate when flow and heat transfer areas were reduced to simulate SG tube plugging in Cases 07 and 08.

Table 3. Countercurrent natural circulation parameters and benchmark results.

Parameter	Target Value[a]	Benchmark Result		
		Cases 01 and 02	Cases 03 through 06[b]	Cases 07 and 08[c]
Hot/cold SG tube split	53%/47%	53%/47%	53%/47%	53%/47%
Fraction of core decay energy absorbed in each U-tube SG	0.135	0.132	0.133	0.134
Hot mixing fraction	0.865	0.866	0.866	0.864
Cold mixing fraction	0.865	0.866	0.864	0.866
Recirculation ratio	1.92	1.92	1.93	1.92

a. Based on Westinghouse experimental data.
b. Benchmarking associated with Cases 01 and 02 was not applicable because servo valves were added to represent all SG plena junctions in these cases.
c. Benchmarking associated with Cases 03 through 06 was not applicable because SG tube plugging was simulated in these cases.

It is important to understand that adjustment of SG plena flow areas and loss coefficients to obtain specific natural circulation behavior was performed during benchmarking calculations only. Thereafter, flow areas and loss coefficients were not altered and natural circulation behavior was calculated by SCDAP/RELAP5 based on thermal-hydraulic conditions and the flow areas and loss coefficients determined during the benchmarking process. Therefore, natural circulation behavior in the station blackout calculations presented in the next section was not 'forced'. Instead, the following results reflect SCDAP/RELAP5 natural circulation predictions consistent with all associated conditions.

4. RESULTS

Highlights in the results from all eight different SCDAP/RELAP5 calculations completed during the course of this analysis are discussed in the following subsections. Before giving those descriptions, it should be noted that a sequence of transient events for all calculations is listed in Table 4 and creep rupture failure timing for all calculations is summarized in Table 5. Those tables may provide information that is helpful in understanding the case-by-case discussions. In addition, a standard set of plotted results was compiled for each calculation. Those plots are provided in Appendices A through H.

Table 4. Sequence of transient events in the SCDAP/RELAP5 station blackout calculations.

Event	Time (in seconds) for Case							
	01	02	03	04	05	06	07	08
TMLB' initiation	0	0	0	0	0	0	0	0
SGB steam valve begins to leak	nc[a]	nc	0	nc	nc	nc	nc	nc
SGA SRV fails open-first challenge	~10	~10	~10	~10	~10	~10	~10	~10
SGB SRV fails open-first challenge	nc	nc	nc	nc	nc	~10	~10	~10

Table 4. Sequence of transient events in the SCDAP/RELAP5 station blackout calculations. (continued)

Event	Time (in seconds) for Case							
	01	02	03	04	05	06	07	08
Pressurizer empties due to shrinkage associated with initial cool down (99% void in bottom of pressurizer)	400	400	397	399	399	189	205	205
SGs dryout (99% void in bottom of SGA/SGB secondaries)	662/ 3,099	662/ 3,099	665/ 3,099	663/ 3,099	663/ 3,099	814/ 872	866/ 925	866/ 925
Pressurizer SRV cycling begins	3,190	4,230[b]	3,190	3,190	3,190	3,120	3,150	3,150
Pressurizer fills due to heating following SG dryout (1% void in top of pressurizer)	3,720	3,240	3,730	3,720	3,720	3,450	3,470	3,470
Vapor from in-core boiling collects in U-tubes ending liquid full loop natural circulation	4,888	3,206	4,889	4,904	4,897	4,636	4,567	4,567
Collapsed liquid level falls below top of fuel rods (6.804 m above lower head bottom)	5,936	4,635	5,912	5,851	5,912	5,606	5,523	5,523
Vapor in the core exit begins to superheat; hot leg countercurrent circulation begins	6,163	4,970	6,138	6,094	6,127	5,824	5,740	5,740
Collapsed liquid level falls below bottom of fuel rods (2.994 m above lower head bottom)	7,179	6,853	7,109	7,072	7,207	6,860	6,708	6,708
Onset of fuel rod oxidation (> 0.01 kg of H_2 produced)	7,869	6,400	7,849	7,810	7,913	7,500	7,310	7,310
Operators open ECCS vent valves	nc	nc	nc	nc	nc	nc	7,582	7,822
Pressurizer drains and remains empty (99% void in bottom of pressurizer)	8,697	7,459	8,635	8,566	8,452	7,747	8,188	8,033
Pressurizer SRV fails to fully close	nc	nc	9,738[c]	9,352[d]	5,920[e]	5,878[f]	nc	nc
First relocation of absorber materials into the lower head	9,949[g]	8,690[h]	10,020[i]	9,966[j]	9,828[k]	18,440[l]	40,230[m]	np[n]
Pressurizer surge line fails by creep rupture	11,730	9,970	11,120	11,060	10,980	np	34,400	20,790
First relocation of molten fuel into the lower head	np	12,130[o]	20,560[p]	19,870[q]	19,640[r]	20,630[s]	37,760[t]	np
SIT injections	np[u]	np[u]	16,220 and 25,560[u]	16,360, 17,370, and 18,110[u]	16,070 and 24,440[u]	12,160, 15,870, and 23,400[u]	from 7,999 to 41,620	from 8,494 to 49,330[u]

Table 4. Sequence of transient events in the SCDAP/RELAP5 station blackout calculations. (continued)

Event	Time (in seconds) for Case							
	01	02	03	04	05	06	07	08
Bottom of fuel rods reflooded by SIT injection (>2.994 m above lower head bottom)	np	np	16,240[v]	18,120	16,090[v]	12,180[v]	8,021	8,519
Upper plenum stainless steel melts and relocates to lower head	13,050, 13,230, 14,090, and 14,480[w]	np	np	np	18,090[x]	np	35,510 and 36,250[y]	30,270 and 31,830[z]
Hot leg A fails by creep rupture	13,070	15,070	19,430	19,360	18,700	20,720	40,040	31,100
Hot leg B fails by creep rupture	13,250	19,860	20,660	19,980	19,740	21,280	np	np
Oxidation induced stagnation of SGA tube natural circulation	13,570	9,979	16,690	16,400	16,890	14,050	np	np
Oxidation induced stagnation of SGB tube natural circulation	13,570	9,741	16,900	16,430	16,890	14,020	np	np
Loop A RCP loop seal clears and downcomer skirt uncovers; onset of full loop natural circulation	np	np	13,900 and 22,250	10,980	13,800 and 21,680	10,680 and 21,300	np	np
Loop A RCP loop seal refills and/or downcomer skirt re-covers; resumption of hot leg countercurrent natural circulation	np	np	16,270	16,430	16,120	12,210[aa]	np	np
Loop B RCP loop seal clears and down comer skirt uncovers; onset of full loop natural circulation	14,360	np	11,180 and 21,870	14,440	10,940 and 21,080	9,400 and 21,110	np	np
Loop B RCP loop seal refills and/or downcomer skirt re-covers; resumption of hot leg countercurrent natural circulation	np	np	16,270	16,430	16,120	12,210[aa]	np	np
First SG tube creep rupture failure	14,600[ab]	np	10,750[ac]	10,770[ac]	11,190[ac]	10,200[ad]	np	33,420[ae]
Collapsed liquid level falls below bottom of fuel rods for second time	np	np	20,900	np	19,970	20,860	38,200	np
End of calculation	15,000	30,000	25,570	20,000	24,450	23,400	48,750	49,330

a. Not considered in this case.
b. The first pressurizer SRV challenge occurred at 3,190 s when the original design pressure set point was first reached, but regular valve cycling was delayed until the time indicated because set points were reset at the time of the first challenge.
c. One of two pressurizer SRVs fail to fully close (@ 13% of full open area) when surge line creep damage begins to accumulate.
d. One of two pressurizer SRVs fail to fully close (@ 13% of full open area) when surge line temperature exceeds the maximum SGA tube temperature during hot leg countercurrent heating.

e. One of two pressurizer SRVs fail to fully close (@13% of full open area) after water discharge through the valve is complete.
f. Both pressurizer SRVs fail to fully close (@ 13% of full open area) after water discharge through the valves is complete.
g. A total of 2,212 kg of absorber material was ultimately relocated into the lower head.
h. A total of 5,632 kg of absorber material was ultimately relocated into the lower head.
i. A total of 4,920 kg of absorber material was ultimately relocated into the lower head.
j. A total of 5,488 kg of absorber material was ultimately relocated into the lower head.
k. A total of 2,127 kg of absorber material was ultimately relocated into the lower head.
l. A total of 5,661 kg of absorber material was ultimately relocated into the lower head.
m. A total of 5,680 kg of absorber material was ultimately relocated into the lower head.
n. Not predicted before the end of the calculation.
o. A total of 7,650 kg UO_2, 1,336 kg ZrO_2, 1,880 kg Zr, and 1,032 kg of stainless steel was ultimately relocated into the lower head.
p. A total of 50,290 kg UO_2, 9,289 kg ZrO_2, and 4,031 kg Zr was ultimately relocated into the lower head.
q. A total of 66,960 kg UO_2, 8,214 kg ZrO_2, 8,592 kg Zr, and 2,679 kg of stainless steel was ultimately relocated into the lower head.
r. A total of 40,070 kg UO_2, 7,389 kg ZrO_2, and 3,220 kg Zr was ultimately relocated into the lower head.
s. A total of 67,790 kg UO_2, 8,135 kg ZrO_2, 8,918 kg Zr, and 415 kg of stainless steel was ultimately relocated into the lower head.
t. A total of 65,450 kg UO_2, 13,230 kg ZrO_2, 4,843 kg Zr, and 507 kg of stainless steel was ultimately relocated into the lower head.
u. SITs were not emptied by the end of the calculation.
v. A second reflood by SIT injection was in progress at the end of this calculation.
w. A total of 17,720 kg of upper plenum steel was relocated.
x. A total of 2,114 kg of upper plenum steel was relocated.
y. A total of 16,210 kg of upper plenum steel was relocated.
z. A total of 14,470 kg of upper plenum steel was relocated.
aa. A second RCP loop seal refilling was in progress just before the end of this calculation.
ab. For SGA and SGB tubes with stress multipliers of unity. See Table 5 for a summary of the timing of all creep rupture failures.
ac. For SGA tubes with a stress multiplier of 4.0. See Table 5 for a summary of the timing of all creep rupture failures.
ad. For SGB tubes with a stress multiplier of 4.0. See Table 5 for a summary of the timing of all creep rupture failures.
ae. For SGA tubes with a stress multiplier of 7.5. See Table 5 for a summary of the timing of all creep rupture failures.

4.1. Case 01

As indicated in Table 1, this calculation was designed to simulate a station blackout accident where the RCS and SGB remain at set point pressures while SGA is depressurized. SGA depressurization was achieved by assuming that SGA SRVs fail to close when first challenged.

This case began with a complete loss of AC power while the reactor was operating at normal steady state conditions. Accordingly, the reactor scrammed, RCPs and feedwater pumps tripped, and turbine stop valves closed (thereby isolating the SGs) at time 0 due to the loss of power. The RCS pressure initially decreased as shown in Figure 6 because the RCS was cooled by heat transfer to water remaining in the SGs at the time of SG isolation. SGA provided most of the initial cooling because the secondary saturation temperature was significantly reduced through depressurization of that generator. However, without a source of feedwater, heat transfer from the RCS diminished as SG inventories were boiled away. Consequently, the RCS pressure began to increase after the dryout of SGA at 662 s and SGB at 3,099 s; ultimately reaching pressurizer SRV opening set points at 3,190 s. The RCS pressure generally remained between opening and closing set points of the pressurizer SRVs thereafter as indicated in the figure.

Table 5. Summary of SCDAP/RELAP5 predicted creep rupture timing.

Component		Time (in seconds) for Case							
		01	02	03	04	05	06	07	08
Surge line		11,730	9,970	11,120	11,060	10,980	np	34,400	20,790
Hot leg A		13,070	15,070	19,430	19,360	18,700	20,720	40,040	31,100
Hot leg B		13,250	19,860	20,660	19,980	19,740	21,280	np	np
SGA tubes w/ stress multipliers	7.5	nc[a]	nc	nc	nc	nc	nc	np	33,420
	7.0	nc	nc	nc	nc	nc	nc	np	40,460
	6.5	nc	nc	nc	nc	nc	nc	np	40,470
	6.0	nc	nc	nc	nc	nc	nc	np	40,480
	5.5	nc	nc	nc	nc	nc	nc	np	40,510
	5.0	nc	nc	nc	nc	nc	nc	np	np
	4.5	nc	nc	nc	nc	nc	nc	np	np
	4.0	nc	nc	10,750	10,770	11,190	21,060	np	np
	3.5	nc	nc	11,180	10,880	14,260	21,600	np	np
	3.0	nc	nc	11,430	10,980	15,680	np	np	np
	2.5	nc	nc	14,790	11,070	16,340	np	np	np
	2.0	nc	nc	16,420	11,160	19,730	np	np	np
	1.5	nc	nc	20,820	11,760	19,760	np	np	np
	1.0	14,600	np[b]	np	np	np	np	np	np
SGB tubes w/ stress multipliers	7.5	nc	nc	nc	nc	nc	nc	np	40,470
	7.0	nc	nc	nc	nc	nc	nc	np	40,480
	6.5	nc	nc	nc	nc	nc	nc	np	40,510
	6.0	nc	nc	nc	nc	nc	nc	np	np
	5.5	nc	nc	nc	nc	nc	nc	np	np
	5.0	nc	nc	nc	nc	nc	nc	np	np
	4.5	nc	nc	nc	nc	nc	nc	np	np
	4.0	nc	nc	11,420	np	19,890	10,200	np	np
	3.5	nc	nc	11,620	np	19,960	10,920	np	np
	3.0	nc	nc	13,570	np	20,530	21,170	np	np
	2.5	nc	nc	20,960	np	np	np	np	np
	2.0	nc	nc	np	np	np	np	np	np
	1.5	nc	nc	np	np	np	np	np	np
	1.0	14,600	np	np	np	np	np	np	np

a. Not considered in this case.
b. Not predicted before the end of the calculation.

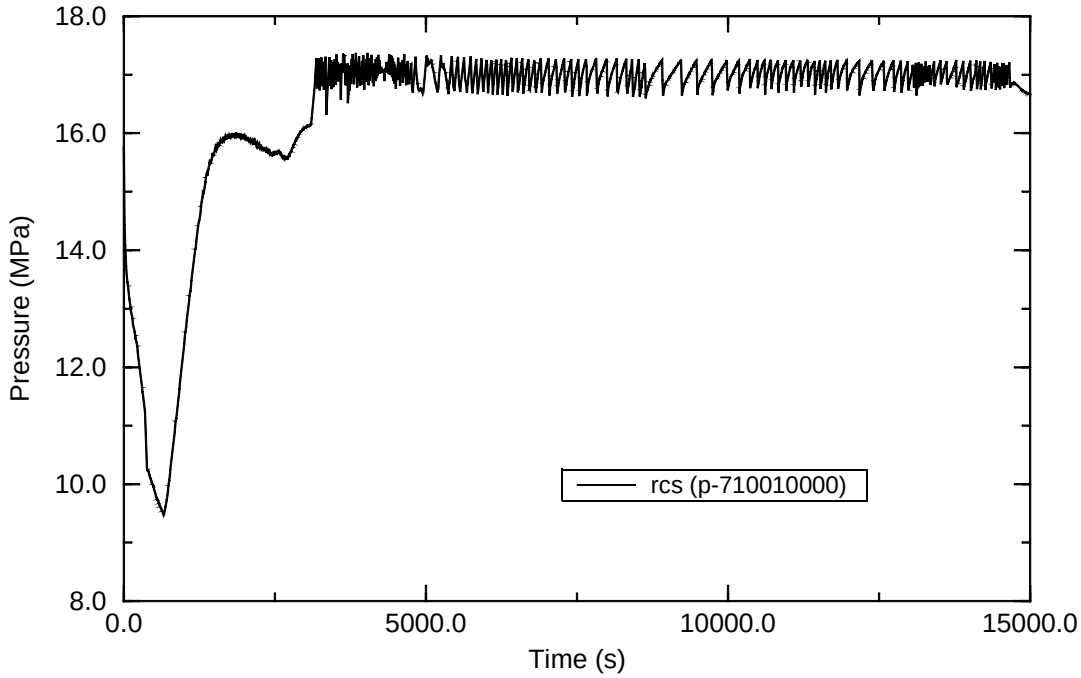

Figure 6. Case 01 RCS pressure.

RCS inventory was lost through the cycling pressurizer SRVs, which led to core uncovery and heatup. Fuel rod oxidation, which began shortly after core uncovery was complete, was an important part of the heatup. Decay heat and the energy associated with the exothermic oxidation process was distributed into the RCS piping by hot leg countercurrent natural circulation, resulting in creep rupture failures of the surge line at 11,730 s, hot leg A at 13,070 s, hot leg B at 13,250 s, and tubes in both SGs by 14,600 s. However, the oxidation excursion shown in Figure 7 also led to stagnation of natural circulation flows in the SG tubes of both loops.

As oxidation progressed, steam/hydrogen mixtures entered the hot leg countercurrent natural circulation flow path and ultimately filled SG U-tubes as indicated in Figure 8. As oxidation ended, hydrogen concentrations entering the top half of the hot leg began to diminish, producing a density gradient between vapors in the SG U-tubes and vapors in the hot leg. By 13,570 s, the density gradient was large enough to result in stagnation of natural circulation flow in the tube bundle as shown in Figure 9.

About 790 s after SG tube flow stagnation, the bottom of the reactor vessel downcomer skirt was uncovered and water was predicted to clear from RCP loop seals in the B loop. When those loop seals cleared, full loop natural circulation flow developed in the B loop with a corresponding increase of flow in SGB “hot” tubes as shown in Figure 10. Flow in SGB “cold” tubes remained near zero because fixed loss coefficients assigned to SG plena junctions for hot leg countercurrent natural circulation were not generally applicable to full loop flow conditions. (This flow discrepancy was addressed in Cases 03 through 08 through the use of servo valves to represent all SG plena junctions.) Increased flow through the SGB “hot” tubes had a direct and immediate impact on the “hot” tube temperature as shown in Figure 11. The lower level of “cold” tube heating (also shown in the figure) was primarily achieved indirectly through heating of

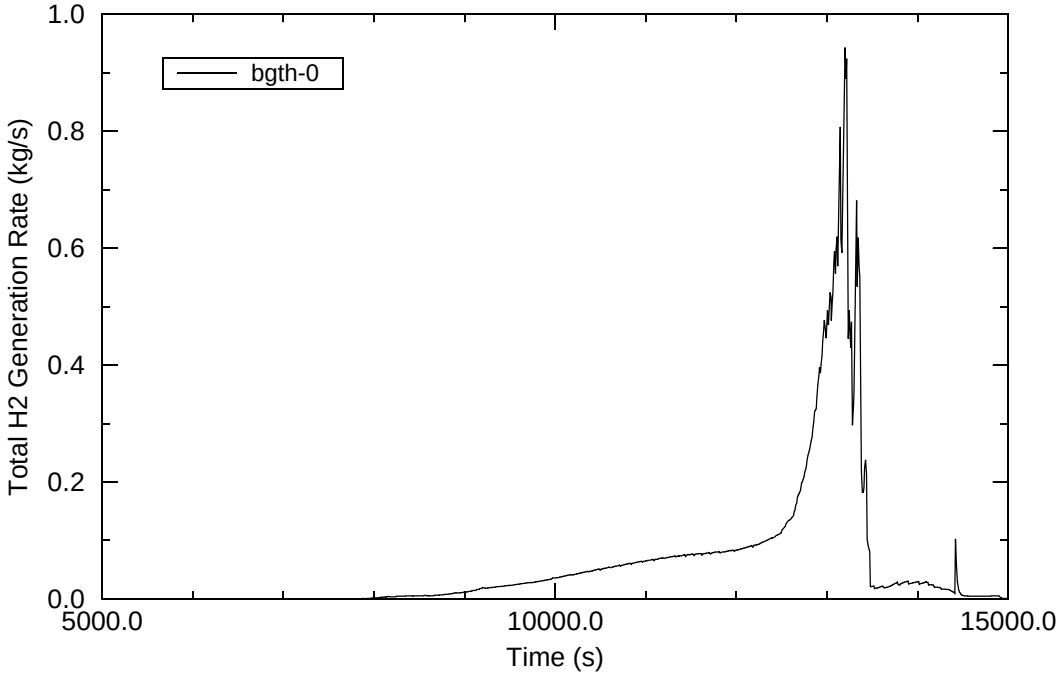

Figure 7. Case 01 hydrogen generation (oxidation) rate.

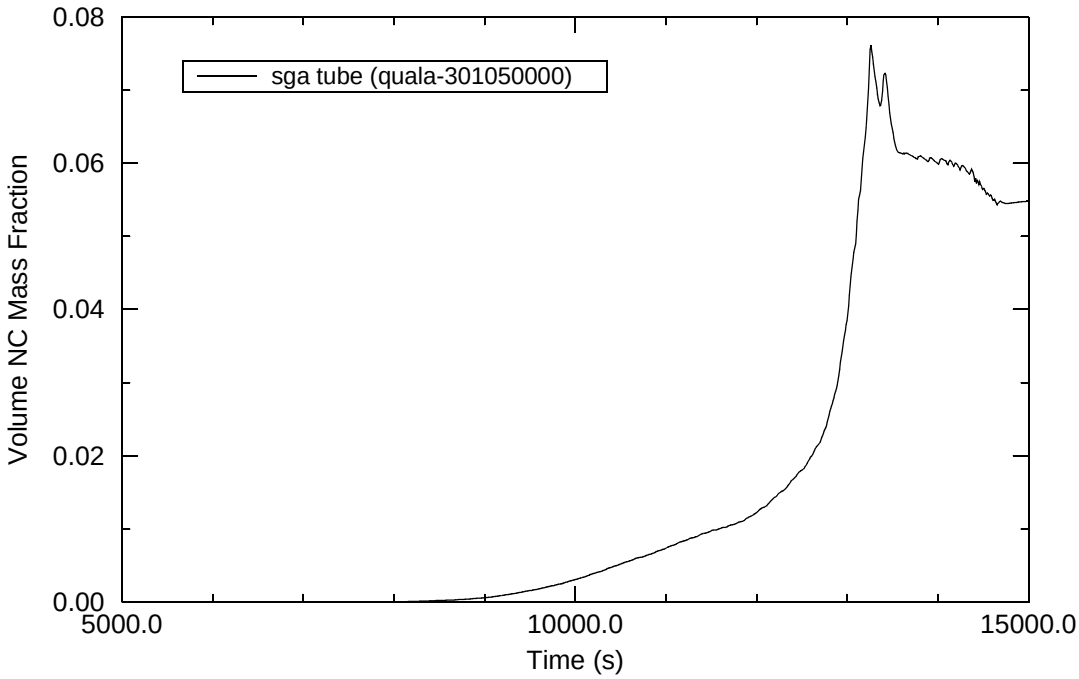

Figure 8. Non-condensable quality in the top of SGA U-tubes in Case 01.

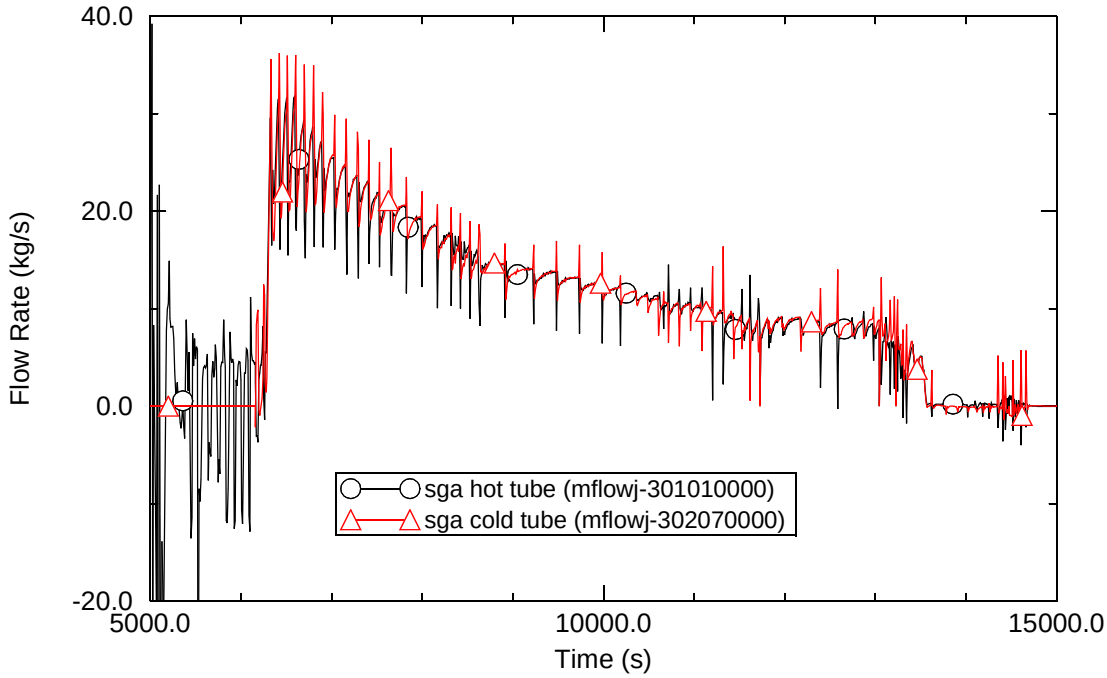

Figure 9. Mass flow rates in hot and cold SGA tubes in Case 01.

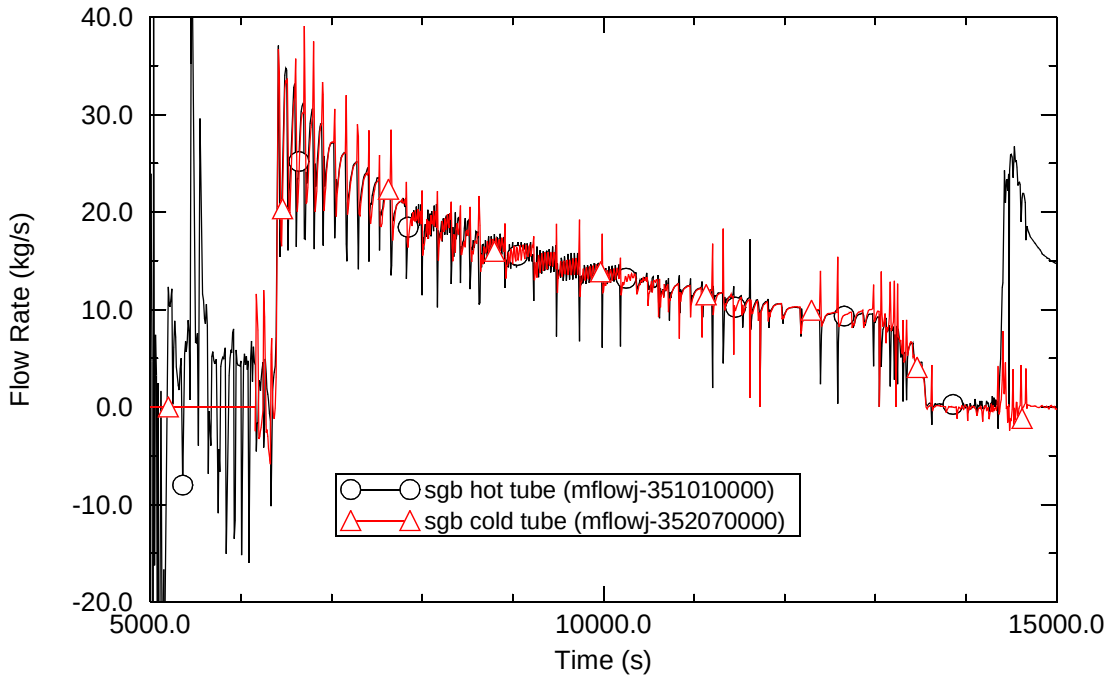

Figure 10. Mass flow rates in hot and cold SGB tubes in Case 01.

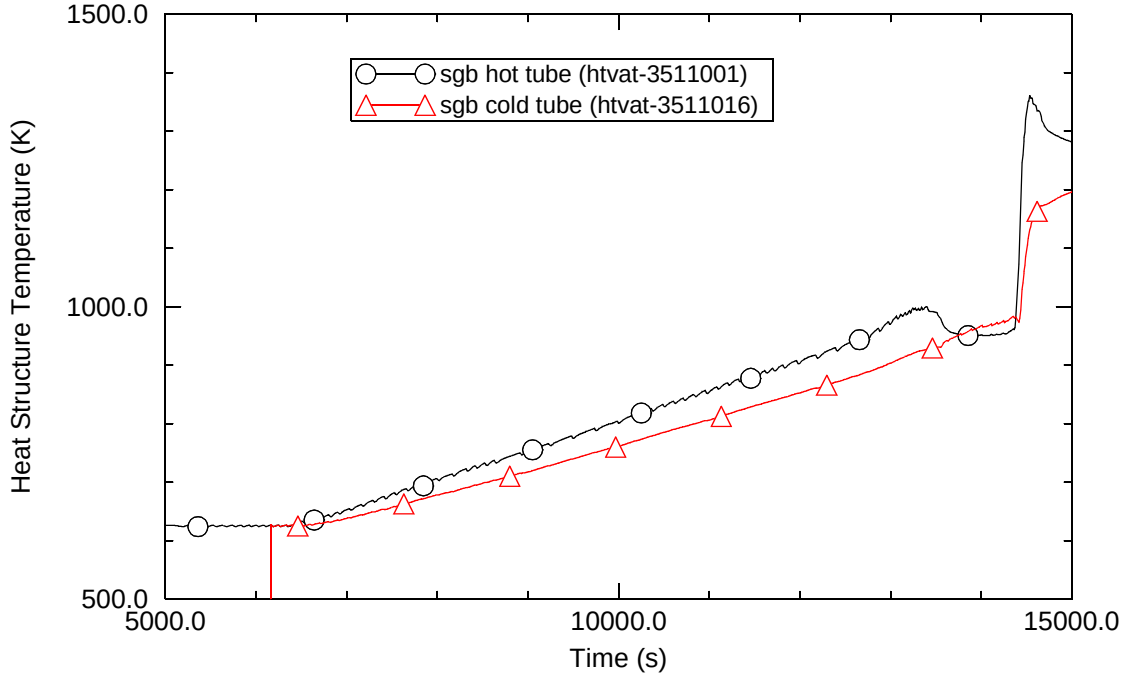

Figure 11. Volume-averaged temperatures of hot and cold SGB tubes in Case 01.

vapor in the SG secondary (because tube flows remained near zero and therefore did not significantly contribute to direct heating). Heat transfer associated with the onset of full loop natural circulation provided cooling sufficient to initiate some RCS pressure reduction as indicated in Figure 6. In addition, "hot" tube heating as a result of full loop natural circulation directly led to creep rupture failure of SGB tubes at 14,600 s, which happened to coincide with failure of SGA tubes. It is important to note that the predicted failure of SGB tubes would have been delayed if full loop natural circulation flows were appropriately balanced at the SG inlet plenum.

SCDAP/RELAP5 results in this case indicate that the surge line and both hot legs fail before SG tubes for the conditions analyzed. The margin between surge line and SG tube failure was 2,870 s, given that the tubes were assumed to be defect free. (Some consideration of tube defects is incorporated into Cases 03 through 08.) In addition, results from this calculation indicate that oxidation can lead to stagnation of natural circulation flows in the SG tubes. Without RCP loop seal clearing, this flow stagnation could be an important factor retarding tube heating and reducing the associated potential for tube failure. If loop seal clearing does occur, modeling of SG plena junctions must include provisions to allow an appropriate transition from hot leg countercurrent to full loop natural circulation in order to properly simulate subsequent tube heating.

4.2. Case 02

This calculation was designed for similarity to a calculation submitted to the NRC by the ANO2 licensee. It is also similar to Case 01, with the single exception that the station blackout was allowed to

progress at a reduced RCS pressure (see Table 1). The RCS pressure reduction was achieved by arbitrarily reducing pressurizer SRV open and close set points by 6.9 MPa when the valves were first challenged. This reduction was thought to be sufficient to evaluate impacts associated with transient progression at a reduced pressure without adding the complications that would accompany SIT injections (at even lower RCS pressures).

Case 02 results were identical to Case 01 results until the first pressurizer SRV challenge at 3,190 s. At that time, pressurizer open and close set points were reduced (by 6.9 MPa). The valves then remained open until the reduced closing pressure was reached at about 4,176 s. Periodic valve cycling between the reduced set points followed at 4,230 s.

Transient events between the first pressurizer SRV challenge and the time of surge line failure in Case 02 were earlier than the same events in Case 01. For example, full loop natural circulation of liquid ended at 4,888 s, core uncovery was complete by 7,179 s, and fuel rod oxidation began at 7,869 s in Case 01. Those events occurred earlier in Case 02 at 3,206 s, 6,853 s, and 6,400 s, respectively. The events were earlier in Case 02 as a result of the RCS inventory that was lost when pressurizer SRVs were opened to reduce the RCS pressure. Because core uncovery and the onset of oxidation occurred earlier, surge line failure in Case 02 was predicted 1,760 s before surge line failure in Case 01. However, Case 02 events were later than corresponding events in Case 01 after surge line failure. That occurred because early oxidation in Case 02 led to early stagnation of hot leg countercurrent natural circulation as shown in Figure 12. RCP loop seal clearing was not predicted. Therefore, early stagnation of natural circulation in Case 02 delayed hot leg failures (compared to Case 01) and precluded all SG tube failures (given that the tubes were assumed to be defect free).

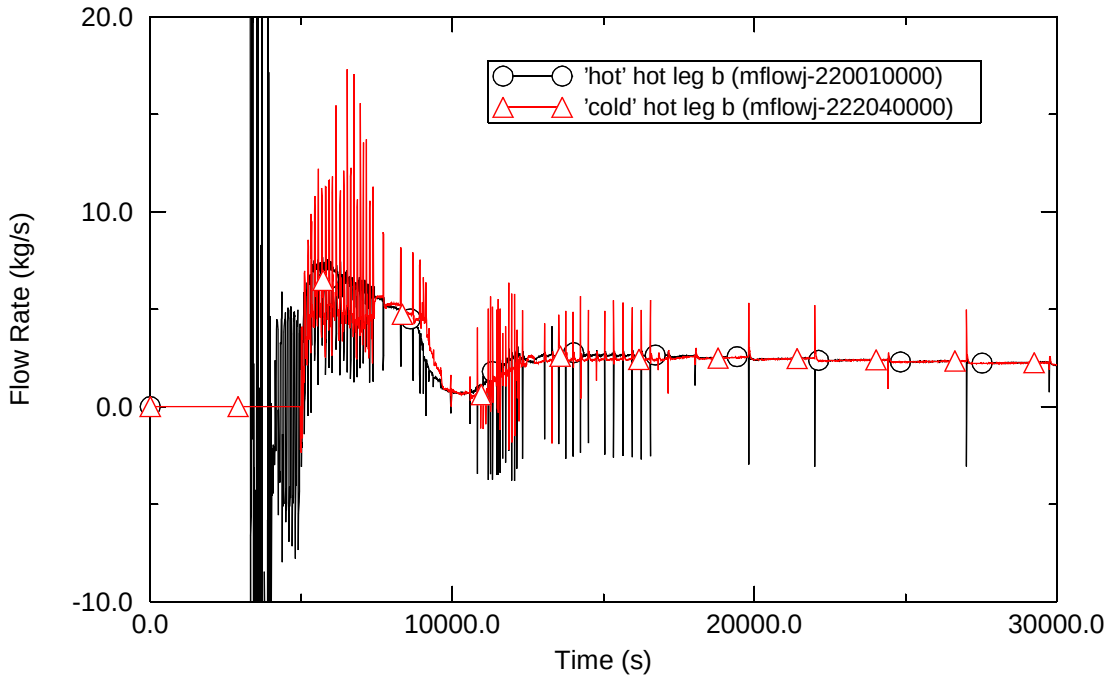

Figure 12. Hot leg B mass flows in Case 02.

4.3. Case 03

As indicated in Table 1, Cases 03 through 06 were designed to evaluate effects associated with various failure-to-fully-close scenarios involving pressurizer SRVs during station blackout accidents. All of these scenarios were loosely based on results from relief valve experiments conducted by the Electric Power Research Institute.[5] Those experiments seemed to indicate that relief valves could generally be expected to operate satisfactorily under a wide range of fluid conditions except for some failures to fully close (although the valves always closed to within 13% of their full open position). In Case 03, it was specifically assumed that one of two pressurizer SRVs would stop at 13% of its full open area during the first attempt to close following a non-zero calculation of surge line creep damage. (Note that this failure does not prevent valve movement in the range of 13 to 100% of full stroke.) The timing of this valve failure, while basically arbitrary, was an attempt to select one of the latest times to accomplish RCS depressurization before surge line creep failure. In addition, Case 03 included SGA depressurization simulated by assuming that SGA SRVs fail to close when first challenged and SGB steam valve leakage through a flow area of 9.3e-5 m^2 (to approximate a secondary depressurization rate of interest to the NRC).

The early RCS pressure response in this calculation was similar to the prediction for Case 01. Specifically, the RCS pressure initially decreased as shown in Figure 13 because the RCS was cooled by heat transfer to water remaining in the SGs at the time of SG isolation. Without a source of feedwater, however, heat transfer from the RCS diminished as SG inventories were boiled away and RCS pressures began to increase, ultimately reaching pressurizer SRV opening set points at 3,190 s. The RCS pressure remained between opening and closing set points of the pressurizer SRVs until 9,738 s, when it was assumed that one of two SRVs would fail to fully close.

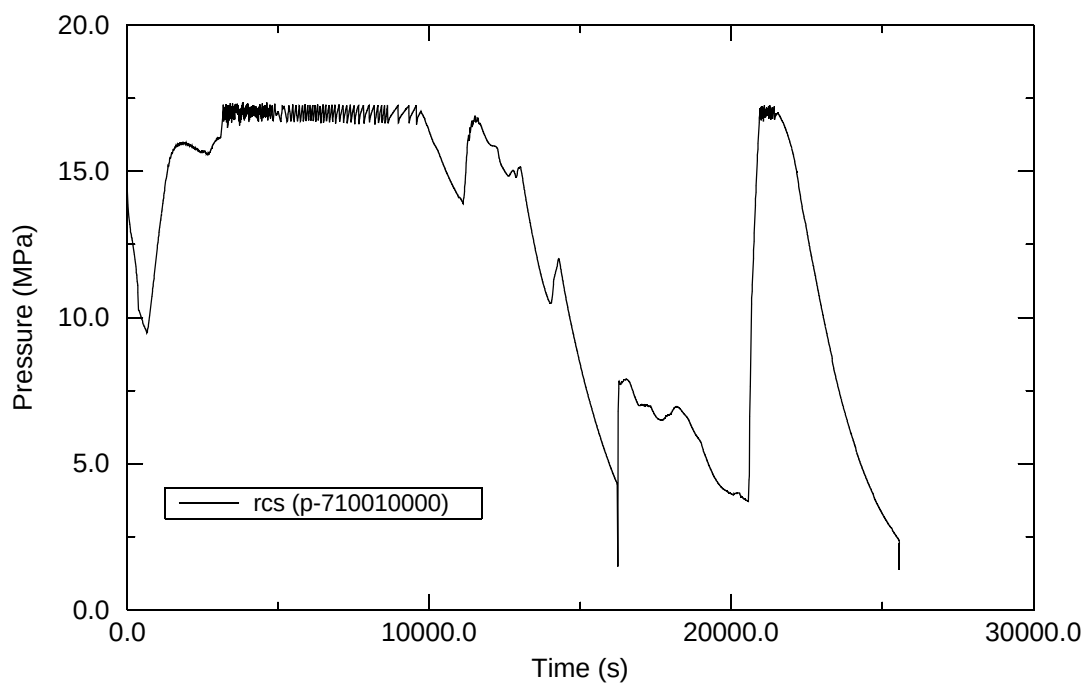

Figure 13. Case 03 RCS pressure.

With one of two pressurizer SRVs partially open, an immediate RCS pressure reduction began as shown in Figure 13. However, that pressure reduction was interrupted three times. The first interruption occurred at ~11,180 s, when the bottom of the reactor vessel downcomer skirt was uncovered and water in one of two RCP loop seals in loop B cleared. As a result, water from the lower head and loop seal was swept into the core, producing a pressure increase due to boiling as indicated in the figure. RCP loop seal clearing in loop A resulted in a similar interruption in the RCS pressure reduction at ~13,900 s. The third interruption occurred when SIT injection began at 16,220 s. Steam generated during SIT injection was being vented through the partially-open pressurizer SRV and a corresponding RCS pressure reduction was in progress when molten fuel relocated into the lower head (at 20,560 s). Boiling associated with the relocation produced a sharp pressure increase limited only by cyclic operation of both pressurizer SRVs. After venting a sufficient amount of steam, cyclic operation of the valves ended, leaving one of the two valves partially open. The RCS pressure was then reduced to the SIT pressure (through the partially-open SRV) as the calculation ended at 25,570 s.

Hot leg countercurrent natural circulation transformed to full loop natural circulation when RCP loop seals cleared. Tube flows shown in Figure 14 illustrate that natural circulation transition for SGB. A period of oxidation-induced flow stagnation in the tubes (from ~16,900 to ~21,870 s) followed by a second period of full loop natural circulation is also shown in the figure. The effects of the various flow regimes can be seen in temperature histories provided in Figure 15 for the inlet of the "hot" and "cold" portions of the tube bundle. Specifically, SG tube temperatures climbed steadily from 6,138 to 11,180 s as a result of hot leg countercurrent natural circulation. Consistent with the characteristic countercurrent flow pattern, "hot"

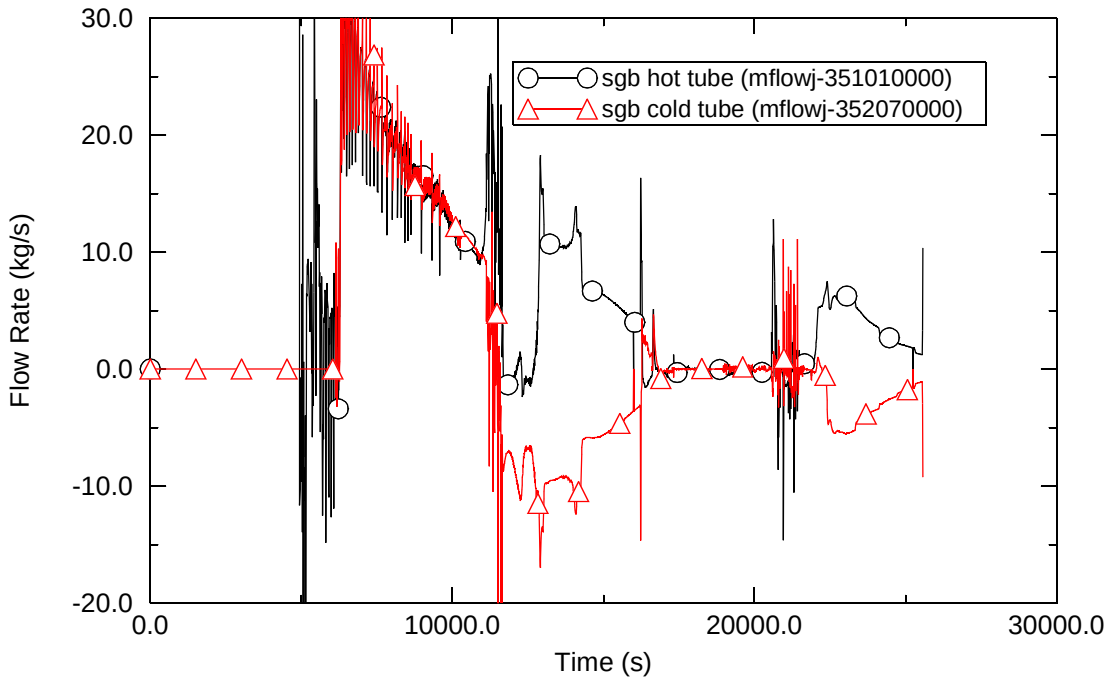

Figure 14. SGB tube mass flows in Case 03.

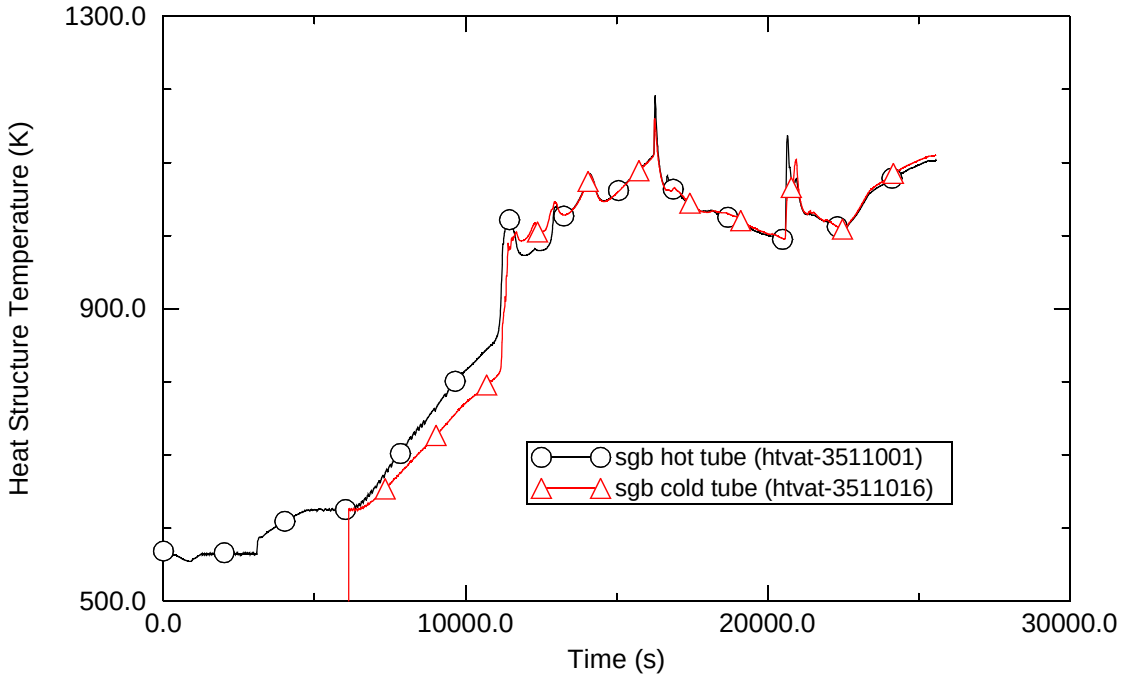

Figure 15. SGB tube temperatures in Case 03.

tube temperatures climbed faster than "cold" tube temperatures during this period. Tube temperatures increased sharply when hot steam was pushed out of the core and into the RCS piping by the pressurization associated with RCP loop seal clearing. "Hot" and "cold" tube temperatures then continued to climb, essentially in equilibrium, as a result of full loop natural circulation. (In contrast to Case 01, tube temperatures appropriately approached equilibrium during full loop natural circulation in this case because of modeling improvements provided through the use of servo valves at all SG plena junctions.) Gradual tube cooling during the subsequent period of flow stagnation was finally followed by heating associated with full loop circulation that was in progress at the end of the analysis.

As indicated in Figure 15, SGB tube temperatures generally remained between 1,000 and 1,100 K during the calculation (while SBA tube temperatures climbed somewhat higher). Heating to those temperatures was sufficient to lead to creep failures in degraded (flawed) SG tubes beginning as early as 10,750 s. However, pristine (unflawed) SG tubes were not predicted to fail before the end of the calculation at 25,570 s. Furthermore, the surge line and hot legs A and B were predicted to fail at 11,120 s, 19,430 s, and 20,660 s, respectively. After simple analysis, results in this case indicate that the surge line will fail before all SGA tubes where degradation is represented by stress multiplication of 3.5 or less and before all SGB tubes where degradation is represented by stress multiplication of 4.0 or less. (See Table 5.) In addition, results from this calculation indicate that using servo valves to model SG plena junctions allows an appropriate transition from hot leg countercurrent to full loop natural circulation and appropriately simulates subsequent tube heating if loop seal clearing occurs.

4.4. Case 04

This calculation was designed for similarity to Case 03 except SGB steam valve leakage was not included and the timing associated with the pressurizer SRV failure-to-close assumption was altered (see Table 1). The decision to drop steam valve leakage was based on a comparison of results from Cases 01 and 02 with results from Case 03, which indicated that SGB dryout was unaffected by the steam valve leakage assumed in Case 03. Because that comparison implied that the SGB heat sink was not impacted, there was no apparent justification for imposing similar steam valve leakage in this calculation. The alteration of timing associated with the pressurizer SRV failure was based on a review of Case 03 results, which indicated that surge line failure will occur before SG tube failure (except for those tubes with relatively high levels of degradation). From those results, it was reasoned that SG tube failures may occur even earlier (with respect to surge line failure) if RCS depressurization began earlier (before significant surge line heating). Accordingly, it was assumed that one of two pressurizer SRVs would stop at 13% of its full open area during the first attempt to close after the surge line temperature first exceeds SGA tube temperatures during hot leg countercurrent natural circulation heating. (Note that this failure does not prevent valve movement in the range of 13 to 100% of full stroke.)

The surge line temperature first exceeded the temperature of the hottest tube in SGA at ~9,346 s in this case. As a result, one of two pressurizer SRVs did not fail to fully close until 9,352 s, which was only 386 s earlier than the pressurizer SRV failure-to-close event in Case 03. Because the timing of pressurizer SRV failures in Cases 03 and 04 was similar, the results were generally similar as indicated in Tables 4 and 5. However, Case 04 results did indicate that the surge line will fail before all SGA tubes where degradation is represented by stress multiplication of 2.5 or less, which contrasts with a Case 03 surge line failure before SGA tubes with stress multiplication of 3.5 or less. Therefore, this result confirms that SG tube failures can occur earlier (with respect to surge line failure) when RCS depressurization begins earlier. It is worth noting that SGB tube failures were not predicted in this case primarily because SGB was not depressurized (through steam valve leakage or by any other means). Consequently, SGB tubes were subjected to compressive or buckling loads (instead of tensile or bursting loads) during significant portions of the transient. SCDAP/RELAP5 does not currently contain models for calculating failures associated with compressive loading, although it is believed that temperatures substantially higher than those leading to (tensile) creep failure would normally be required.

In addition to differences associated with SGB tube failures, results provided in Table 4 indicate that the timing for SIT reflooding of the bottom of the core was the only other substantial difference between Cases 03 and 04. Specifically, the bottom of the core was not reflooded by SIT injection in Case 04 until 18,120 s, a delay of 1,880 s relative to Case 03. This result was predicted despite the fact that initial SIT injections occurred at essentially the same time in the two cases. Reflooding the core in Case 04 was delayed primarily because SIT injection water was split between empty RCP loop seals and the reactor vessel. In other words, some of the injected water refilled RCP loop seals while the remainder was added to vessel inventory. Injection water was not split in Case 03. Instead, all injection water was added directly to the reactor vessel. The distribution of injection water was apparently affected by differences in hydrogen concentrations in the two cases.

At the time of the initial SIT injection in Case 04, steam/hydrogen mixtures in the SG tubes were relatively rich in hydrogen. A much lower hydrogen concentration existed in the SGs in Case 03 as indicated in Figure 16. Those differences occurred because of differences in the timing associated with the initial SIT injections. Specifically, approximately 220 kg of hydrogen had been generated by the time of the ini-

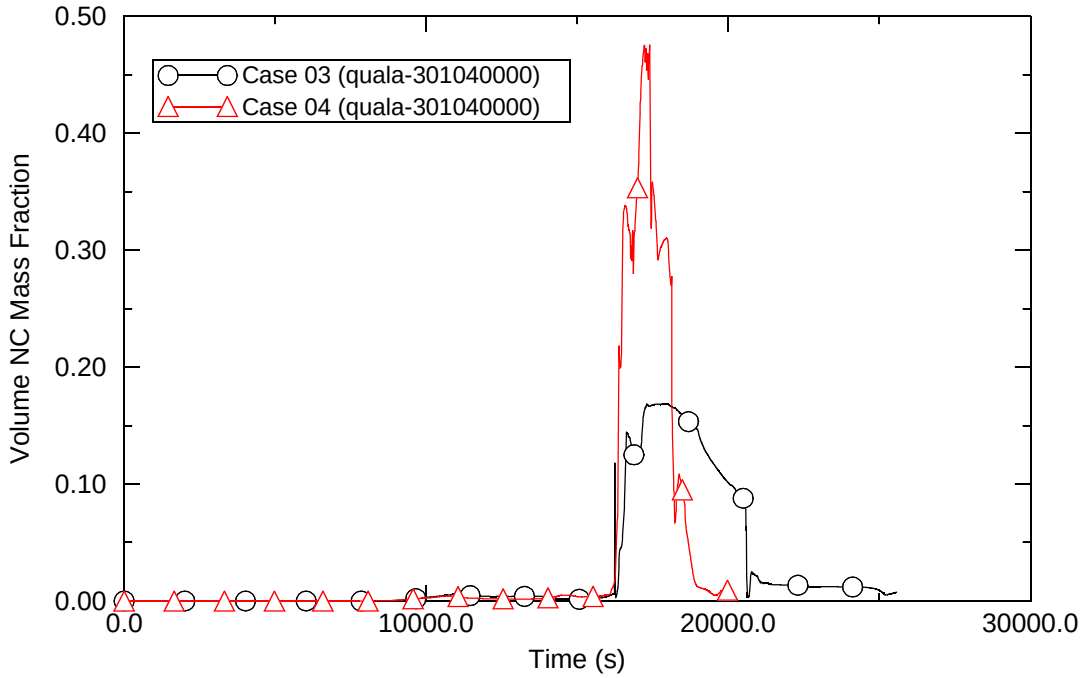

Figure 16. Non-condensable quality in SGA tubes in Cases 03 and 04.

tial SIT injection in Case 04 while only 120 kg of hydrogen had been generated by the time of the initial SIT injection in Case 03 (see Figure 17). As a result, vapor in the SGs in Case 04 was rich in hydrogen relative to Case 03. At the time of the initial SIT injection, relatively light SG vapors in Case 04 were readily displaced, allowing free flow of injected water toward the empty RCP loop seals. In Case 03, however, heavier vapors in the SGs promoted flow of injected water toward the reactor vessel. This result indicates that relatively small changes in the sequence of events (i.e., a 386 s shift in the timing of the pressurizer SRV failure-to-close event) can affect transient results.

4.5. Case 05

This calculation was designed for similarity to Case 04 except the timing associated with the pressurizer SRV failure was altered (see Table 1). In this case, it was assumed that one of two pressurizer SRVs would stop at 13% of its full open area during the first attempt to close after water discharge through the SRVs was complete. (Note that this failure does not prevent valve movement in the range of 13 to 100% of full stroke.) The reasoning here was that discharging water may contribute to galling that may prevent complete valve closure.

Water was discharged through the pressurizer SRVs between ~3,670 and ~5,850 s as indicated in Figure 18. Consistent with the identified assumption, one of two pressurizer SRVs stopped at 13% of the full open area at 5,920 s (during the first attempt to close after 5,850 s). It is worth noting that galling associated with water discharge could have led to SRV failure ~2,180 s earlier, although the impact of an earlier failure was not evaluated. In addition, one partially-open SRV did not provide adequate RCS pressure control so pressurizer SRV cycling continued (from 5,920 s) until 7,504 s.

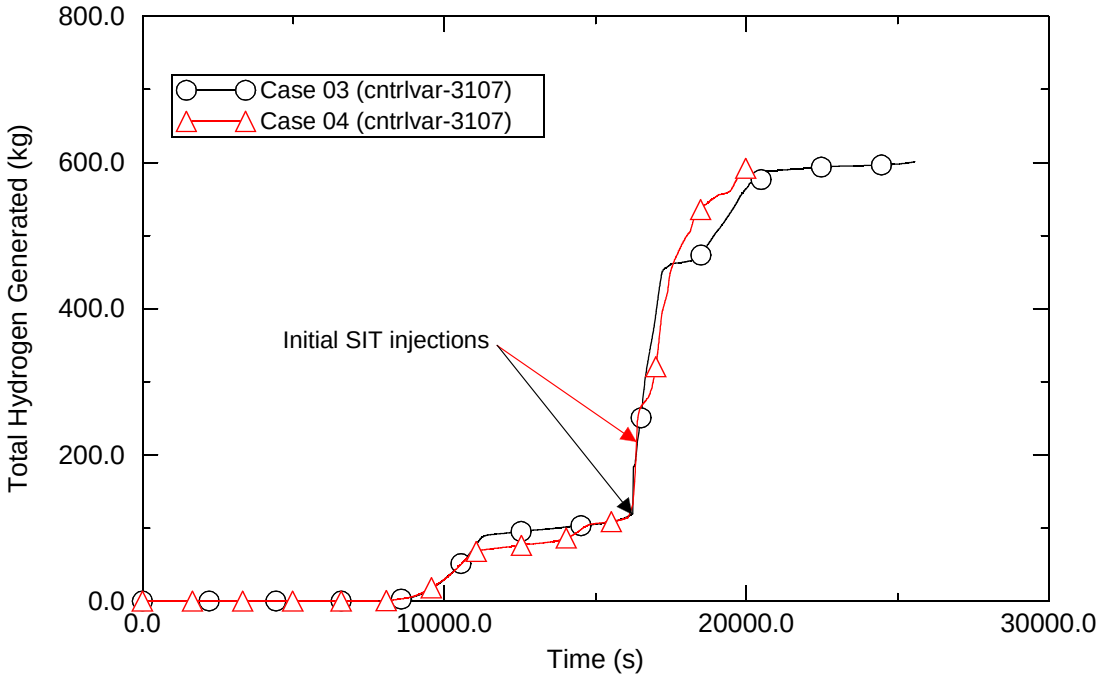

Figure 17. Total hydrogen generated in Cases 03 and 04.

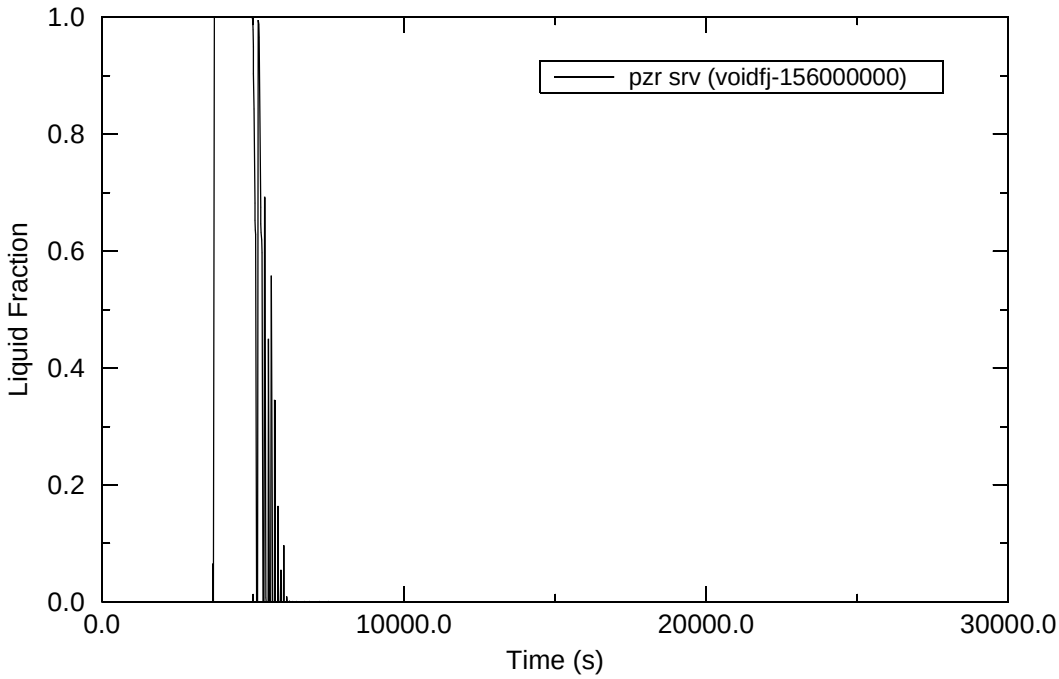

Figure 18. Pressurizer SRV liquid fraction in Case 05.

As indicated in Table 4, transient progression in Case 05 was quite similar to transient progression in Case 04 despite the fact that the pressurizer SRV failure-to-close event was 3,432 s earlier in Case 05. (This provides some indication that evaluation of an even earlier galling failure in Case 05 may not have produced significantly different results.) RCP loop seals did not refill during SIT injection in this case (for reasons discussed in Section 4.4), so the delay in reflooding the bottom of the core as predicted in Case 04 did not occur. Otherwise, the timing of SG tube failures was the only notable difference between Cases 04 and 05.

Differences in the timing of SG tube failures were simply related to the order of RCP loop seal clearing. Specifically, RCP loop seals in loop B cleared before RCP loop seals in loop A in Case 05 and RCP loop seals in loop A cleared before RCP loop seals in loop B in Case 04. Because some increase in SG tube temperature occurs following loop seal clearing, SGA tubes in Case 04 tended to be hotter than SGA tubes in Case 05 and SGB tubes in Case 05 tended to be hotter than SGB tubes in Case 04 as indicated in Figures 19 and 20. Consequently, SGA tubes in Case 04 tended to fail earlier than SGA tubes in Case 05 and SGB tubes in Case 05 tended to fail earlier than SGB tubes in Case 04. Those trends are reflected in results provided in Table 4. (Note that an RCS repressurization associated with molten core relocation was an important contributor to SGB tube failures in Case 05. Case 04 was terminated before effects on SGB tubes from a similar relocation were recorded.) In any event, results from this case indicate that the surge line will fail before all SG tubes where degradation is represented by stress multiplication of 4.0 or less (see Table 5).

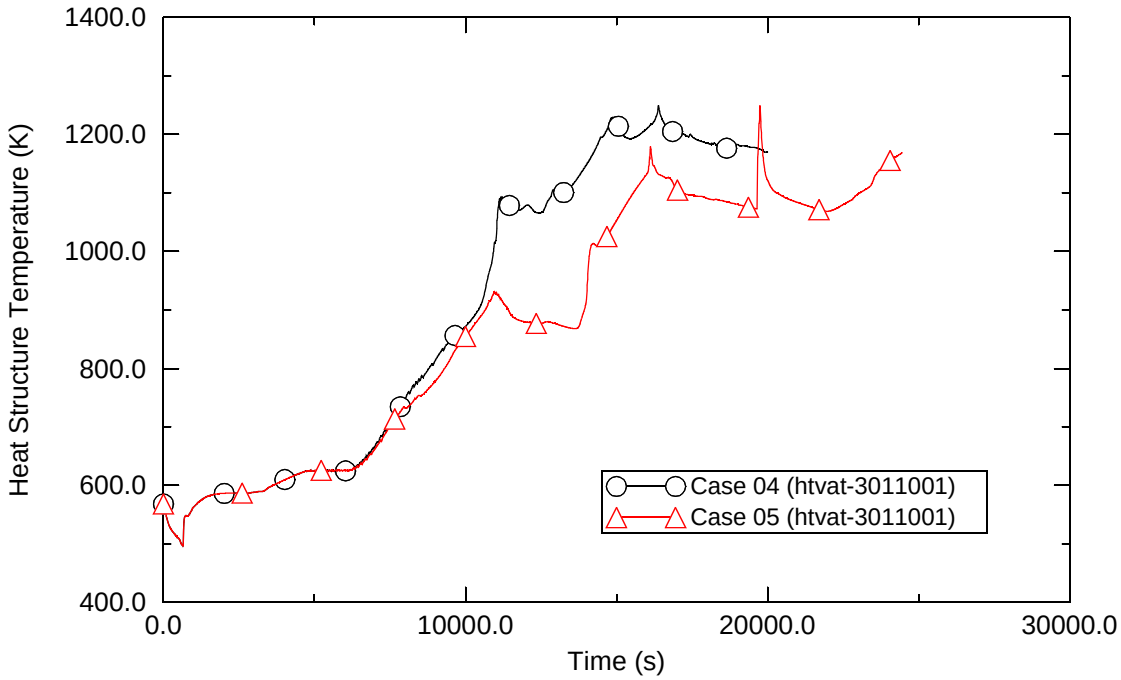

Figure 19. SGA hot tube temperatures in Cases 04 and 05.

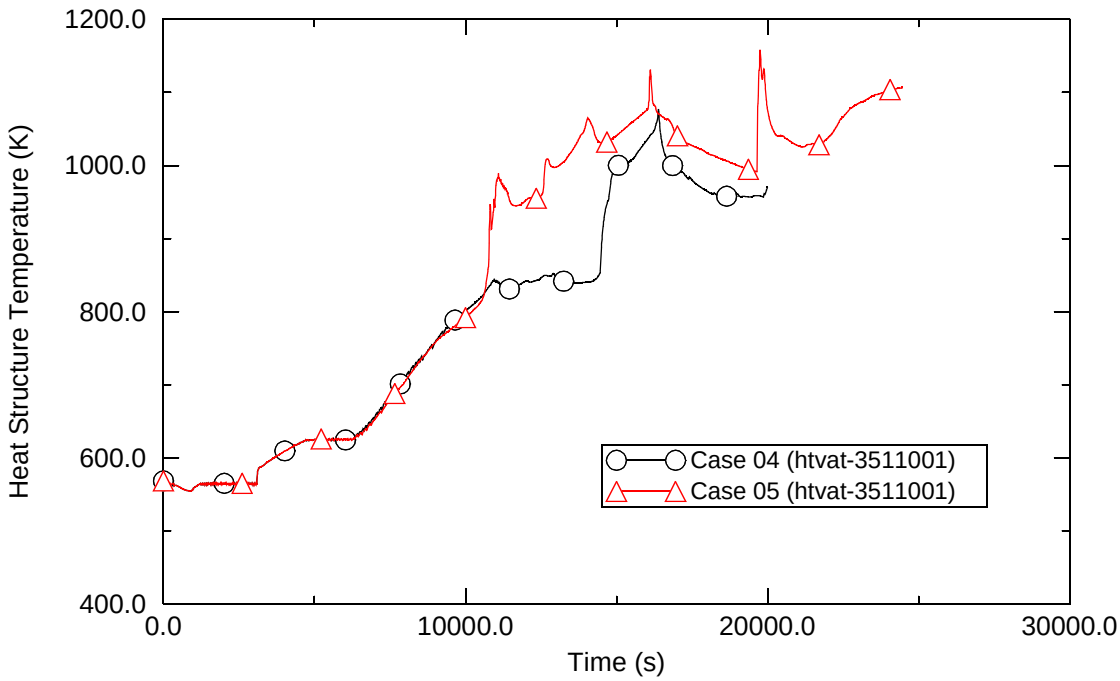

Figure 20. SGB hot tube temperatures in Cases 04 and 05.

4.6. Case 06

This case was the last in a series of calculations (comprised of Cases 03 through 06) designed to evaluate effects associated with various failure-to-fully-close scenarios involving pressurizer SRVs during station blackout accidents. In this case, it was assumed that *both* pressurizer SRVs would stop at 13% of their full open area during the first attempt to close after water discharge through the valves was complete. (Note that these failures do not prevent valve movements in the range of 13 to 100% of full stroke.) In addition, depressurization of *both* SGs was simulated by assuming that SG SRVs fail to close when first challenged.

Like all other station blackout scenarios considered, this case began with a complete loss of AC power while the reactor was operating at normal steady state conditions. Accordingly, the reactor scrammed, RCPs and feedwater pumps tripped, and turbine stop valves closed (thereby isolating the SGs) at time 0 due to the loss of power. The RCS pressure initially decreased because the RCS was cooled by heat transfer to water remaining in the SGs at the time of SG isolation. The initial RCS pressure decrease in this case was substantial, and well below that achieved in Case 05 as shown in Figure 21, because secondary saturation temperatures were significantly reduced through depressurization of both SGs. Without a source of feedwater, however, heat transfer from the RCS diminished as SG inventories were boiled away and RCS pressures began to increase, ultimately reaching pressurizer SRV opening set points at 3,120 s. The RCS pressure remained between opening and closing set points of the pressurizer SRVs until 5,878 s, when it was assumed that both pressurizer SRVs would fail to fully close. However, results indicated that partially-opening both SRVs did not provide adequate RCS pressure control so pressurizer SRV cycling continued (from 5,878 s) until 6,508 s.

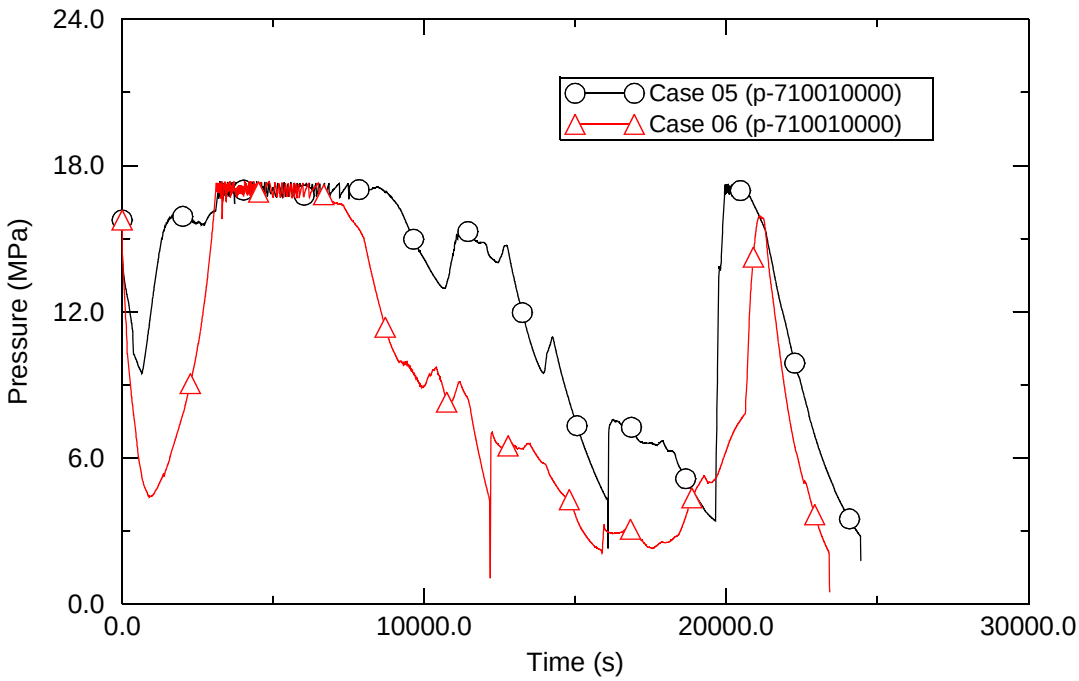

Figure 21. RCS pressures in Cases 05 and 06.

The RCS pressure dropped rapidly after 6,508 s as a result of steam flow through the partially-open pressurizer SRVs. RCP loop seal clearing in loops B and A resulted in pressure fluctuations at ~10,400 s and ~11,180 s, respectively. Otherwise, the RCS pressure decreased steadily until 12,160 s when the first SIT injection occurred. Steam generated during the first SIT injection was ultimately vented through the partially-open pressurizer SRVs, allowing a second SIT injection at 15,870 s. Several relocations of molten control rod absorber materials and core stainless steel into water in the lower head resulted in a gradual RCS pressure increase beginning at 18,440 s. The gradual pressure increase was interrupted at 20,630 s by a large relocation of molten fuel into the lower head. Boiling associated with that relocation produced a sharp pressure increase as shown in Figure 21. Partially-open pressurizer SRVs limited the pressure increase to ~16 MPa and thereafter reduced the RCS pressure to the SIT pressure as the calculation ended at 23,400 s.

As indicated in Figure 21, the partial opening of both pressurizer SRVs resulted in a substantially lower RCS pressure in this case as compared to the RCS pressure in Case 05 (where only one of two pressurizer SRVs was partially open). The relatively low RCS pressure in this case had important effects with respect to surge line integrity. Specifically, creep damage in any component is a function of the time the component is held at elevated pressures and temperatures. However, the surge line was subjected to relatively low pressures in this case. In addition, flow through the surge line toward partially-open pressurizer SRVs is pressure dependent. Because the pressure in this case was relatively low, surge line flows, and the associated heating of the surge line, were relatively low. Consequently, creep failure of the surge line was not predicted before the end of the calculation.

Early failures of degraded (flawed) tubes in SGB were predicted however (see Table 5). The early tube failures (at 10,200 s for degradation corresponding with stress multiplication of 4.0 and at 10,920 s for degradation corresponding with stress multiplication of 3.5) occurred as a result of heating associated with RCP loop seal clearing (after 9,400 s) as indicated in Figure 22. All other creep failure predictions were clustered around the RCS pressurization event associated with the relocation of molten fuel into the lower head. Those results indicate that hot leg failures (in both loops) will occur before the failure of pristine (unflawed) SG tubes. Furthermore, hot leg failures (in both loops) will occur before the failure of SGA tubes with degradation corresponding with stress multiplication of 3.5 or lower and before the failure of SGB tubes with degradation corresponding with stress multiplication of 2.5 or lower.

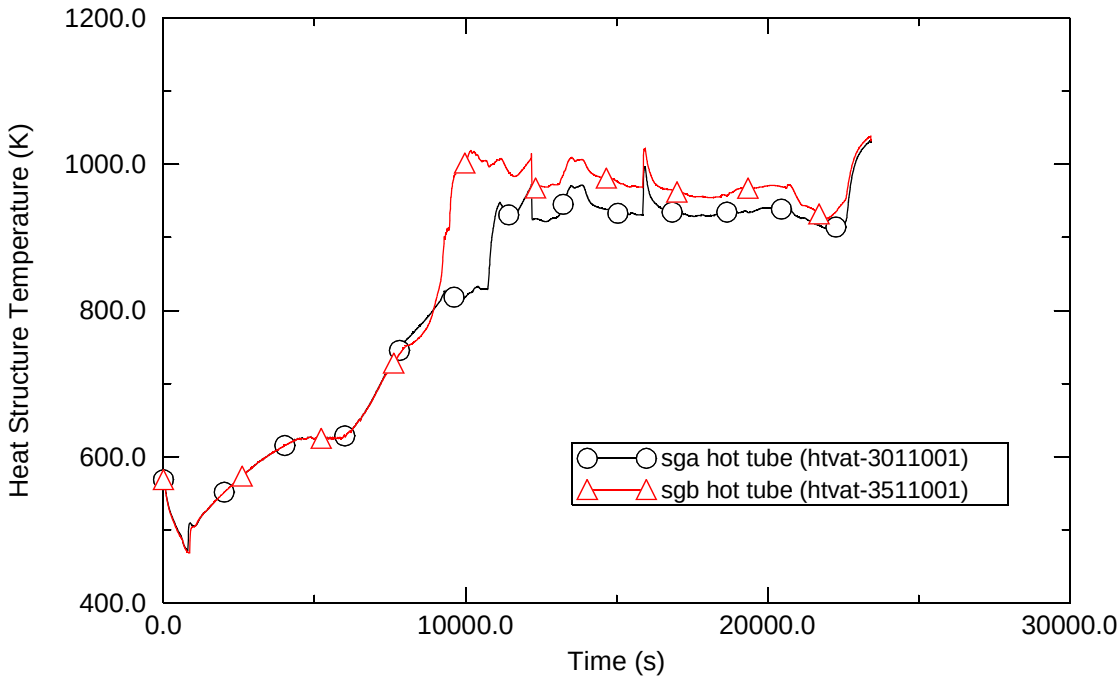

Figure 22. SG hot tube temperatures in Case 06.

4.7. Case 07

As indicated in Table 1, Cases 07 and 08 were designed to evaluate the effects of operator actions during station blackout accidents. Fourteen (14) levels of SG tube degradation (from none to almost enough to cause spontaneous rupture at normal operating conditions) were used in both cases for the calculation of tube creep damage. Furthermore, both cases included early depressurization of both SG secondaries through failed SRVs and SG heat transfer area reductions consistent with the current estimate of tube plugging at ~17.7%. In this particular case, it was assumed that operators would open ECCS vent valves 1,380 s (23 minutes) after core exit temperatures reach 700 K (800°F). This delay is consistent with the licensee's *initial* evaluation of human error probabilities and the time required before the probability of this action not being taken falls below 0.25.

This case began with a complete loss of AC power while the reactor was operating at normal steady state conditions. Accordingly, the reactor scrammed, RCPs and feedwater pumps tripped, and turbine stop valves closed (thereby isolating the SGs) at time 0 due to the loss of power. The RCS pressure initially decreased as indicated in Figure 23 as a result of cooling associated with the transfer of decay heat from the RCS to water remaining in SG secondaries at the time of isolation. Without a source of feedwater, however, heat transfer from the RCS diminished as SG inventories were boiled away. Therefore, the RCS pressure began to increase after the dryout of SGA at 866 s and SGB at 925 s; ultimately reaching pressurizer SRV opening set points at 3,150 s. Loss of RCS inventory through subsequent cycling of the pressurizer SRVs led to an RCS heatup, including detection of a temperature of 700 K (800°F) at the exit of the center core channel at 6,202 s. Consistent with the specified operator actions, pressurizer SRVs were subsequently opened at 7,582 s to simulate operator opening of ECCS vent valves. It is worth noting that the operator response was not actually taken until 874 s after core uncovery was complete, even though a core exit temperature of 700 K (800°F) was detected only 679 s after initial voiding developed in the top of the core. Consequently, the core exit temperature increased from 700 to 991 K by the time operator action was completed as indicated in Figures 24 and 25.

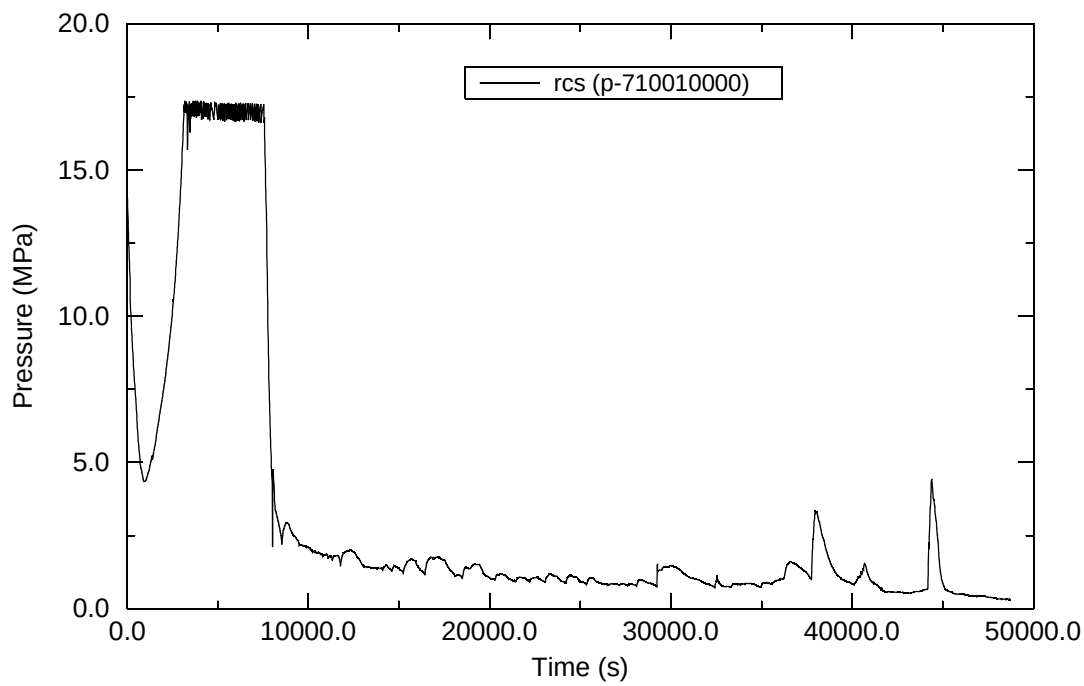

Figure 23. RCS pressure in Case 07.

The RCS was depressurized (through open pressurizer SRVs) to the initial SIT pressure (of ~4.31 MPa) by 7,999 s. At that time, the SITs began discharging cool water (322 K) into the RCS, causing pressure fluctuations by condensing steam at interfaces with the cool water and then creating more steam as the water contacted hot core surfaces. When steam was created, the RCS pressure increased and SIT injections stopped until enough of the steam was released (through the simulated ECCS vent path) to allow the RCS pressure to drop below the remaining pressure in the SITs. The SITs then injected more water, repeating the cycle at a reduced pressure. This process continued until the SITs were emptied at 41,620 s.

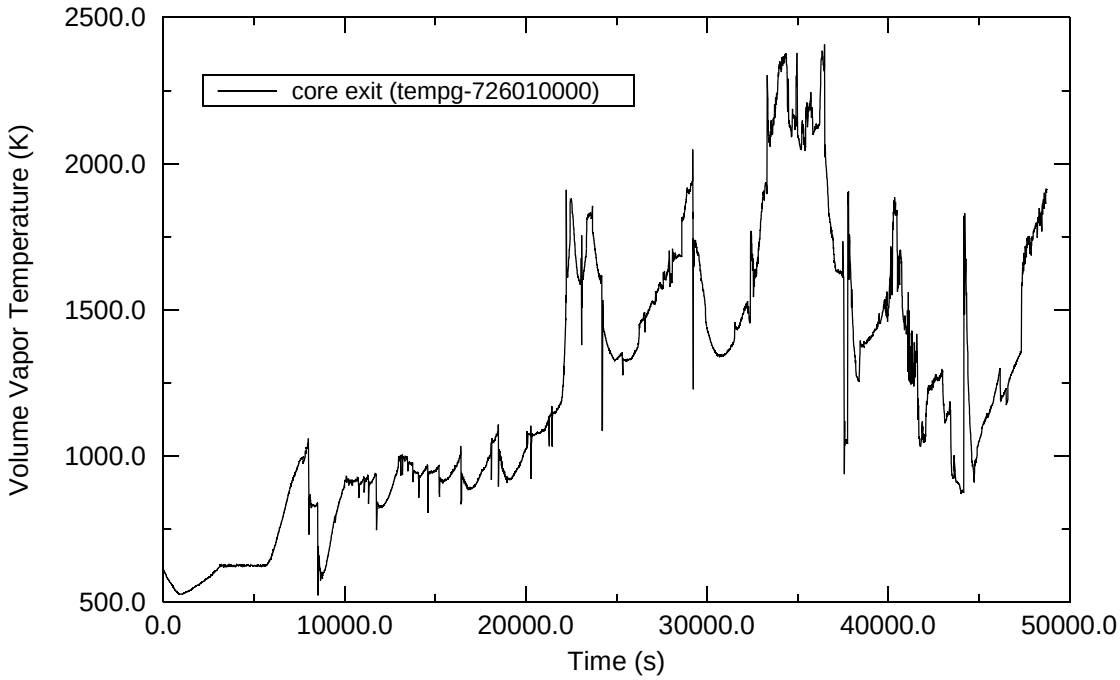

Figure 24. Core exit temperature in Case 07.

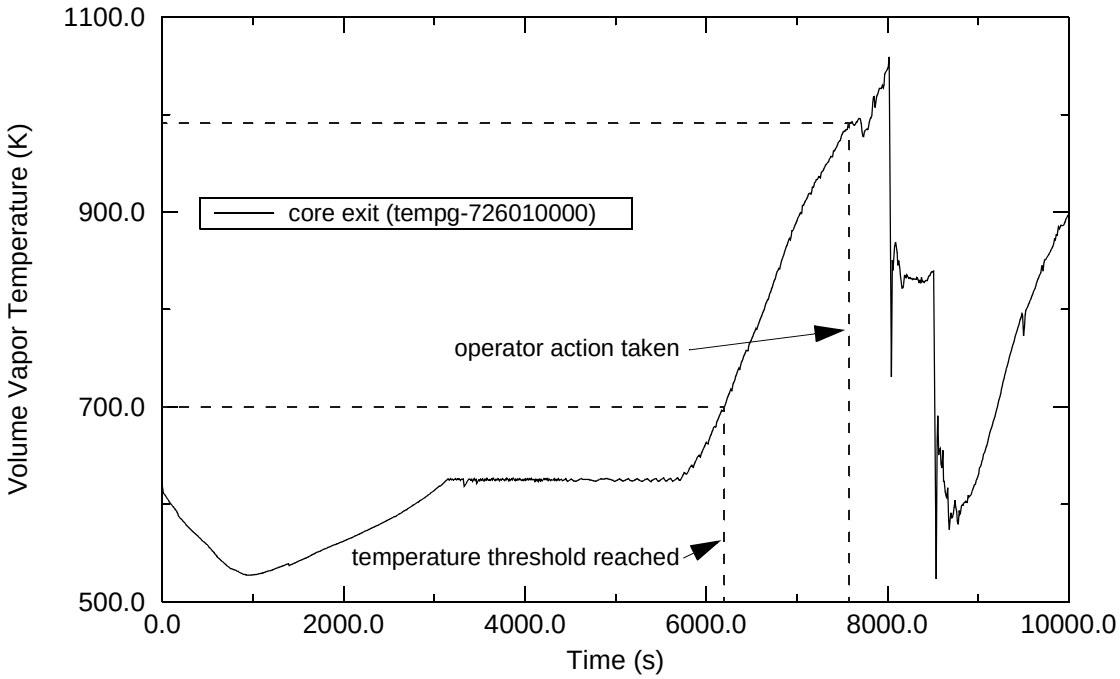

Figure 25. Core exit temperature near the time of operator action in Case 07.

Flow of hot steam from the core toward the open pressurizer SRVs was the primary mechanism for heating the surge line and hot leg A. That heating led to surge line and hot leg A creep failure predictions at 34,400 s and 40,040 s, respectively. Breaks were not initiated in the SCDAP/RELAP5 model to simulate these failures. Instead, the calculation was allowed to proceed to determine the earliest possible timing of SG tube failures. However, SG tubes were not predicted to fail at any stress multiplication level before the end of the calculation at 48,750 s.

SG tube failures did not occur primarily because natural circulation and any corresponding tube heatup was minimized by flow toward the open pressurizer SRVs. In loop A, flow moved from the reactor vessel through the hot leg and surge line toward the pressurizer while SG tube flow essentially stagnated. In loop B, a hot leg countercurrent natural circulation pattern was established, but it was significantly weakened (and tube heating was reduced accordingly) by the general tendency for all flow to move toward the open valves. Some SG tube temperature spiking was predicted in both loops similar to that shown in Figure 26. Although the spiking was not high enough to result in SG tube creep failure, a limited discussion regarding the nature of the more significant spikes (at ~8,000, ~29,100, ~37,800, and ~44,200 s) may be helpful.

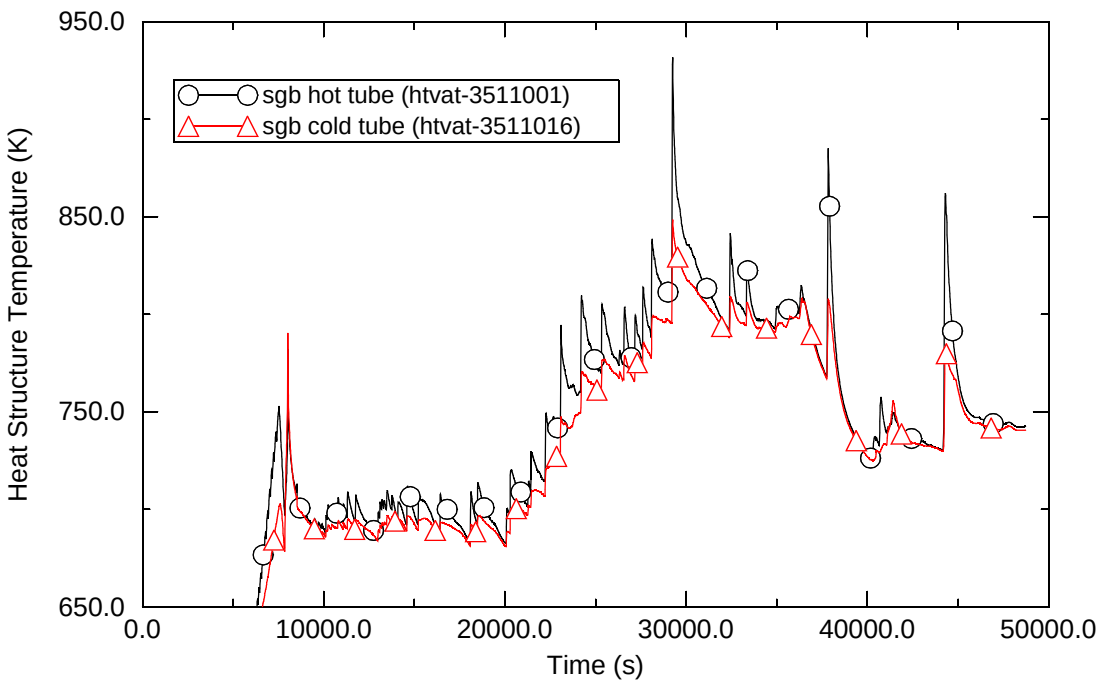

Figure 26. SGB tube temperatures in Case 07.

All temperature spikes occurred as a result of in-vessel boiling. Boiling actually results in a pressure increase, which can force hot steam from the reactor vessel into the RCS piping and thereby increase all piping temperatures. SG tube temperatures can be readily affected because the tubes are relatively thin. The first SIT injection and clearing of one of two RCP loop seals in both loops were sources for vessel water addition at ~8,000 s, which led to in-vessel boiling. The first SIT injection actually caused loop seal clearing through the combined effects of a relatively low pressure in the cold legs and a relatively high

pressure in the vessel/hot legs. Cold leg pressures decreased because steam in the cold legs was condensed by the injection of SIT water. Vessel/hot leg pressures then increased because injected water was boiled in the core. The resulting pressure differential across the loop seals led to loop seal clearing, although full loop natural circulation was not established at that time because the reactor vessel liquid level was above the bottom of the downcomer skirt.

A relatively large SIT injection was the source for water addition and in-vessel boiling that produced the SG tube temperature spike at ~29,100 s. However, SIT injections were not factors in temperature spikes at ~37,800 and ~44,200 s. At those times, pressures (and SG tube temperatures) increased primarily because water in the reactor vessel lower head was boiled following the relocation of molten fuel. The first relocation of molten fuel from the core into the lower head at ~37,800 s produced in-vessel boiling just sufficient to uncover the bottom of the downcomer skirt. At that time, resulting pressures were high enough to push a limited amount of water from liquid filled loop seals toward the vessel, thereby replenishing the liquid level (to a point above the bottom of the downcomer skirt) and blocking development of full loop natural circulation. A larger relocation of molten fuel at ~44,200 s resulted in complete boiling of all water that remained in the lower head and a corresponding increase in SG tube temperatures. Because all RCP loop seals were refilled by the final SIT injection (at 41,620 s), however, development of full loop natural circulation was also precluded following vessel dryout.

Before the end of the calculation (and after the prediction of surge line creep rupture), the surge line reached temperatures near 1,770 K. Given that stainless steel melts between solidus and liquidus temperatures of 1,675 and 1,727 K, the possibility of surge line survival is very unlikely. At the same time, SG tube integrity was not seriously challenged during the calculation because the tubes remained near 800 K with no pressure differential. Furthermore, if a break in the RCS was (more realistically) introduced at the time of the predicted surge line failure, one would expect quick depletion of remaining SIT inventory with minimal re-pressurization (because a break as large as the surge line should readily vent most of the generated steam). A gradual boil-off would then be required before significant heating of any RCS piping could resume. It is expected that the effects of any subsequent heating of the RCS piping would be focussed on the surge line and hot leg, consistent with the break flow path. Therefore, it seems clear that operator actions to open ECCS vent valves (as modeled in this case) will result in surge line failure well before any possibility of SG tube failure. In addition, any challenge to SG tube integrity appears to be minimal even if the expected surge line failure were modeled, indicating that the operator action considered in this case will be successful with respect to ensuring that tube failures will not occur before other RCS pressure boundary failures.

4.8. Case 08

Like Case 07, this calculation was designed to evaluate the effects of operator actions during station blackout accidents (see Table 1). In this particular case, it was assumed that operators would open ECCS vent valves 1,620 s (27 minutes) after core exit temperatures reach 700 K (800°F). This delay is 240 s (4 minutes) longer than assumed in Case 07, but consistent with the licensee's *latest* evaluation of human error probabilities and the time required before the probability of this action not being taken falls below 0.25. In addition, an approximation for the effects of the ECCS vent valve discharge piping was included. This was expected to improve prediction of RCS depressurization relative to Case 07 (where pressurizer SRVs were simply opened to simulate the ECCS vent valve flow path.)

Results in this calculation were identical to results in Case 07 up to 7,582 s. Both pressurizer SRVs were fully opened at that time in Case 07 to simulate operators opening ECCS vent valves. In this case, however, there was no simulation of operator action until 7,822 s. At that time, pressurizer SRVs were throttled (partially opened) to simulate operator activation of the vent flow path. It is worth noting that the core exit temperature increased from 700 to 1036 K by the time operator action was actually completed as indicated in Figures 27 and 28.

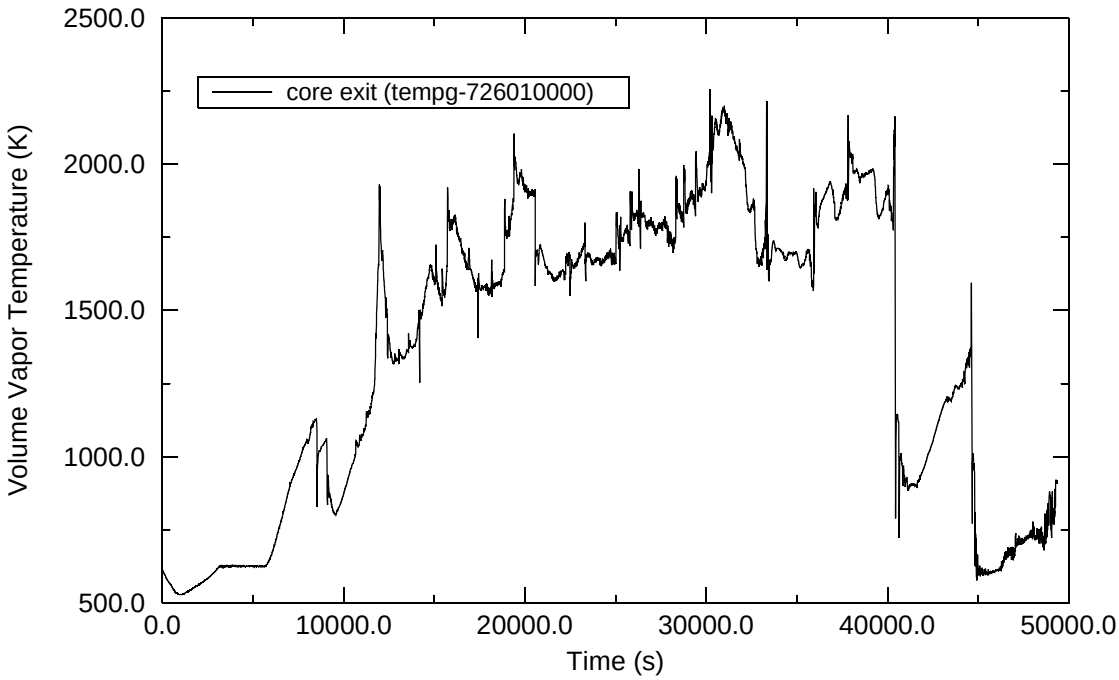

Figure 27. Core exit temperature in Case 08.

Throttling of the pressurizer SRVs was based on a separate SCDAP/RELAP5 model of the ECCS vent valves and all associated piping from the top of the pressurizer to the quench tank as described by the licensee.[6] Steam flows were calculated through the vent valves and the described piping for high (17.2 MPa), intermediate (5 MPa), and low (2.07 MPa) RCS pressures. Pressurizer SRV flow areas were then determined to achieve flow parity in the SCDAP/RELAP5 ANO2 model at all three pressures. Results from that process indicated that throttling both pressurizer SRVs to ~63% of their full open area was necessary to simulate ECCS vent valve flow. It is important to note that this process revealed that ECCS vent valve flows are friction dominated. In other words, flow capacity is not determined by the size of the vent valves. Instead, flow capacity is limited by friction through (what seemed to be) a long and torturous path to the quench tank. This could be quite important because discharge through the pressurizer SRVs is carried through some of the same piping. Although pressurizer SRVs discharge into some of the piping in the ECCS vent valve discharge path, INEEL did not investigate whether the piping between the SRVs and the quench tank had a similar impact on the effective capacity of the pressurizer SRVs. Furthermore, INEEL did not compare these results to the licensee's assessment of the ECCS vent path capabilities in its design basis analyses.

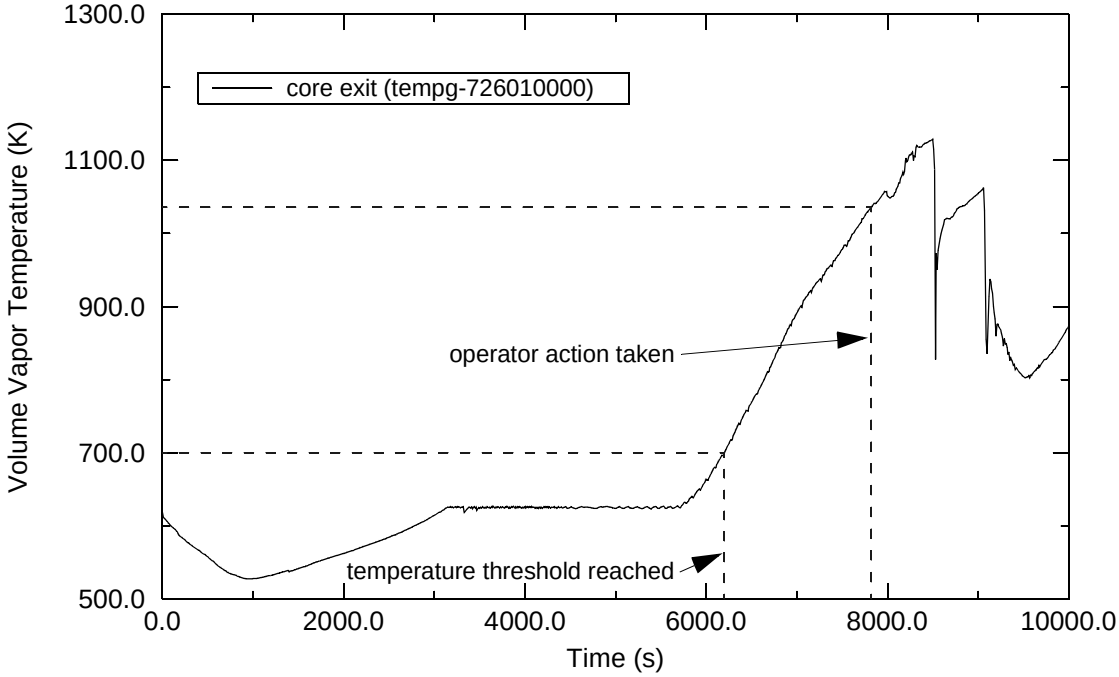

Figure 28. Core exit temperature near the time of operator action in Case 08.

The RCS was depressurized (through throttled pressurizer SRVs) to the initial SIT pressure (of ~4.31 MPa) by 8,494 s. At that time, the first injection of cool water (322 K) from the SITs into the RCS began. The injection was terminated when RCS pressures increased above SIT pressures as a result of in-core boiling of the SIT water and a subsequent injection at a reduced SIT pressure did not restart until sufficient RCS pressure reduction was achieved by venting generated steam through the throttled pressurizer SRVs. In this case, this process was repeated through the remainder of the analysis because the SITs were not emptied by the end of the calculation at 49,330 s.

Like Case 07, the flow of hot steam from the core toward the pressurizer SRVs was the primary mechanism for heating the surge line and hot leg A. That heating led to surge line and hot leg A creep failure predictions at 20,790 s and 31,100 s, respectively. However, those failure predictions are significantly earlier than the predictions in Case 07 (at 34,400 s and 40,040 s, respectively). Those failure timing differences can be traced to differences associated with simulating ECCS vent valve flows.

In Case 07, ECCS vent valve flows were simulated by fully opening both pressurizer SRVs without any consideration of the effects of the vent valve tail piping. In contrast, a detailed analysis of the ECCS vent valve flow path was completed as part of Case 08, indicating that both pressurizer SRVs should be throttled to only ~63% of their full open area in order to more accurately simulate ECCS vent valve flows. Consequently, flows from the core to the pressurizer SRVs were higher in Case 07 than in Case 08. As a result, two phase levels in the core were consistently higher in Case 07 than in Case 08 as indicated in Figure 29. Results provided in Figure 29, which are representative of core wide differences, actually show that significant amounts of water were present in the seventh axial elevation of the center core channel for an extended period of time in Case 07. The same conditions did not occur in Case 08 (as indicated)

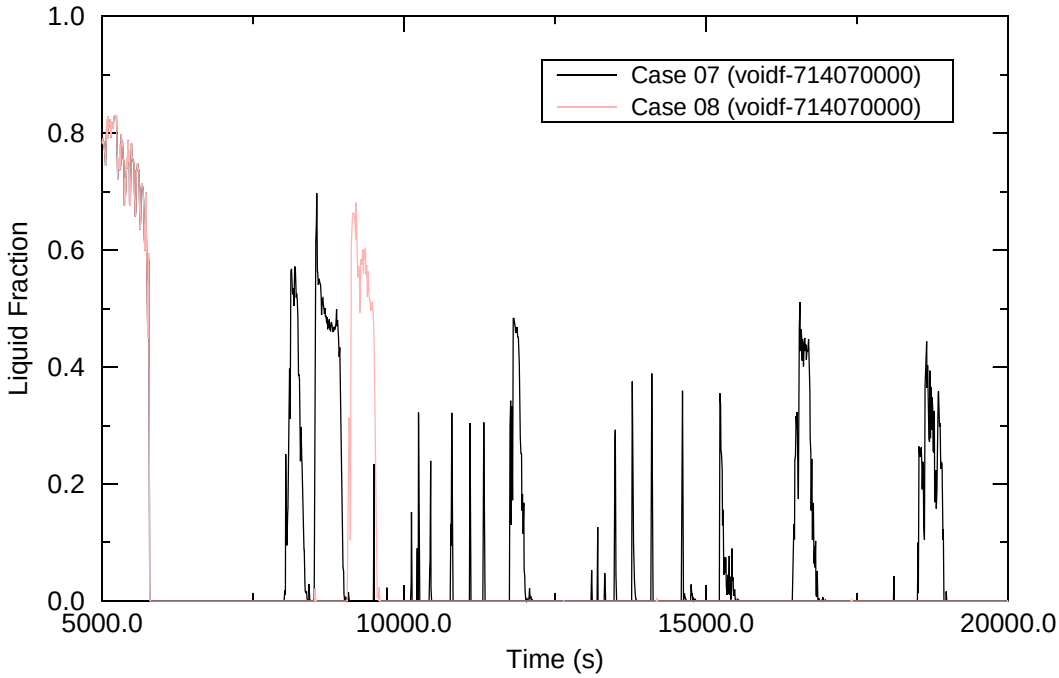

Figure 29. Core liquid fractions at the seventh axial level of the center channel in Cases 07 and 08.

because reduced velocities (and corresponding reductions in interphase drag) did not promote effective entrainment of water available in the lower levels of core. Cooling provided by the relatively high two phase levels in Case 07 delayed the onset of oxidation in Case 07 compared to Case 08 as indicated in Figure 30. Because oxidation significantly contributes to system heating, relatively early oxidation in Case 08 led to relatively early creep failures of the surge line and hot leg.

Breaks were not initiated in the SCDAP/RELAP5 model to simulate these failures. Instead, the calculation was allowed to proceed to determine the earliest possible timing of SG tube failures. Consequently, the hottest tubes in SGA with stress multiplication factors of 7.5 were predicted to fail by creep rupture at 33,420 s, some 12,630 s after surge line failure and 2,320 s after failure of hot leg A. A series of SG tube failures were also clustered around 40,500 s. (Specifically, the hottest tubes in SGA were predicted to fail by creep rupture at 40,460 s with a stress multiplication factor of 7.0, at 40,470 s with a stress multiplication factor of 6.5, at 40,480 s with a stress multiplication factor of 6.0, and at 40,510 s with a stress multiplication factor of 5.5. In addition, the hottest tubes in SGB with stress multiplication factors of 7.5, 7.0, and 6.5 were predicted to fail at 40,470 s, 40,480 s, and 40,510 s, respectively.) (See Tables 4 and 5.) All of these clustered SG tube failures were directly related to an RCS re-pressurization (to ~11 MPa) associated with an SIT injection that produced RCP loop seal clearing in two of four loops (although development of full loop natural circulation did not follow because water remained above the bottom of the reactor vessel downcomer skirt).

Prior to the time of the first SG tube failure, the surge line was heated to temperatures near 1,700 K. Given that stainless steel melts between solidus and liquidus temperatures of 1,675 and 1,727 K, the possibility of surge line survival (from 20,790 s) to the time of the first SG tube failure (at 33,420 s) seems very

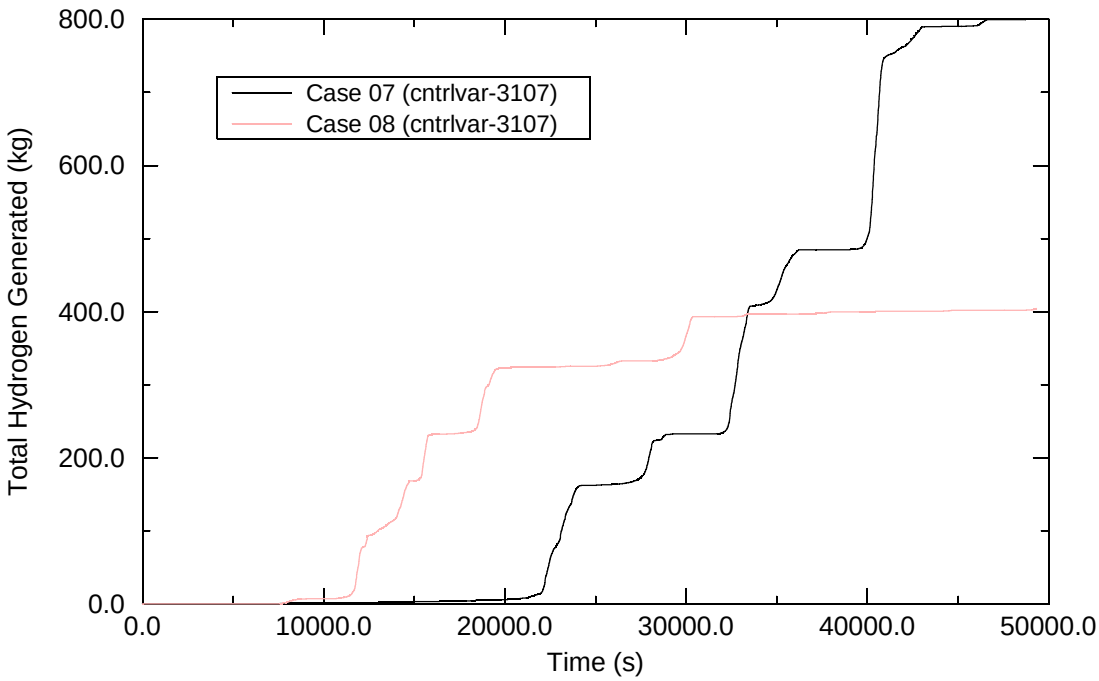

Figure 30. Total hydrogen generation in Cases 07 and 08.

unlikely. Furthermore, if a break in the RCS was (more realistically) introduced at the time of the predicted surge line failure, one would expect quick depletion of remaining SIT inventory with minimal re-pressurization (because a break as large as the surge line should readily vent most of the generated steam). A gradual boil-off would then be required before significant heating of any RCS piping could resume. It is expected that the effects of any subsequent heating of the RCS piping would be focussed on the surge line and hot leg, consistent with the break flow path. Therefore, it seems clear that operator actions to open ECCS vent valves (as modeled in this case) will result in surge line failure well before the first possible SG tube failure. In addition, any challenge to SG tube integrity appears to be minimal even if the expected RCS depressurization due to surge line failure were modeled, indicating that the operator action considered in this case will be successful with respect to ensuring that tube failures will not occur before other RCS pressure boundary failures.

Although current estimates of ANO2 SG tube plugging were included in Cases 07 and 08, it is worth noting that the effects expressly associated with plugging could not be determined. That is because calculations completed during the course of this analysis, including Cases 07 and 08, were not designed to isolate plugging effects. Qualitatively, it would seem that reducing the SG heat transfer area (i.e., eliminating heat transfer to tubes that are plugged) could result in higher temperatures in the remaining (unplugged) tubes because the “total heat load” could be distributed to a “smaller heat sink”. Therefore, neglecting the effects of plugging, as commonly done in many analyses for the NRC, may not be advisable because many PWRs currently operating in the United States have partially plugged SGs and because resulting tube temperatures, and the corresponding predictions of creep failure, may be non-conservative.

5. CONCLUSIONS

Eight different SCDAP/RELAP5 calculations were completed to determine thermal-hydraulic conditions resulting from station blackout accident progression and the impact of those conditions on SG tube integrity. Conclusions pertinent to that effort are summarized below.

Oxidation can lead to stagnation of natural circulation flow in SG U-tubes.

When rapid oxidation of the core begins, steam/hydrogen mixtures enter the hot leg countercurrent natural circulation flow path and ultimately fill SG U-tubes. When the rapid phase of oxidation ends, hydrogen concentrations entering the top half of the hot leg begin to diminish, producing a density gradient between vapors in the SG U-tubes and vapors in the hot leg. This density gradient can be large enough to result in stagnation of natural circulation flow in SG tube bundles. In the current version of SCDAP/RELAP5, the flow stagnation generally persists until a relatively large pressurization event (i.e., an SIT injection or a relocation of molten core materials into water in the lower head) or the onset of full loop natural circulation forces the clearing of relatively light vapors in the tube bundle. The duration of the stagnation period might be reduced, however, if the code was modified to treat the diffusion of hydrogen.

Oxidation-induced stagnation of natural circulation flow can effectively reduce the potential for SG tube failure.

SG tube heating can be effectively eliminated during periods of oxidation-induced stagnation of natural circulation flow in a SG U-tube bundle. This could be very important with respect to the evaluation of severe accident risks because the potential for SG tube failure is significantly reduced without tube heating. Given that level of importance, reliable predictions of flow stagnation and, more importantly, the duration of stagnation period, should be integral to severe accident analyses. Therefore, further evaluation of the possible effects of hydrogen diffusion and the absence of such models in SCDAP/RELAP5 appears to be warranted.

Modeling of SG plena junctions must account for transitions between hot leg countercurrent and full loop natural circulation modes in order to appropriately predict SG tube temperatures.

Natural circulation flows can switch between hot leg countercurrent and full loop natural circulation modes during severe accidents in PWRs with U-tube SGs. Water levels in the reactor vessel and in RCP loop seals determine when these flow transitions occur. However, resulting SCDAP/RELAP5 SG tube temperatures indicated that a single set of flow areas and loss coefficients for all SG plena junctions is not adequate for simulating of both natural circulation modes. Therefore, a more sophisticated model of SG plena junctions is required. Results from this analysis indicate that using servo valves to represent SG plena junctions allows appropriate flow transition and simulation of subsequent tube heating.

The effects of SG tube plugging should not be ignored in severe accident analyses.

Although calculations completed during the course of this analysis were not designed to isolate effects associated with SG tube plugging, it qualitatively appears that reducing the SG heat transfer area (i.e., eliminating heat transfer to tubes that are plugged) could result in higher temperatures in the remaining (unplugged) tubes because the “total heat load” could be distributed to a “smaller heat sink”. Therefore, neglecting the effects of plugging in severe accident analyses may not be advisable because many PWRs

currently operating in the United States have partially plugged SGs and because resulting tube temperatures, and the corresponding predictions of creep failure, may be non-conservative.

ANO2 ECCS vent valve flows are friction dominated and not determined by valve size.

A separate SCDAP/RELAP5 model of the ECCS vent valves and all associated piping from the top of the pressurizer to the quench tank was developed. Results from that model indicated that ECCS vent valve flows are friction dominated. In other words, flow capacity is not determined by the size of the vent valves. Instead, flow capacity is limited by friction through the long and torturous path to the quench tank. This could be quite important because discharge through the pressurizer SRVs is carried through some of the same piping. Although pressurizer SRVs discharge into some of the piping in the ECCS vent valve discharge path, INEEL did not investigate whether the piping between the SRVs and the quench tank had a similar impact on the effective capacity of the pressurizer SRVs. Furthermore, INEEL did not compare these results to the licensee's assessment of the ECCS vent path capabilities in its design basis analyses.

Operators can open ECCS vent valves and successfully ensure that SG tube failures will be delayed until long after other RCS pressure boundary failures.

Two SCDAP/RELAP5 calculations were completed during the course of this analysis to evaluate the effects of operator actions during station blackout accidents. In both cases, the operator action consisted of opening ECCS vent valves to depressurize the RCS at specified times during accident progression in an effort to mitigate accident consequences. And in both cases, the results indicate that SG tube failure can be delayed until long after other RCS pressure boundary failures. Those results held even for the analysis of highly degraded (flawed) SG tubes. Therefore, results from this analysis indicate that the analyzed operator actions will be successful.

Based on the cases considered, surge line and/or hot leg failures will most likely occur before the creep rupture of SG tubes that meet design basis structural integrity limits.

In addition to the evaluation of operator actions, six different SCDAP/RELAP5 calculations were completed to determine thermal-hydraulic conditions that could result from station blackout accidents with variations in RCS and SG secondary pressures. The variations were selected in an attempt to cover those conditions that could reasonably be expected to develop during a station blackout accident and have an impact on SG tube integrity. In all cases, surge line and/or hot leg failures were predicted to occur before failures of pristine (unflawed) SG tubes. Furthermore, surge line and/or hot leg failures were generally predicted to occur before failure of SG tubes with degradation (flaws) represented by stress multiplication as high as ~3. However, these calculations did not consider the effects of simulation uncertainties and variances in material properties that are used by NRC to produce a probabilistic evaluation for the conditional probability that the tubes will not rupture first. Also, this study did not attempt to evaluate the effects of tube leakage that may be induced at high temperatures in tubes that meet the design basis leakage criterion at normal temperatures and the design basis pressure differential. (A stress multiplication factor of about 4.5 for a short, partially through-wall crack could allow it to pop-through and potentially leak under design basis conditions.)

6. REFERENCES

1. The SCDAP/RELAP5 Development Team, *SCDAP/RELAP5/MOD3.2 Code Manuals*, NUREG/CR-6150, Revision 1, INEL-96/0422, Idaho National Engineering and Environmental Laboratory, July 1998.

2. D. L. Knudson (INEEL) letter to R. Lee (NRC), "Revision 1 of Steam Generator Tube Rupture Analyses under JCN W6242", DLK-4-96, June 6, 1996, transmitting D. L. Knudson and K. S. Quick, "A SCDAP/RELAP5 Analysis of the Potential for Steam Generator Tube Rupture in Arkansas Nuclear One Unit 2 - Revision 1", Idaho National Engineering and Environmental Laboratory, June 1996.

3. W. A. Stewart et al., *Natural Circulation Experiments for PWR High Pressure Accidents*, EPRI Project No. RP2177-5, Final Report, Westinghouse Electric Corporation, July 1992.

4. T. J. Leahy (INEEL) letter to S. M. Long (NRC), "Transmittal of Task 1 Letter Report Under Task Order 1 of JCN J2824", CCN 00-007176, April 5, 2000, transmitting D. L. Knudson, "ANO2 SCDAP/RELAP5 Model Modifications", Idaho National Engineering and Environmental Laboratory, April 2000.

5. T. Auble and J. Hosler, *EPRI PWR Safety and Relief Valve Test Program, Safety and Relief Valve Test Report*, Electric Power Research Institute, April 1982.

6. J. Richardson facsimile transmittal to M. Lloyd (both presumably employed by the ANO2 licensee), "Re: K Factors for ECCS Vent", June 16, 2000, forwarded to D. Knudson (INEEL), June 28, 2000.

Appendix A - Selected Results from Case 01

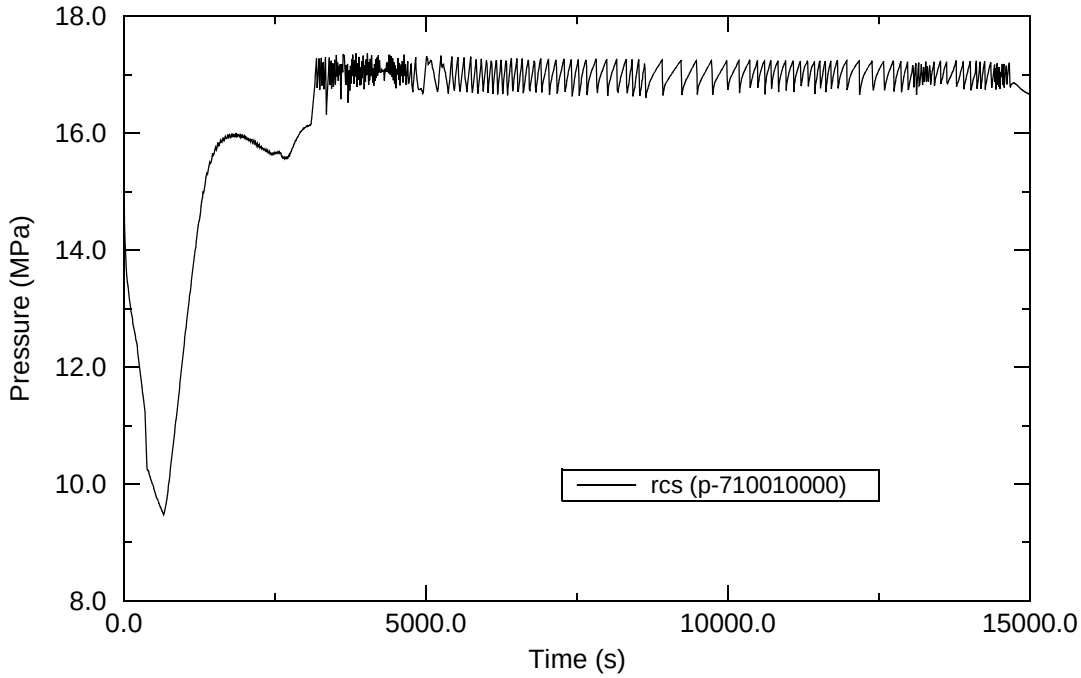

Figure A-1. Case 01 RCS (reactor coolant system) pressure.

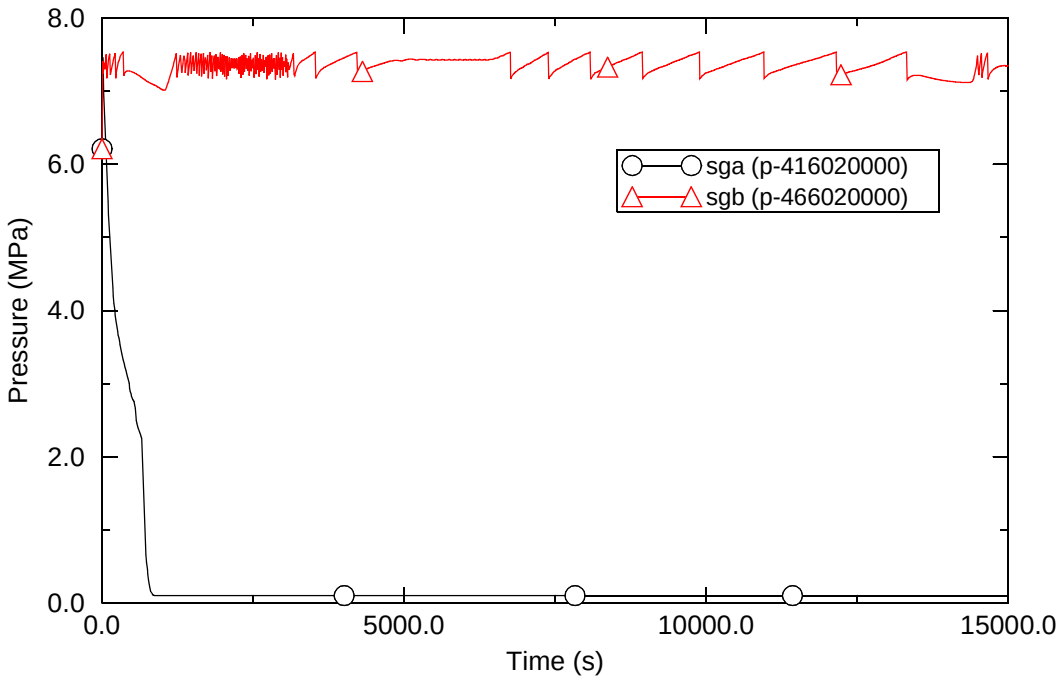

Figure A-2. Case 01 pressures in SGA (steam generator in primary coolant loop with pressurizer) and SGB (steam generator in primary coolant loop without pressurizer).

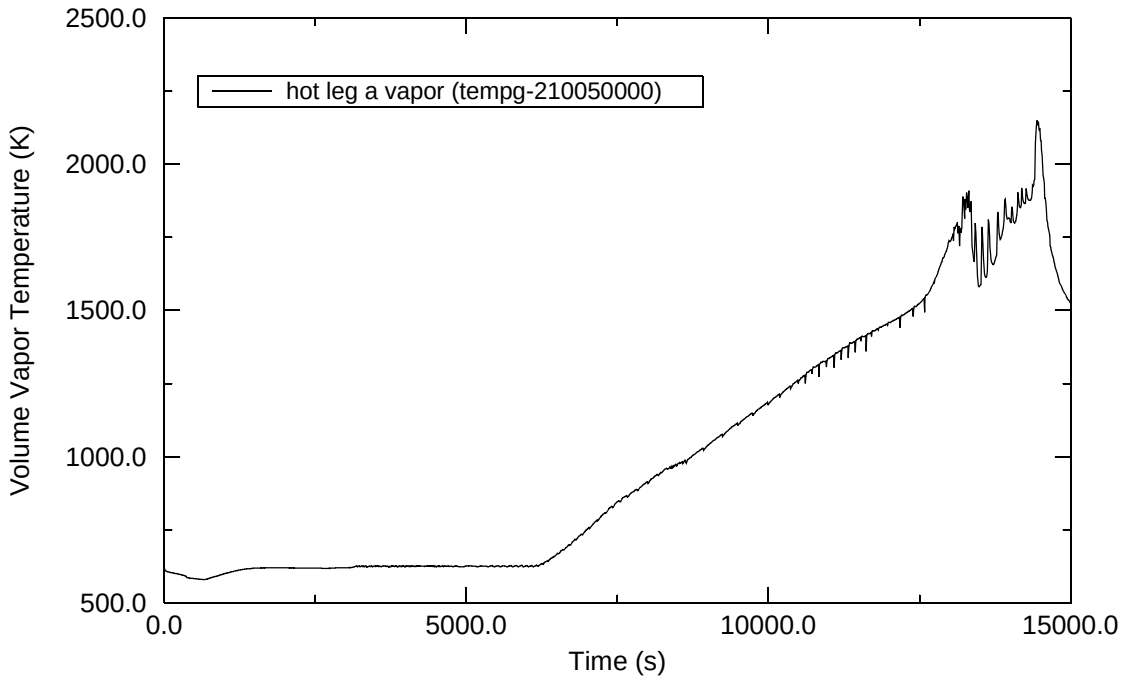

Figure A-3. Case 01 vapor temperature entering SGA inlet plenum from the "hot" part of the hot leg.

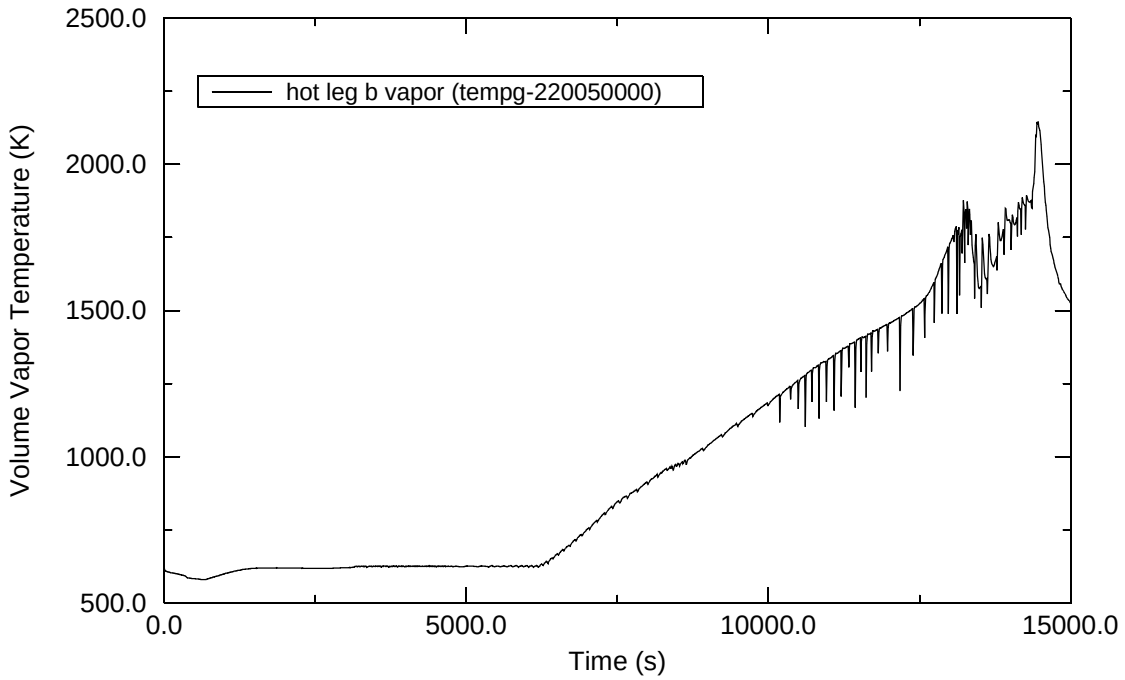

Figure A-4. Case 01 vapor temperature entering SGB inlet plenum from the "hot" part of the hot leg.

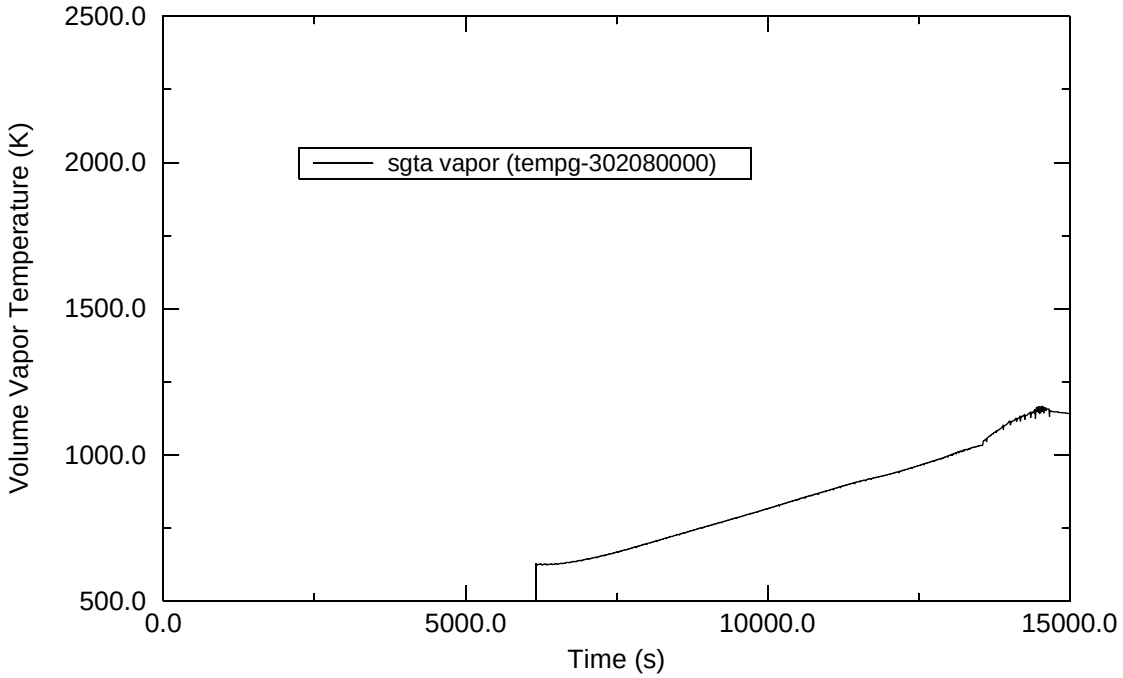

Figure A-5. Case 01 vapor temperature returning to SGA inlet plenum from the "cold" SG tube bundle.

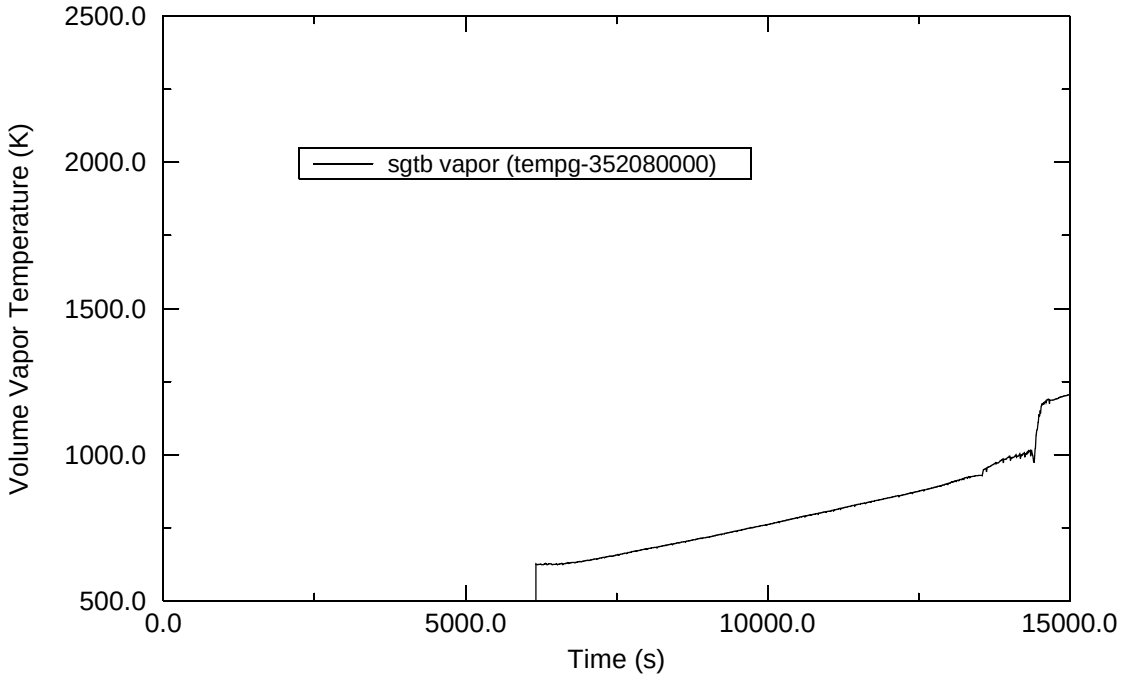

Figure A-6. Case 01 vapor temperature returning to SGB inlet plenum from the "cold" SG tube bundle.

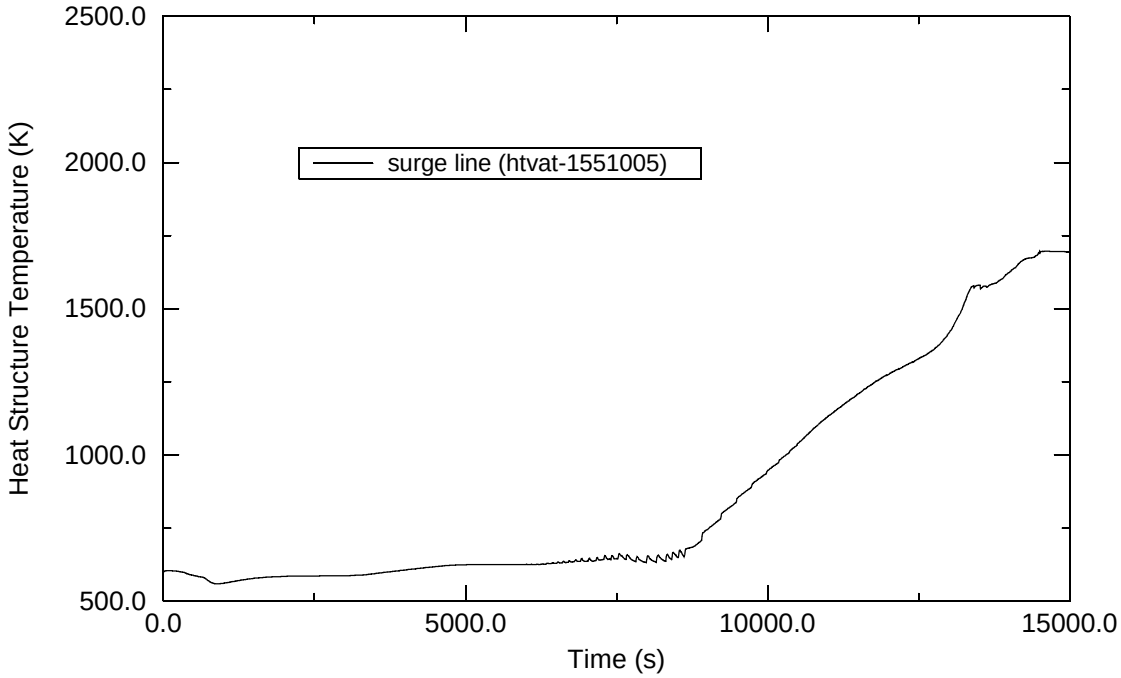

Figure A-7. Case 01 surge line temperature.

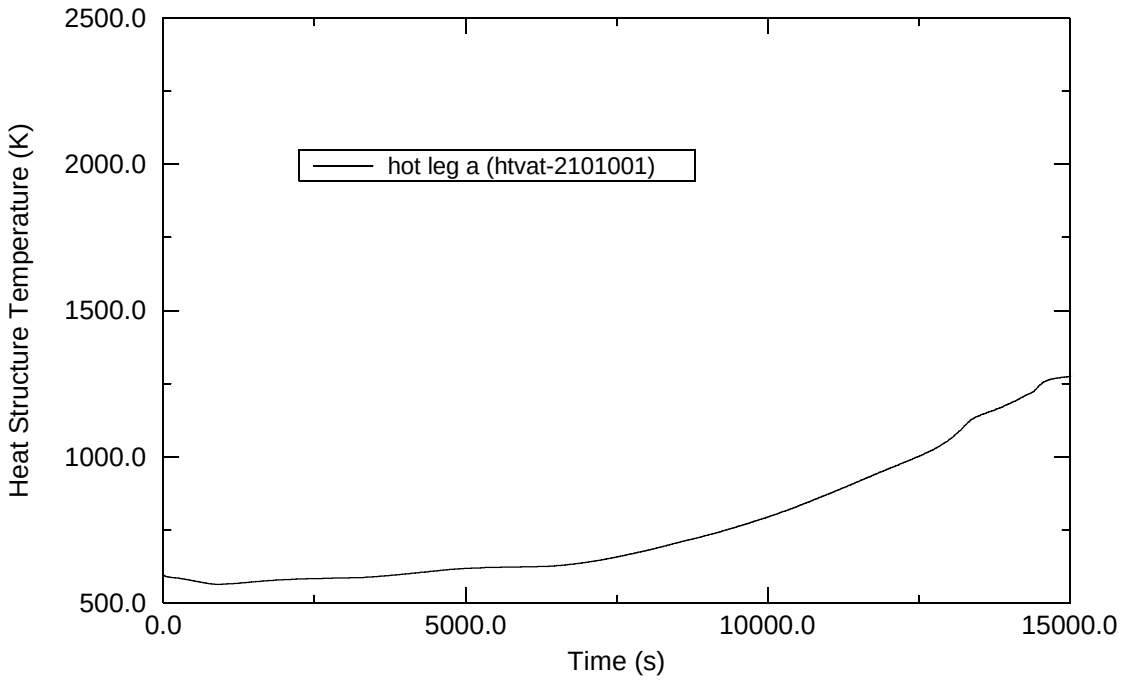

Figure A-8. Case 01 temperature of hot leg A (hot leg in primary coolant loop with pressurizer).

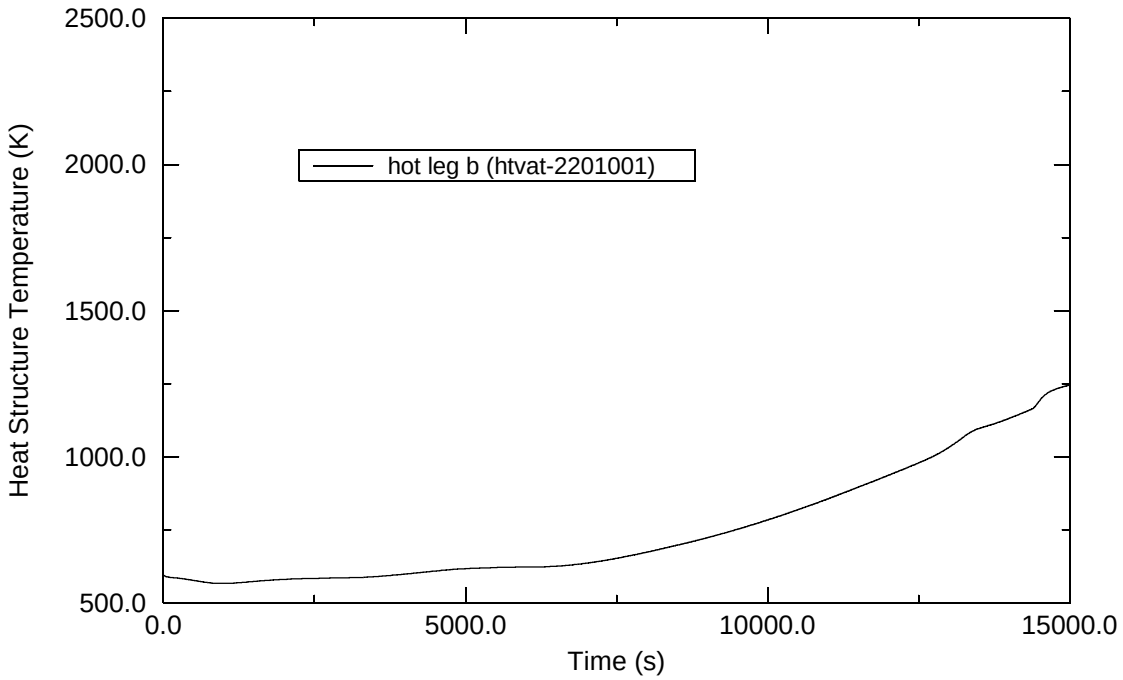

Figure A-9. Case 01 temperature of hot leg B (hot leg in primary coolant loop without pressurizer).

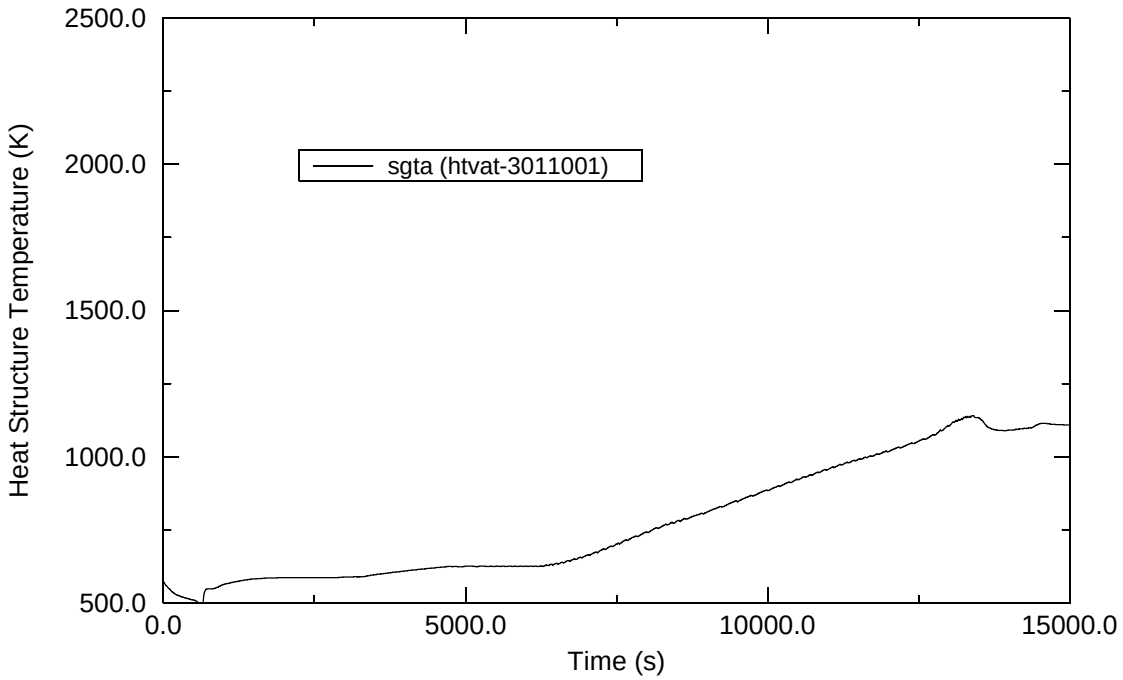

Figure A-10. Case 01 SGA tube temperature.

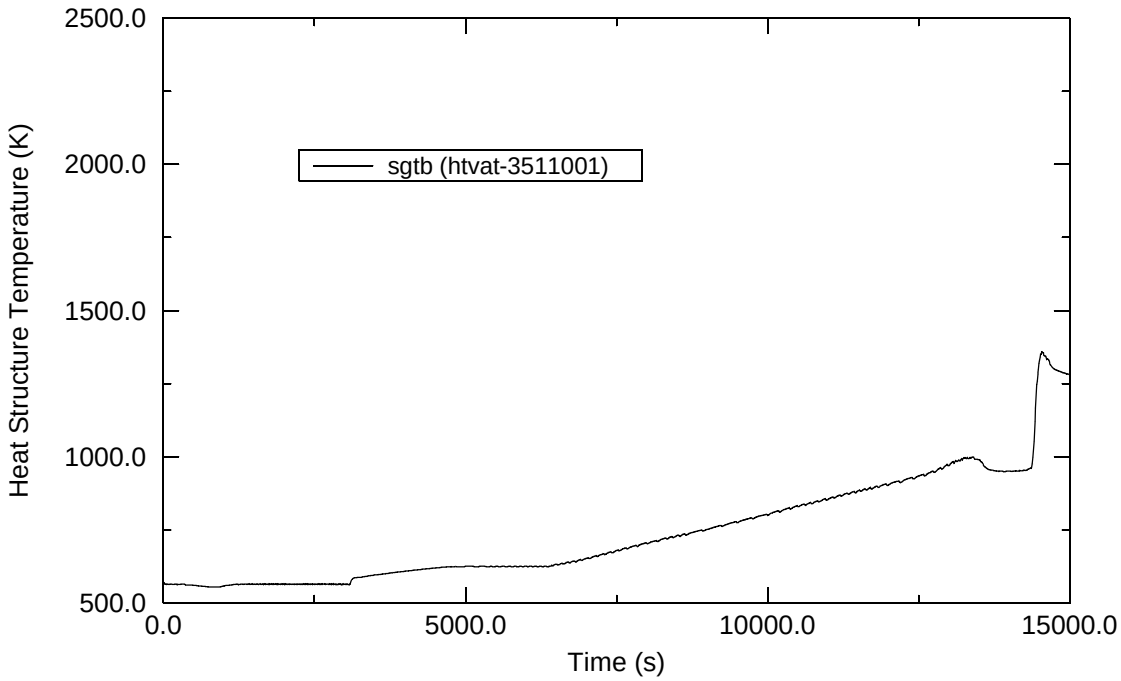

Figure A-11. Case 01 SGB tube temperature.

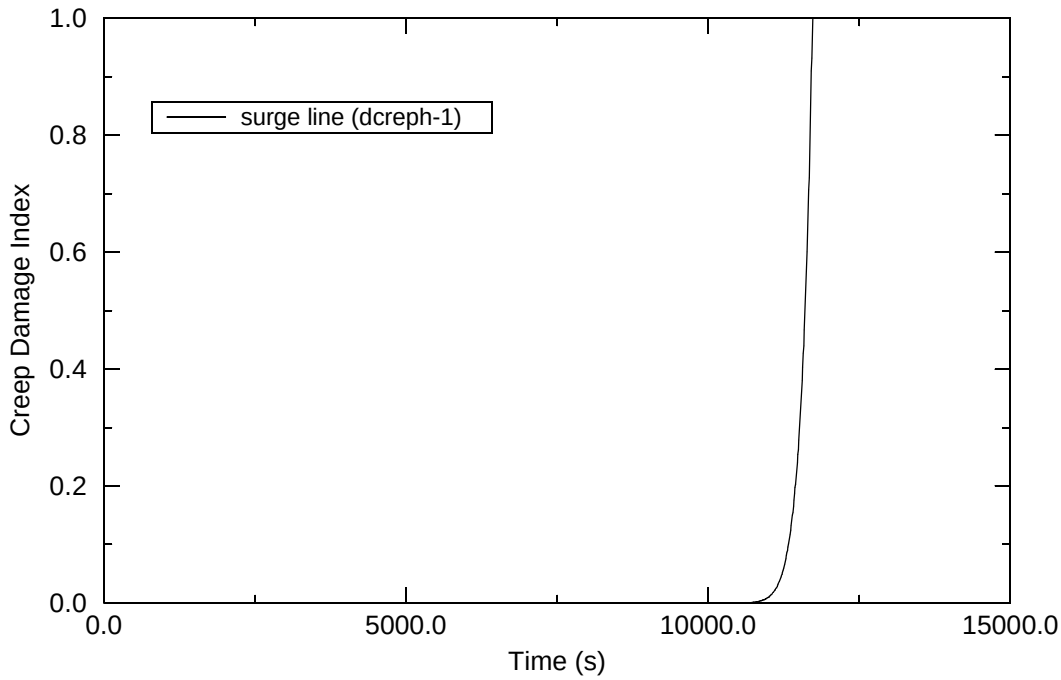

Figure A-12. Case 01 surge line creep damage index.

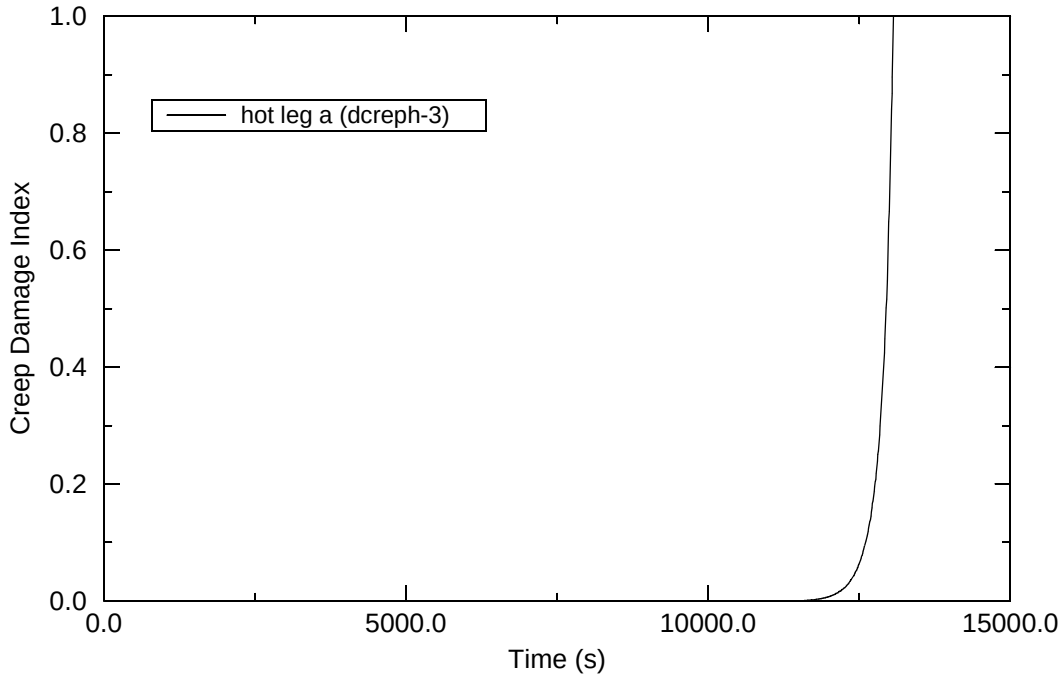

Figure A-13. Case 01 hot leg A creep damage index.

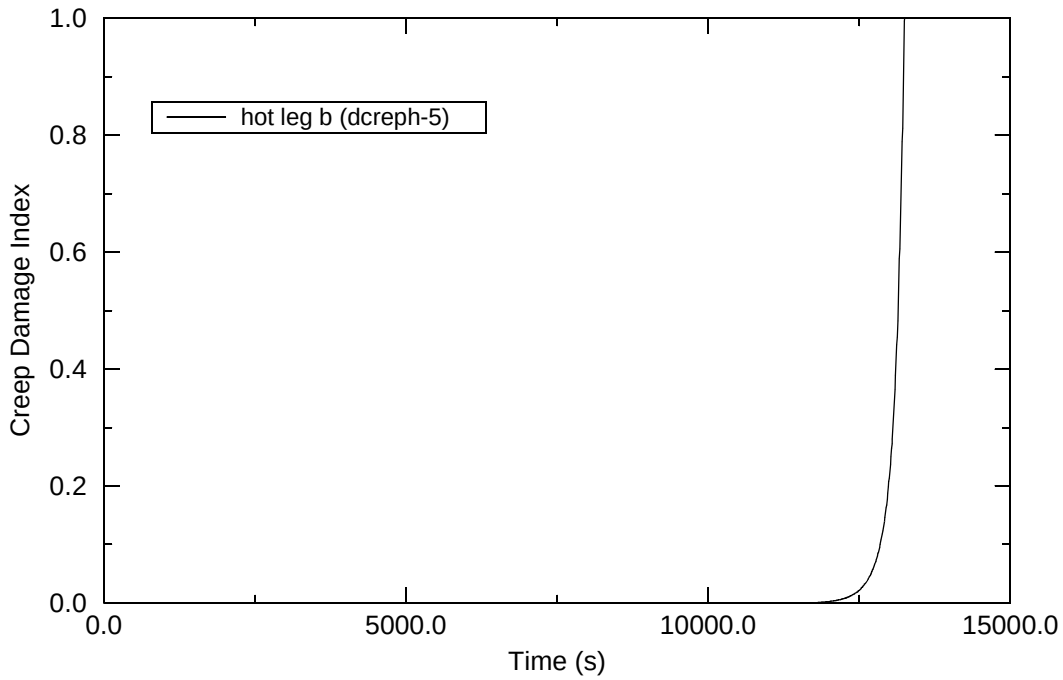

Figure A-14. Case 01 hot leg B creep damage index.

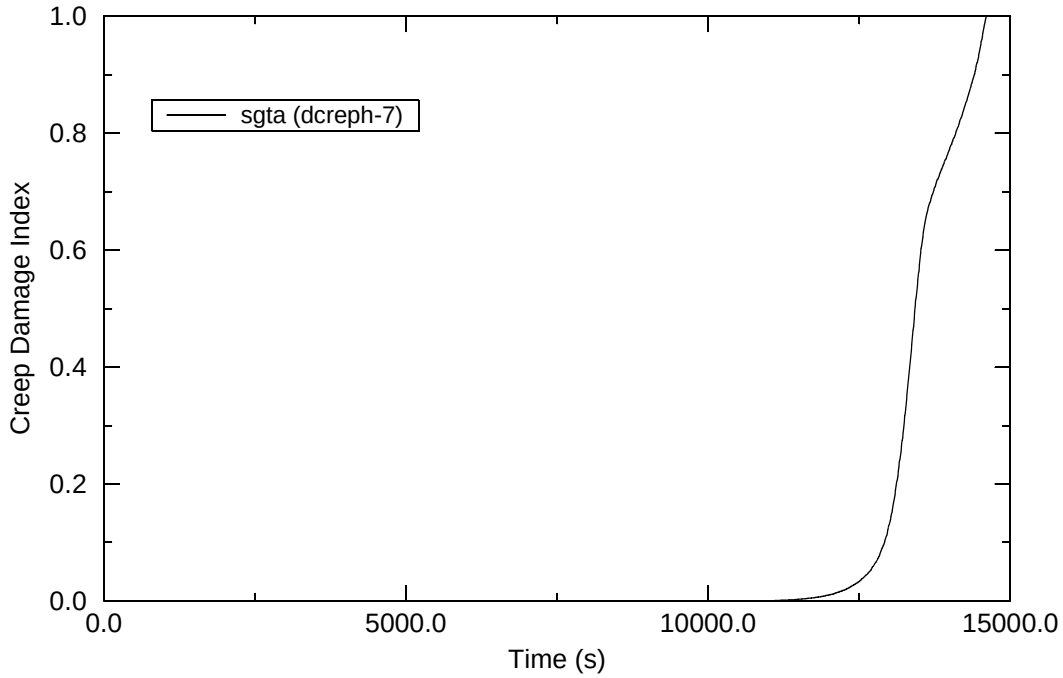

Figure A-15. Case 01 SGA tube creep damage index.

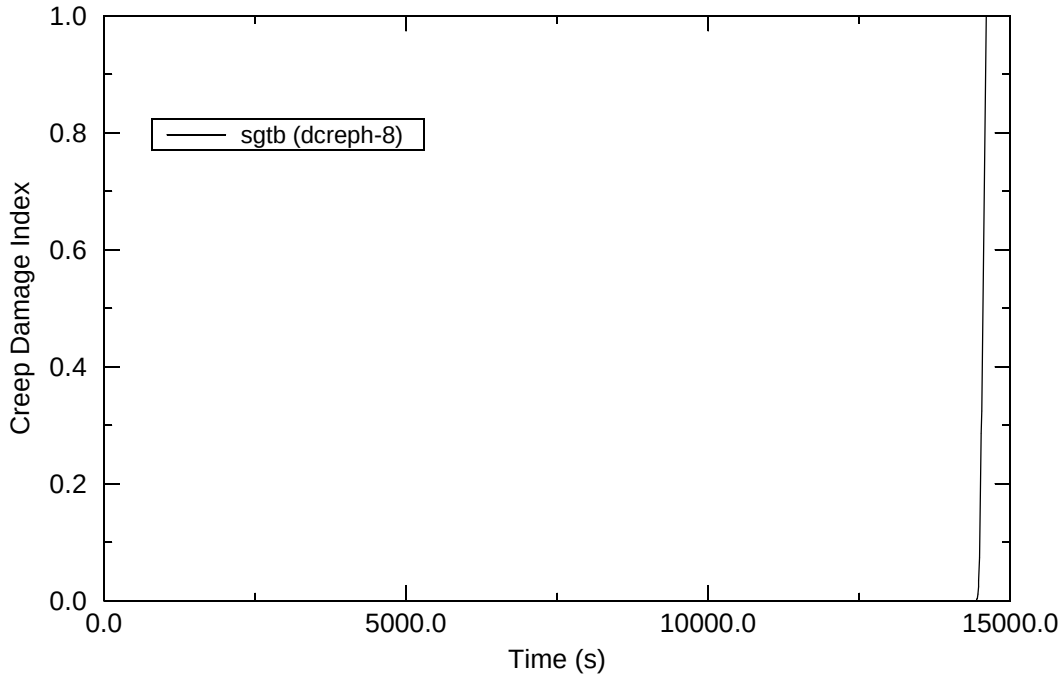

Figure A-16. Case 01 SGB tube creep damage index.

Appendix B - Selected Results from Case 02

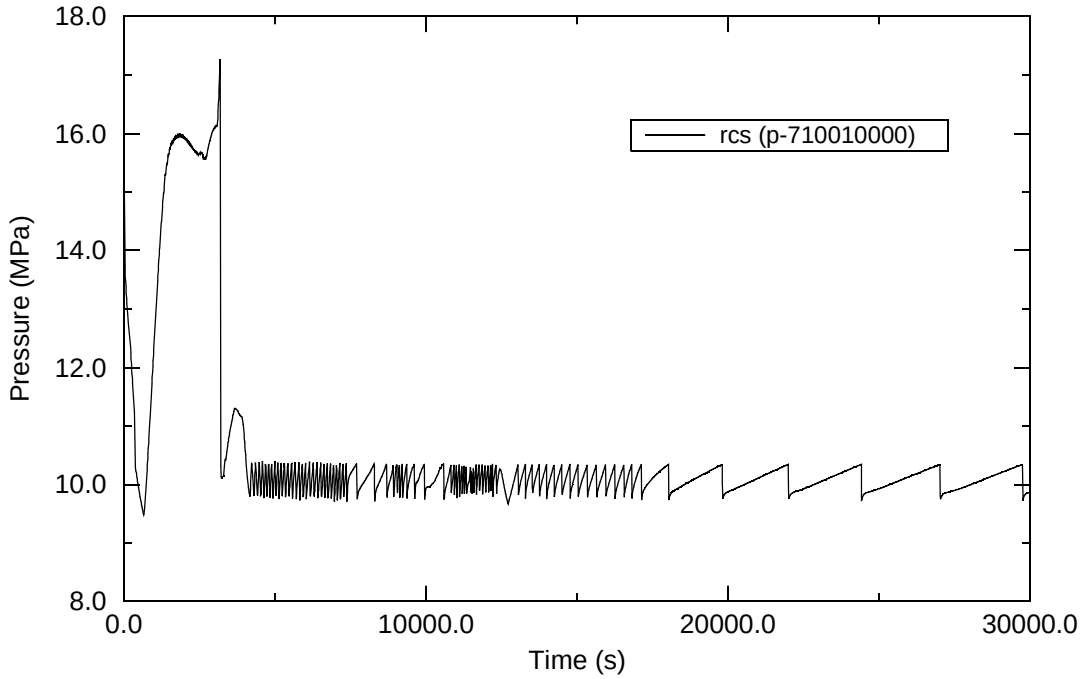

Figure B-1. Case 02 RCS (reactor coolant system) pressure.

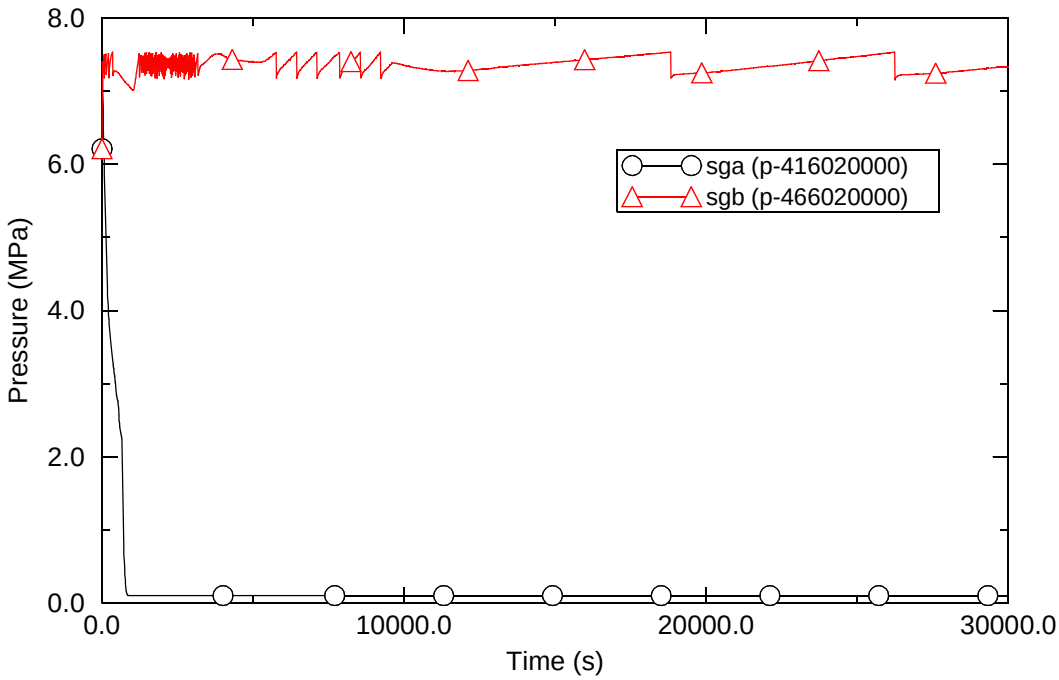

Figure B-2. Case 02 pressures in SGA (steam generator in primary coolant loop with pressurizer) and SGB (steam generator in primary coolant loop without pressurizer).

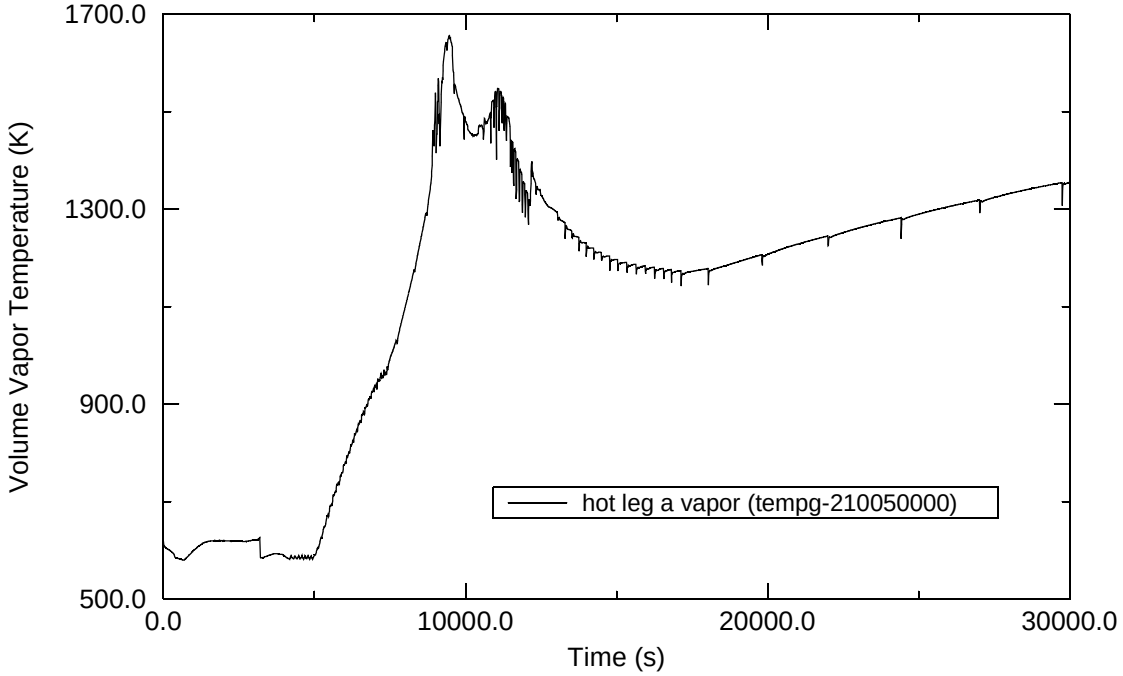

Figure B-3. Case 02 vapor temperature entering SGA inlet plenum from the "hot" part of the hot leg.

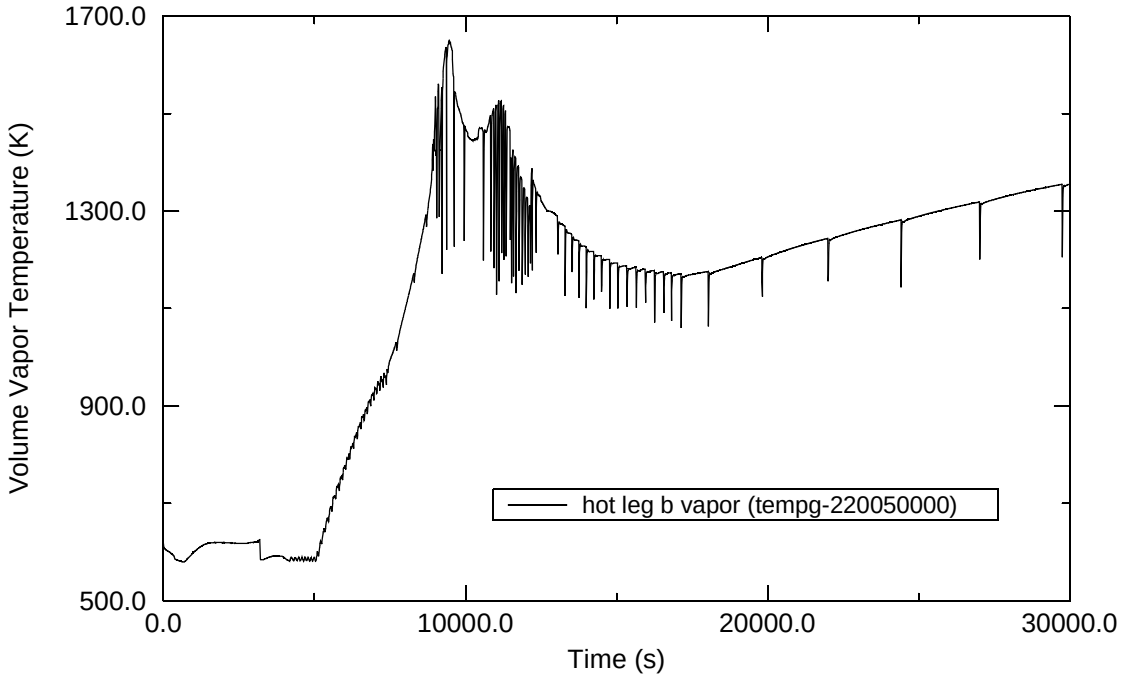

Figure B-4. Case 02 vapor temperature entering SGB inlet plenum from the "hot" part of the hot leg.

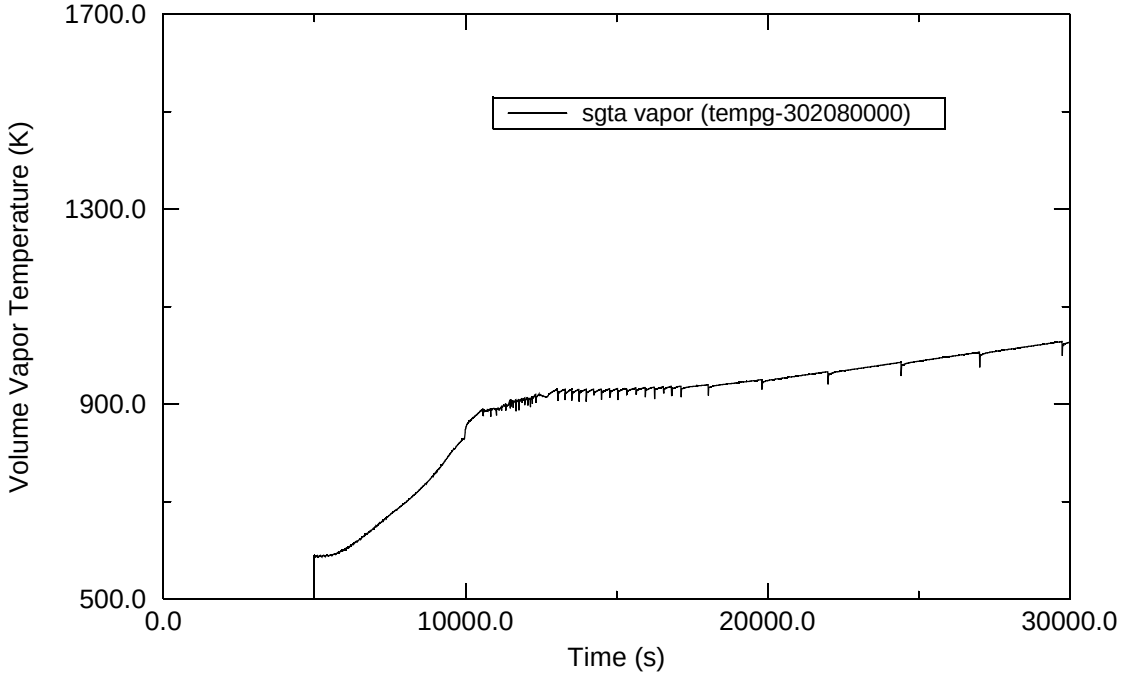

Figure B-5. Case 02 vapor temperature returning to SGA inlet plenum from the "cold" SG tube bundle.

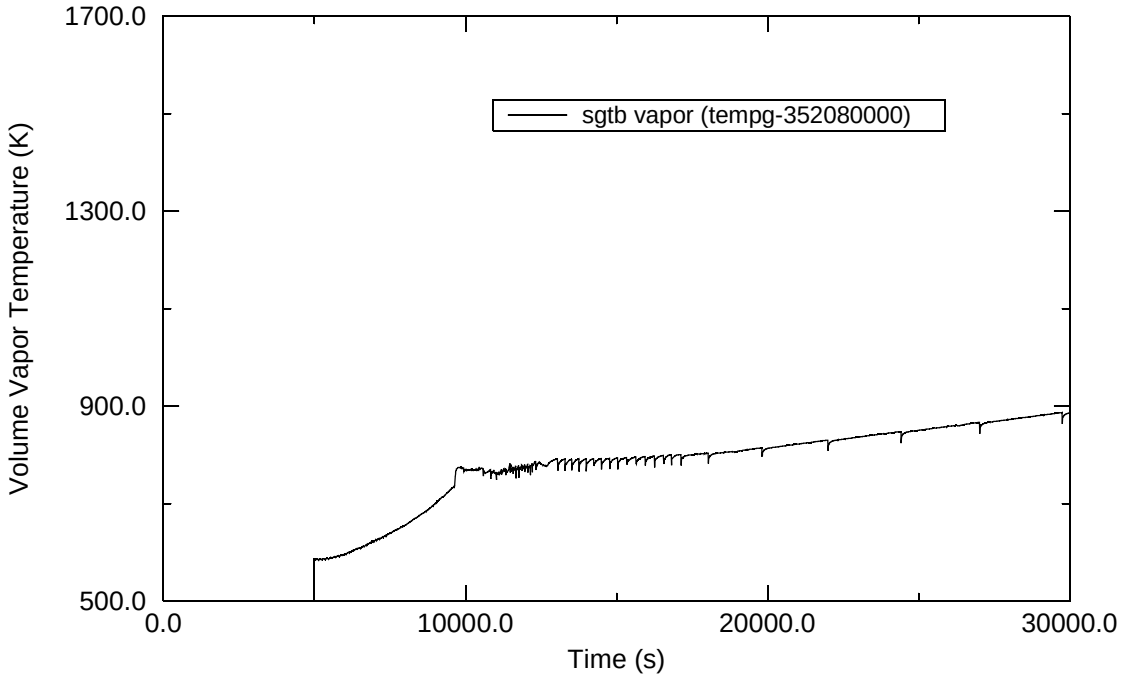

Figure B-6. Case 02 vapor temperature returning to SGB inlet plenum from the "cold" SG tube bundle.

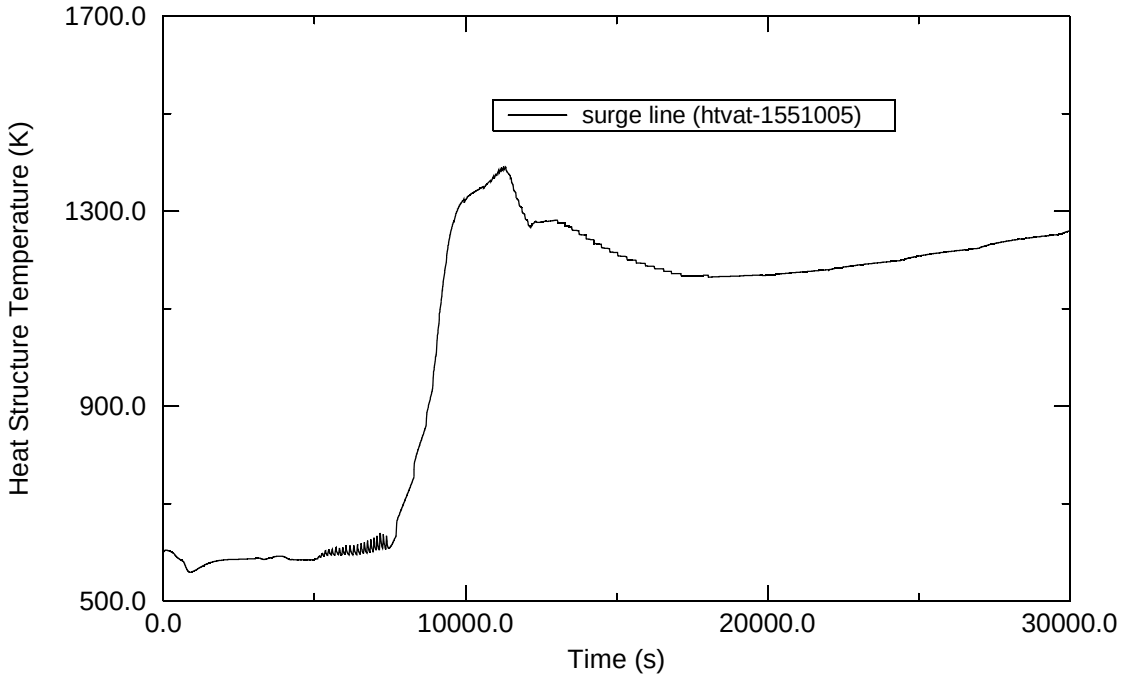

Figure B-7. Case 02 surge line temperature.

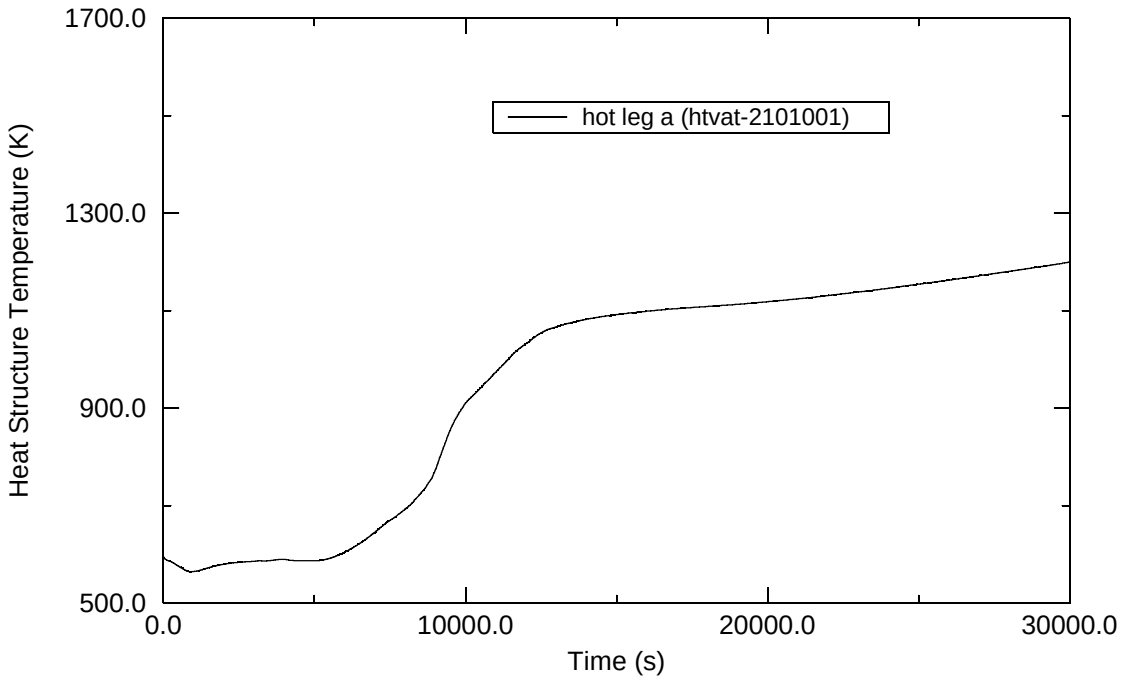

Figure B-8. Case 02 temperature of hot leg A (hot leg in primary coolant loop with pressurizer).

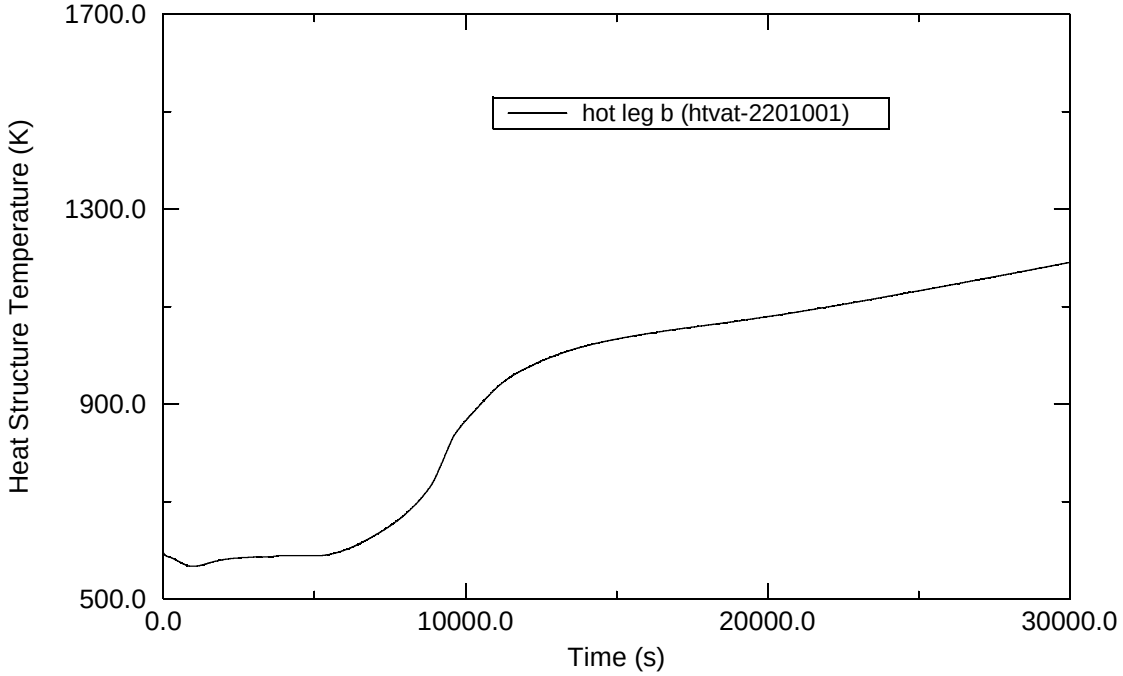

Figure B-9. Case 02 temperature of hot leg B (hot leg in primary coolant loop without pressurizer).

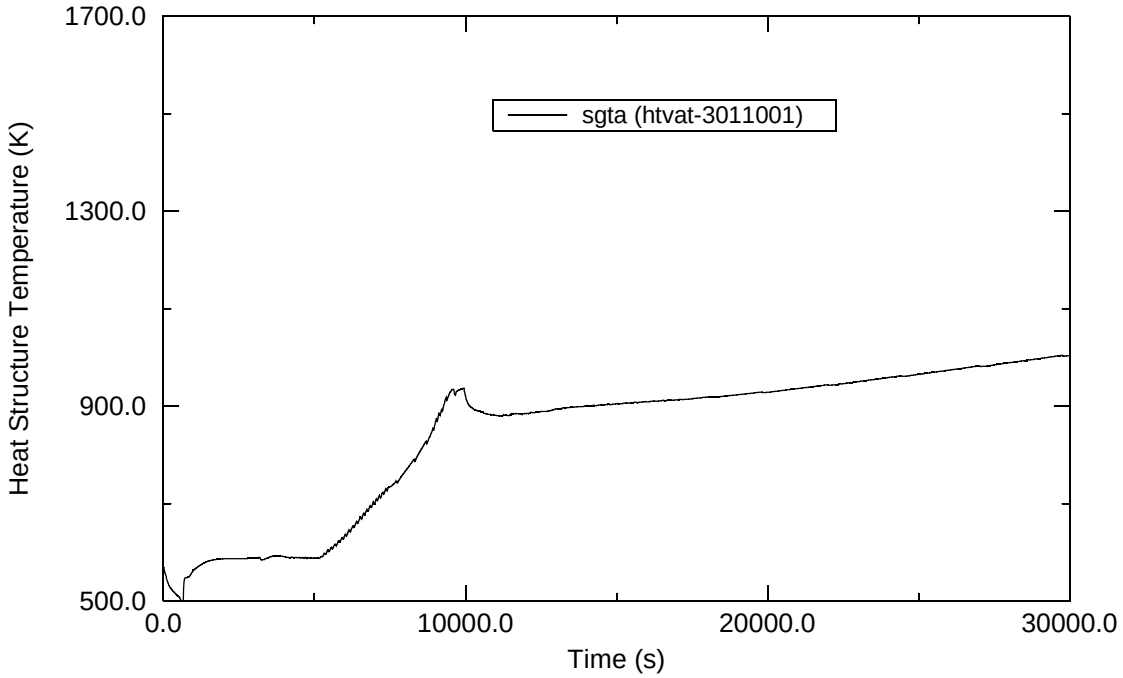

Figure B-10. Case 02 SGA tube temperature.

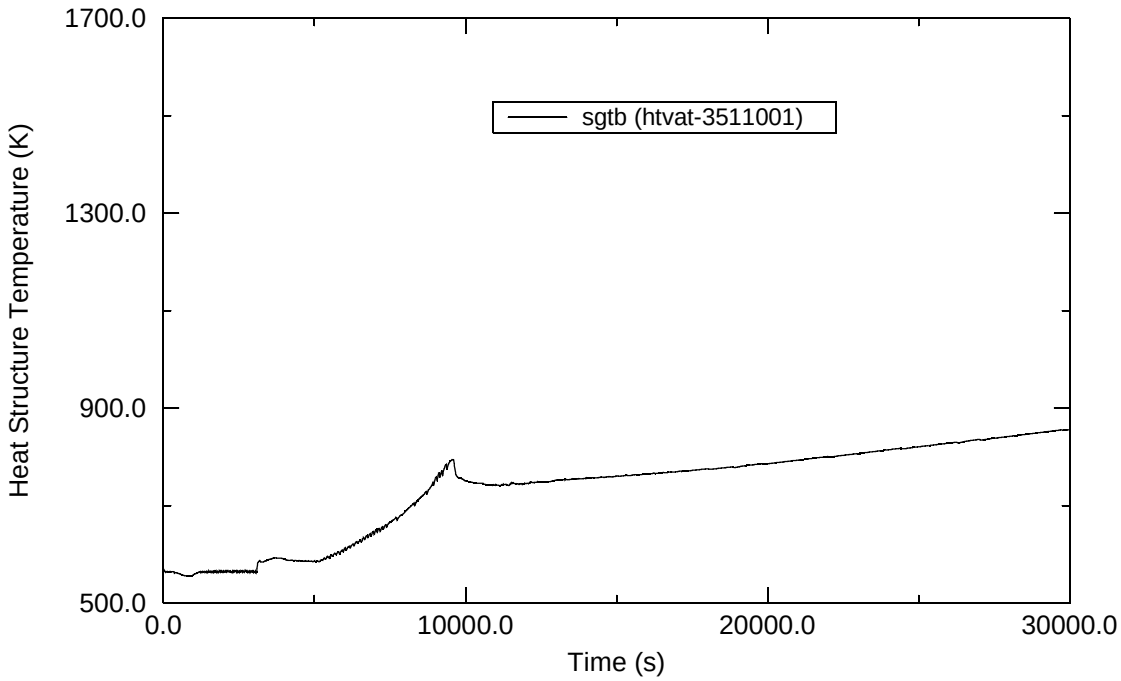

Figure B-11. Case 02 SGB tube temperature.

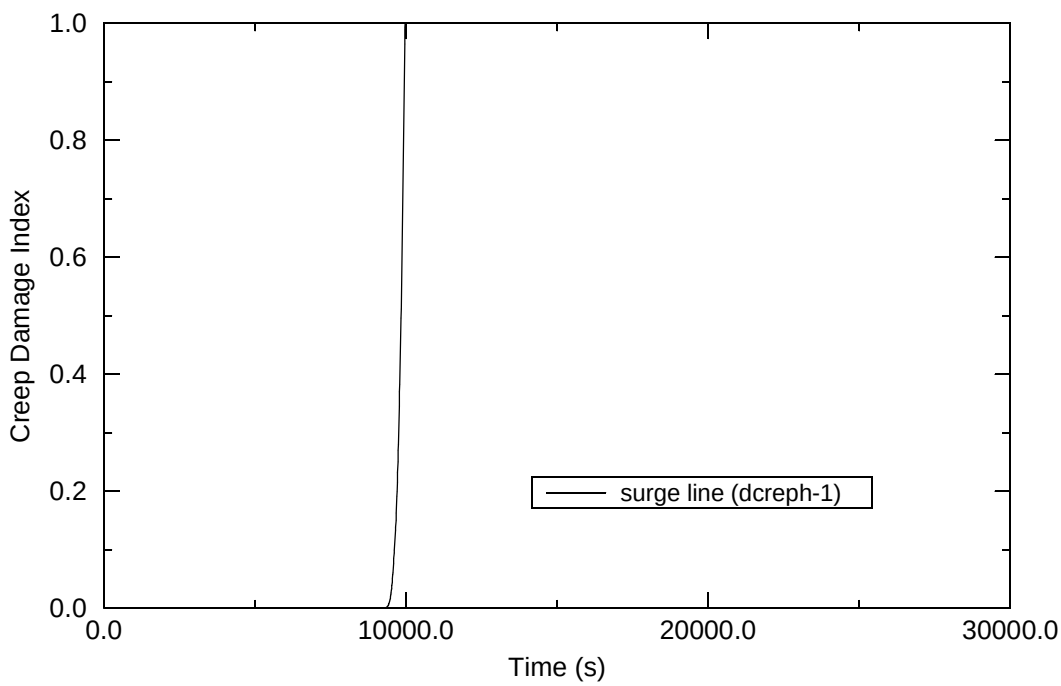

Figure B-12. Case 02 surge line creep damage index.

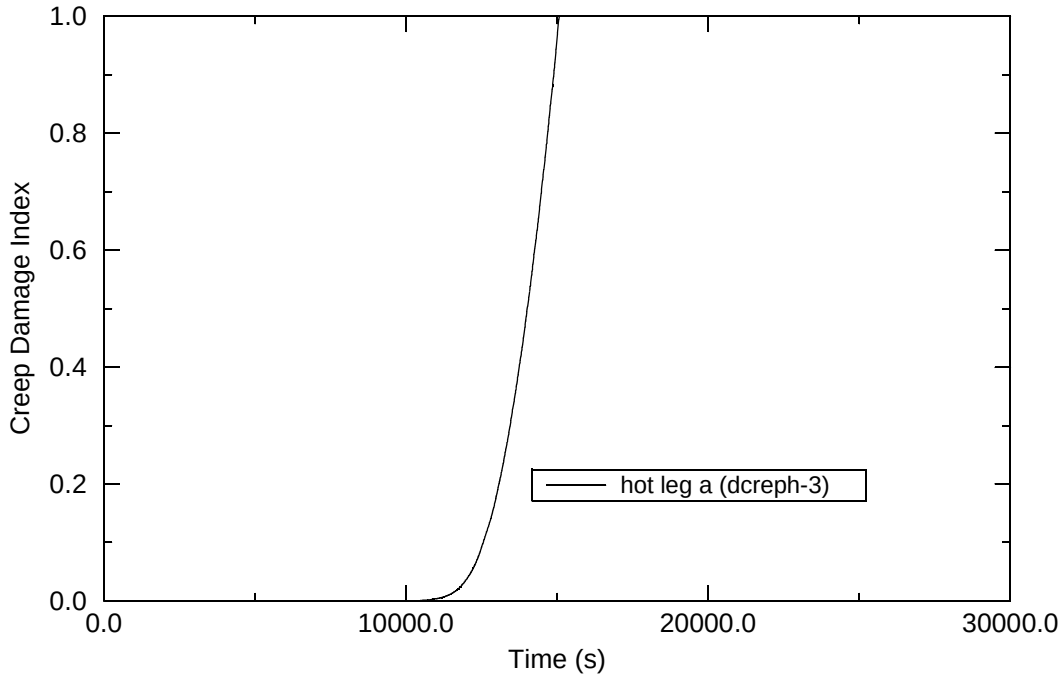

Figure B-13. Case 02 hot leg A creep damage index.

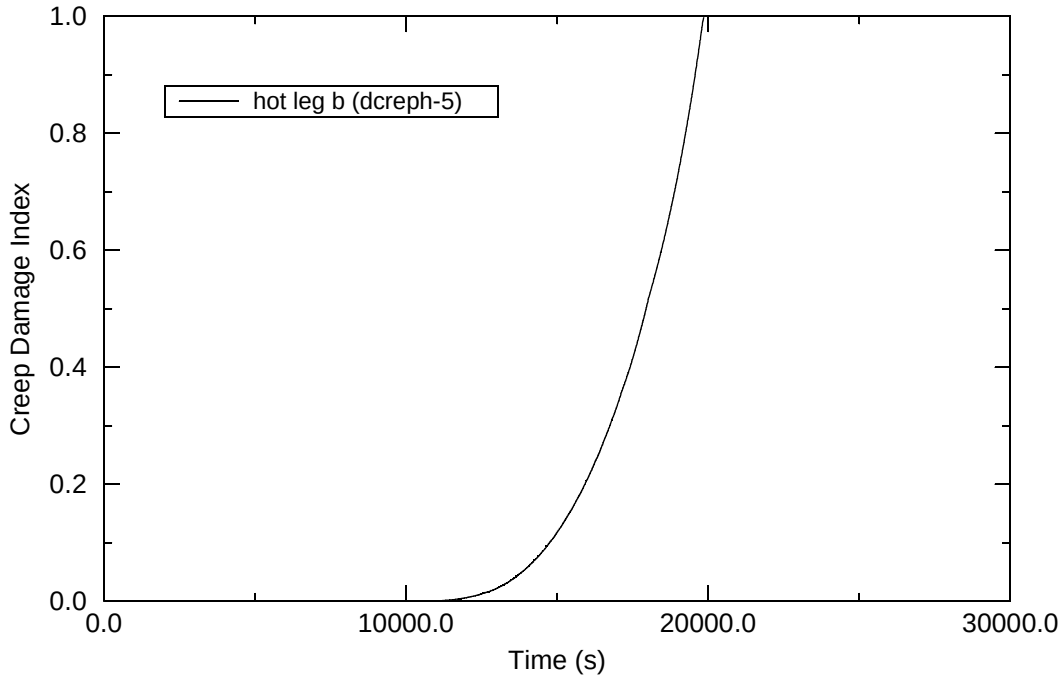

Figure B-14. Case 02 hot leg B creep damage index.

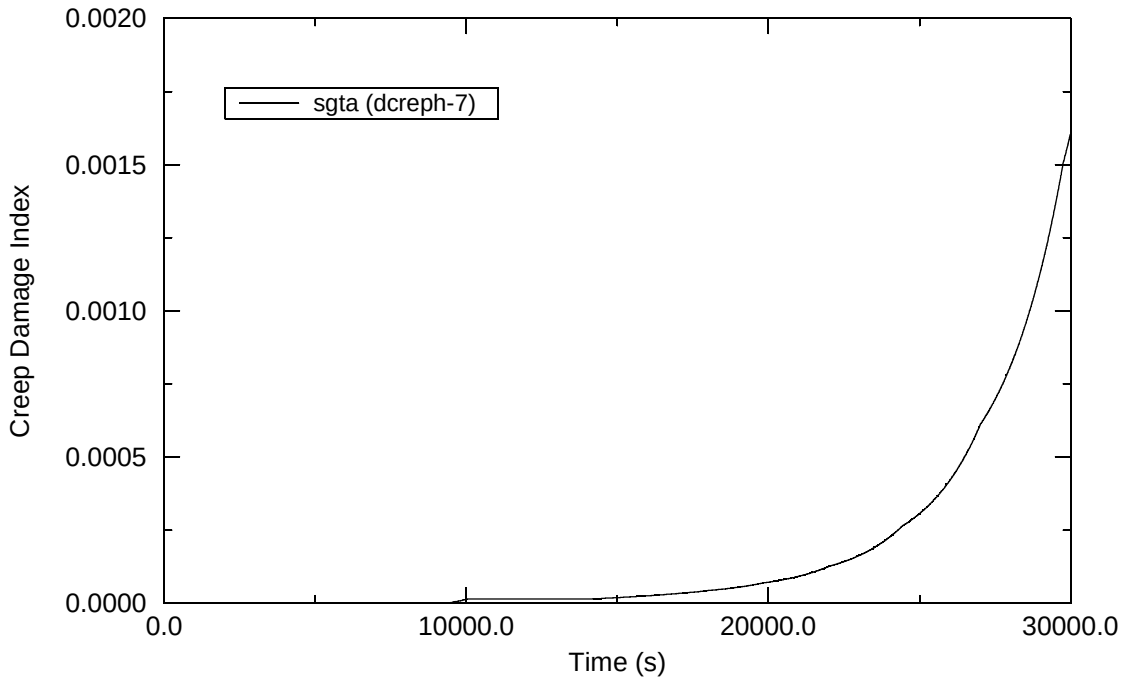

Figure B-15. Case 02 SGA tube creep damage index.

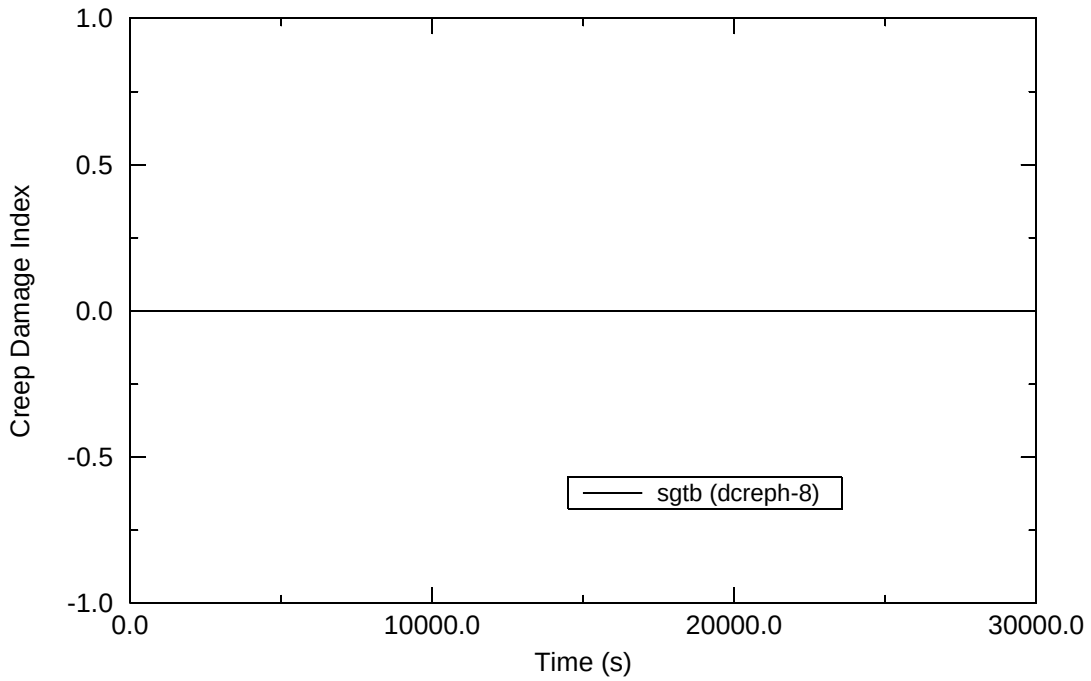

Figure B-16. Case 02 SGB tube creep damage index.

Appendix C - Selected Results from Case 03

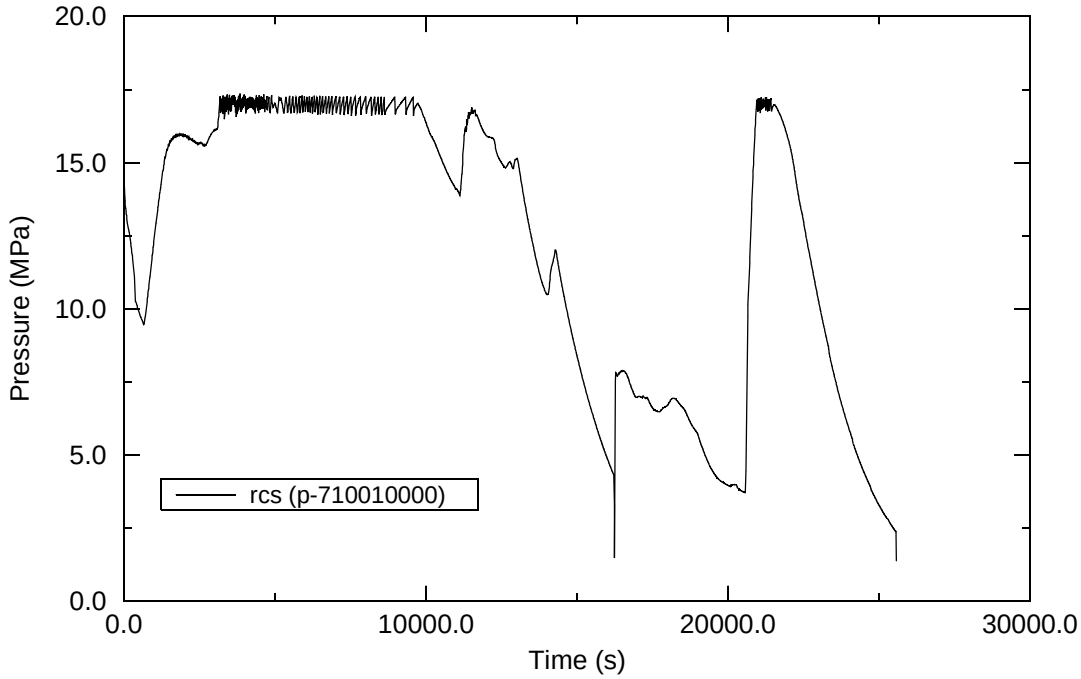

Figure C-1. Case 03 RCS (reactor coolant system) pressure.

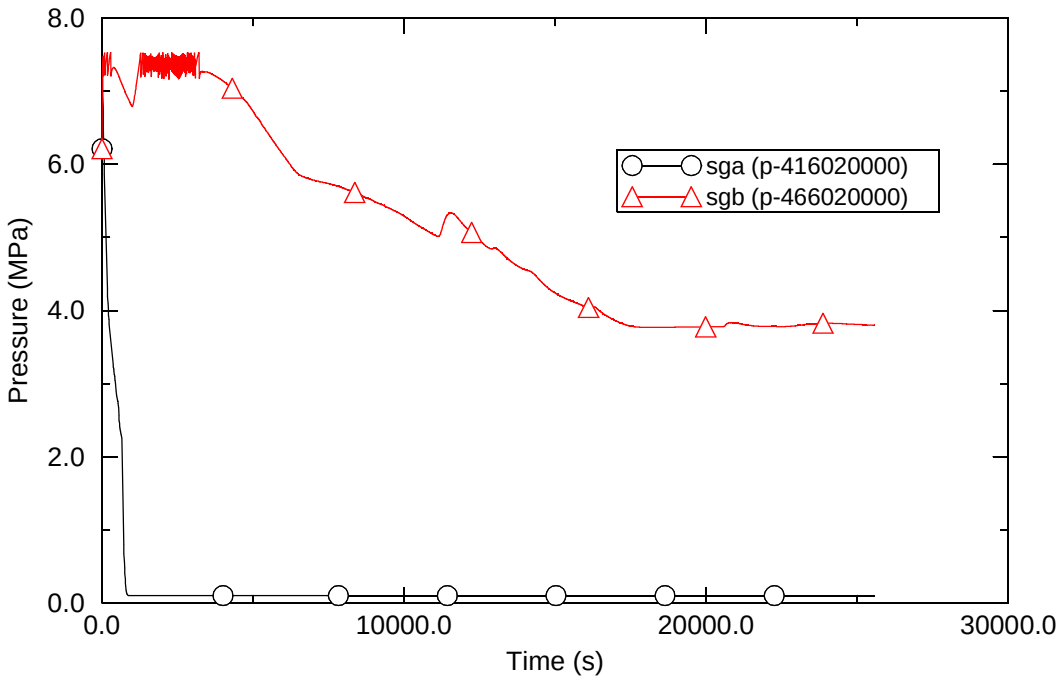

Figure C-2. Case 03 pressures in SGA (steam generator in primary coolant loop with pressurizer) and SGB (steam generator in primary coolant loop without pressurizer).

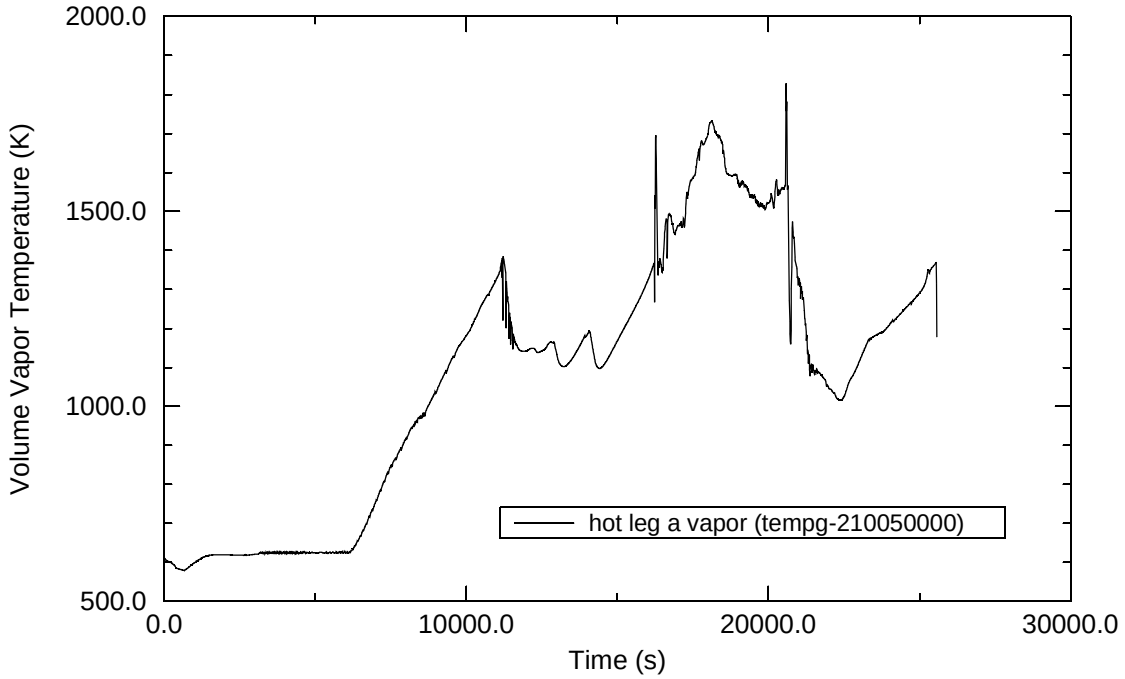

Figure C-3. Case 03 vapor temperature entering SGA inlet plenum from the "hot" part of the hot leg.

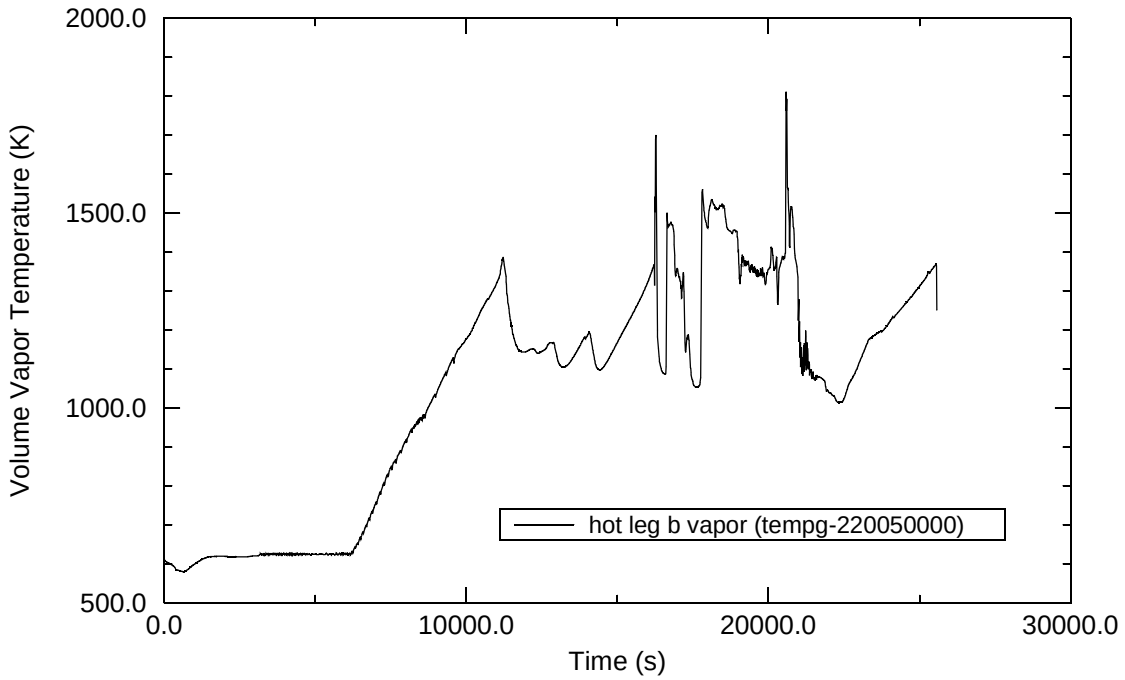

Figure C-4. Case 03 vapor temperature entering SGB inlet plenum from the "hot" part of the hot leg.

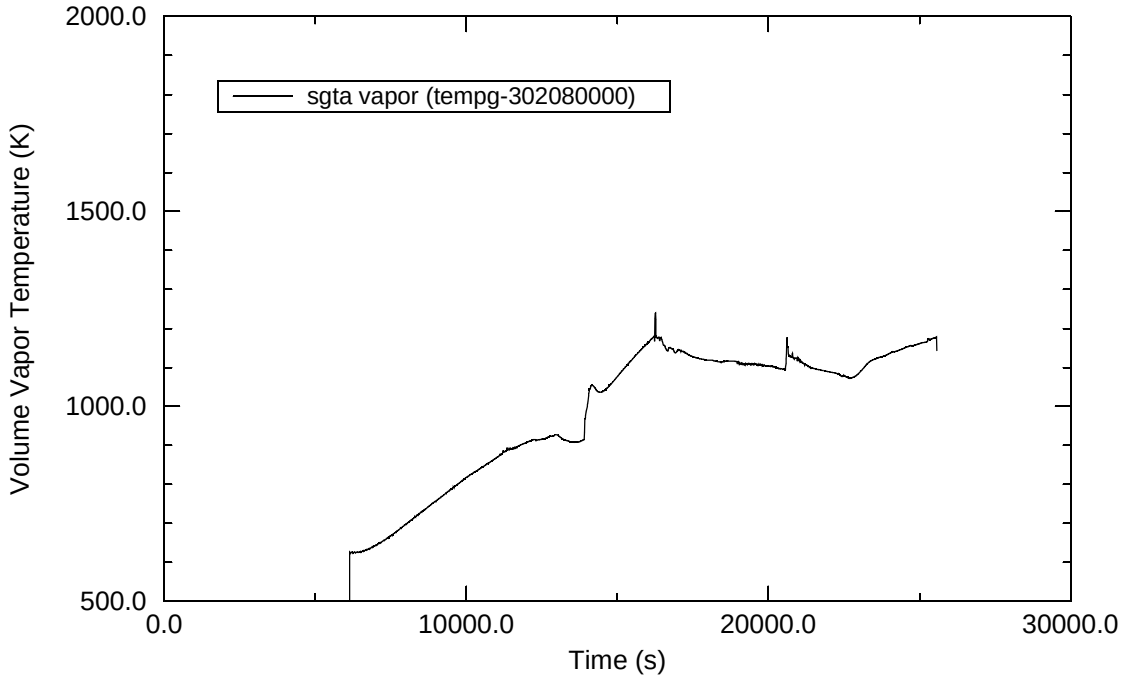

Figure C-5. Case 03 vapor temperature returning to SGA inlet plenum from the "cold" SG tube bundle.

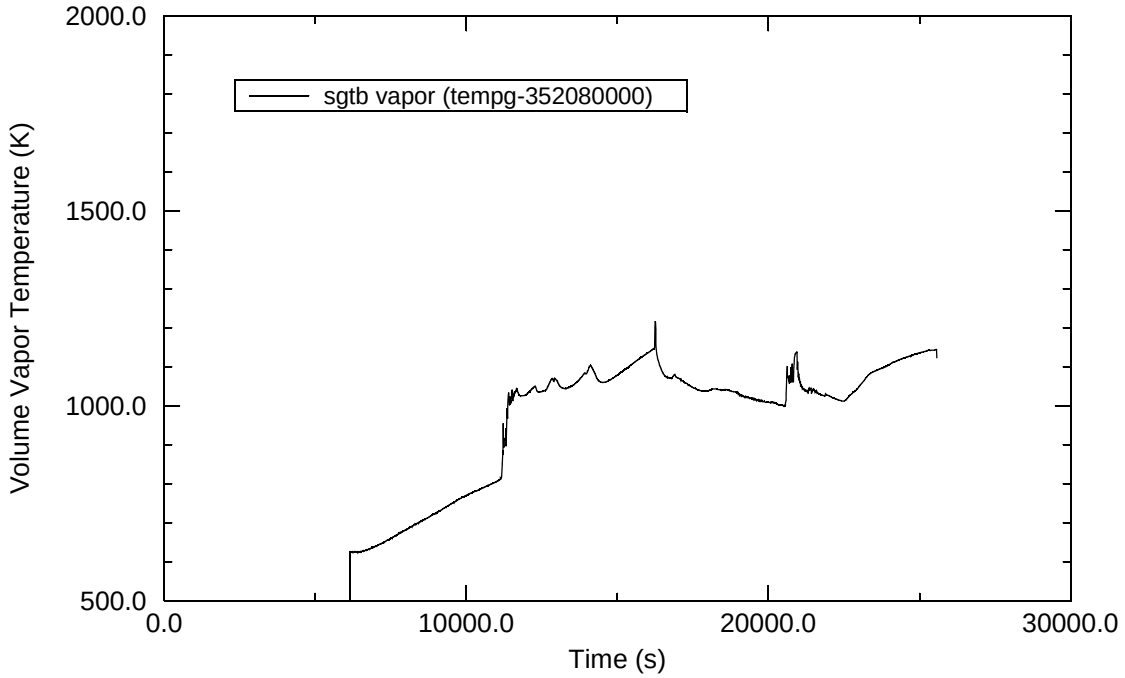

Figure C-6. Case 03 vapor temperature returning to SGB inlet plenum from the "cold" SG tube bundle.

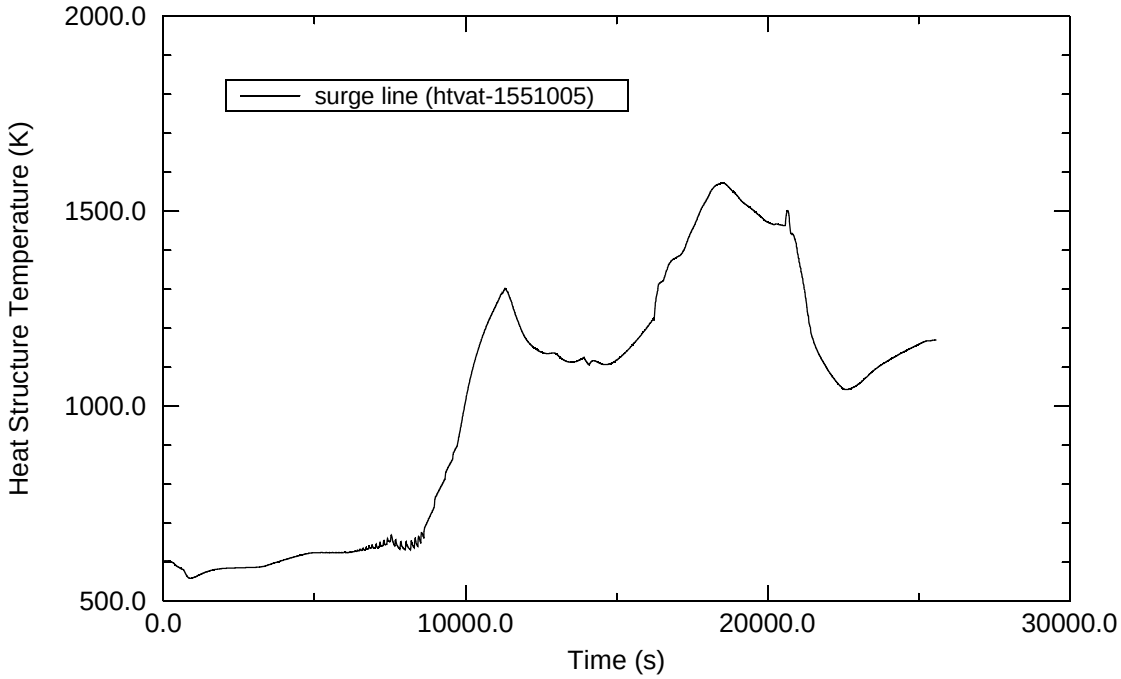

Figure C-7. Case 03 surge line temperature.

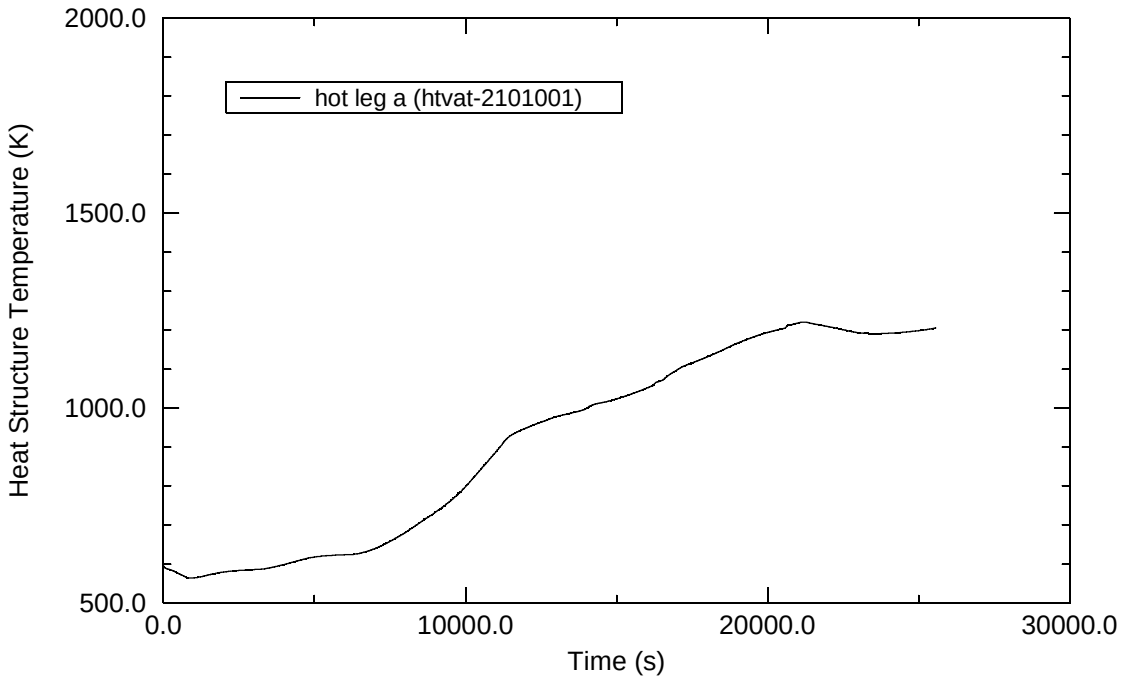

Figure C-8. Case 03 temperature of hot leg A (hot leg in primary coolant loop with pressurizer).

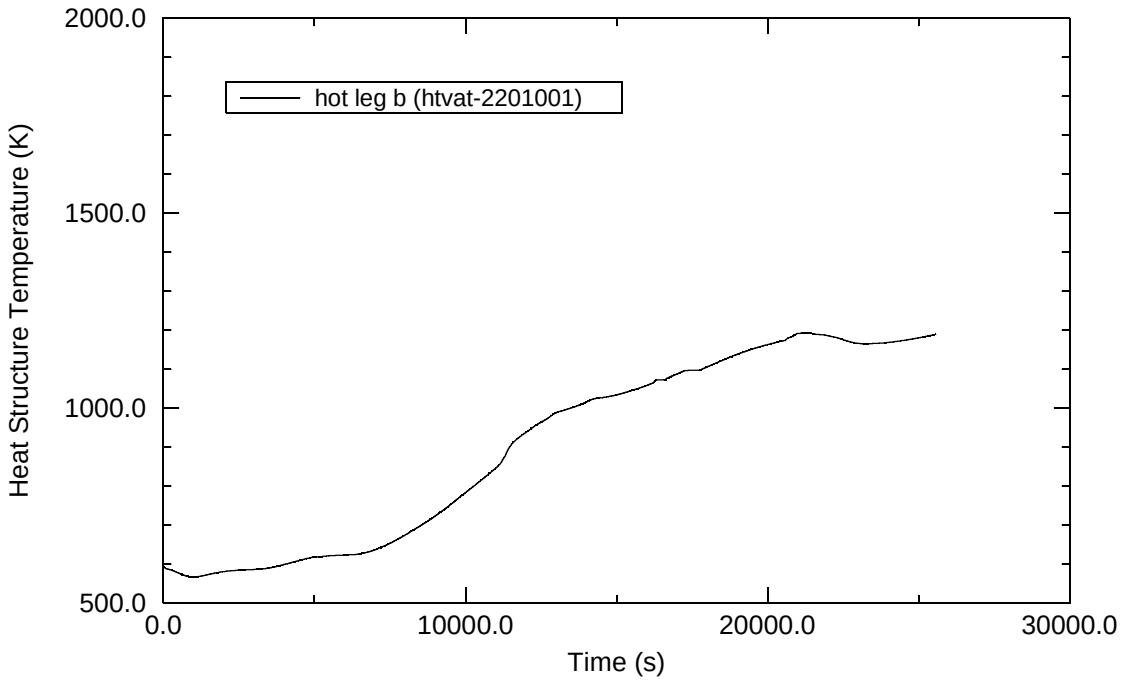

Figure C-9. Case 03 temperature of hot leg B (hot leg in primary coolant loop without pressurizer).

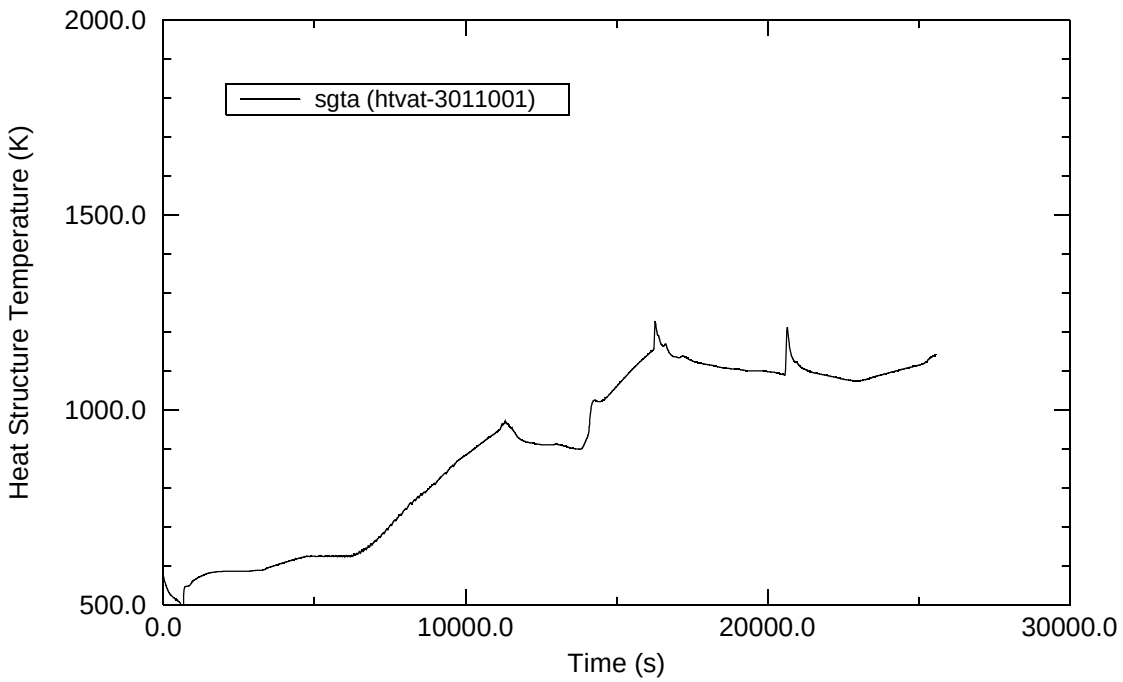

Figure C-10. Case 03 SGA tube temperature.

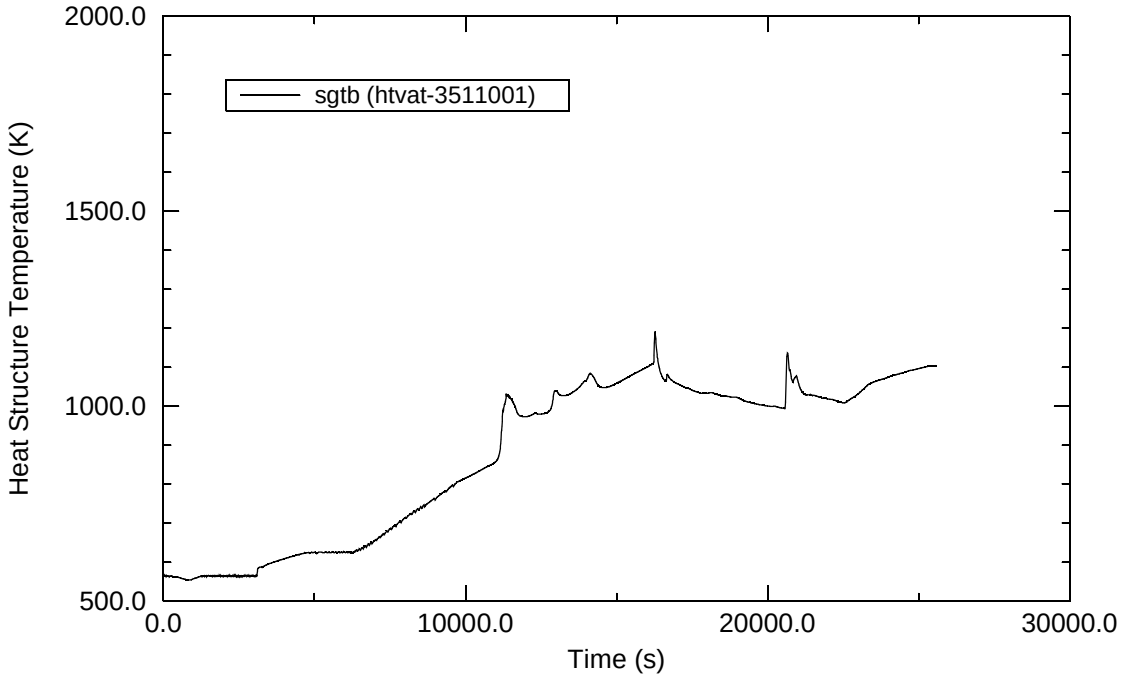

Figure C-11. Case 03 SGB tube temperature.

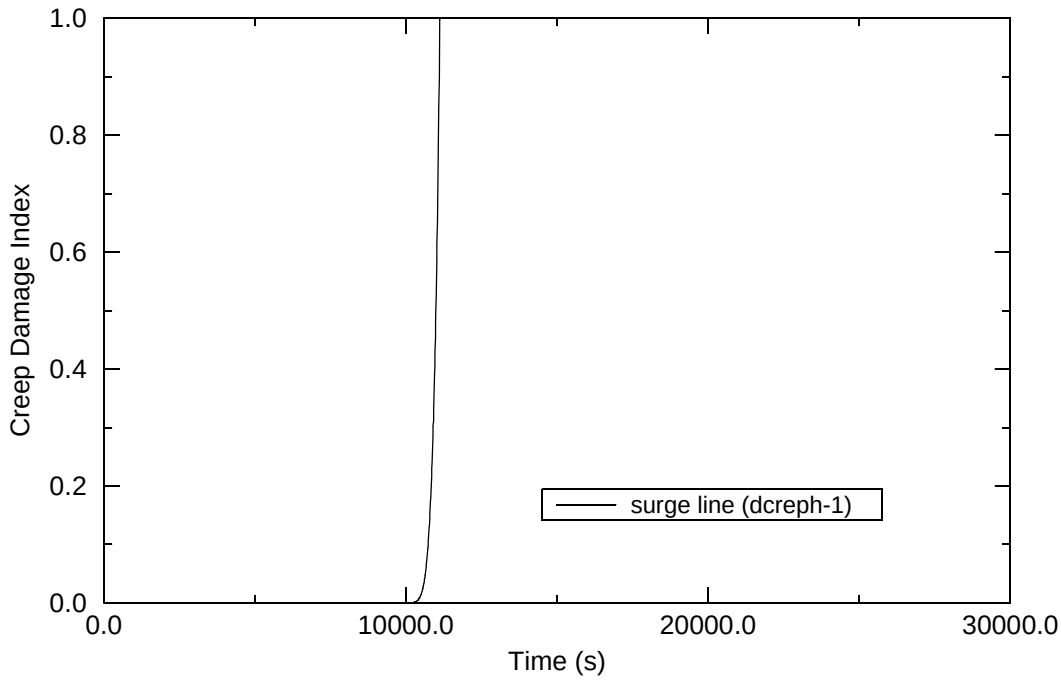

Figure C-12. Case 03 surge line creep damage index.

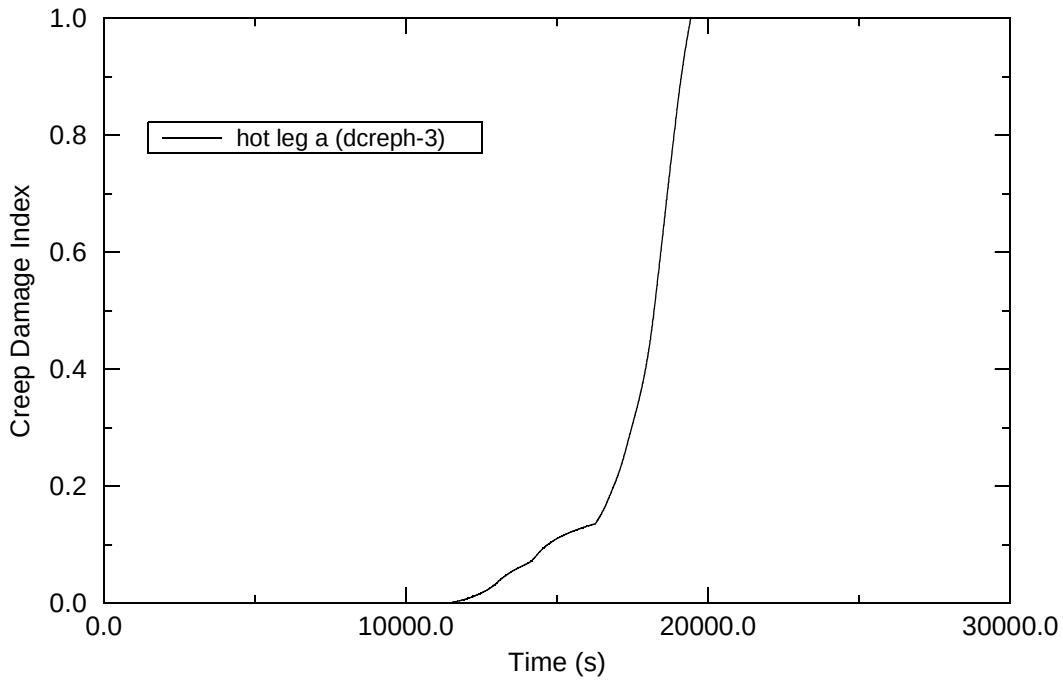

Figure C-13. Case 03 hot leg A creep damage index.

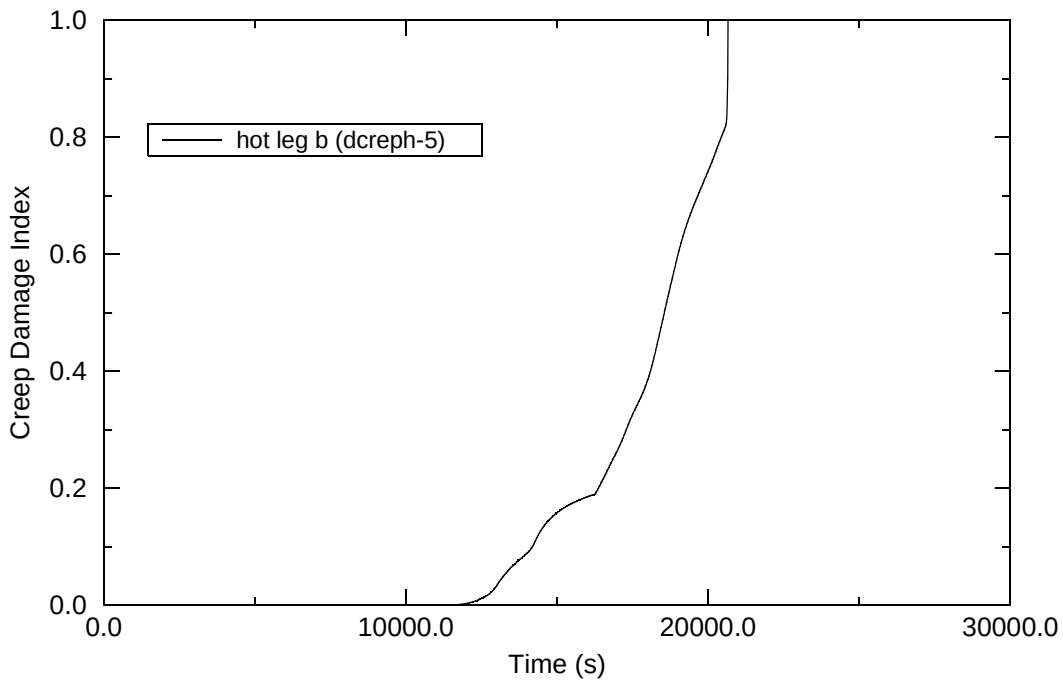

Figure C-14. Case 03 hot leg B creep damage index.

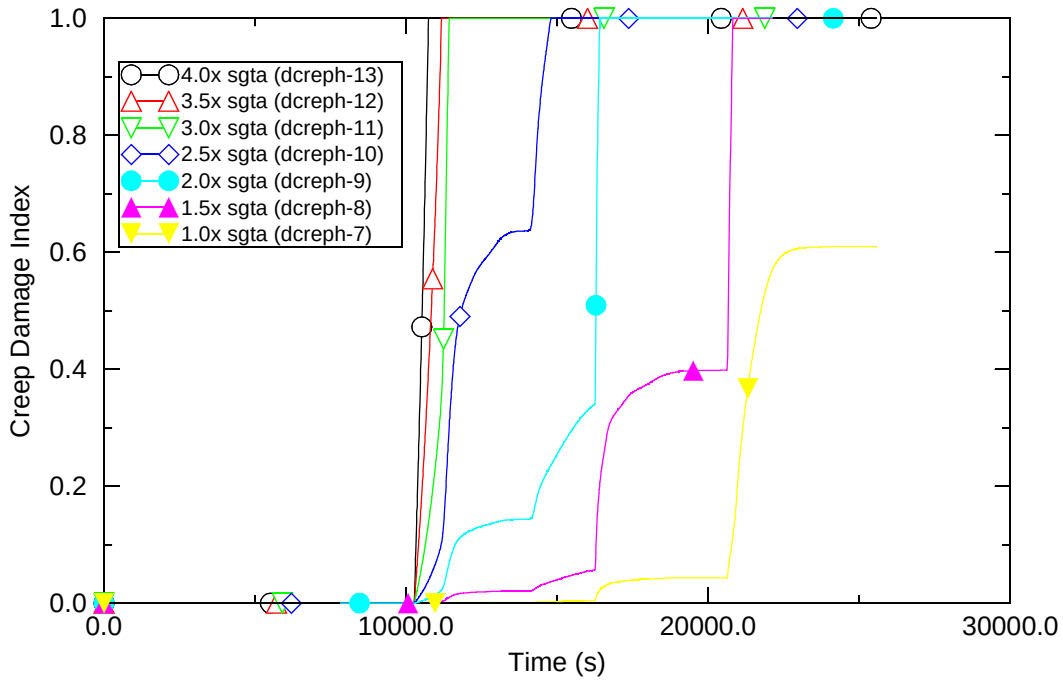

Figure C-15. Case 03 SGA tube creep damage indices.

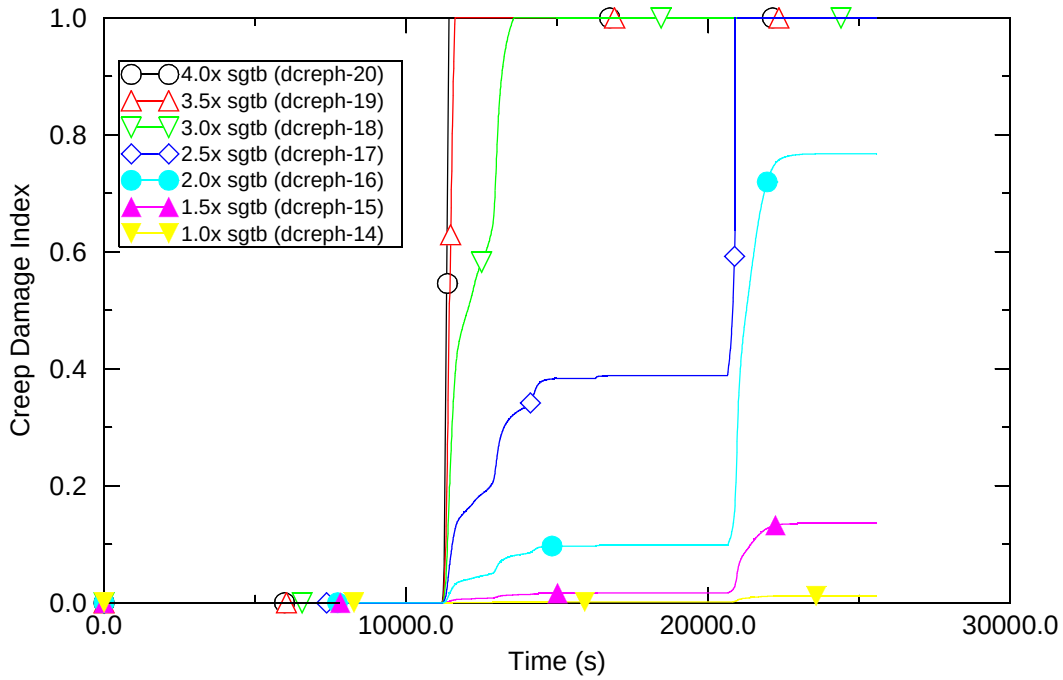

Figure C-16. Case 03 SGB tube creep damage indices.

Appendix D - Selected Results from Case 04

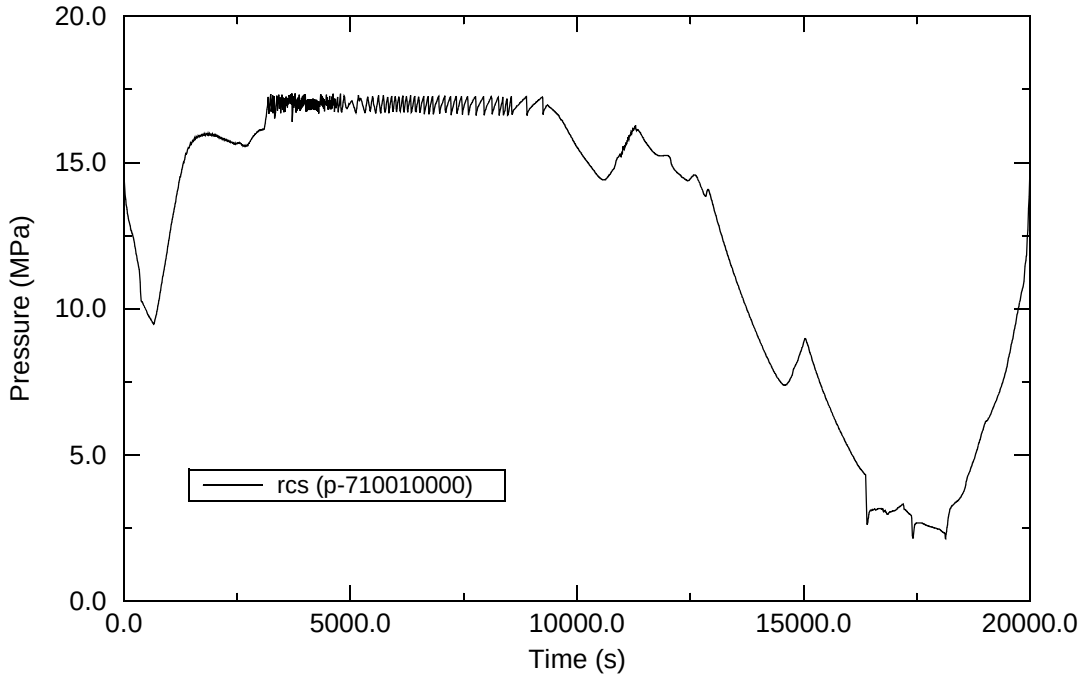

Figure D-1. Case 04 RCS (reactor coolant system) pressure.

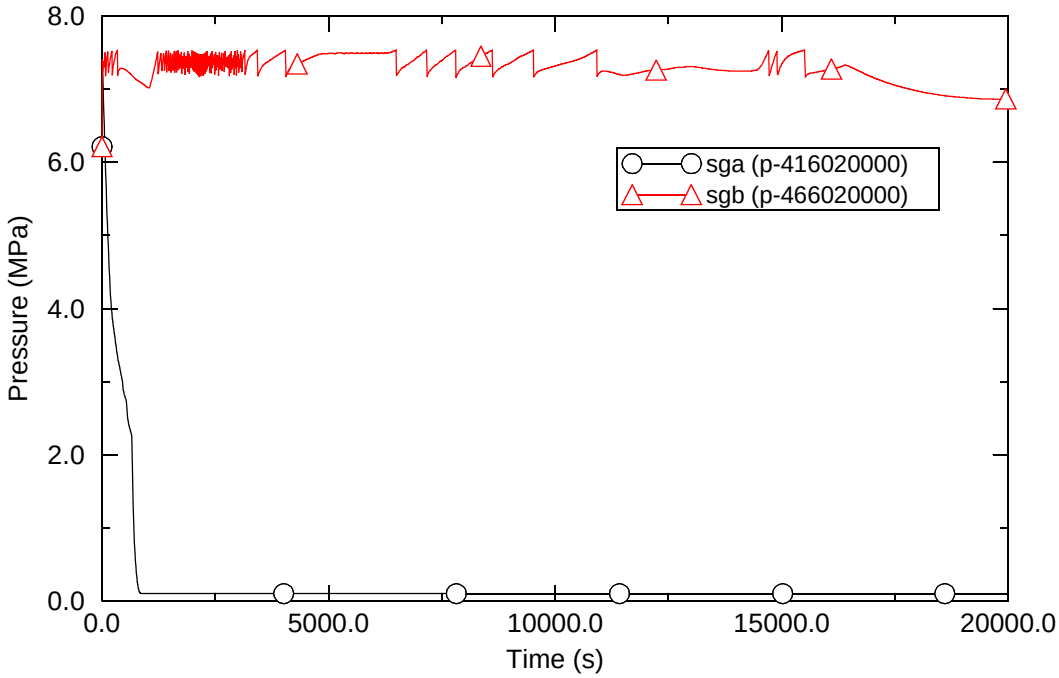

Figure D-2. Case 04 pressures in SGA (steam generator in primary coolant loop with pressurizer) and SGB (steam generator in primary coolant loop without pressurizer).

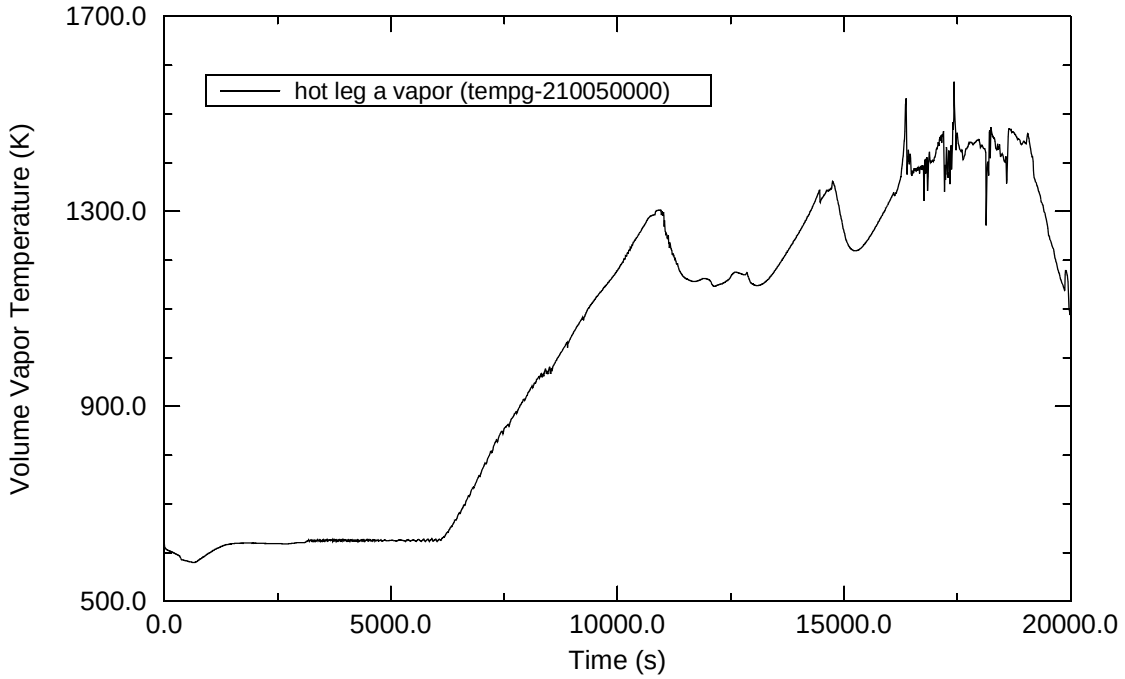

Figure D-3. Case 04 vapor temperature entering SGA inlet plenum from the "hot" part of the hot leg.

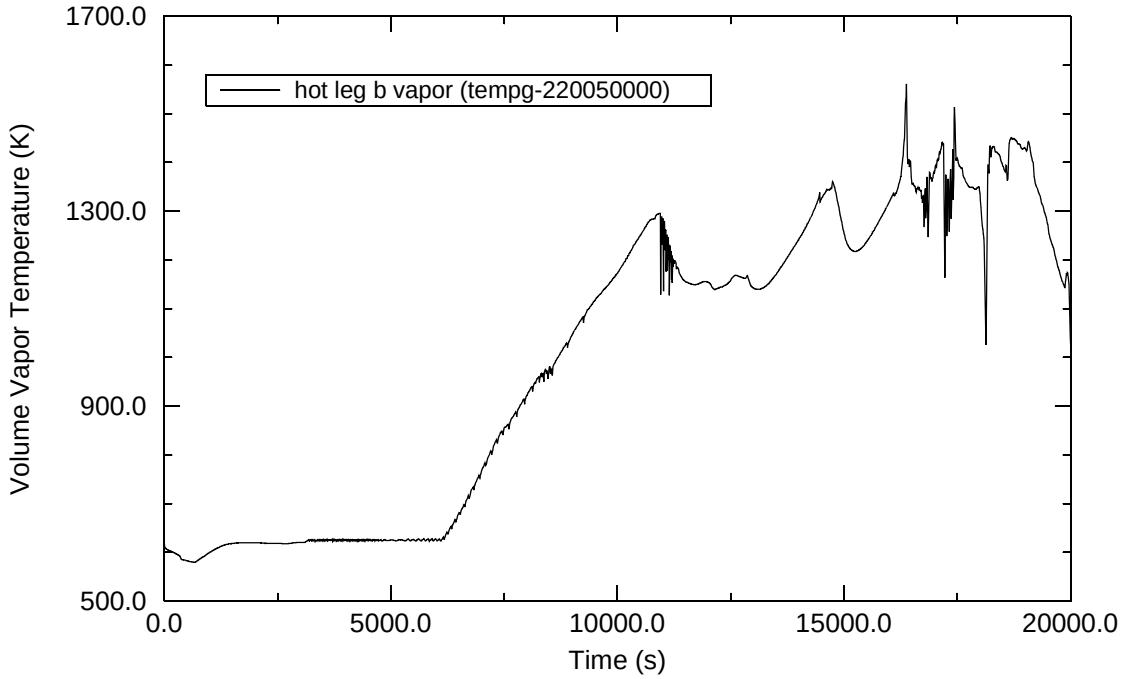

Figure D-4. Case 04 vapor temperature entering SGB inlet plenum from the "hot" part of the hot leg.

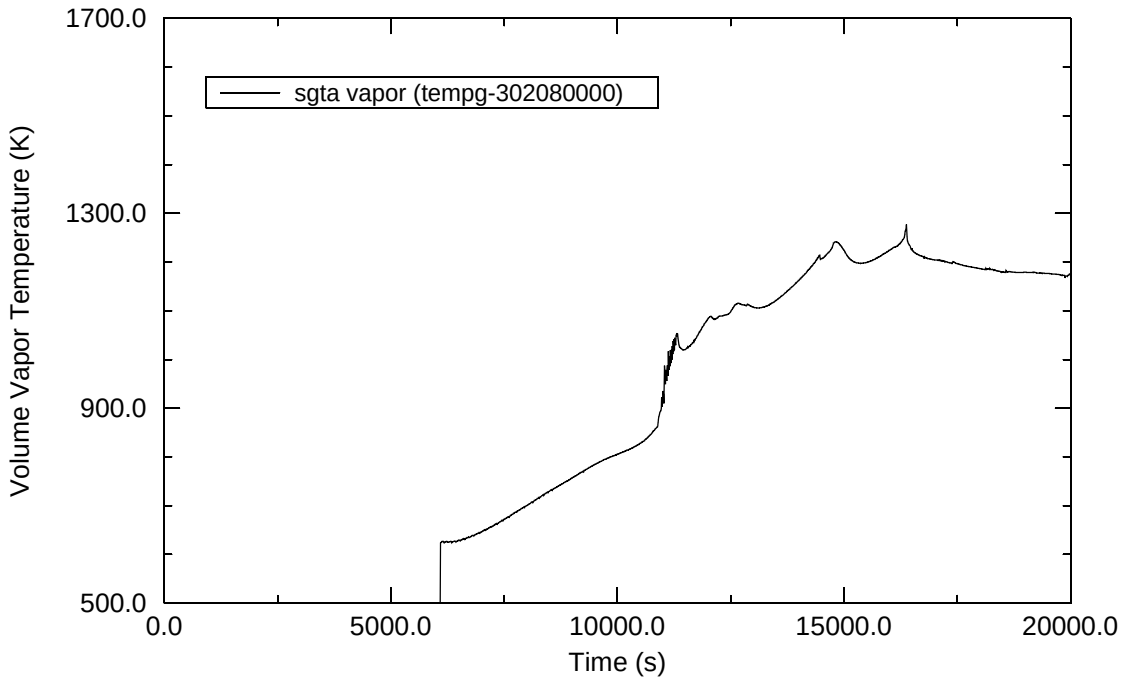

Figure D-5. Case 04 vapor temperature returning to SGA inlet plenum from the "cold" SG tube bundle.

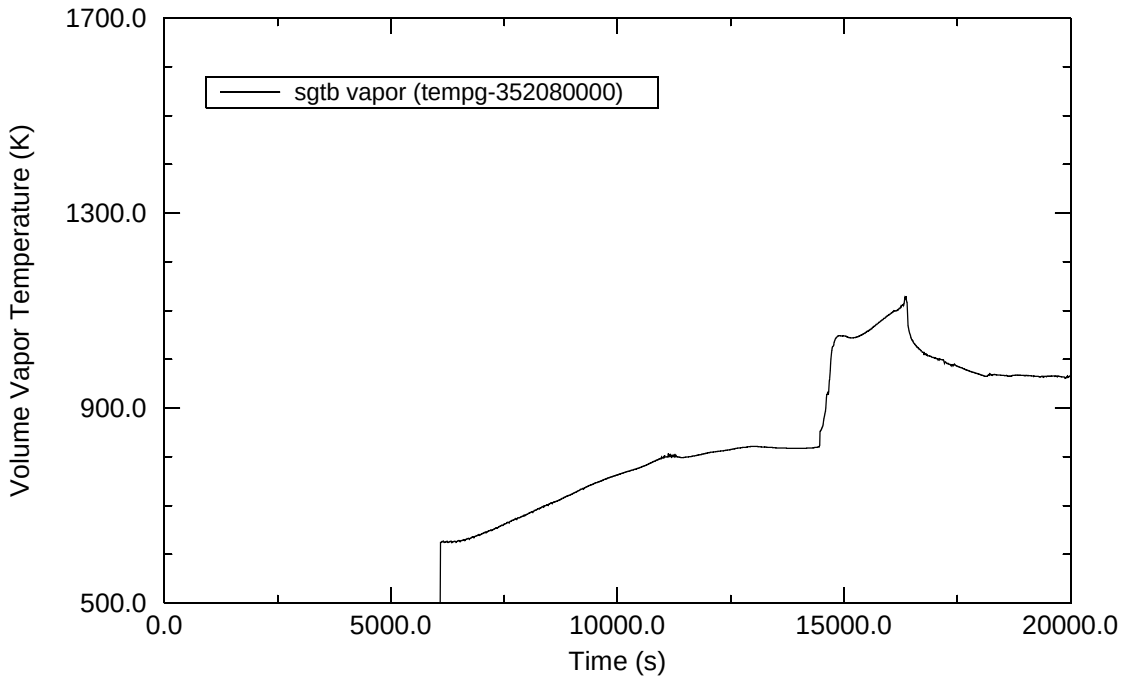

Figure D-6. Case 04 vapor temperature returning to SGB inlet plenum from the "cold" SG tube bundle.

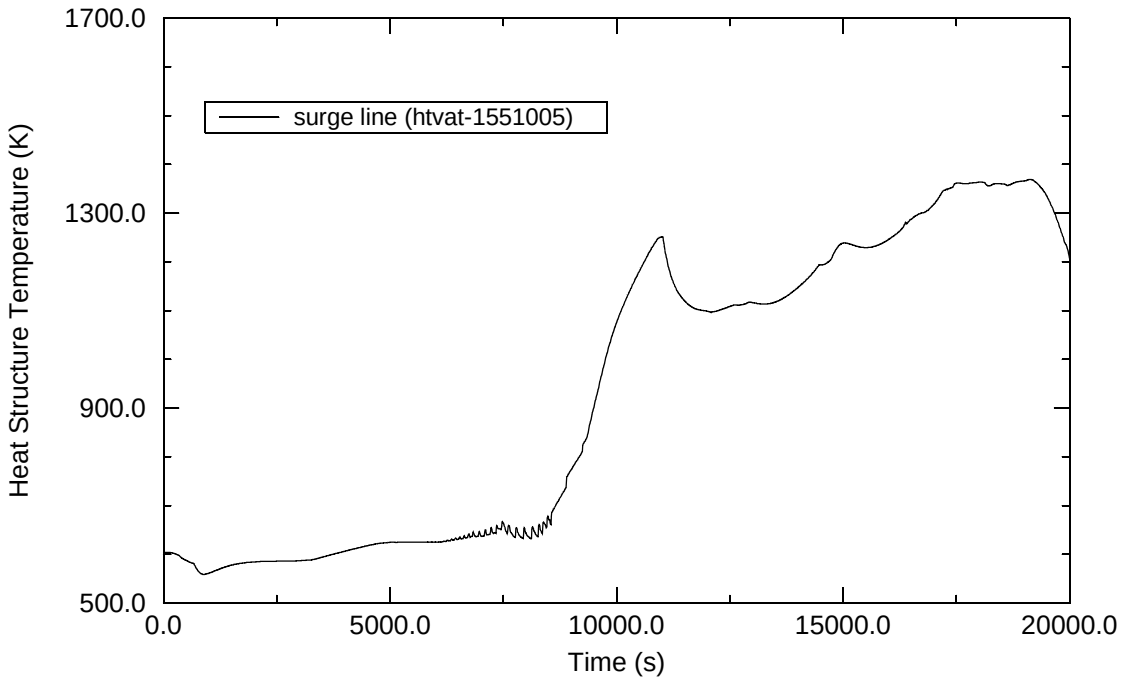

Figure D-7. Case 04 surge line temperature.

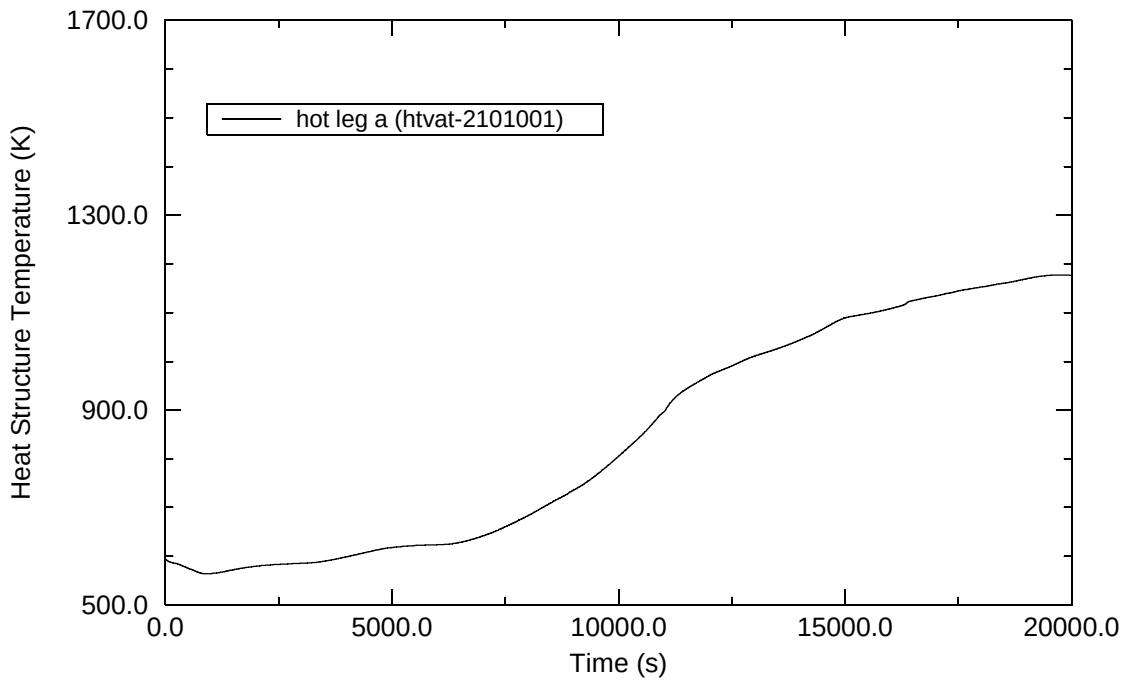

Figure D-8. Case 04 temperature of hot leg A (hot leg in primary coolant loop with pressurizer).

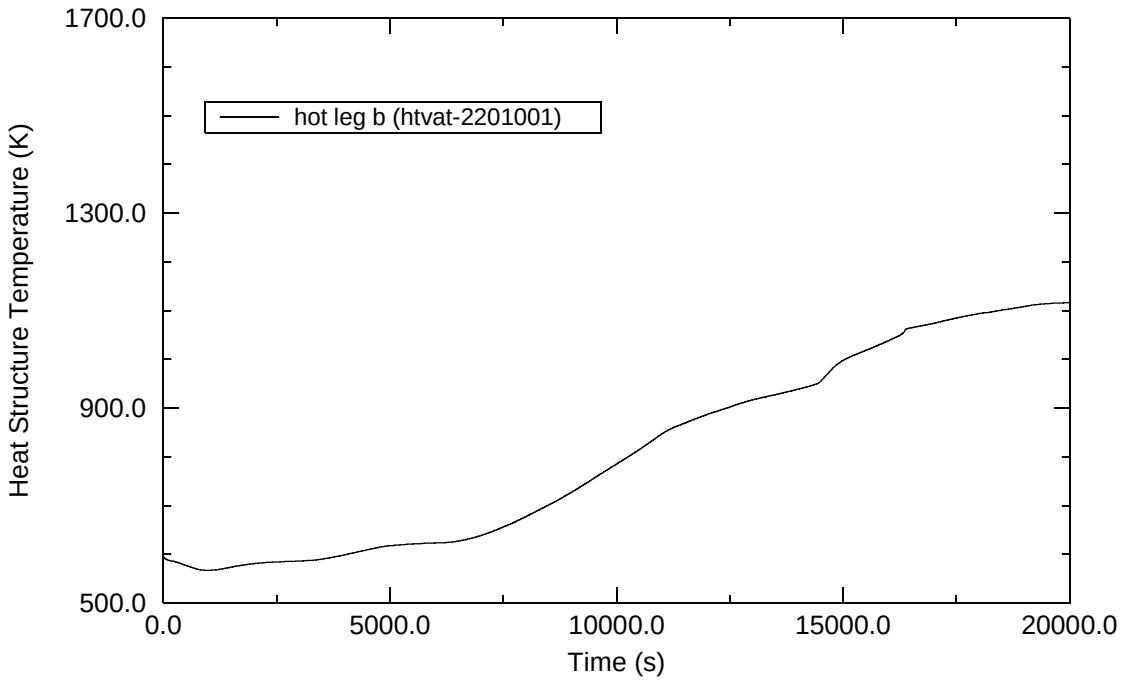

Figure D-9. Case 04 temperature of hot leg B (hot leg in primary coolant loop without pressurizer).

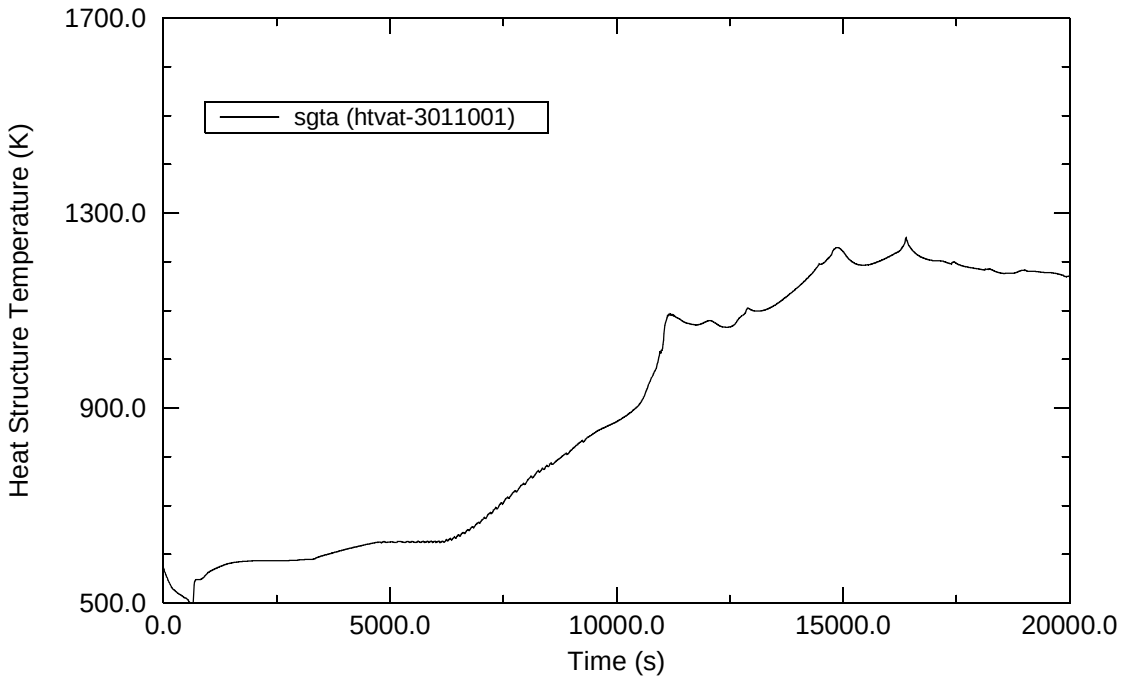

Figure D-10. Case 04 SGA tube temperature.

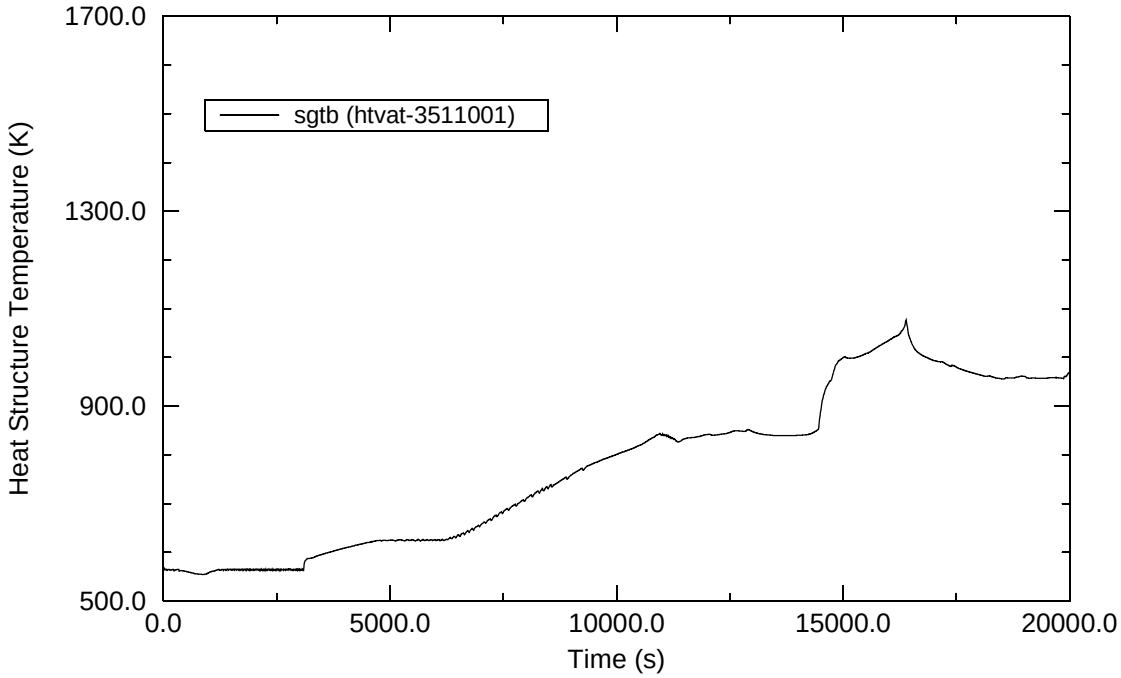

Figure D-11. Case 04 SGB tube temperature.

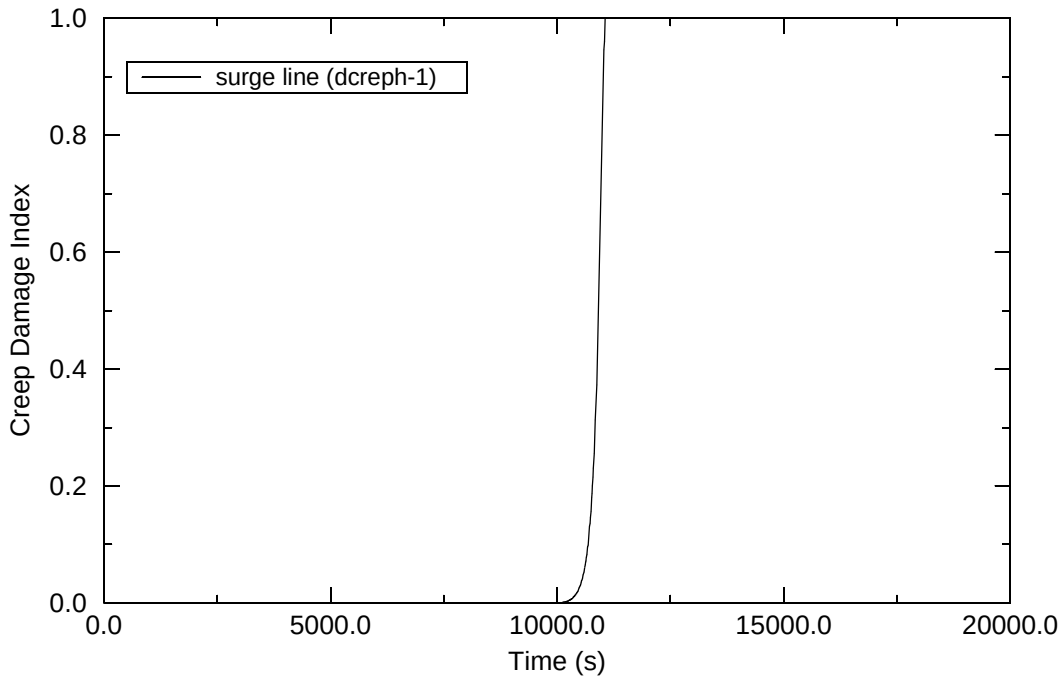

Figure D-12. Case 04 surge line creep damage index.

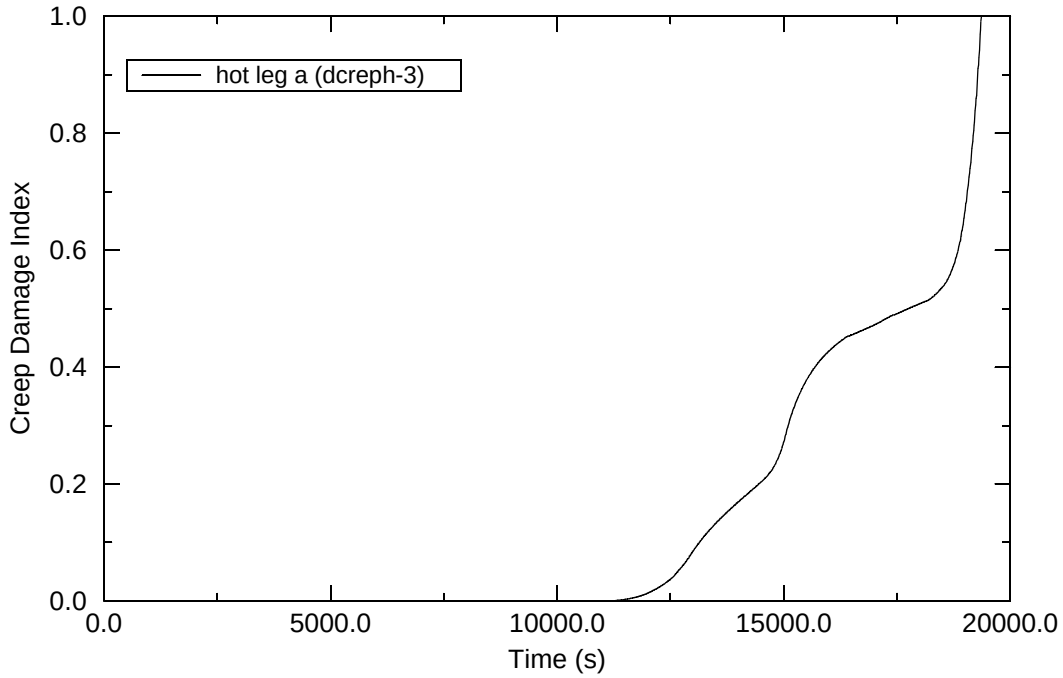

Figure D-13. Case 04 hot leg A creep damage index.

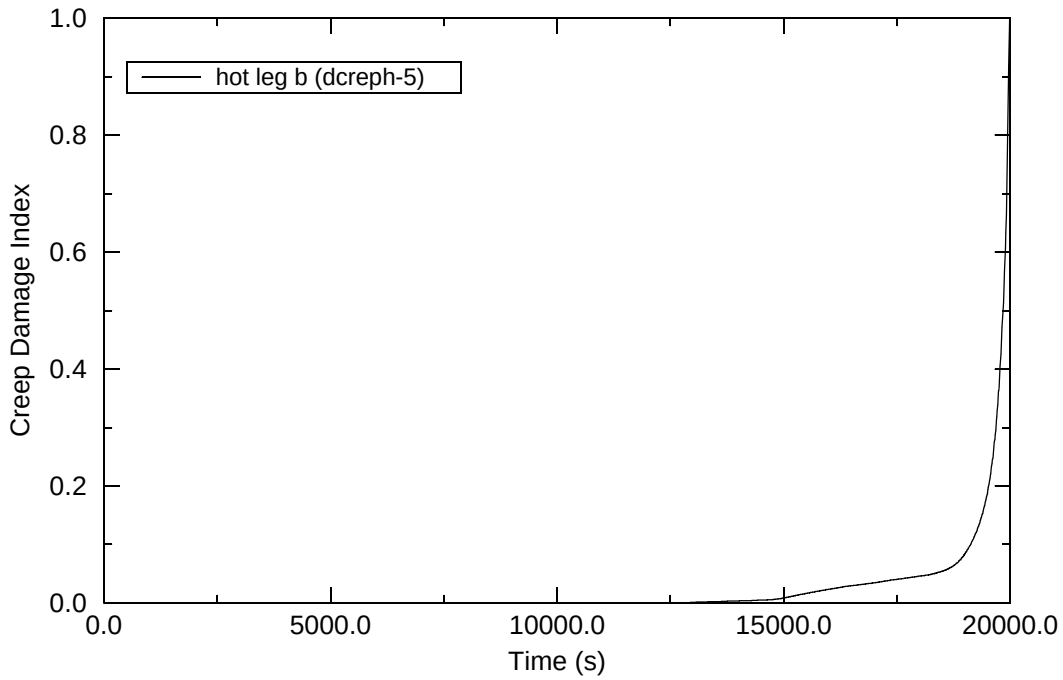

Figure D-14. Case 04 hot leg B creep damage index.

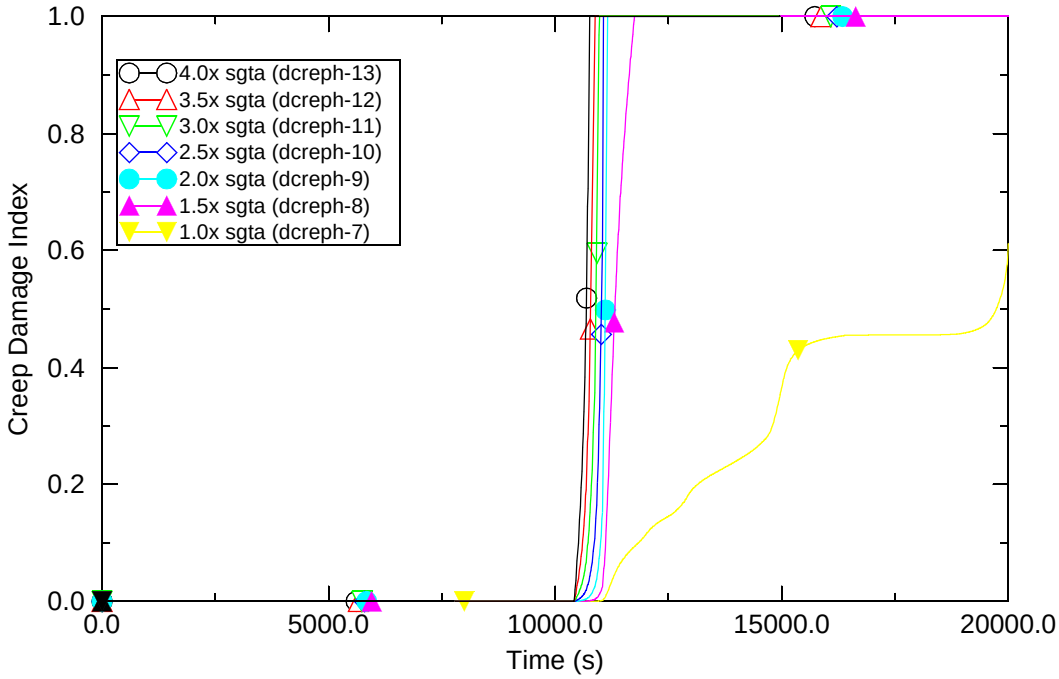

Figure D-15. Case 04 SGA tube creep damage indices.

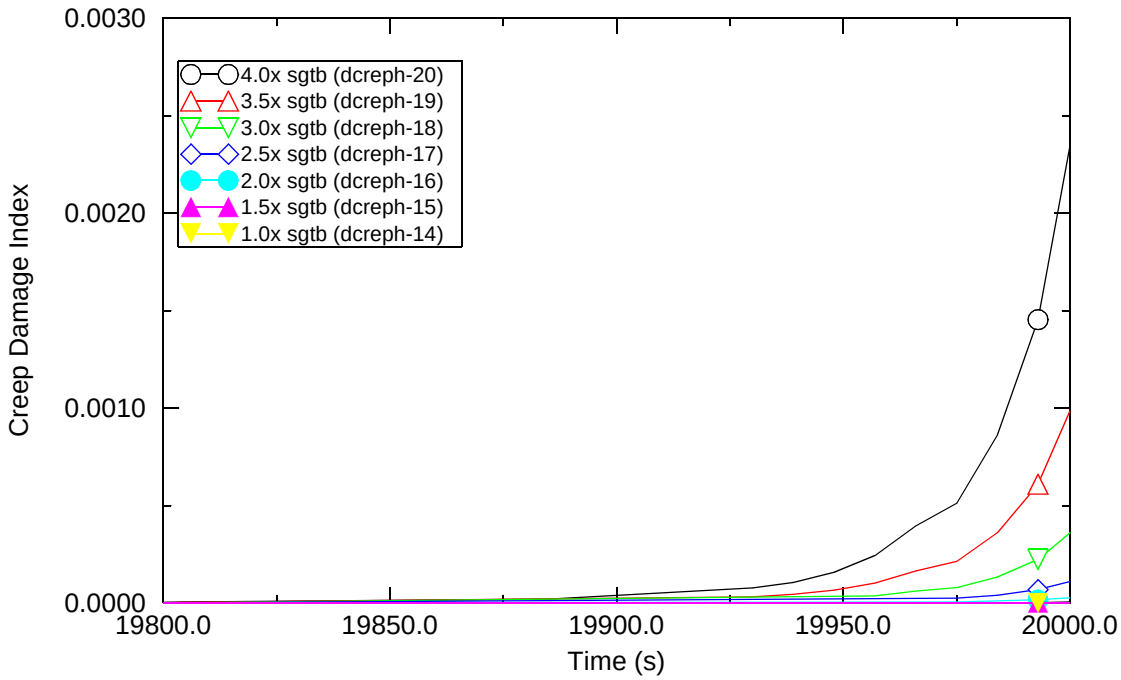

Figure D-16. Case 04 SGB tube creep damage indices.

Appendix E - Selected Results from Case 05

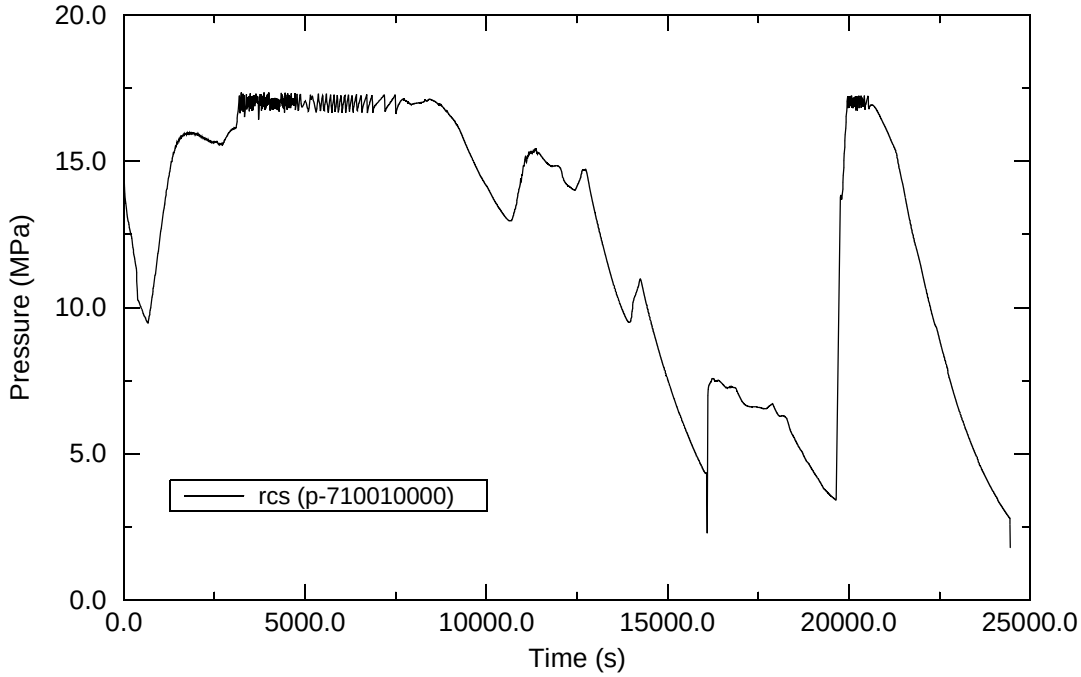

Figure E-1. Case 05 RCS (reactor coolant system) pressure.

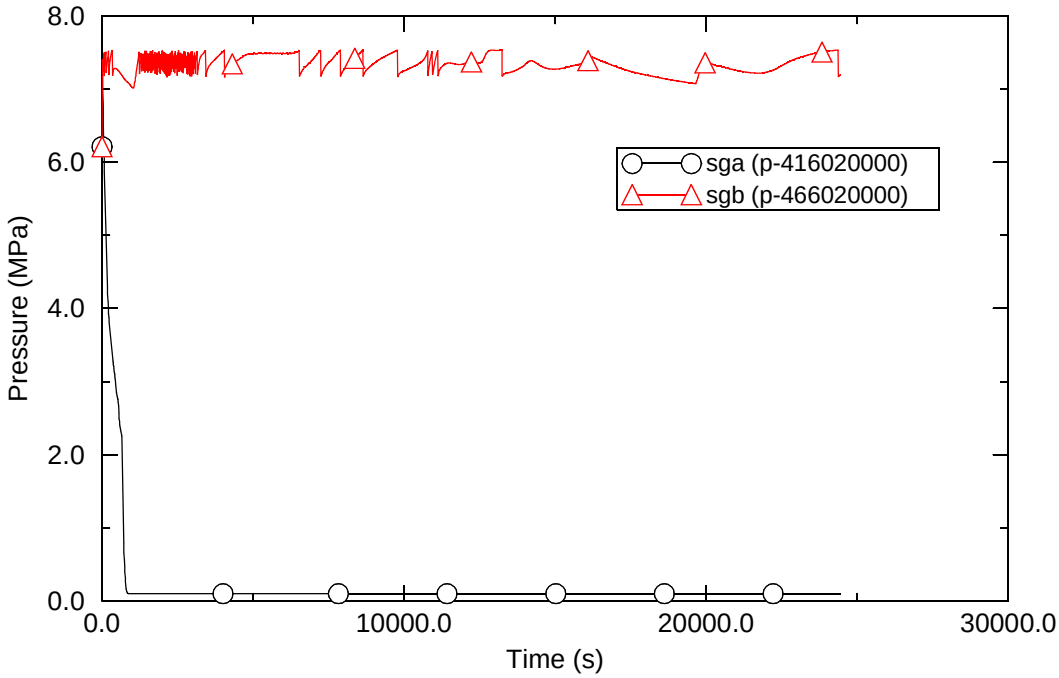

Figure E-2. Case 05 pressures in SGA (steam generator in primary coolant loop with pressurizer) and SGB (steam generator in primary coolant loop without pressurizer).

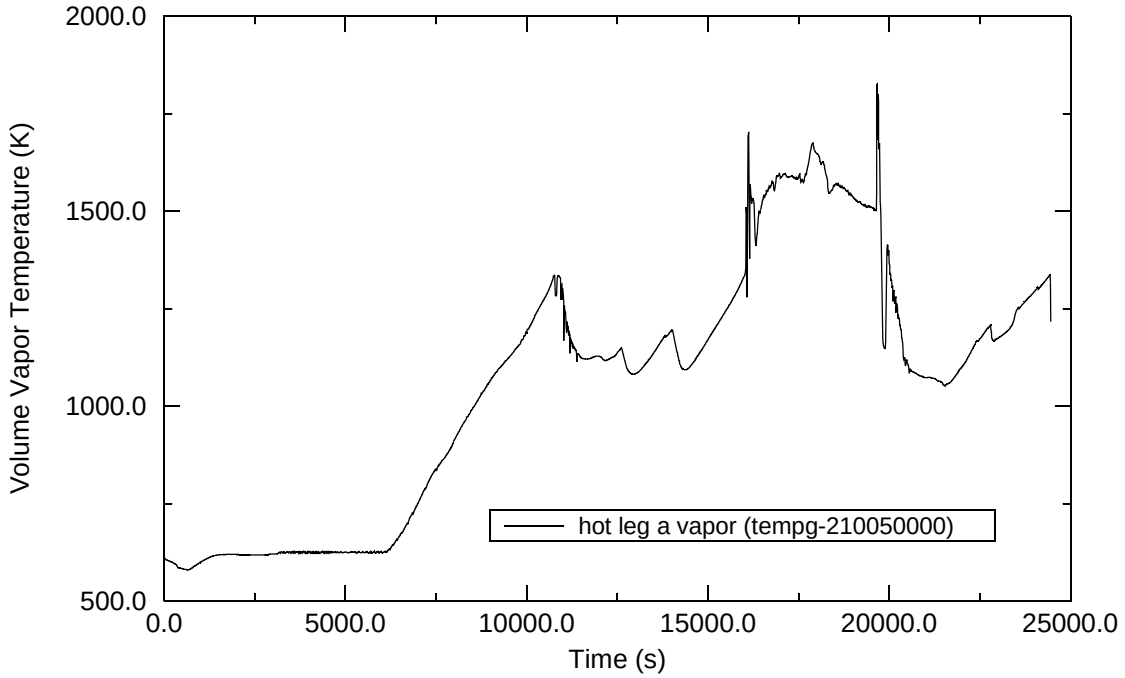

Figure E-3. Case 05 vapor temperature entering SGA inlet plenum from the "hot" part of the hot leg.

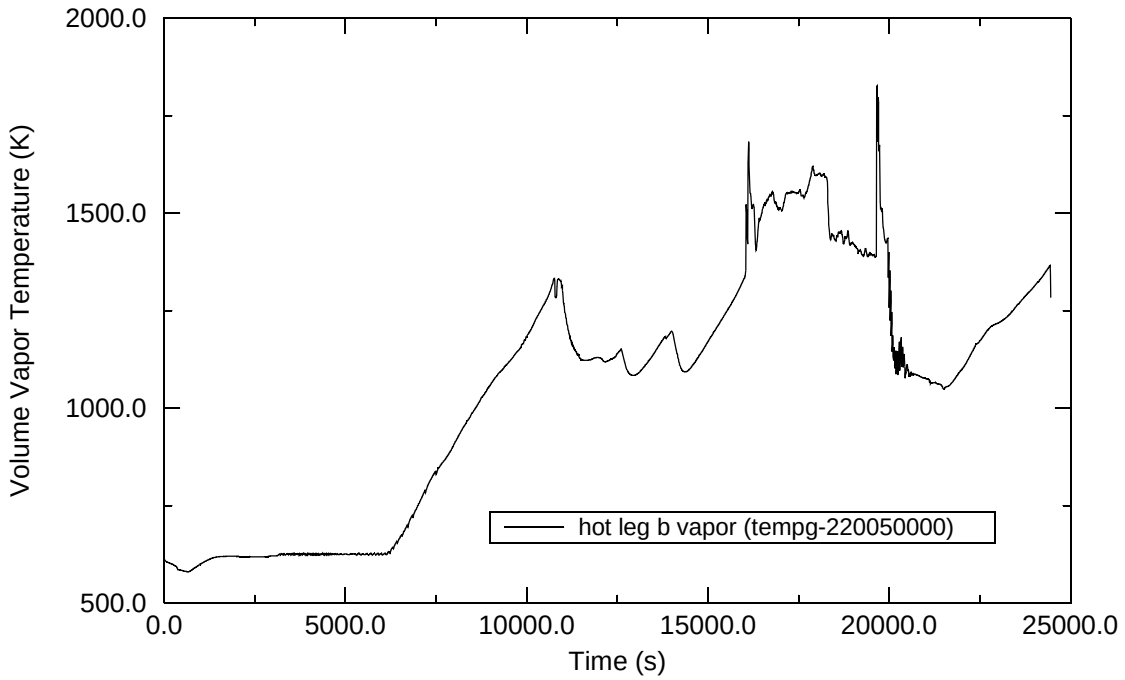

Figure E-4. Case 05 vapor temperature entering SGB inlet plenum from the "hot" part of the hot leg.

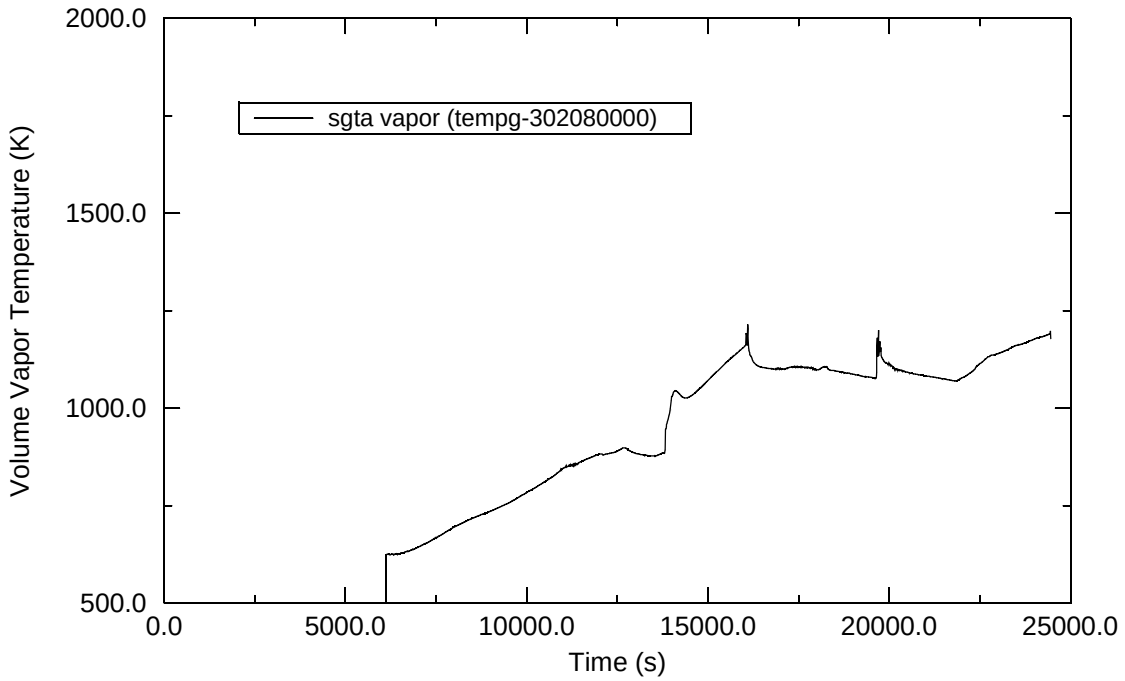

Figure E-5. Case 05 vapor temperature returning to SGA inlet plenum from the "cold" SG tube bundle.

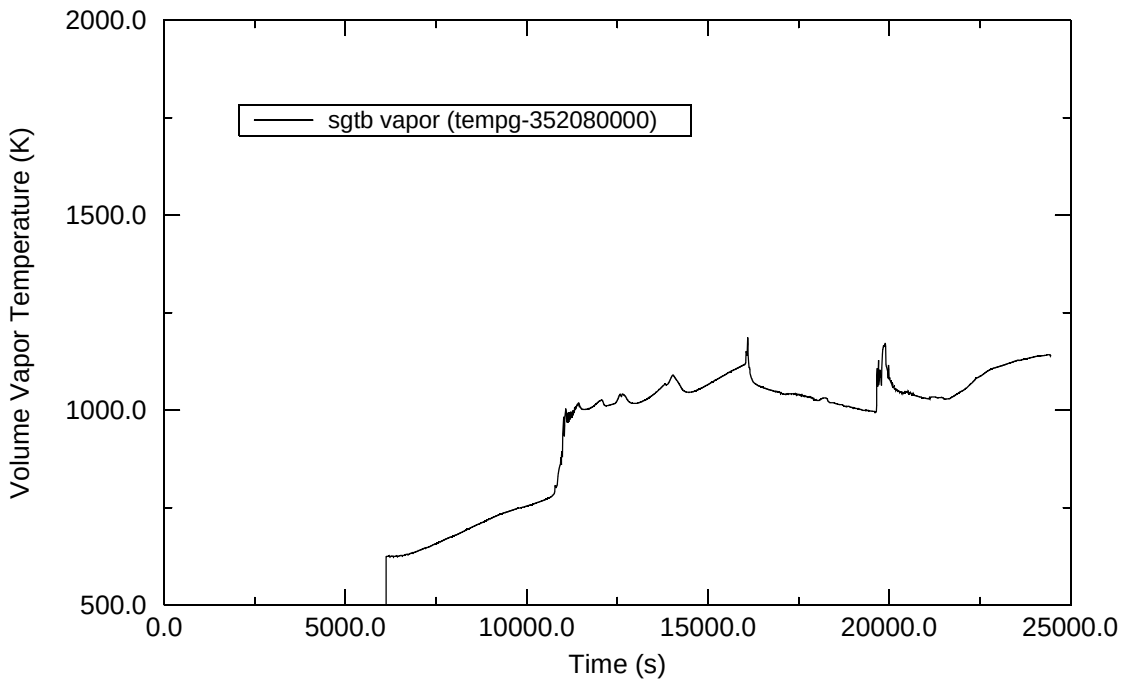

Figure E-6. Case 05 vapor temperature returning to SGB inlet plenum from the "cold" SG tube bundle.

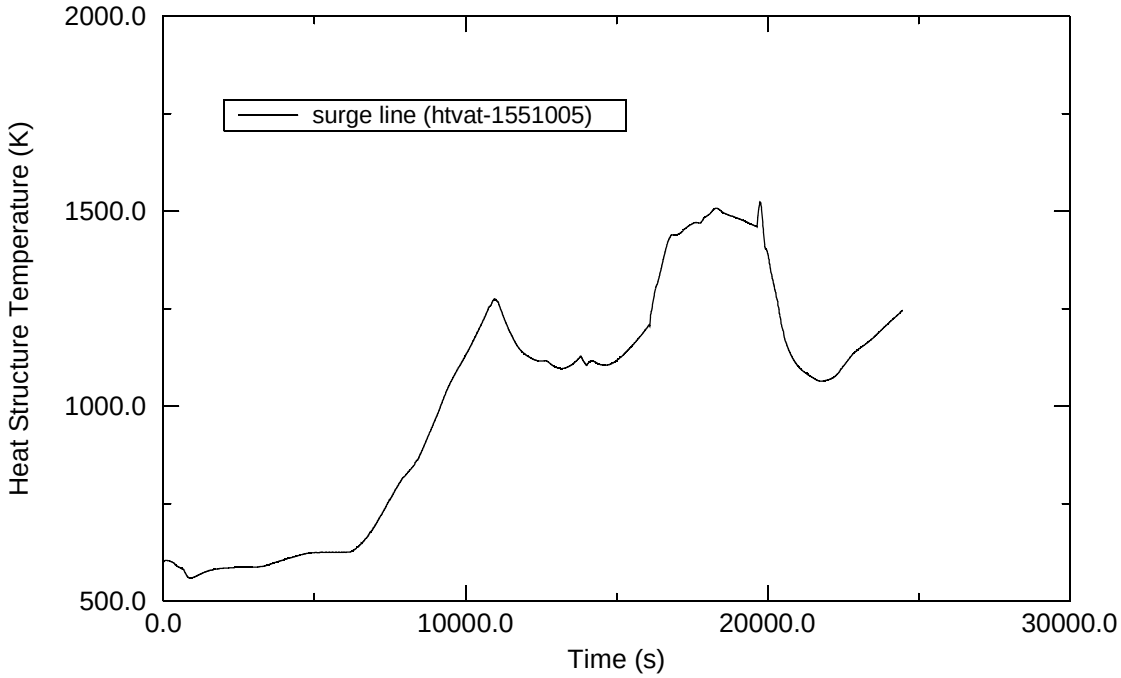

Figure E-7. Case 05 surge line temperature.

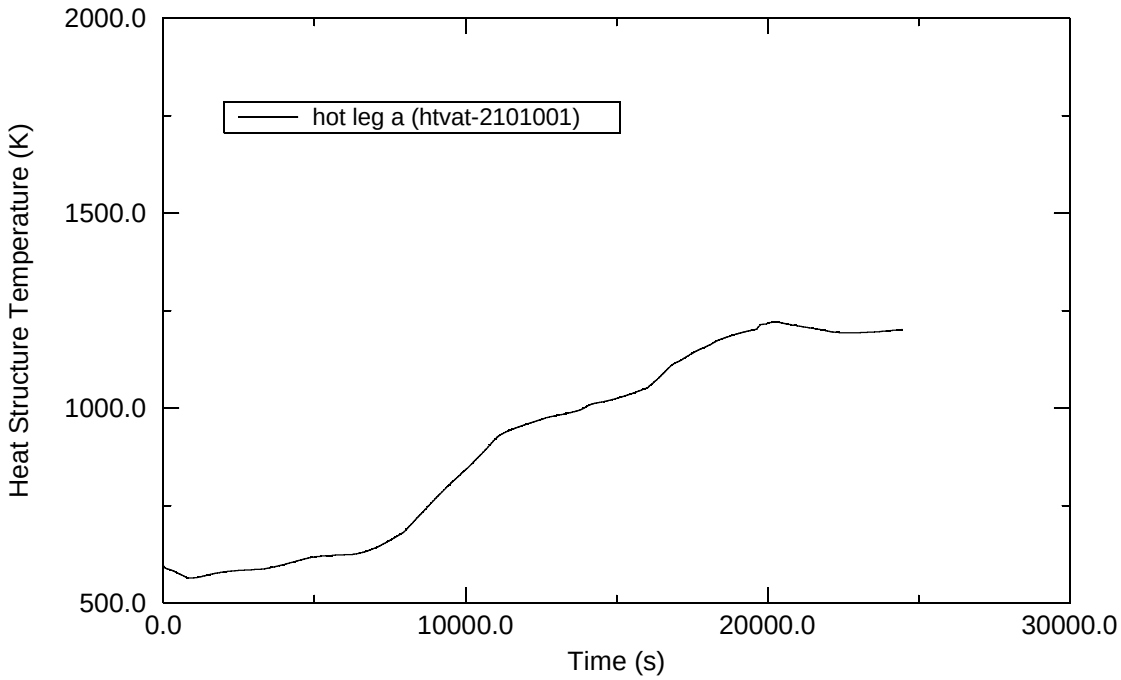

Figure E-8. Case 05 temperature of hot leg A (hot leg in primary coolant loop with pressurizer).

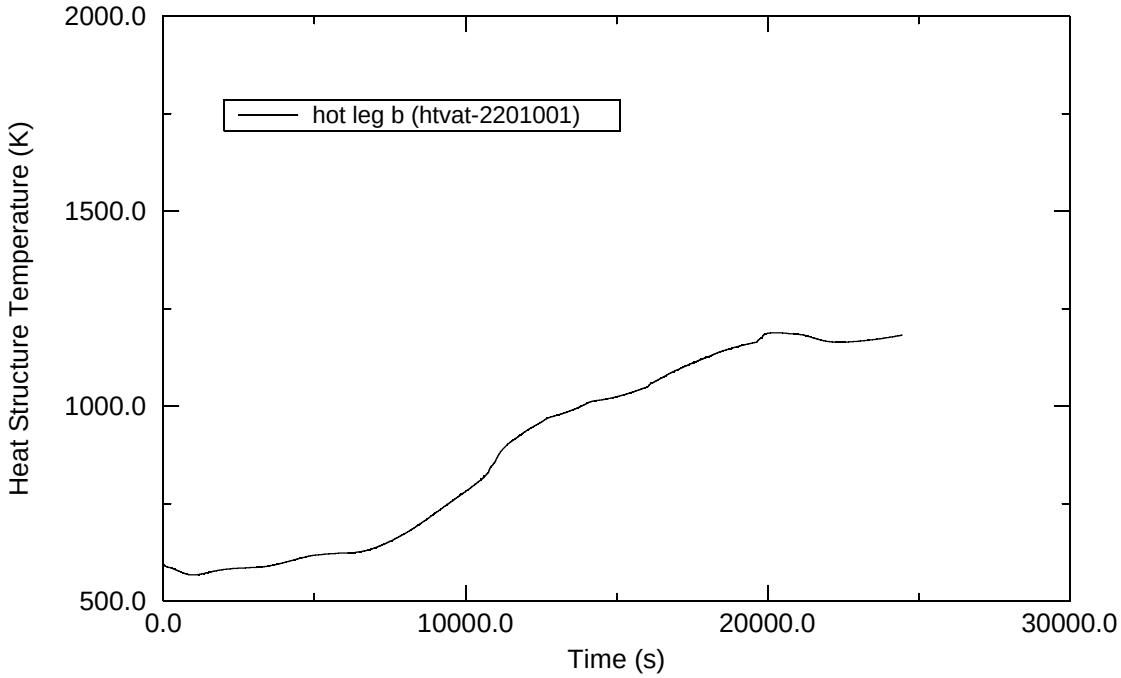

Figure E-9. Case 05 temperature of hot leg B (hot leg in primary coolant loop without pressurizer).

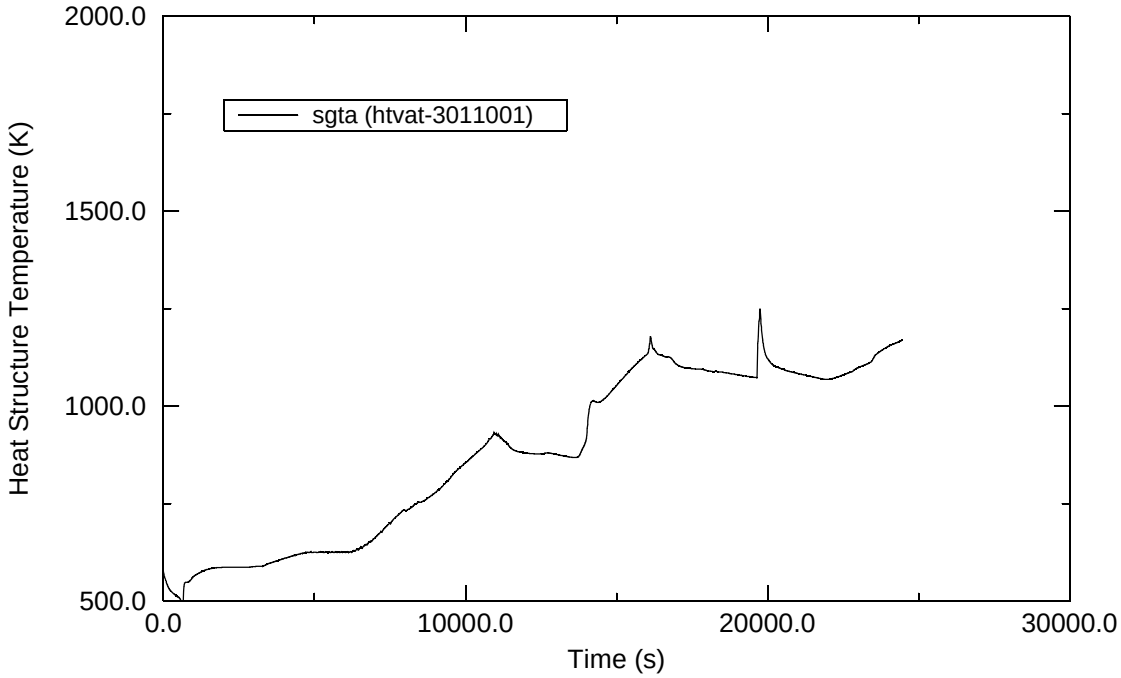

Figure E-10. Case 05 SGA tube temperature.

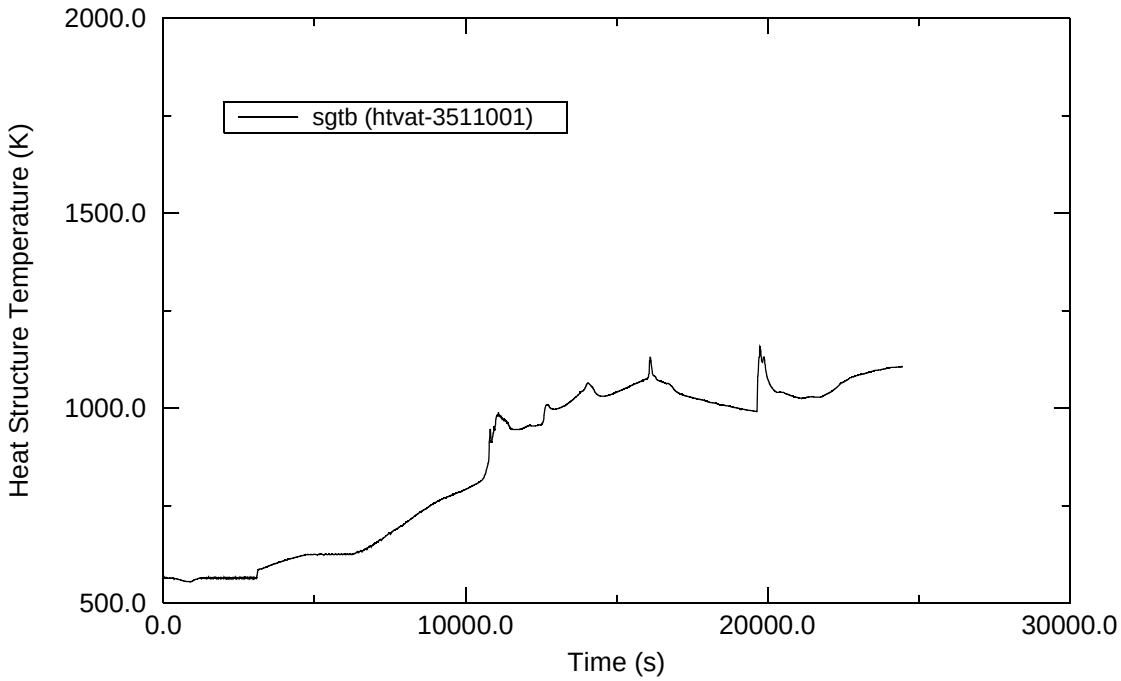

Figure E-11. Case 05 SGB tube temperature.

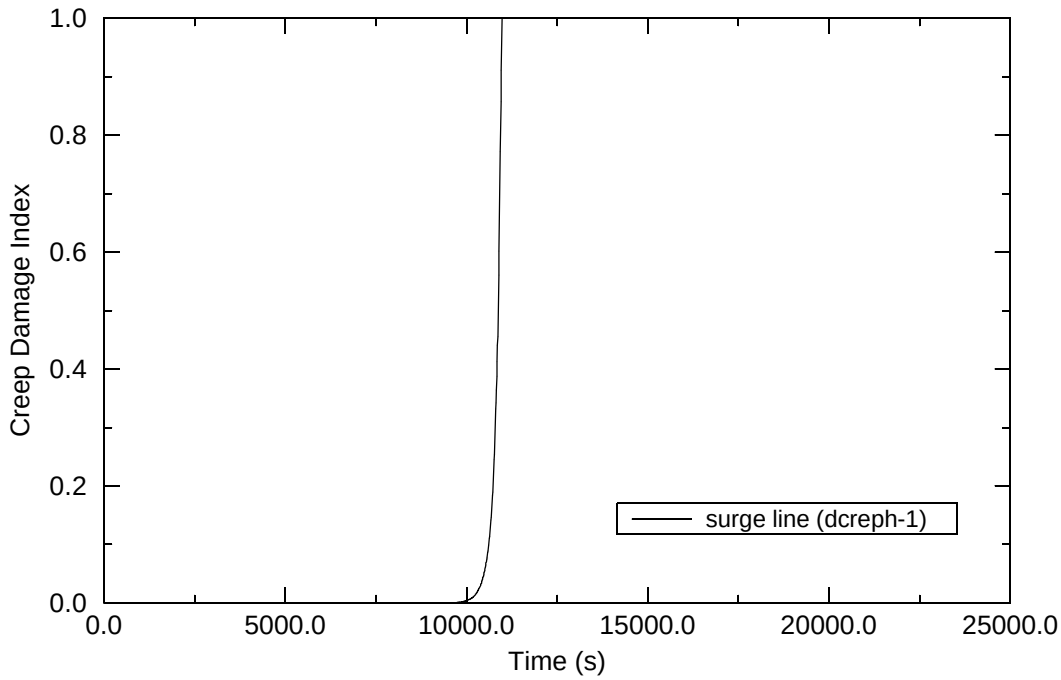

Figure E-12. Case 05 surge line creep damage index.

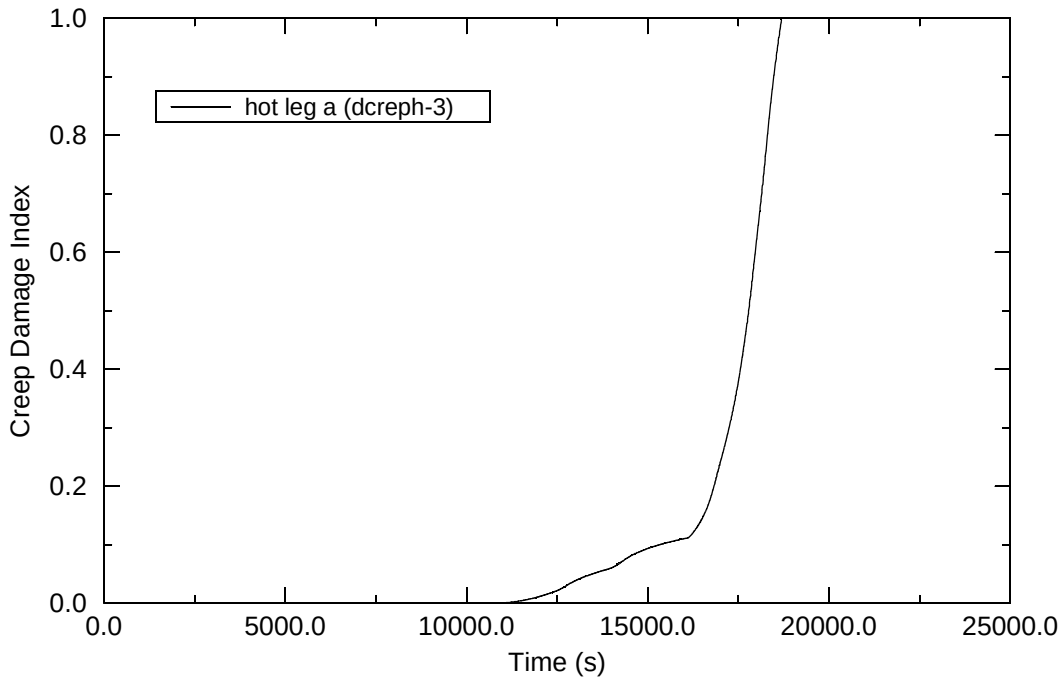

Figure E-13. Case 05 hot leg A creep damage index.

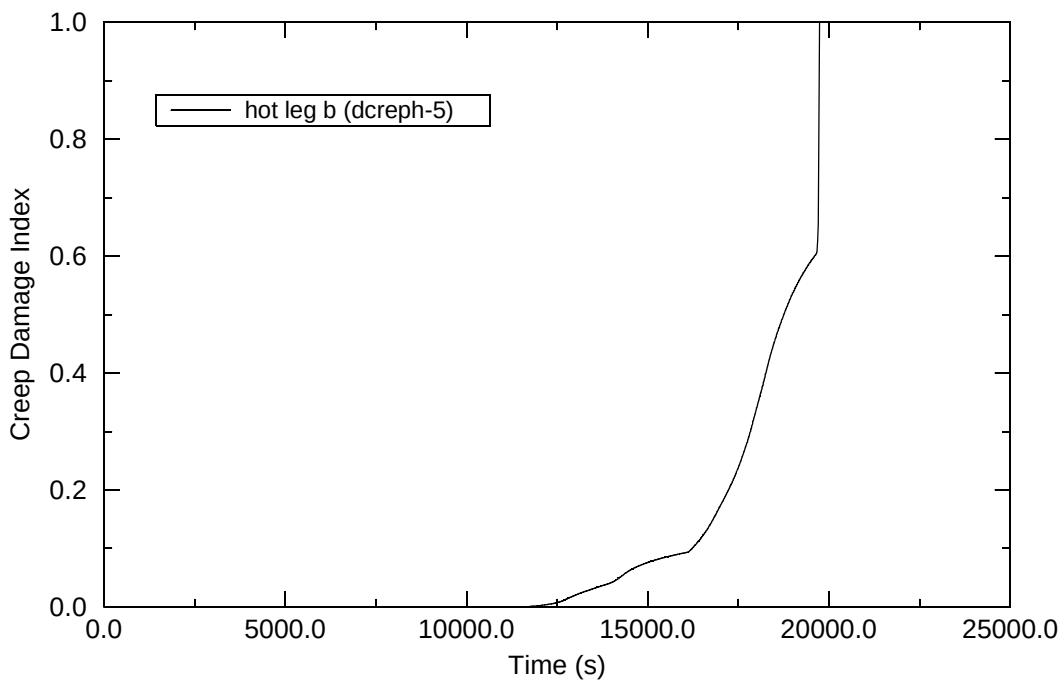

Figure E-14. Case 05 hot leg B creep damage index.

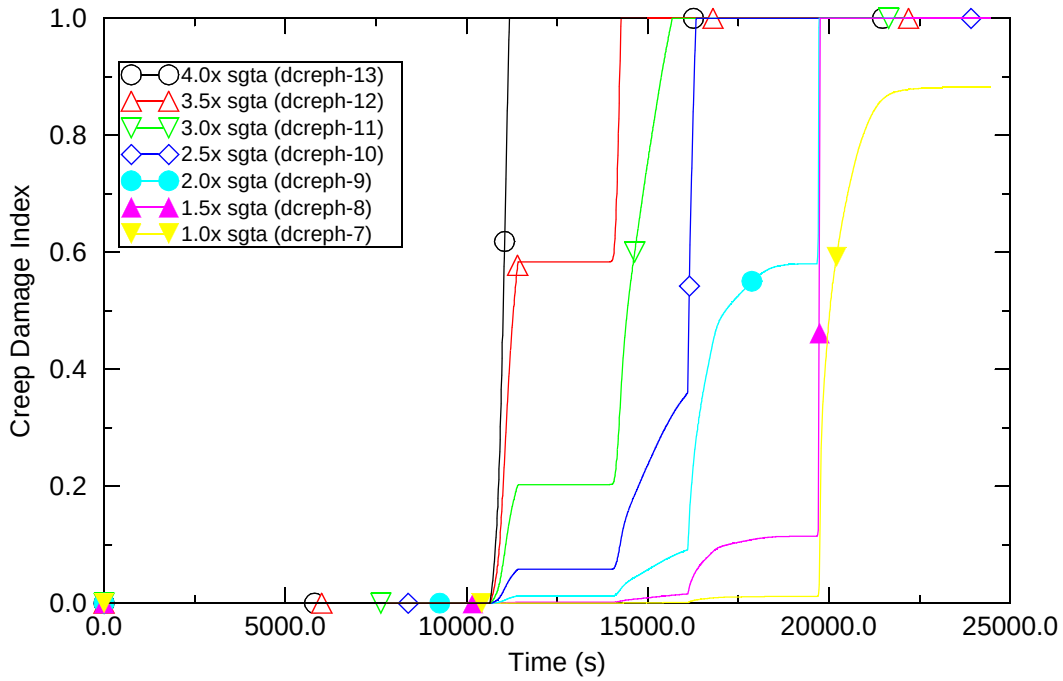

Figure E-15. Case 05 SGA tube creep damage indices.

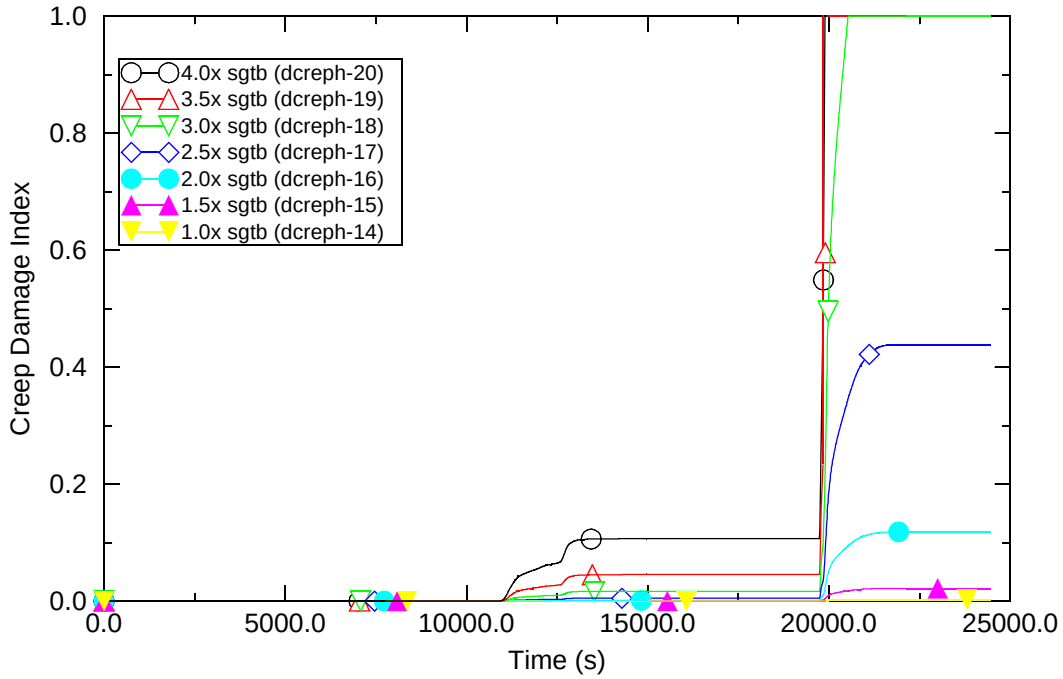

Figure E-16. Case 05 SGB tube creep damage indices.

Appendix F - Selected Results from Case 06

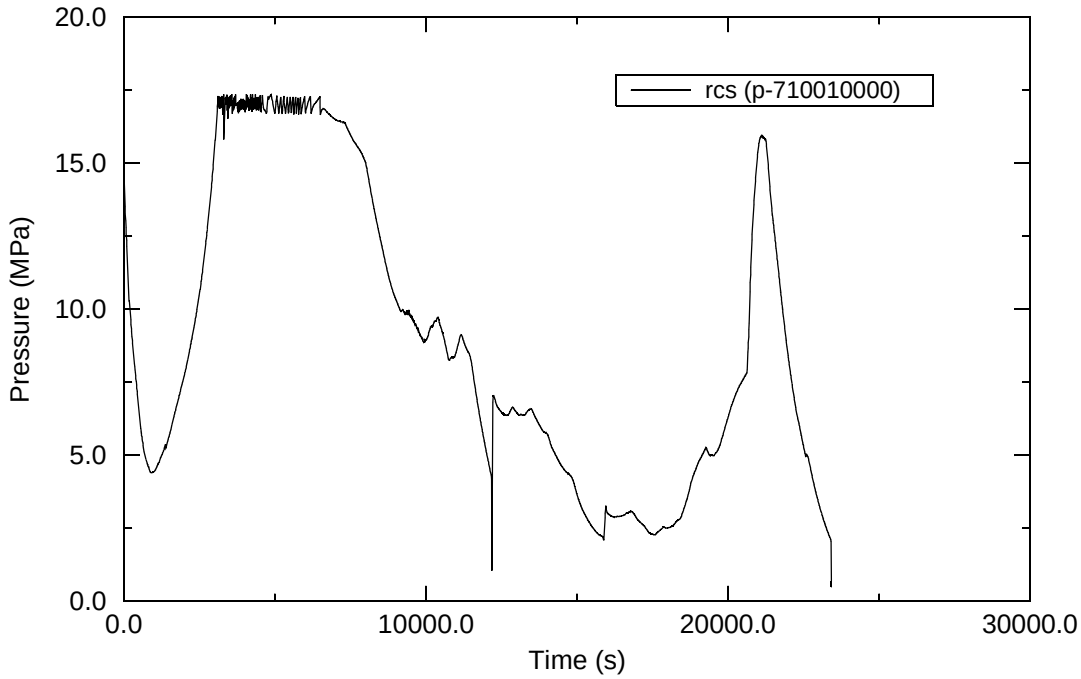

Figure F-1. Case 06 RCS (reactor coolant system) pressure.

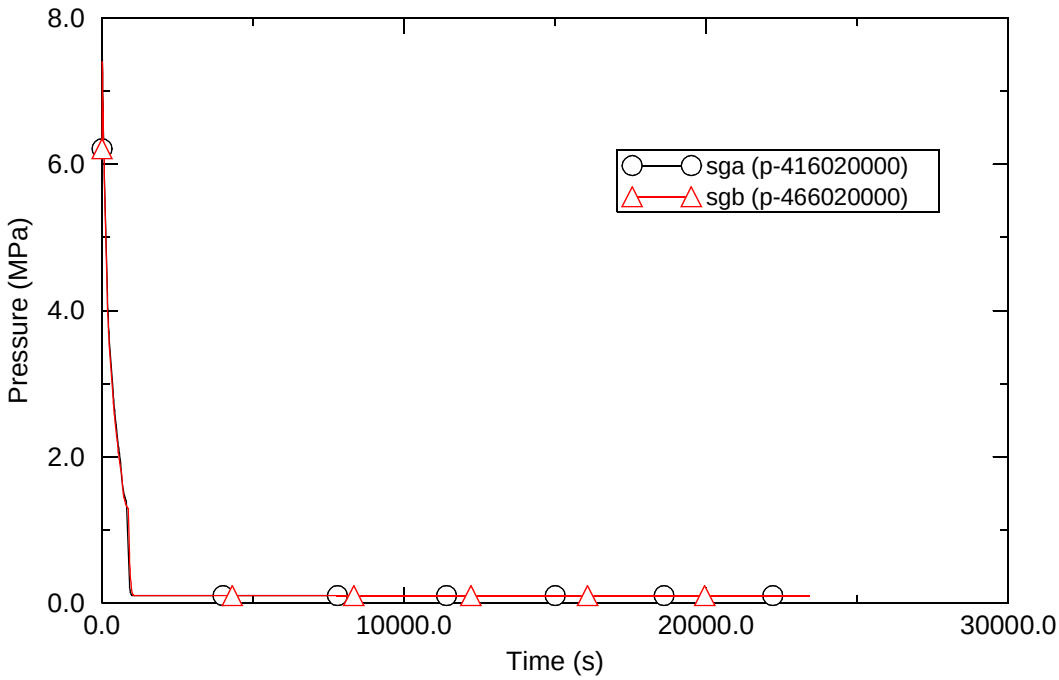

Figure F-2. Case 06 pressures in SGA (steam generator in primary coolant loop with pressurizer) and SGB (steam generator in primary coolant loop without pressurizer).

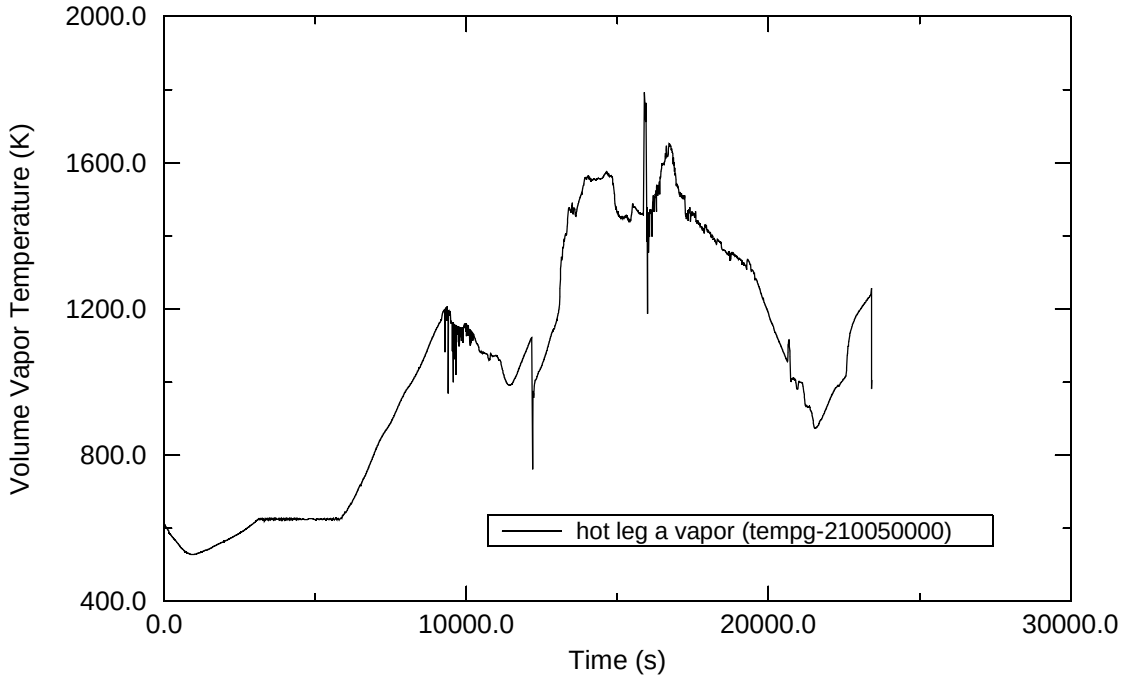

Figure F-3. Case 06 vapor temperature entering SGA inlet plenum from the "hot" part of the hot leg.

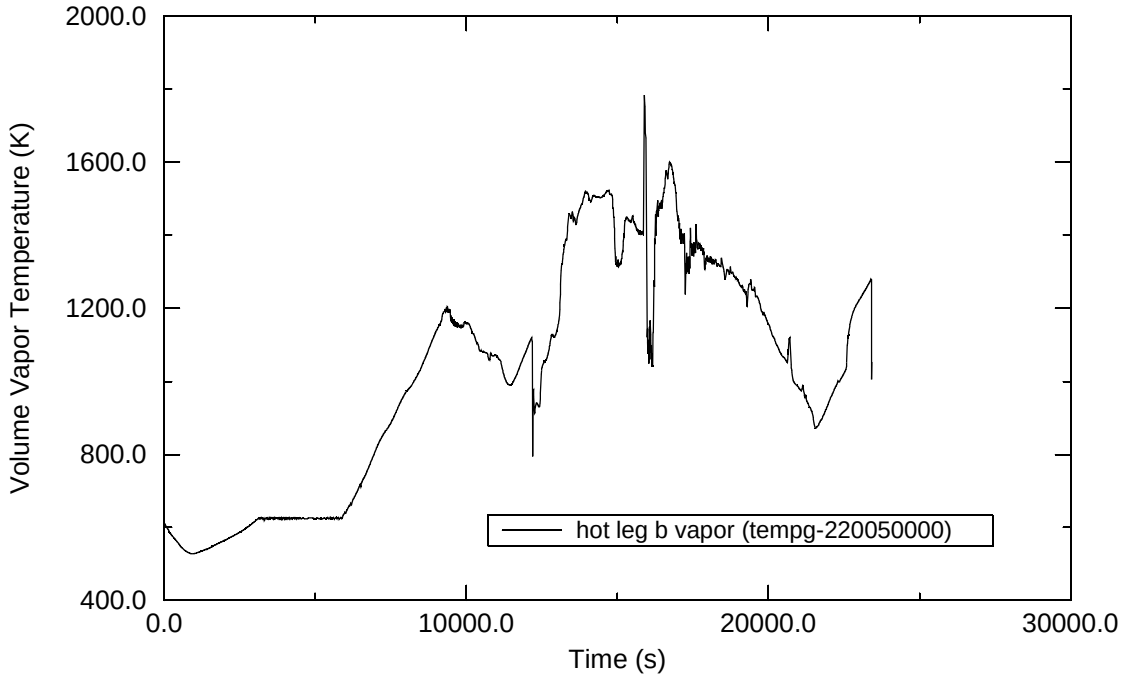

Figure F-4. Case 06 vapor temperature entering SGB inlet plenum from the "hot" part of the hot leg.

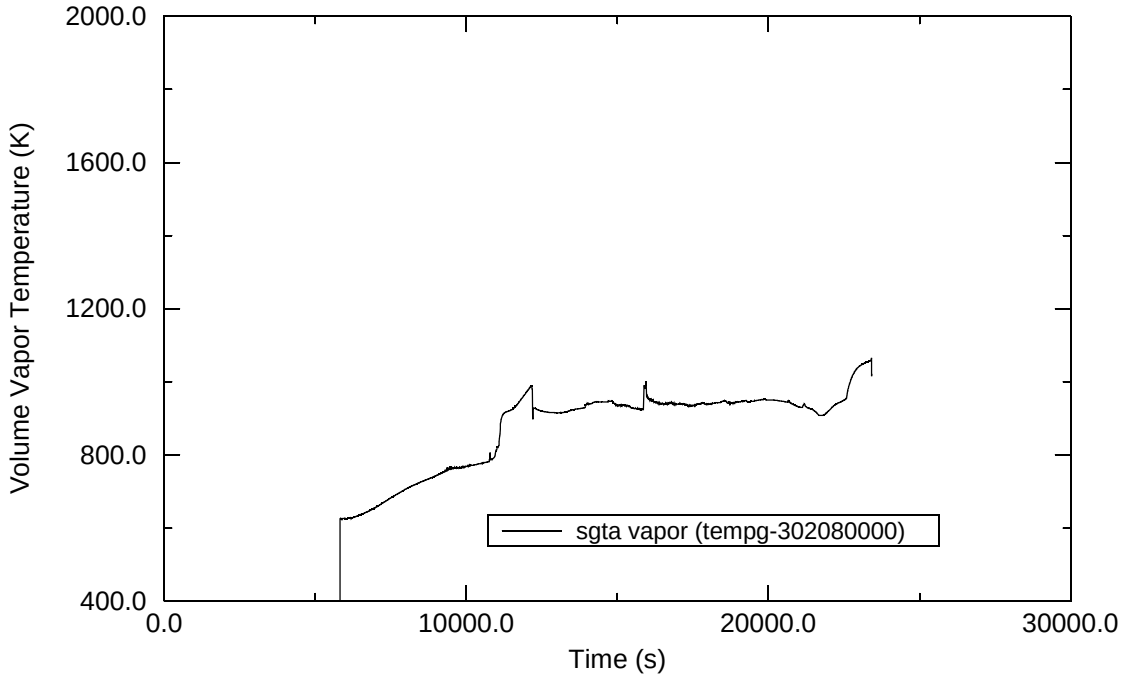

Figure F-5. Case 06 vapor temperature returning to SGA inlet plenum from the "cold" SG tube bundle.

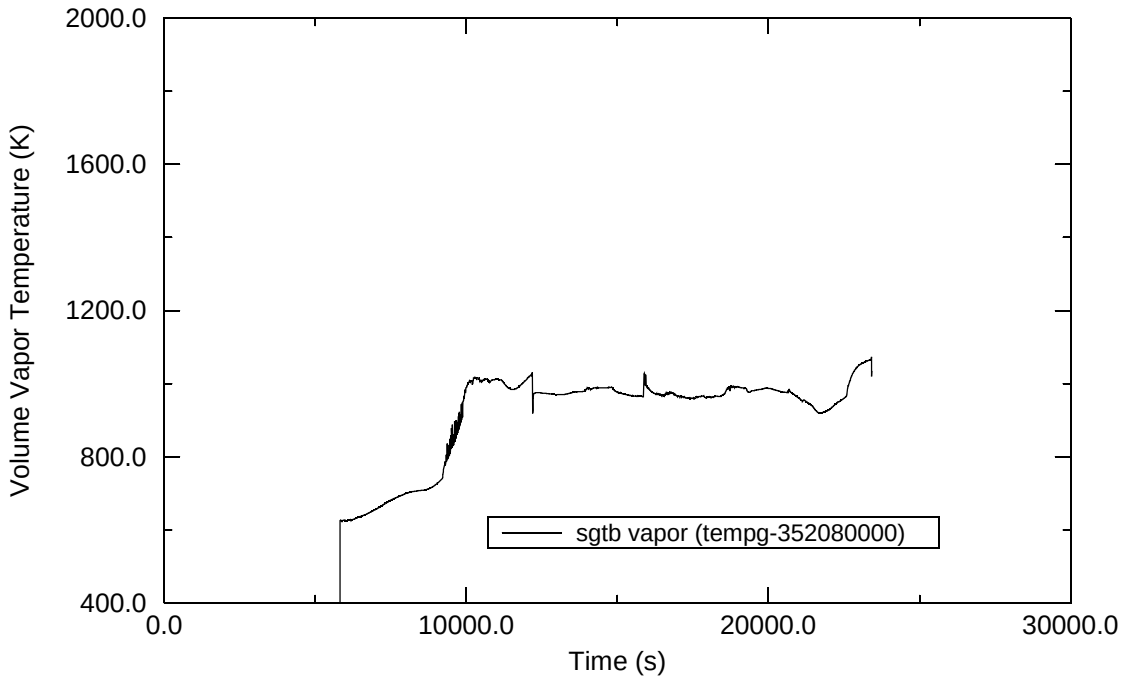

Figure F-6. Case 06 vapor temperature returning to SGB inlet plenum from the "cold" SG tube bundle.

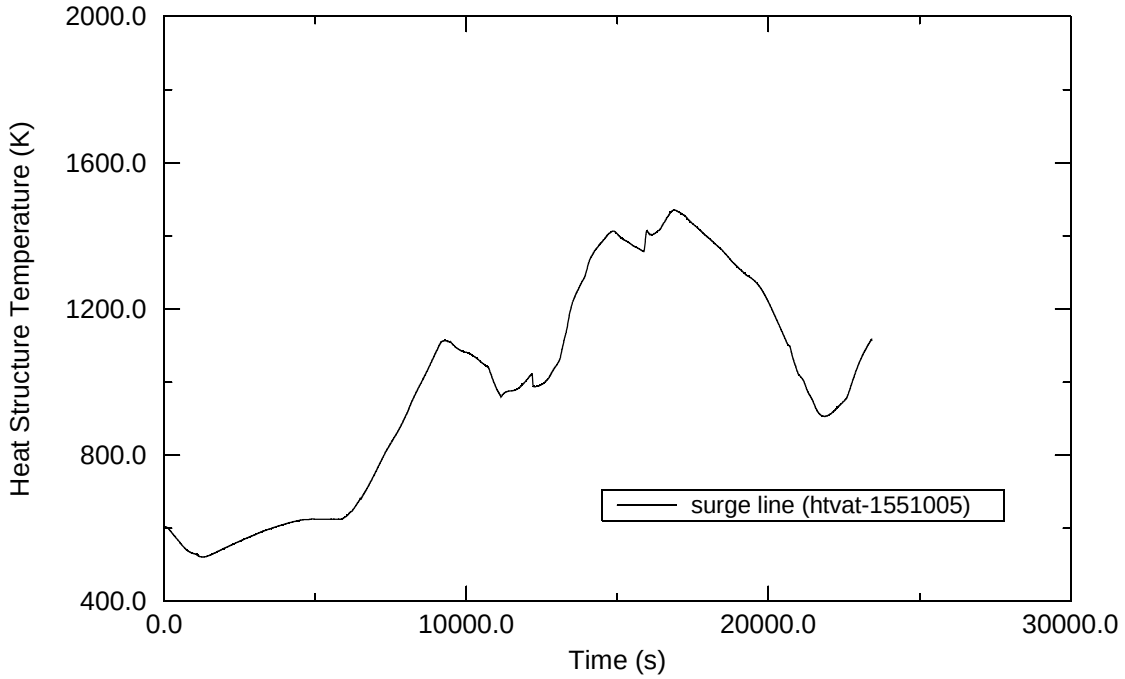

Figure F-7. Case 06 surge line temperature.

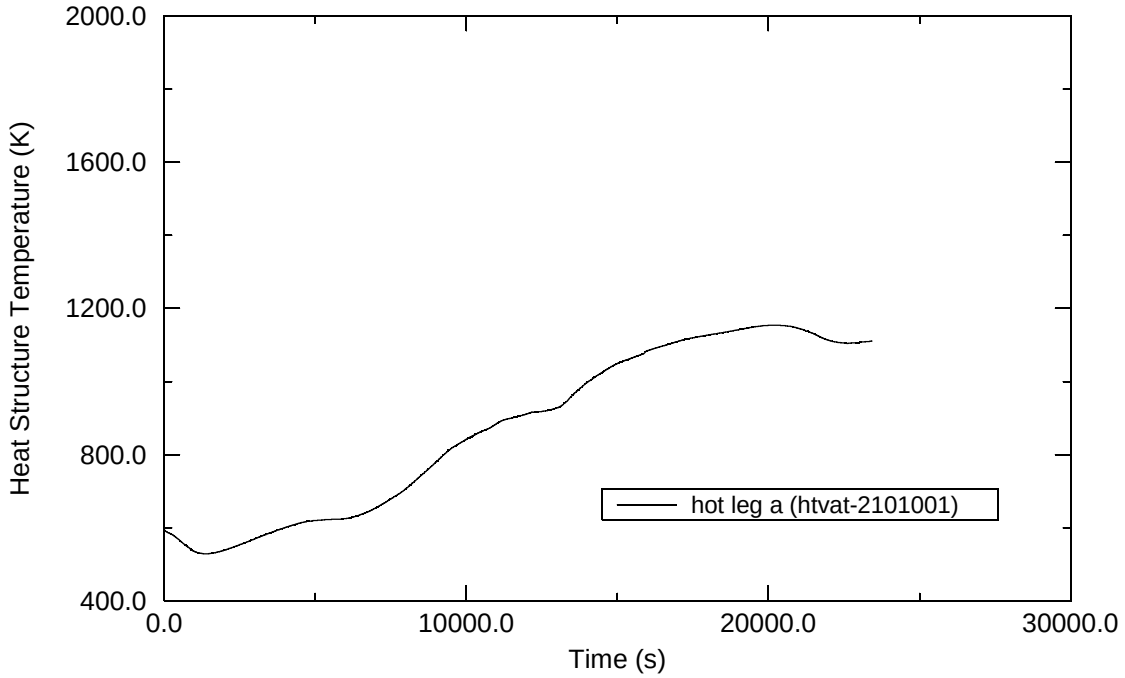

Figure F-8. Case 06 temperature of hot leg A (hot leg in primary coolant loop with pressurizer).

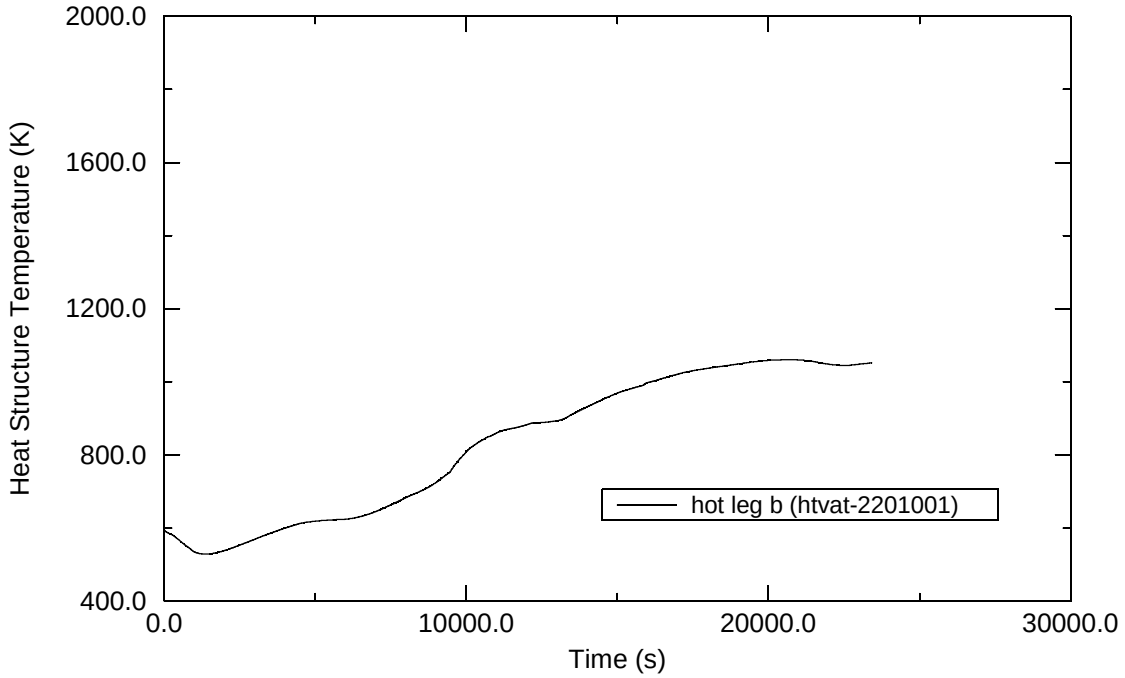

Figure F-9. Case 06 temperature of hot leg B (hot leg in primary coolant loop without pressurizer).

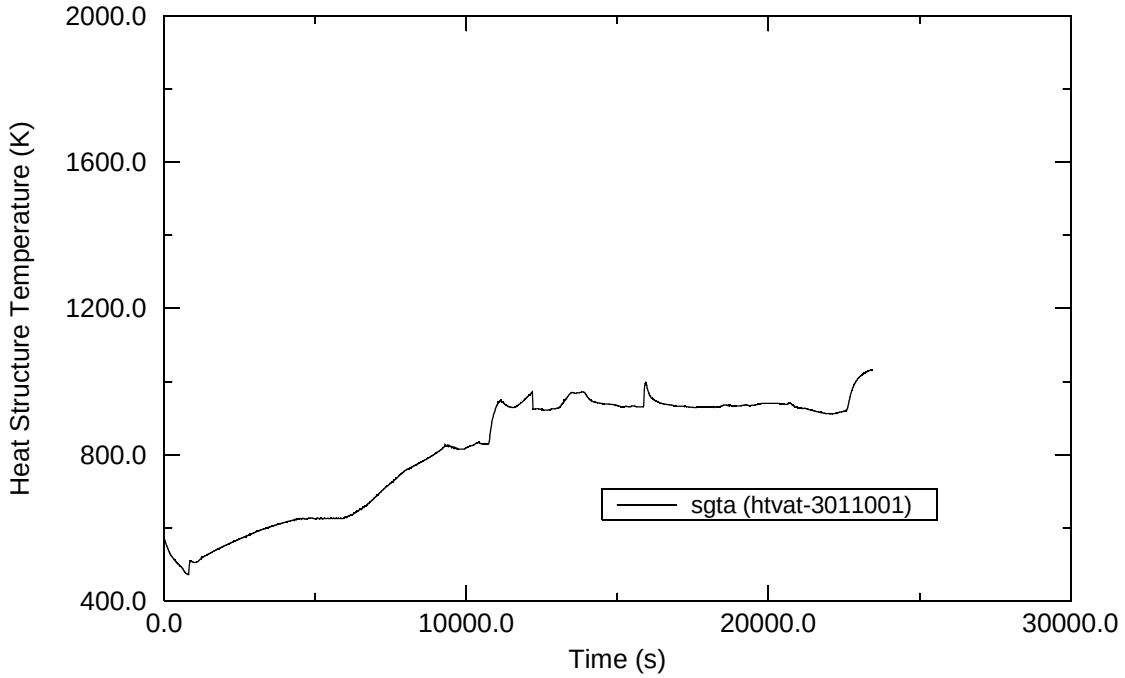

Figure F-10. Case 06 SGA tube temperature.

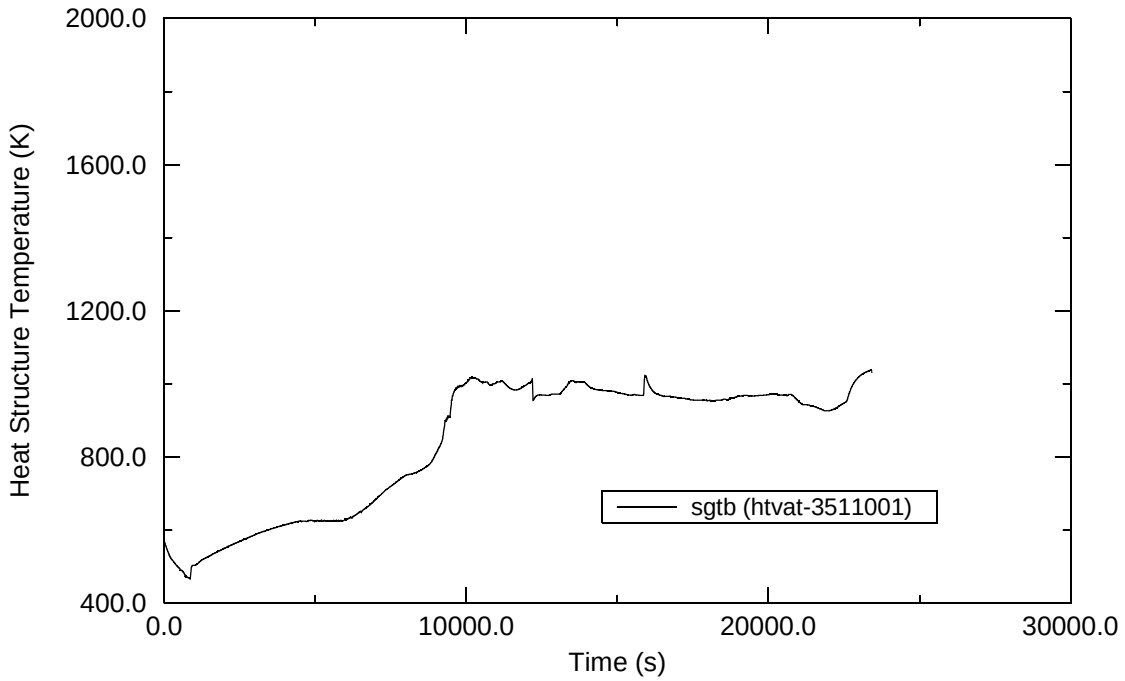

Figure F-11. Case 06 SGB tube temperature.

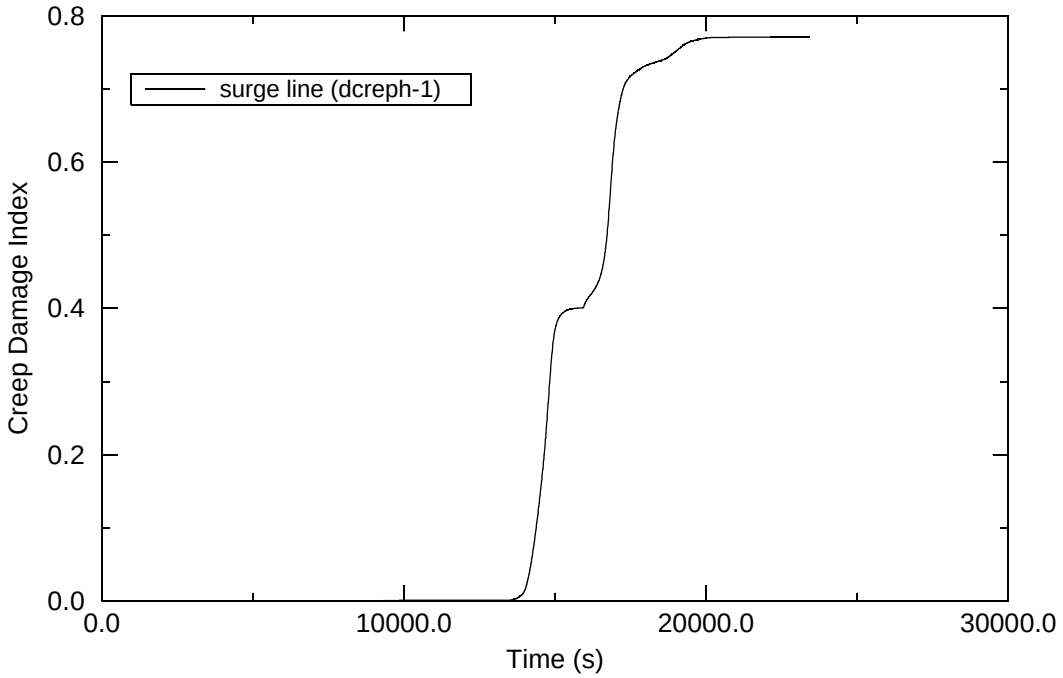

Figure F-12. Case 06 surge line creep damage index.

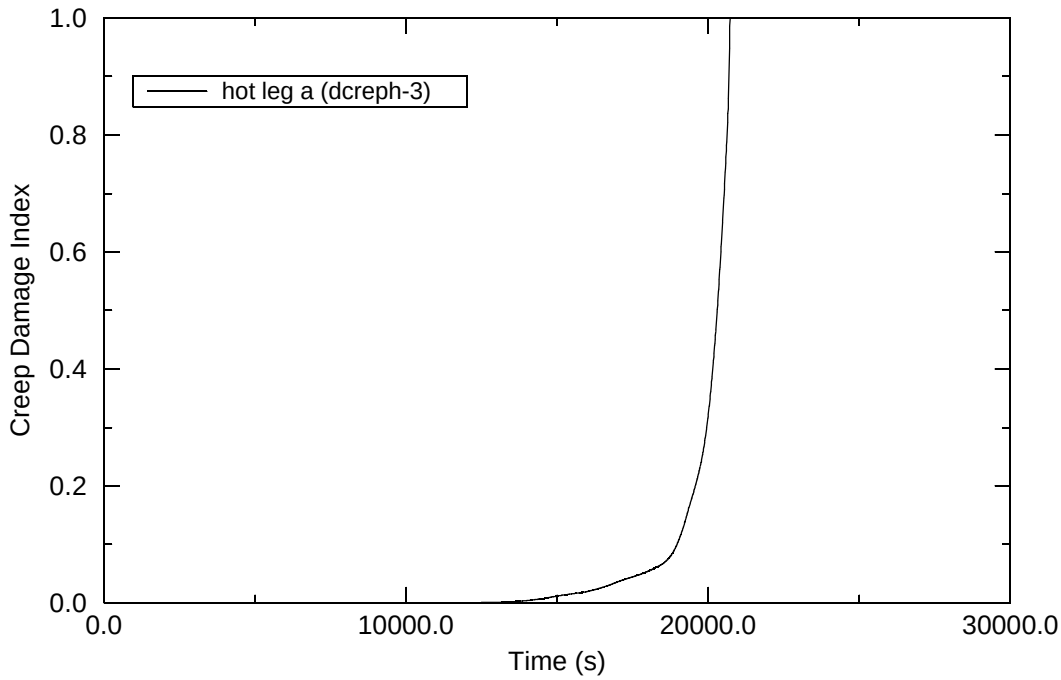

Figure F-13. Case 06 hot leg A creep damage index.

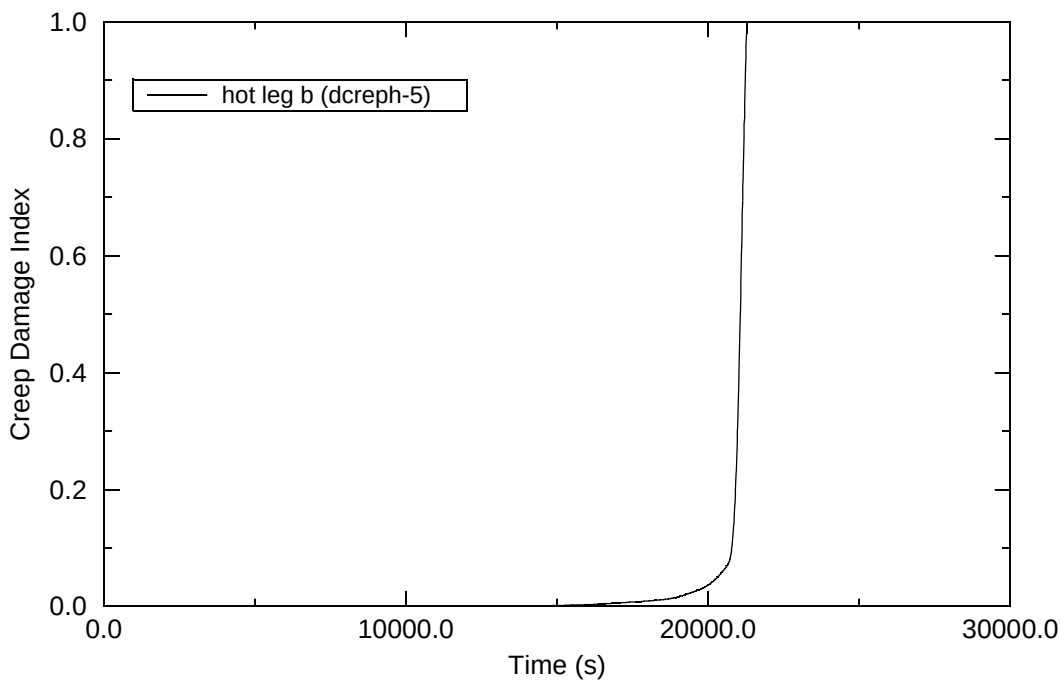

Figure F-14. Case 06 hot leg B creep damage index.

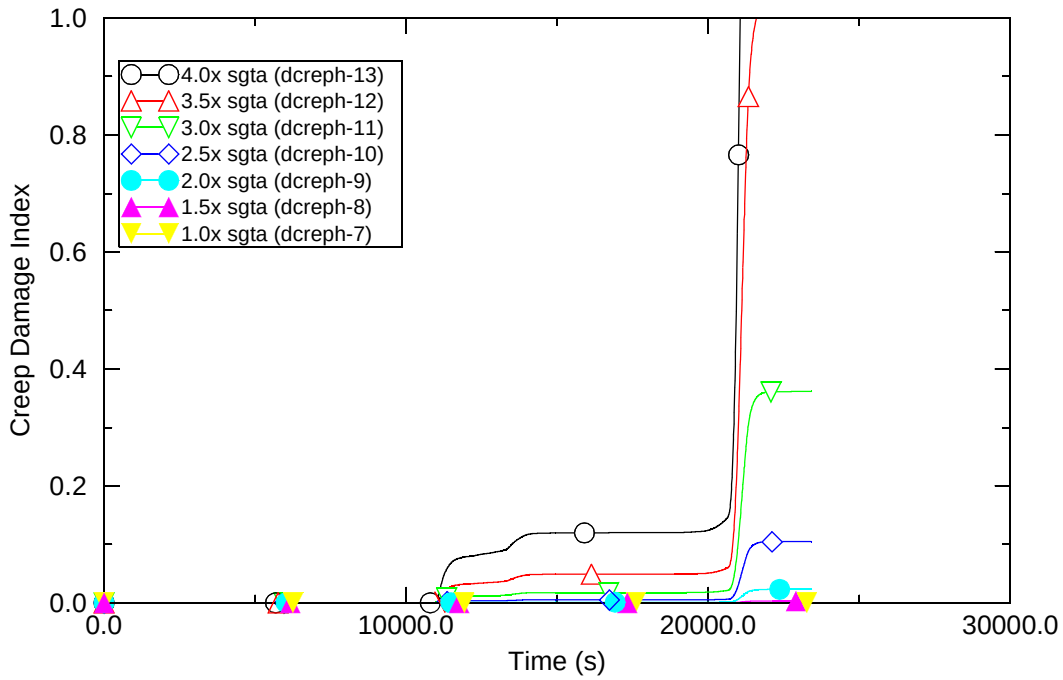

Figure F-15. Case 06 SGA tube creep damage indices.

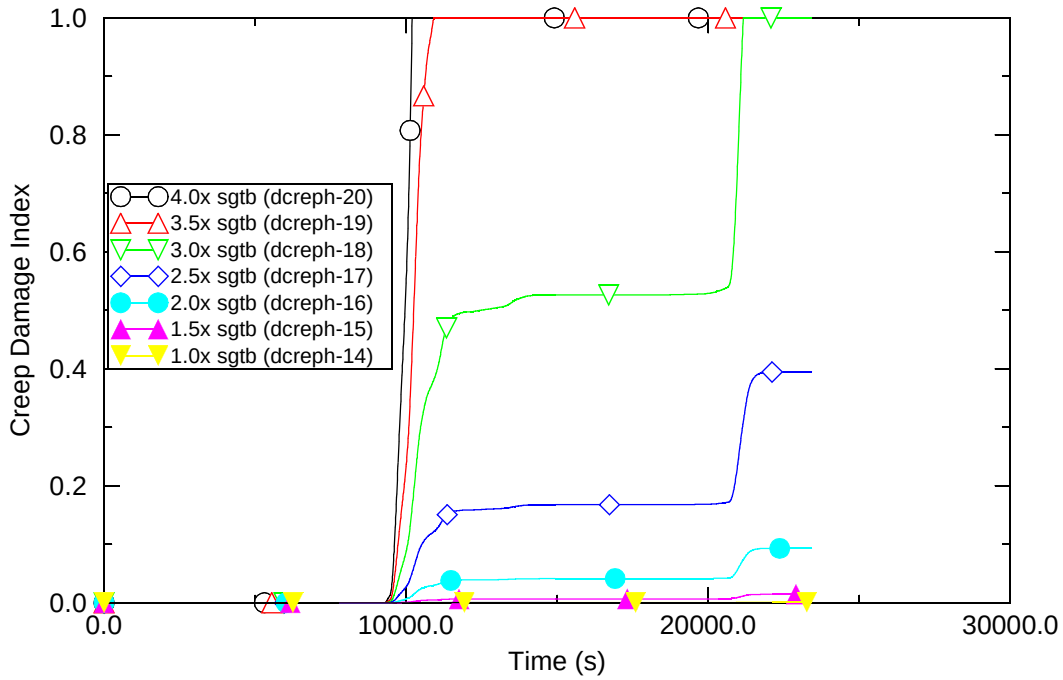

Figure F-16. Case 06 SGB tube creep damage indices.

Appendix G - Selected Results from Case 07

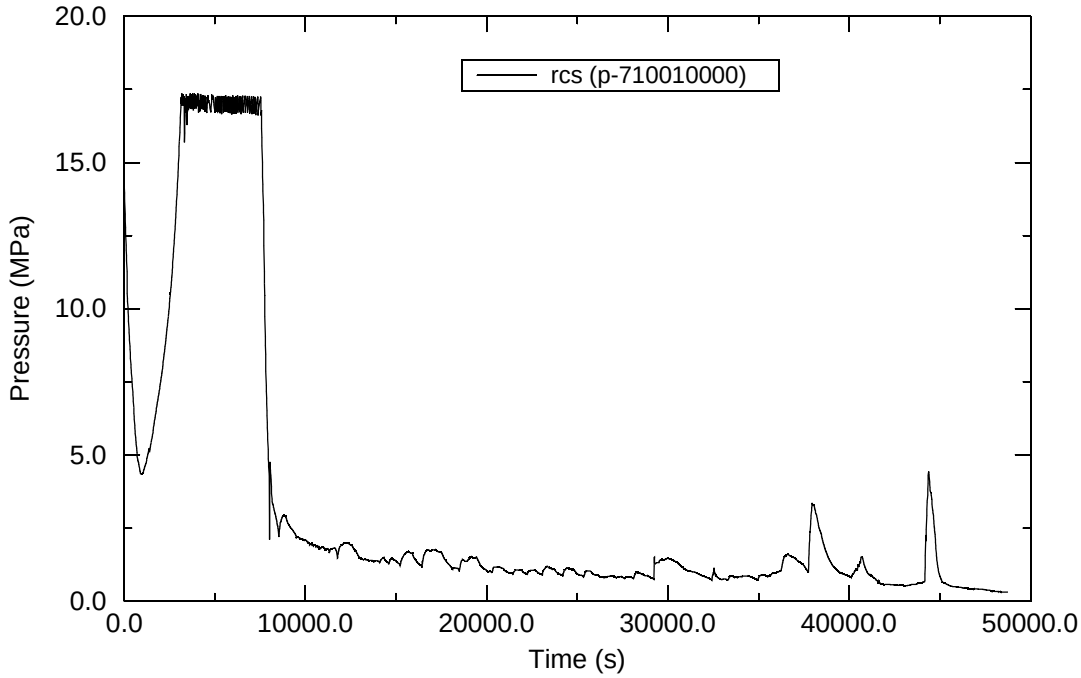

Figure G-1. Case 07 RCS (reactor coolant system) pressure.

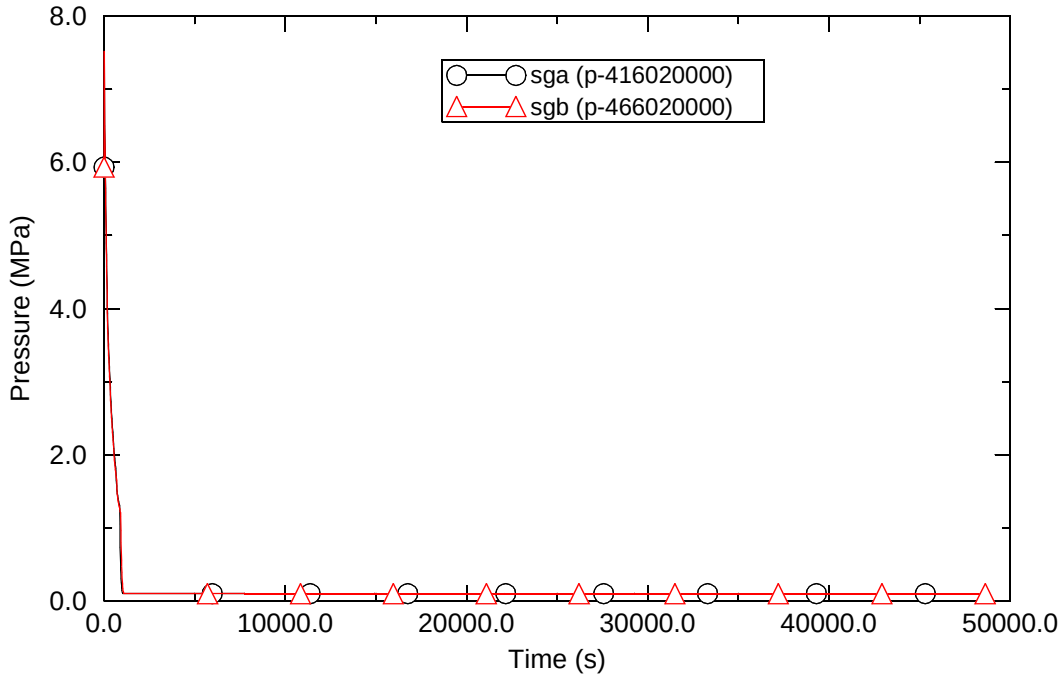

Figure G-2. Case 07 pressures in SGA (steam generator in primary coolant loop with pressurizer) and SGB (steam generator in primary coolant loop without pressurizer).

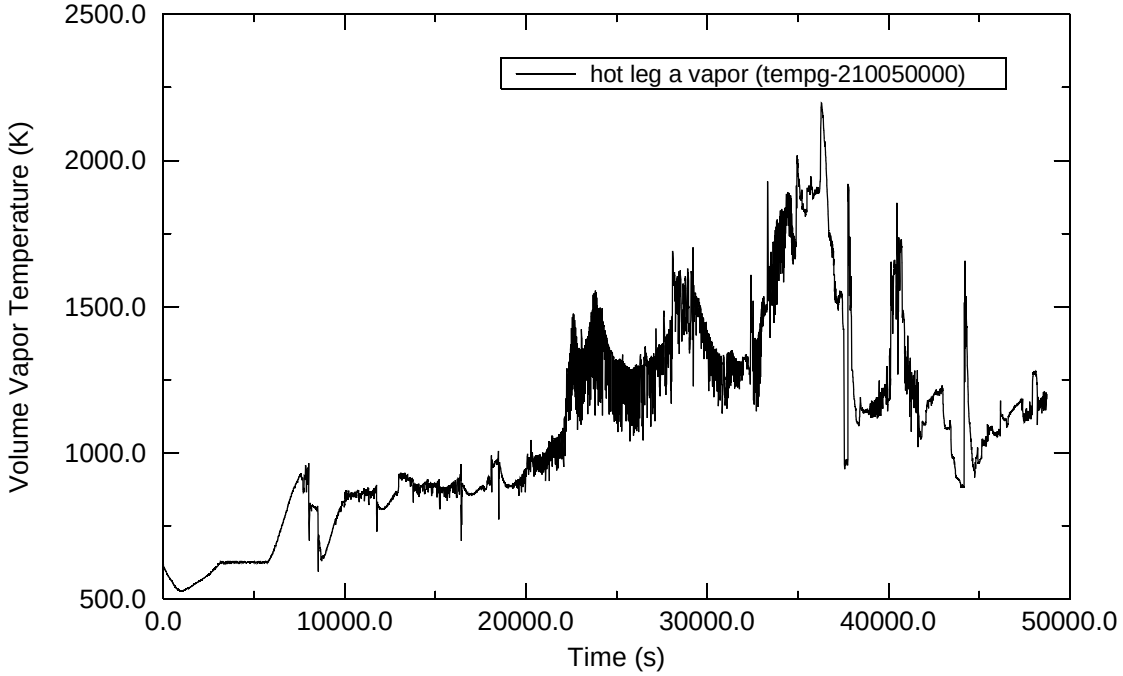

Figure G-3. Case 07 vapor temperature entering SGA inlet plenum from the "hot" part of the hot leg.

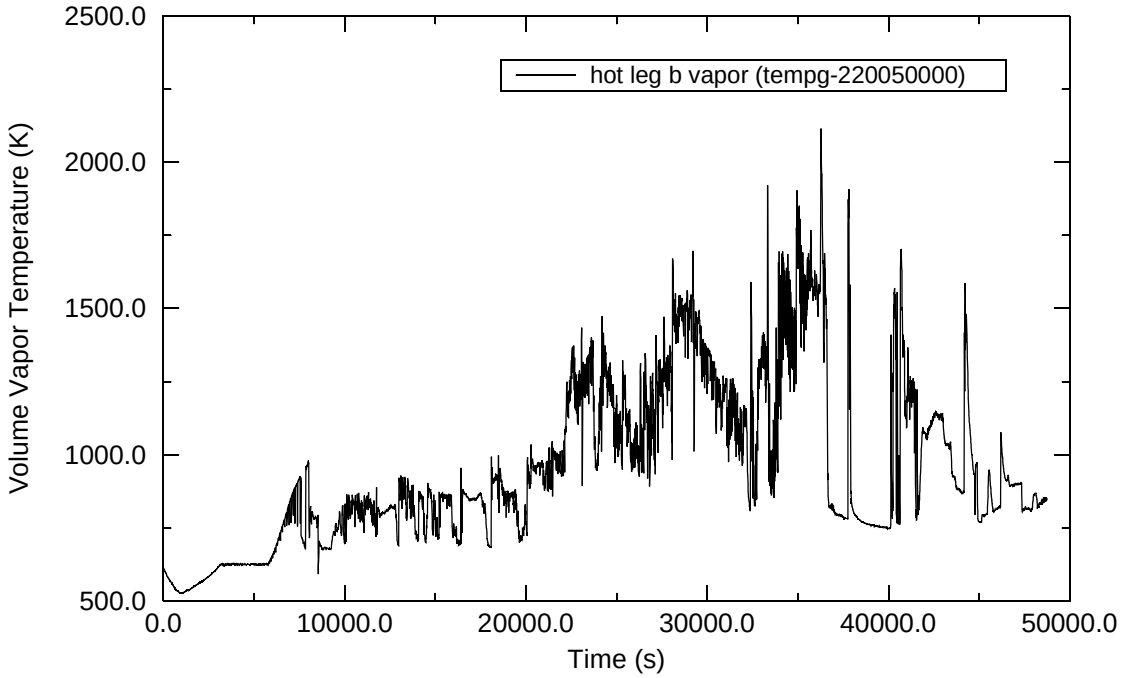

Figure G-4. Case 07 vapor temperature entering SGB inlet plenum from the "hot" part of the hot leg.

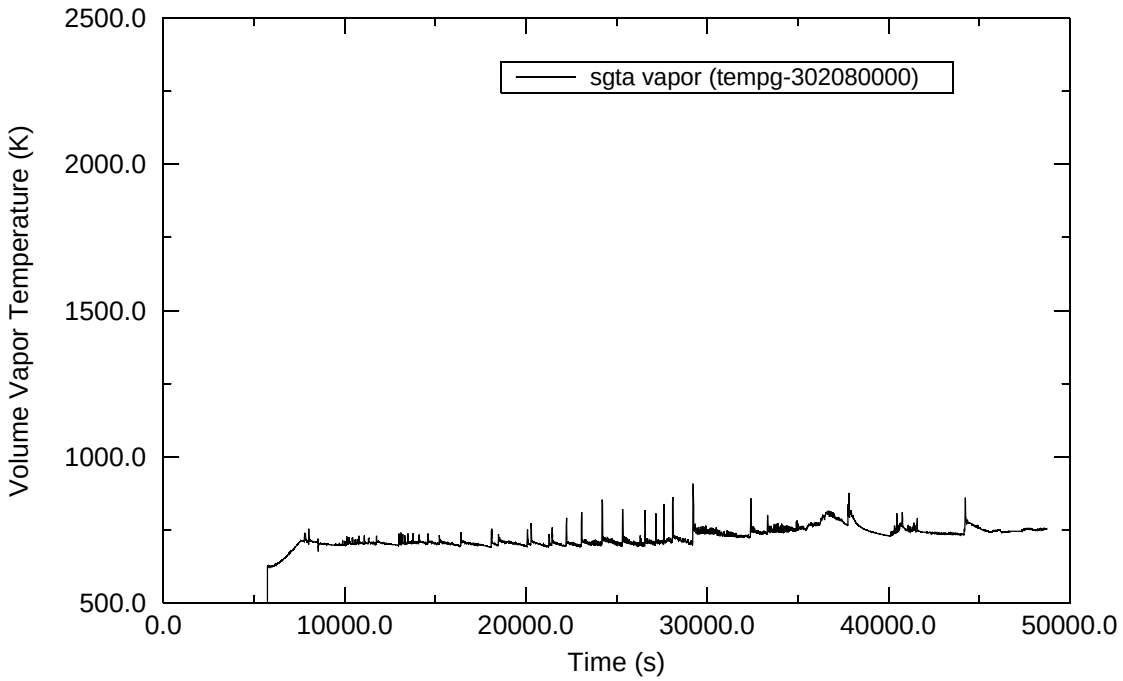

Figure G-5. Case 07 vapor temperature returning to SGA inlet plenum from the "cold" SG tube bundle.

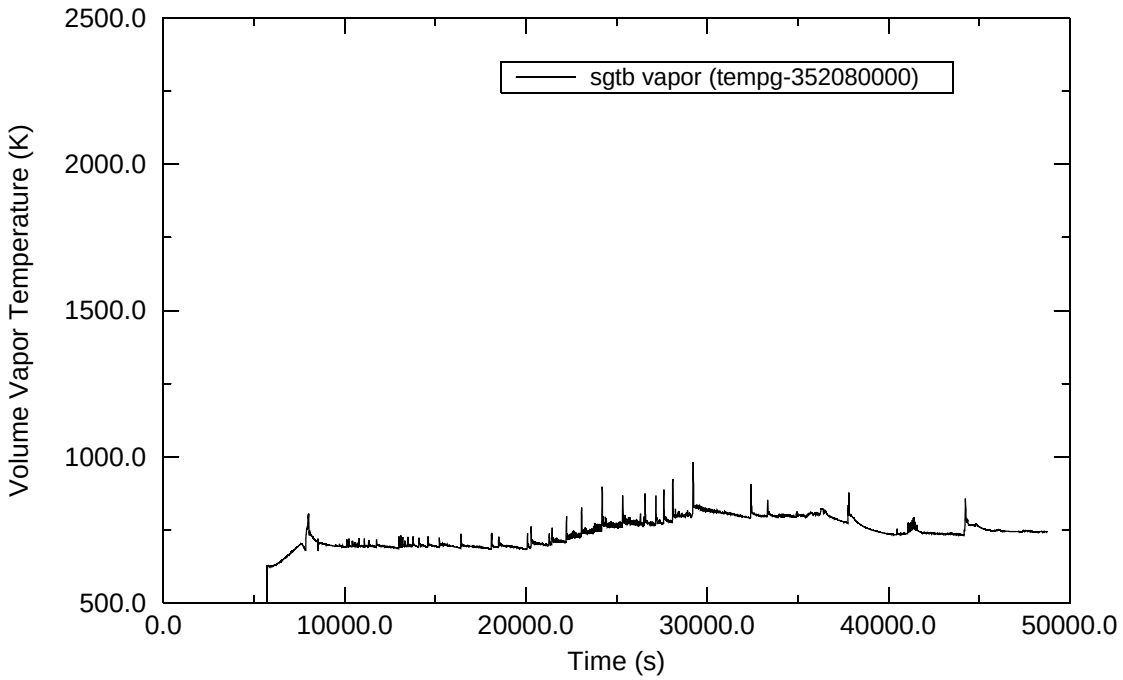

Figure G-6. Case 07 vapor temperature returning to SGB inlet plenum from the "cold" SG tube bundle.

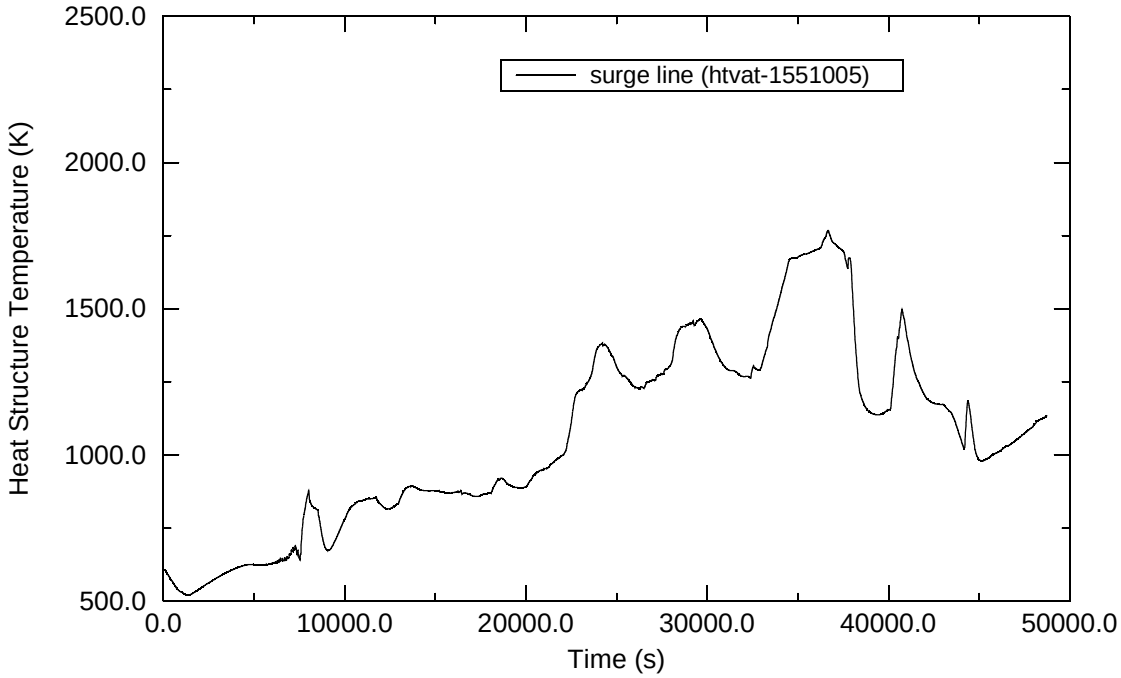

Figure G-7. Case 07 surge line temperature.

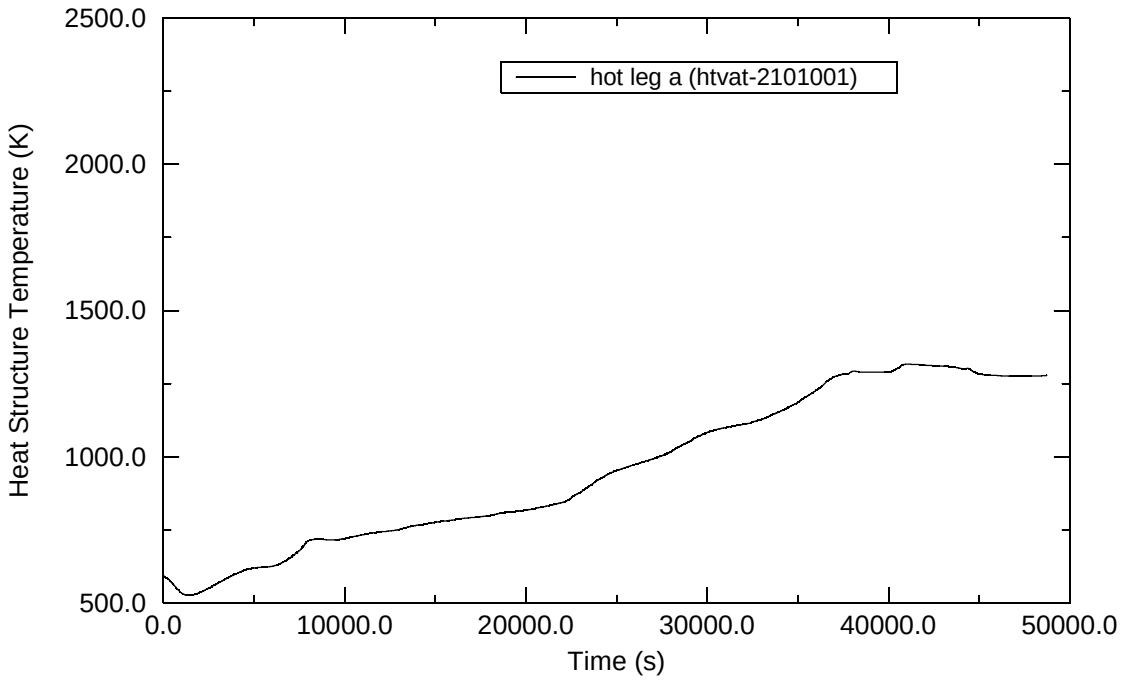

Figure G-8. Case 07 temperature of hot leg A (hot leg in primary coolant loop with pressurizer).

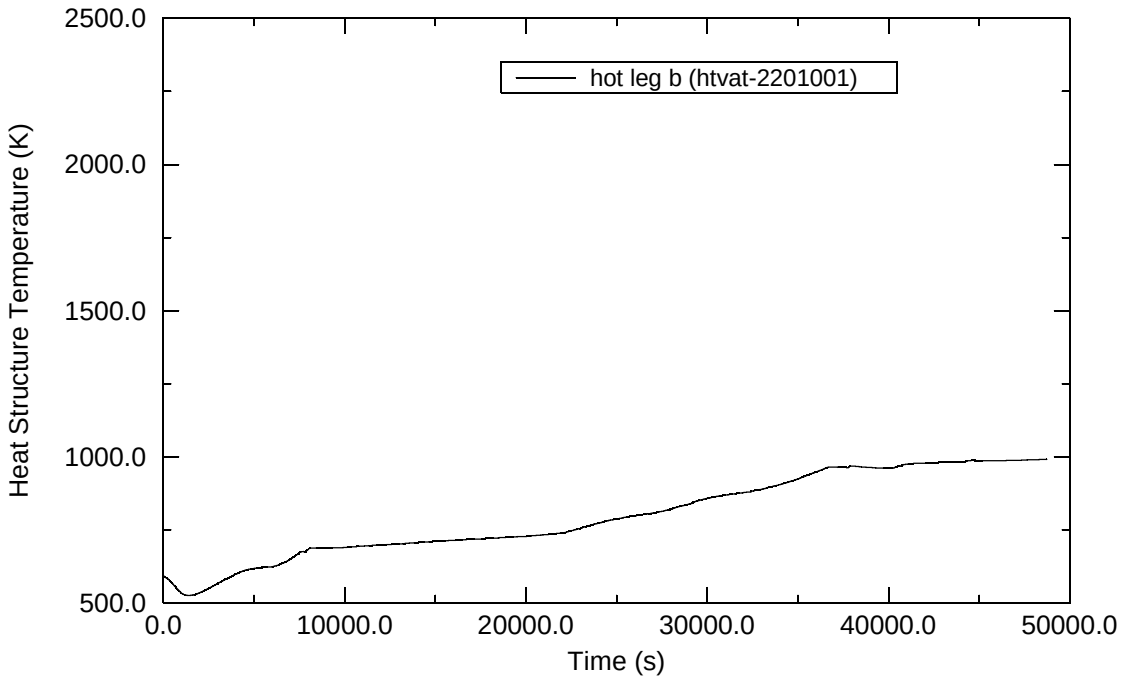

Figure G-9. Case 07 temperature of hot leg B (hot leg in primary coolant loop without pressurizer).

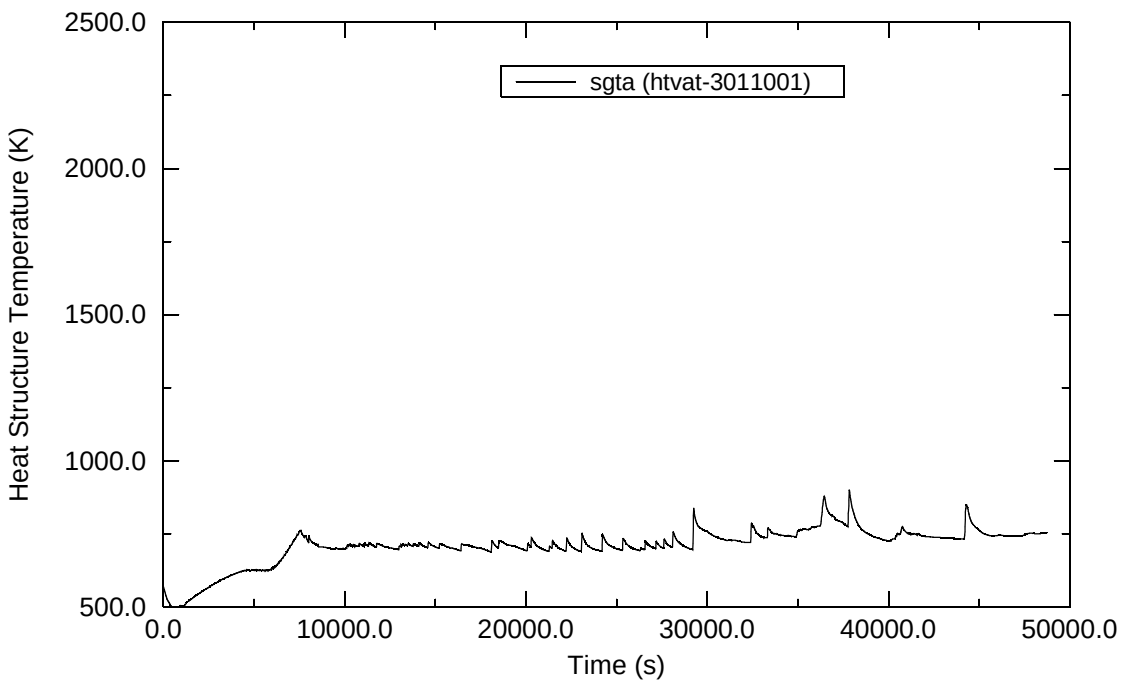

Figure G-10. Case 07 SGA tube temperature.

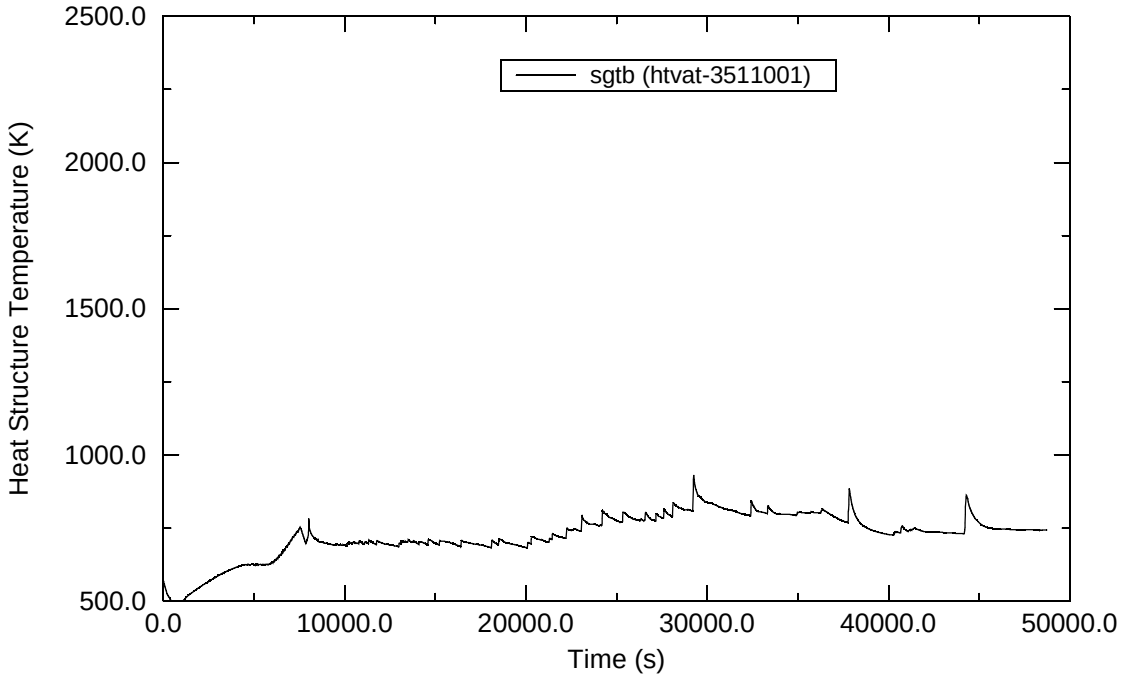

Figure G-11. Case 07 SGB tube temperature.

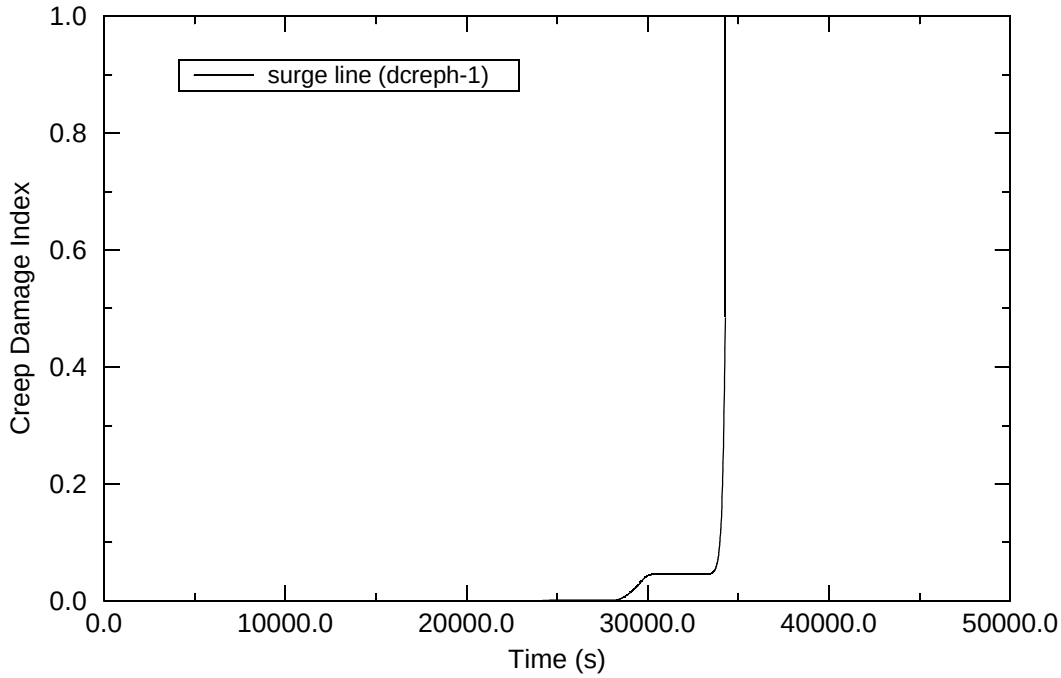

Figure G-12. Case 07 surge line creep damage index.

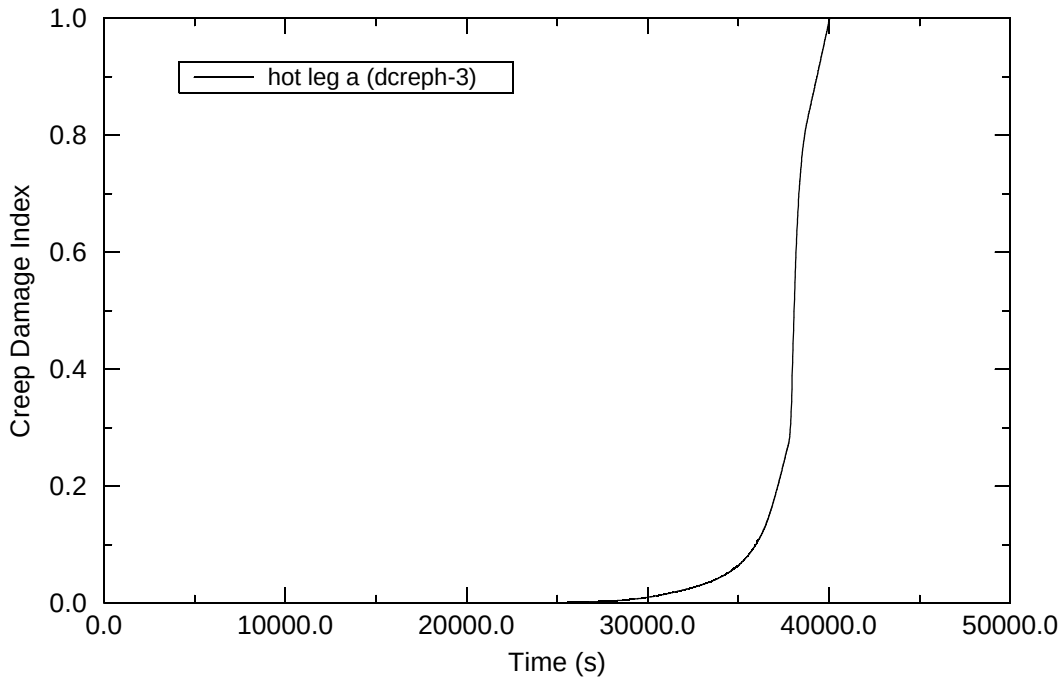

Figure G-13. Case 07 hot leg A creep damage index.

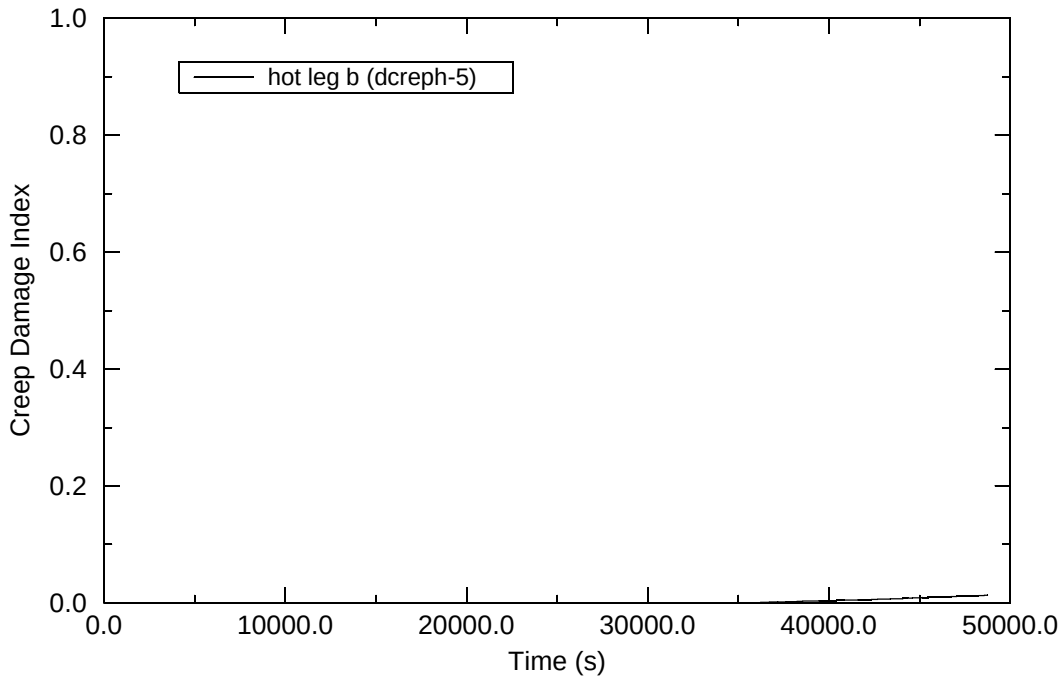

Figure G-14. Case 07 hot leg B creep damage index.

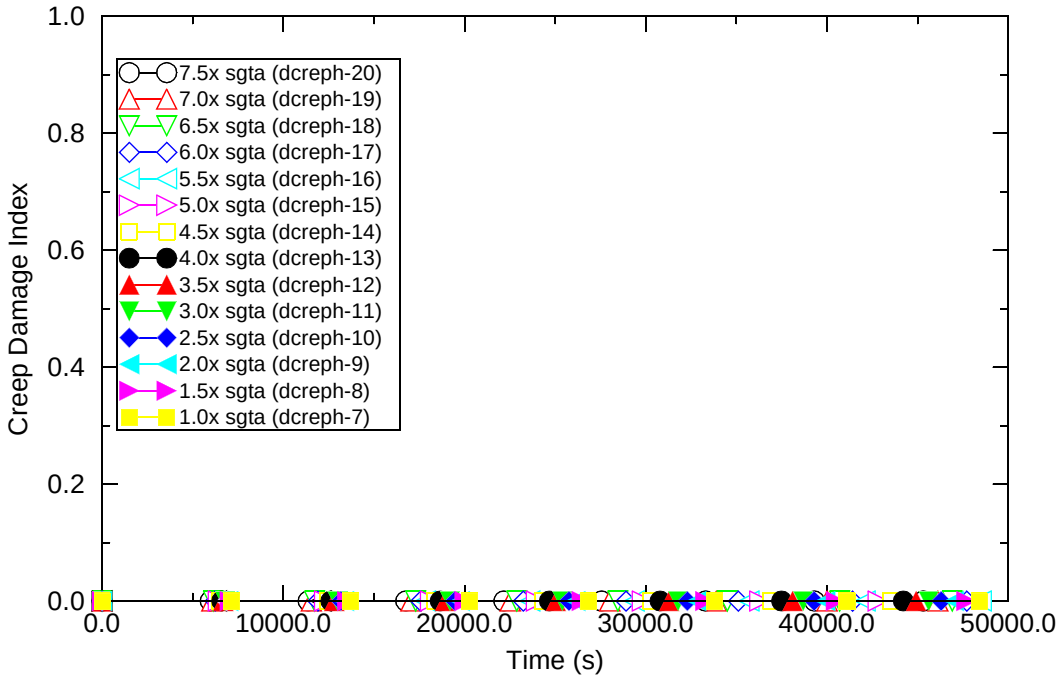

Figure G-15. Case 07 SGA tube creep damage indices.

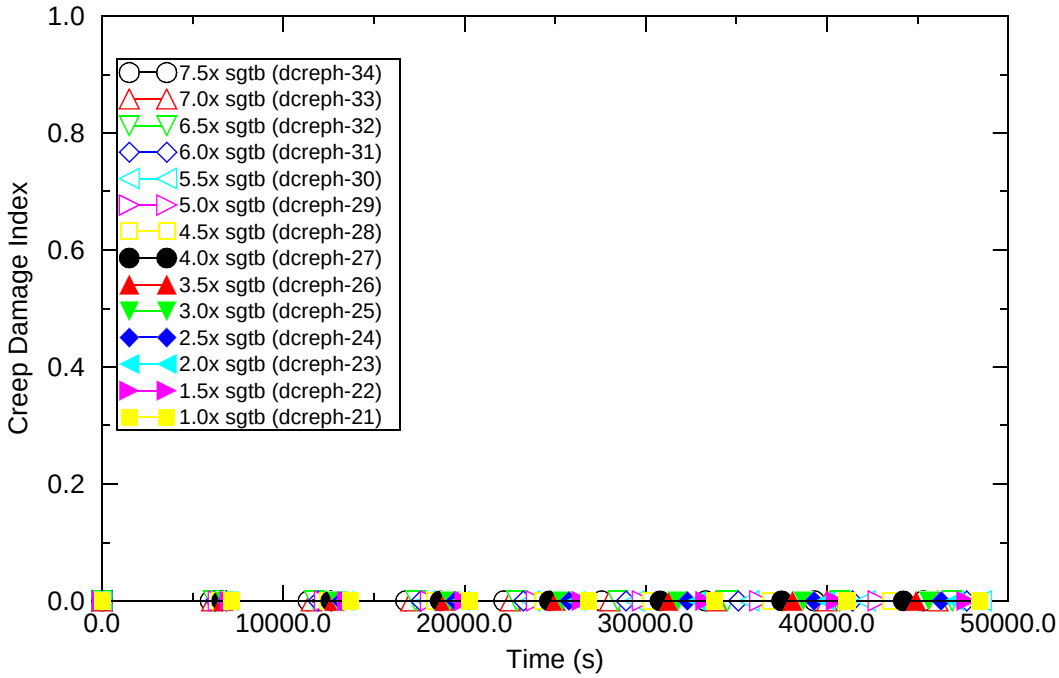

Figure G-16. Case 07 SGB tube creep damage indices.

Appendix H - Selected Results from Case 08

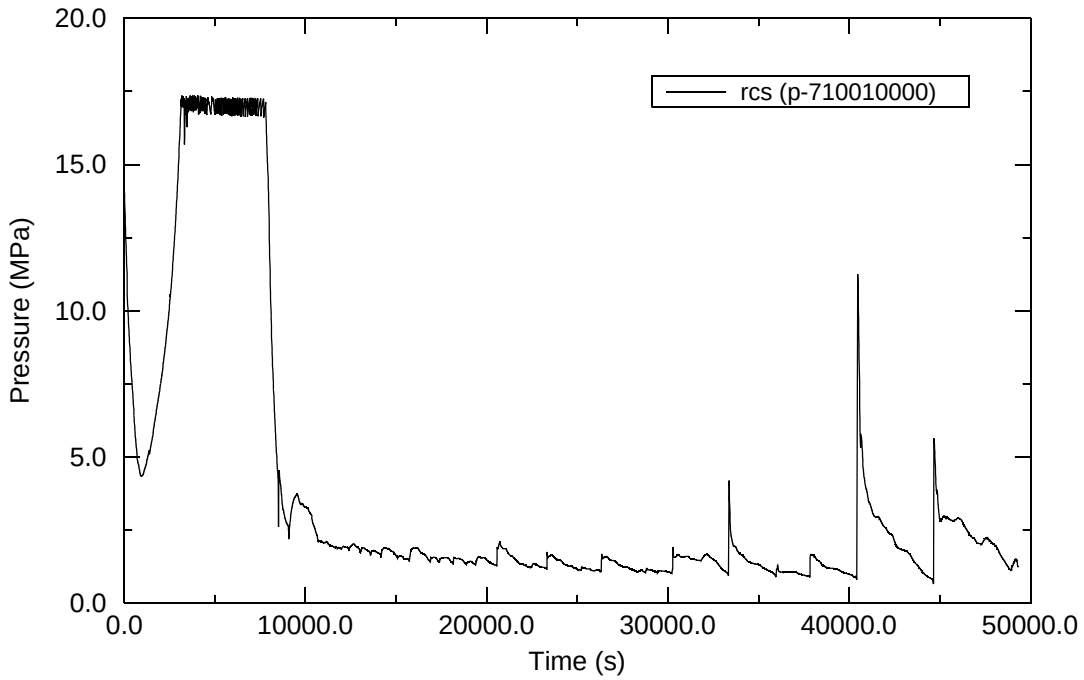

Figure H-1. Case 08 RCS (reactor coolant system) pressure.

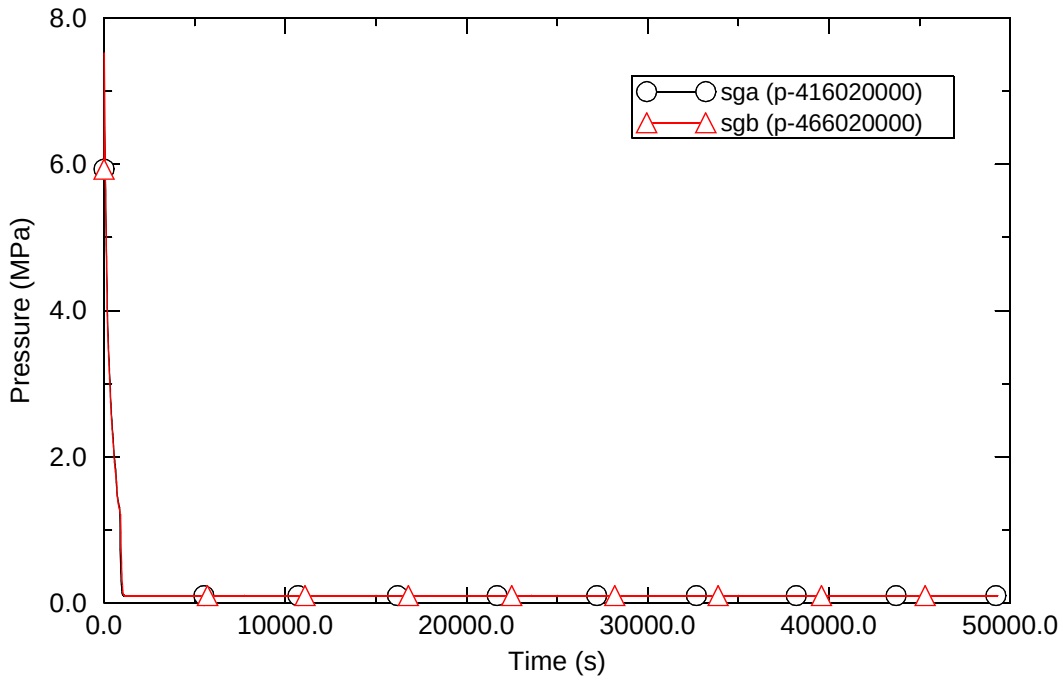

Figure H-2. Case 08 pressures in SGA (steam generator in primary coolant loop with pressurizer) and SGB (steam generator in primary coolant loop without pressurizer).

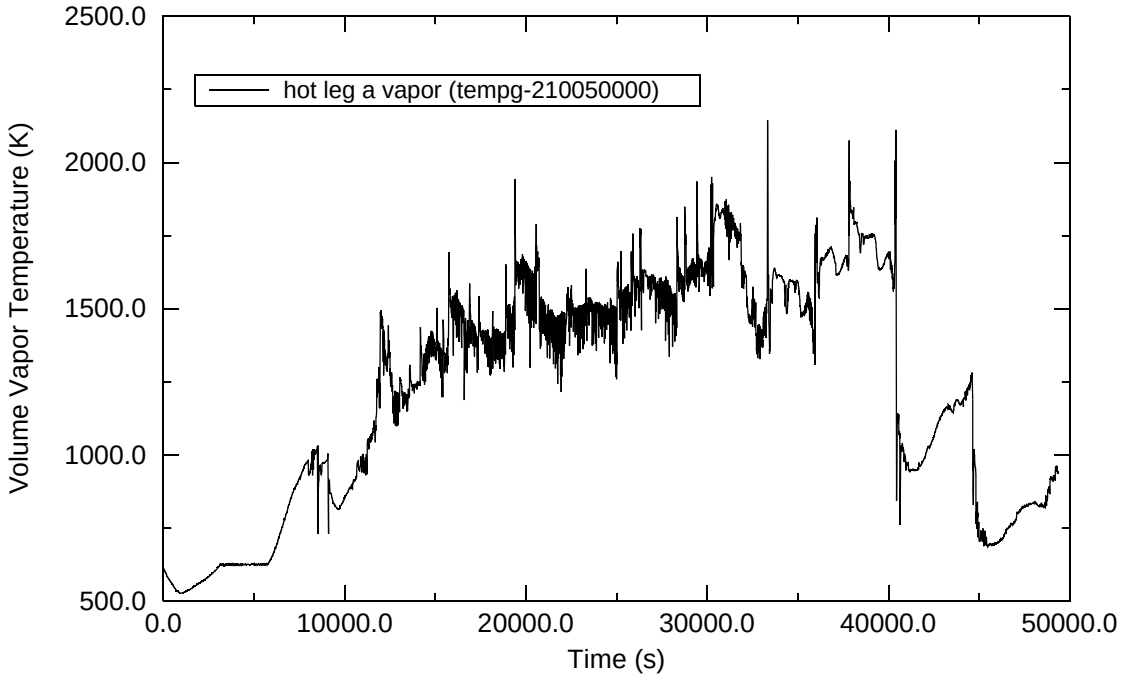

Figure H-3. Case 08 vapor temperature entering SGA inlet plenum from the "hot" part of the hot leg.

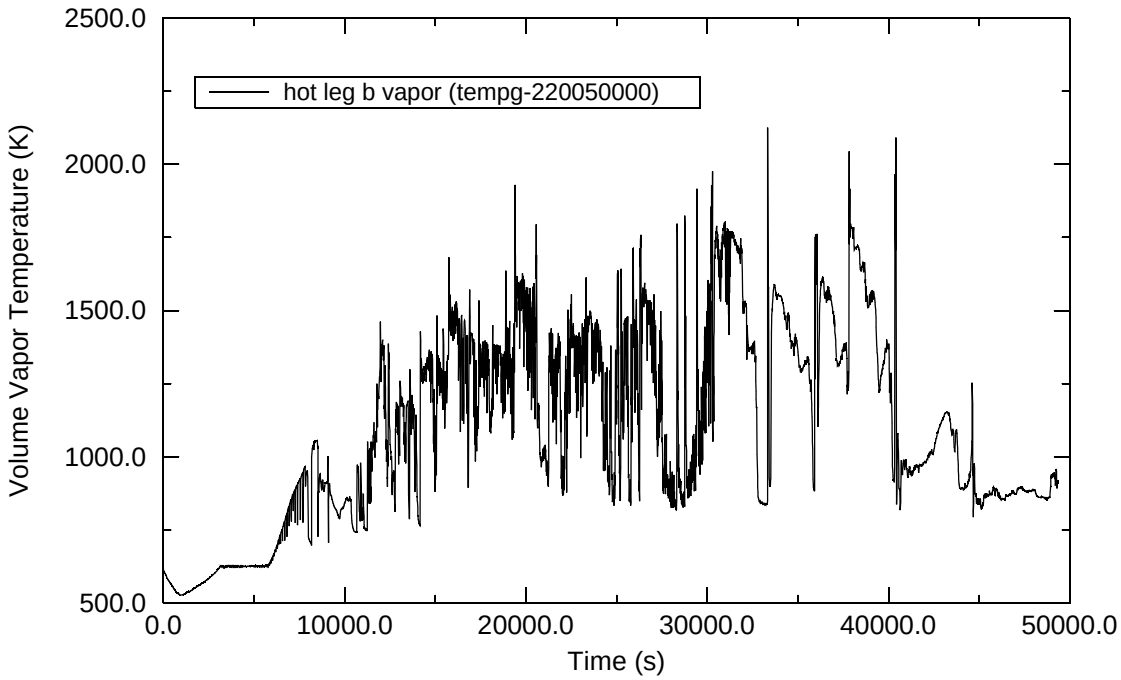

Figure H-4. Case 08 vapor temperature entering SGB inlet plenum from the "hot" part of the hot leg.

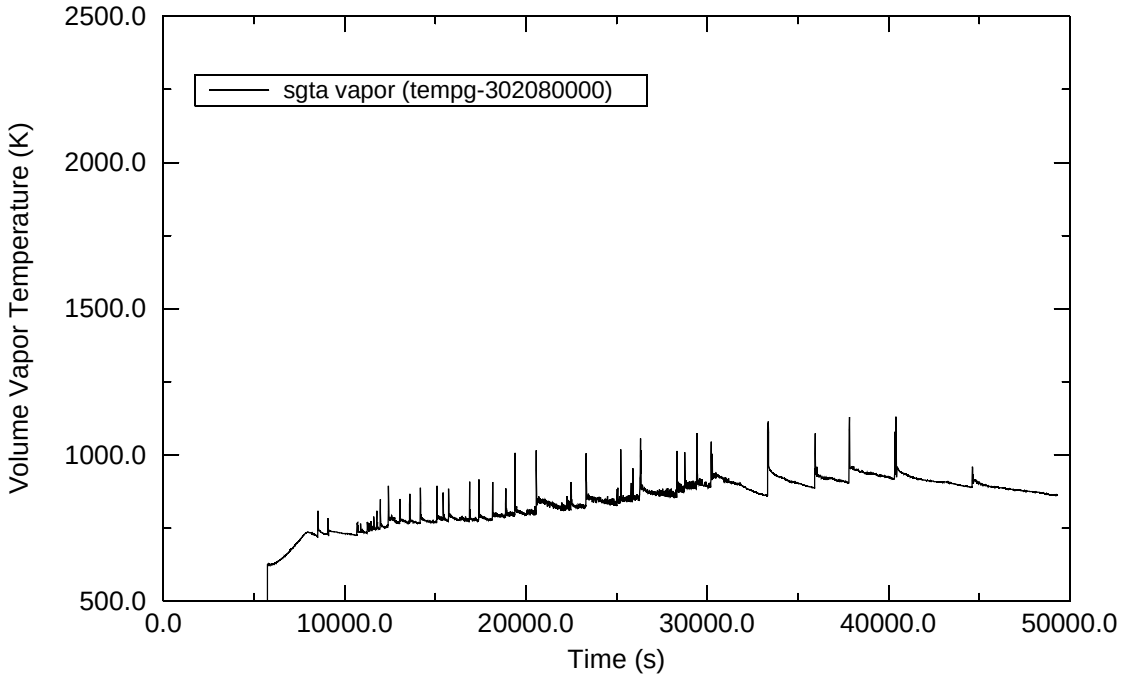

Figure H-5. Case 08 vapor temperature returning to SGA inlet plenum from the "cold" SG tube bundle.

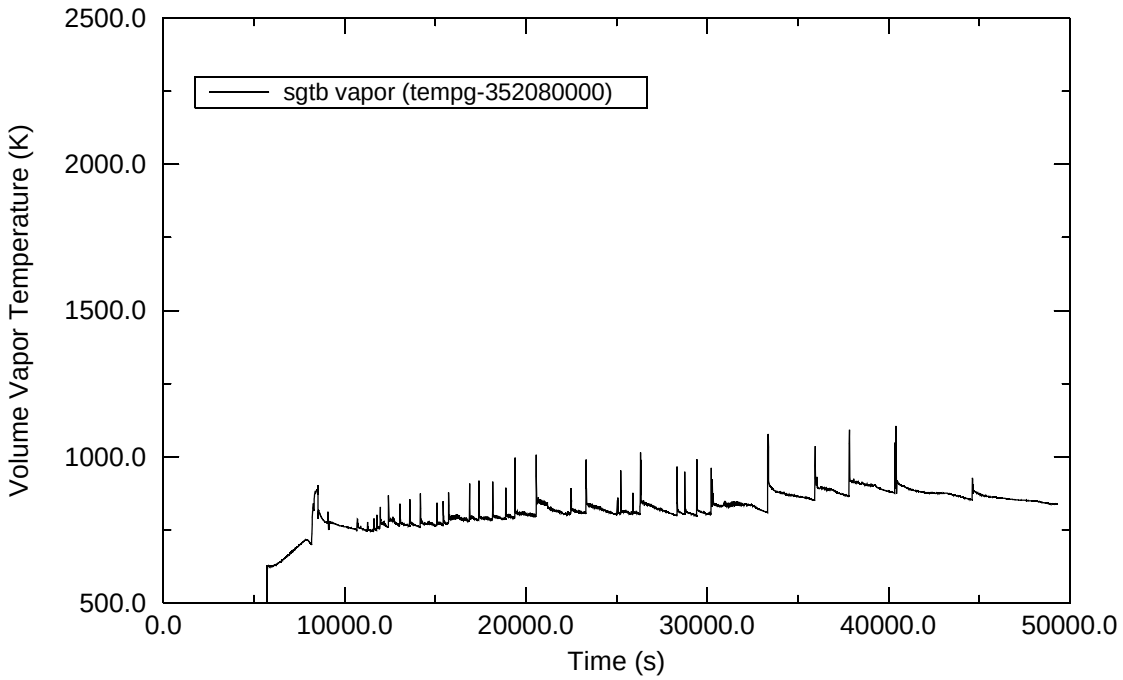

Figure H-6. Case 08 vapor temperature returning to SGB inlet plenum from the "cold" SG tube bundle.

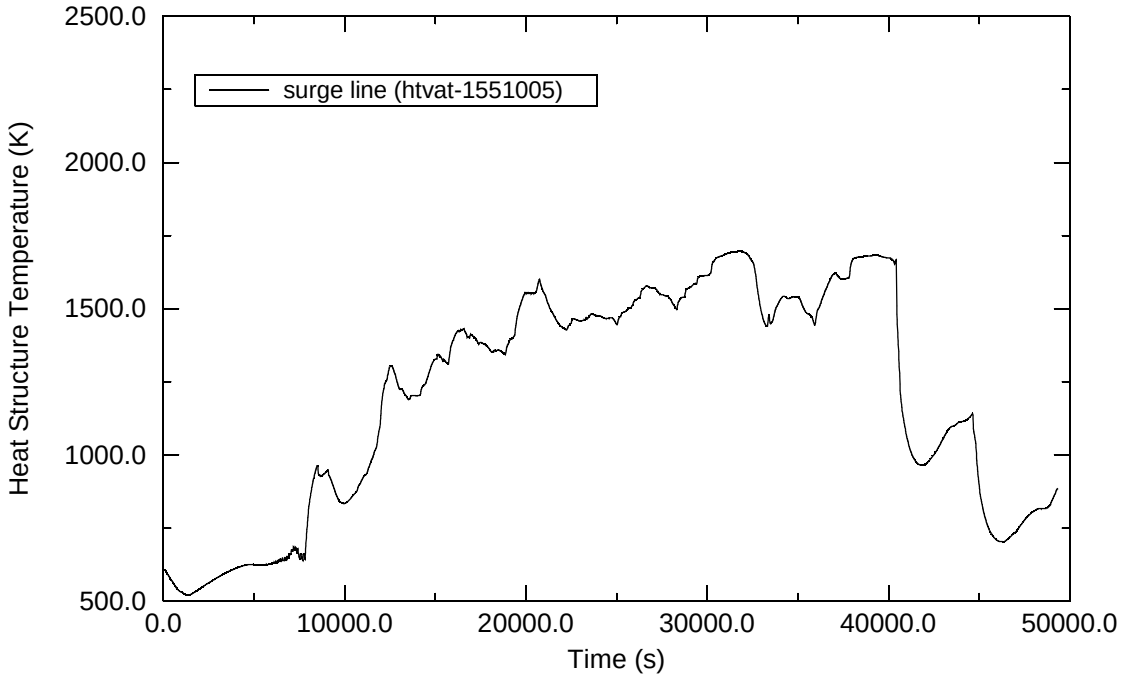

Figure H-7. Case 08 surge line temperature.

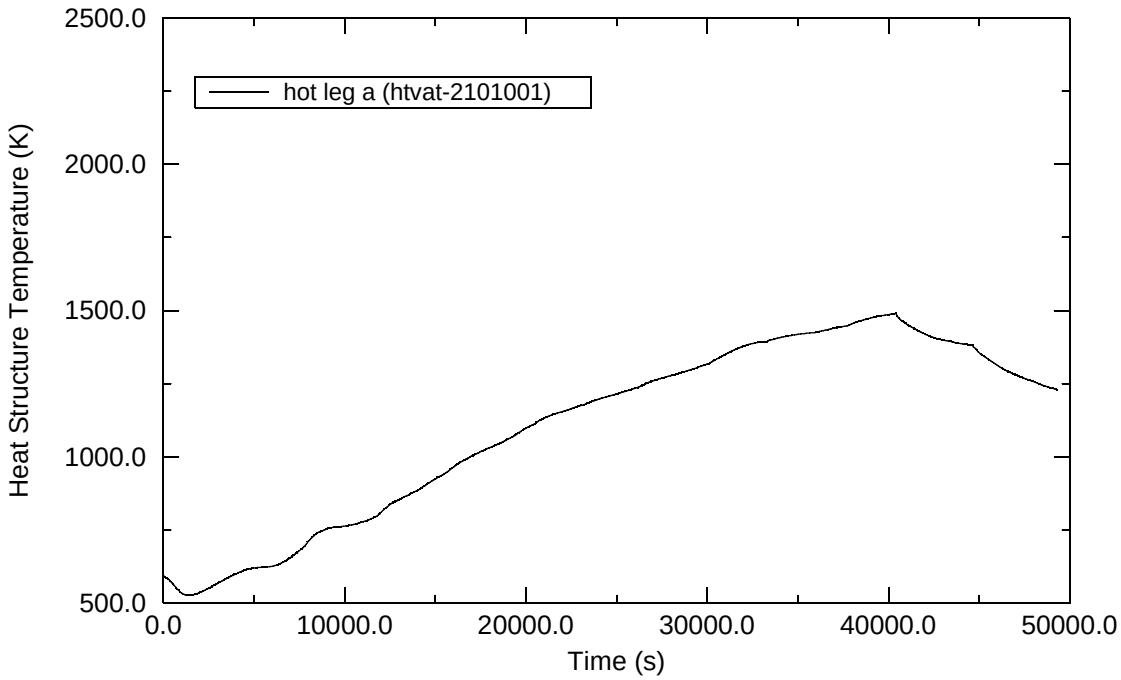

Figure H-8. Case 08 temperature of hot leg A (hot leg in primary coolant loop with pressurizer).

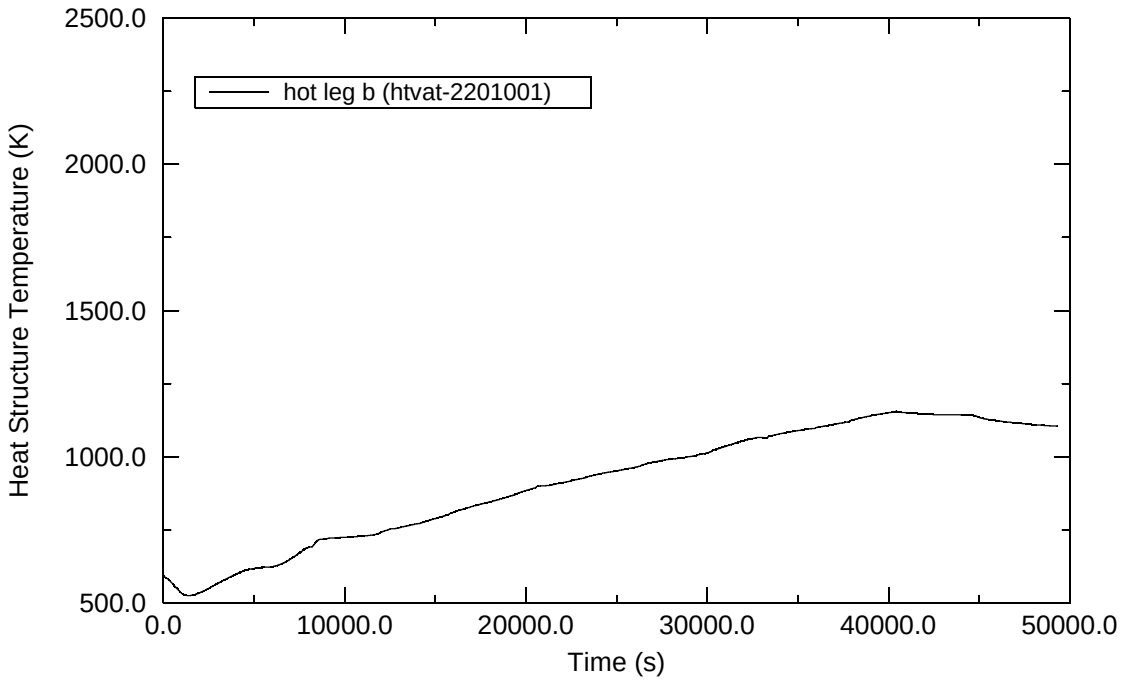

Figure H-9. Case 08 temperature of hot leg B (hot leg in primary coolant loop without pressurizer).

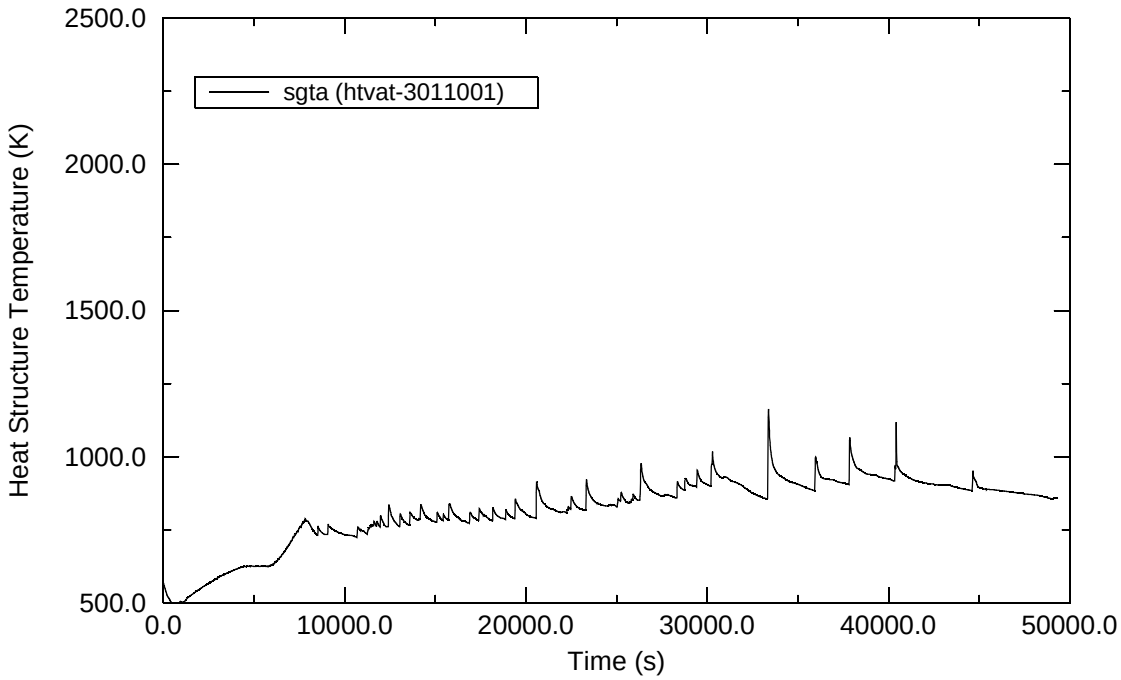

Figure H-10. Case 08 SGA tube temperature.

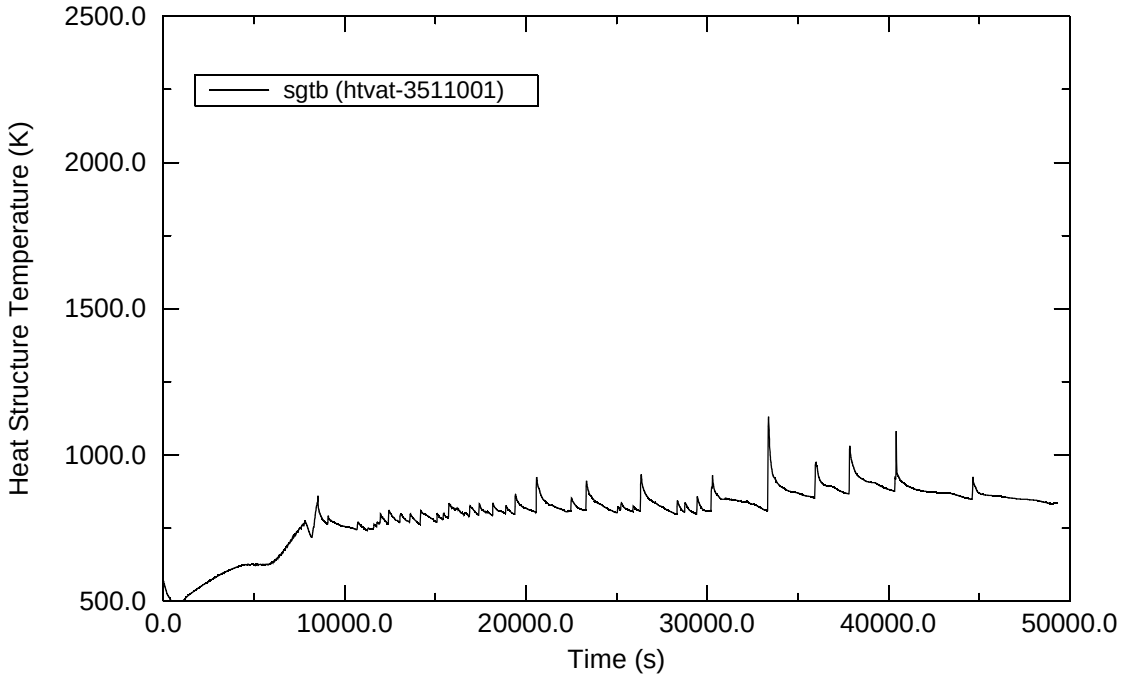

Figure H-11. Case 08 SGB tube temperature.

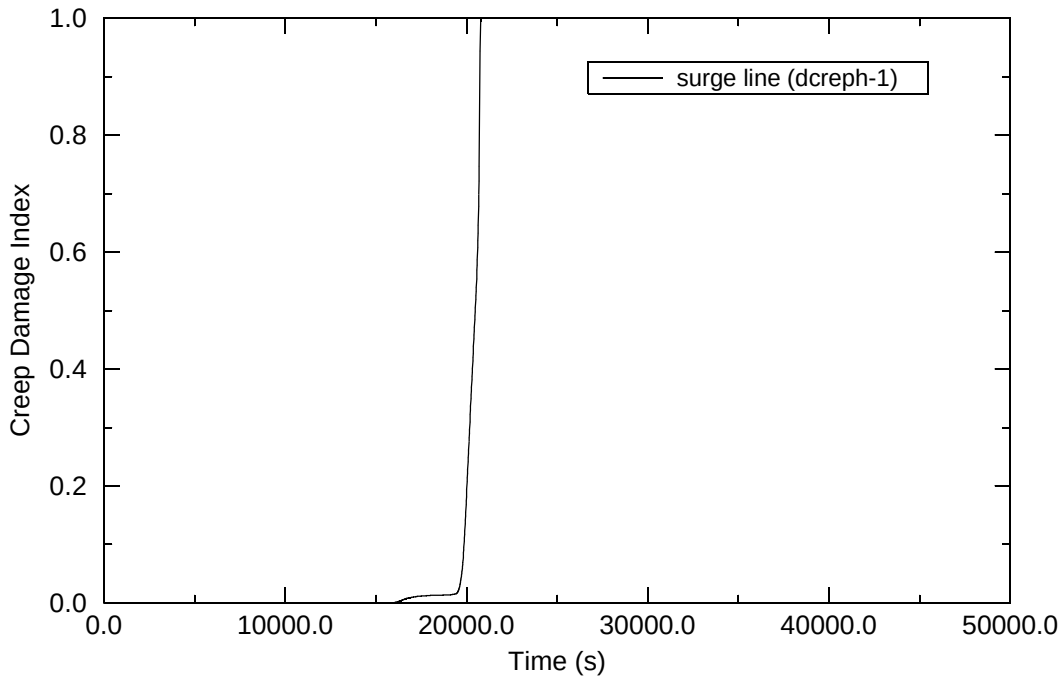

Figure H-12. Case 08 surge line creep damage index.

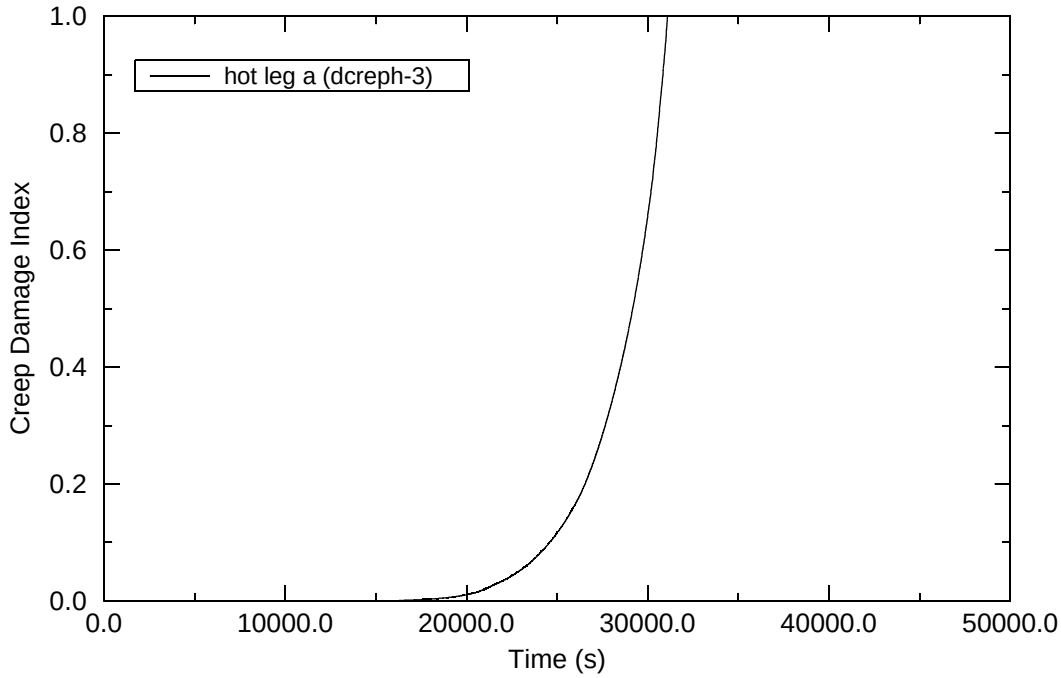

Figure H-13. Case 08 hot leg A creep damage index.

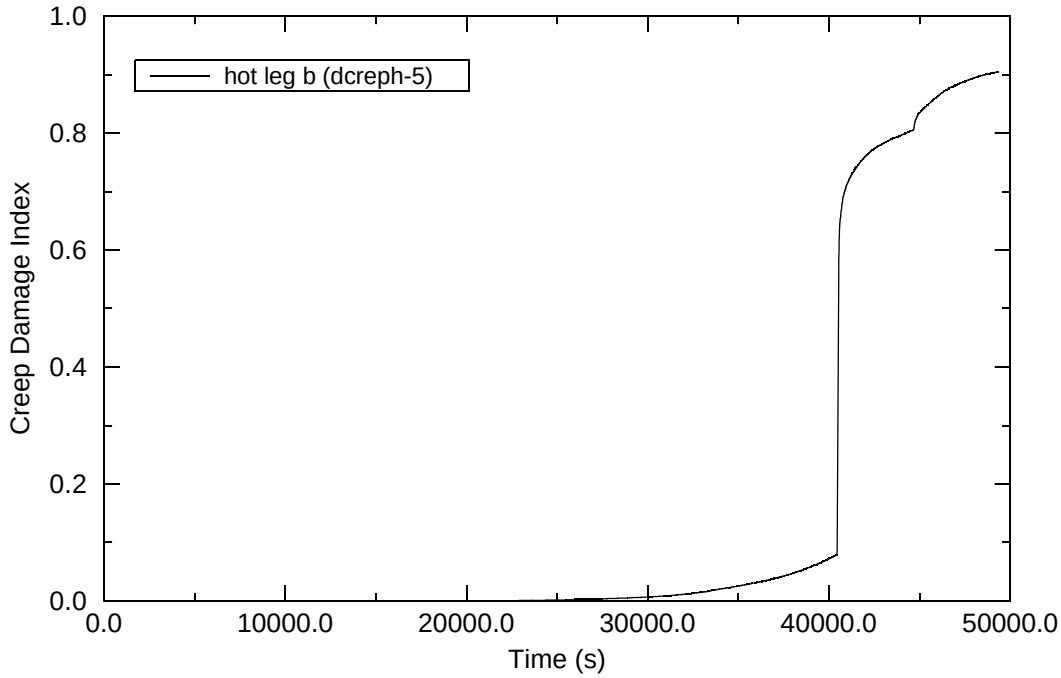

Figure H-14. Case 08 hot leg B creep damage index.

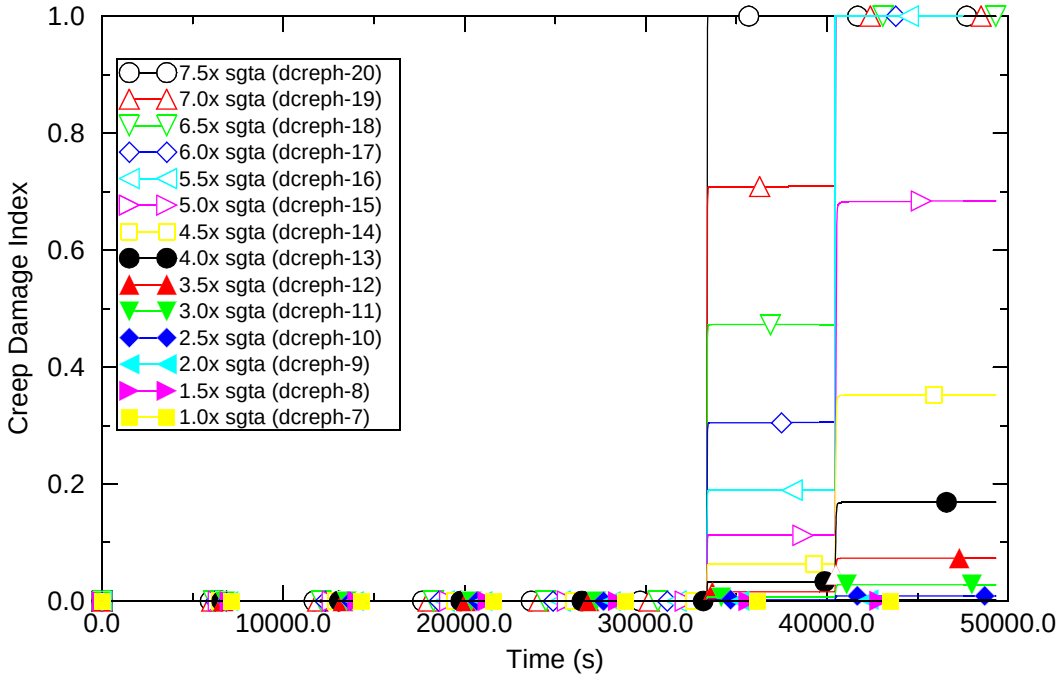

Figure H-15. Case 08 SGA tube creep damage indices.

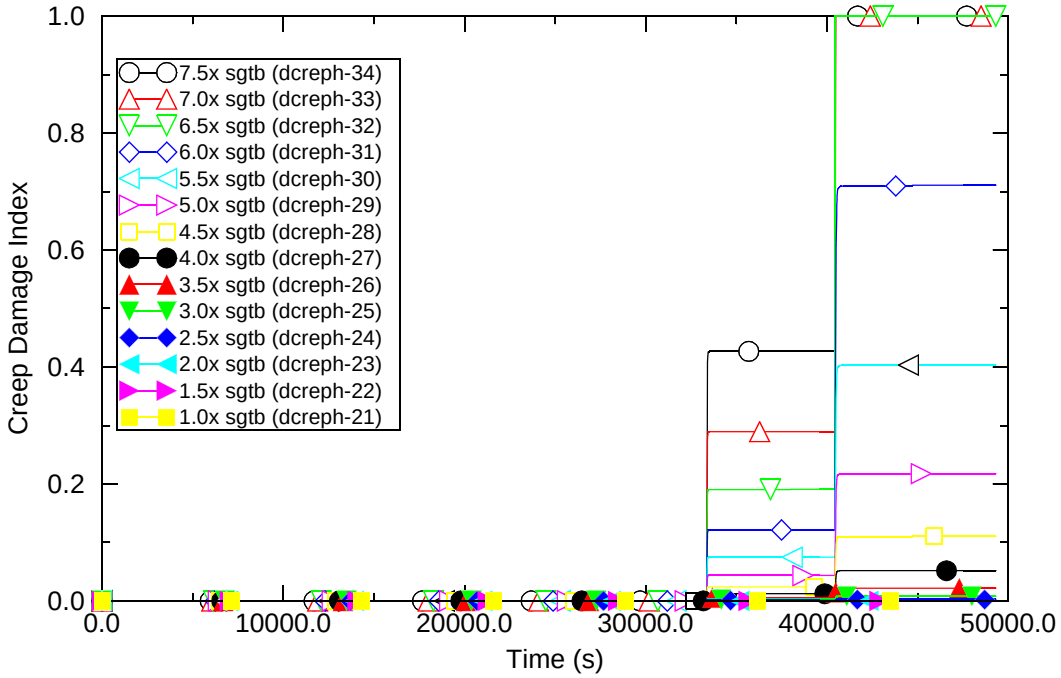

Figure H-16. Case 08 SGB tube creep damage indices.